UNIVERSITY OF SOUTHAMPTON

FACULTY OF NATURAL AND ENVIRONMENTAL SCIENCES

School of Chemistry

MAIN GROUP AND TRANSITION METAL-BASED CHELATES FOR PET APPLICATIONS

by

Francesco Matteo Monzittu

Thesis for the degree of Doctor of Philosophy

April 2018

UNIVERSITY OF SOUTHAMPTON

ABSTRACT

FACULTY OF NATURAL AND ENVIRONMENTAL SCIENCES

Chemistry

Doctor of Philosophy

MAIN GROUPS AND TRANSITION METAL-BASED CHELATES FOR PET APPLICATIONS

by Francesco Matteo Monzittu

$[AlCl_3(BnMe_2\text{-tacn})]$ was radiolabelled by Cl/^{18}F halide exchange reactions in the presence of 2.99 mol. equiv. of KF at pH 4 CH_3CO_2Na buffer solution with addition of ^{18}F-target water, to give $[Al^{18}F^{19}F_2(BnMe_2\text{-tacn})]$ with RCY up to 24 %. The radio-product was purified through a simple SPE purification protocol in 99 % RCP and it shows excellent stability in 50 % EtOH/PBS solution for >3h.

$[GaF_3(BnMe_2\text{-tacn})]$ can be successfully ^{18}F-radiolabelled using a precursor concentration as low as 27 nM through ^{18}F/^{19}F isotopic exchange reactions, using ^{18}F-target water in a 75 % MeCN/H_2O solution, in good RCYs (37 ± 5 %) within 10 minutes. The RCY of the reaction starting with a precursor concentration of 268 nM and 2.68 µM were 66 ± 4 % and 73 ± 4 %, respectively. $[Ga^{18}F^{19}F_2(BnMe_2\text{-tacn})]$ was purified through an SPE cartridge and formulated in 20 % EtOH/water solution showing a RCP of 99 % at t = 0 which decreases to 77-88 % after 2 h. The effect on the RCP of temperature, pH, addition of ascorbic acid, an excess of Cl^- or OH^- in solution were investigated.

The coordination chemistry of Group 13 metal fluorides towards O-donor ligands was developed. The $MF_3{\cdot}3H_2O$ (M = Al, Ga, In) were synthesised and the more readily soluble molecular species $[MF_3(OH_2)_2(DMSO)]$ (M = Al, Ga) were used as synthons for reactions with other ligands. The complexes were characterised by ^{1}H, ^{19}F{^{1}H}, microanalysis and IR spectroscopy. The stability of $[GaF_3(OH_2)_2(dmso)]$ was tested to determine whether it could be used as a radiolabelling precursor.

The coordination chemistry of the Group 3, Sc(III), Y(III), and lanthanides, La(III) and Lu(III), trichlorides and trifluorides (Sc only) towards neutral N-donor ligands was developed. The complexes were characterised by ^{1}H, ^{19}F{^{1}H} and ^{45}Sc NMR spectroscopy, as appropriate, together with IR spectroscopy and microanalysis. The crystal structures of $[ScCl_3(terpy)]$, $[MCl_3(terpy)(OH_2)]$ (M = Y, Lu), $[YI_3(Me_3\text{-tacn})]{\cdot}MeCN$, $[\{YI_2(Me_3\text{-tacn})\}_2(\mu\text{-}O)]{\cdot}MeCN$, $[\{La(terpy)(OH_2)Cl_2\}_2(\mu\text{-}Cl)_2]$, $[ScF_2Cl(Me_3\text{-tacn})]$ and $[ScF_2(Me_3\text{-tacn})(\mu\text{-}F)SnMe_3Cl]$ are reported. The first three examples of scandium fluoride complexes with neutral ligands are reported, $[ScF_3(BnMe_2\text{-tacn})]$, $[ScF_3(Me_3\text{-tacn})]$ and $[ScF_3(terpy)]$. These complexes were obtained by halide exchange reactions using the trichloride analogues, by reaction with $[Me_4N]F$ or Me_3SnF as the fluoride source.

The first row transition metal fluorides chemistry with terpy and Me_3-tacn was explored in order to identify promising systems for ^{18}F radiolabelling. The complexes $[MF_3(L)]$ (M = Cr, Mn, Fe, Co; L = Me_3-tacn, terpy) were synthesised and fully characterised by UV-vis and IR spectroscopy, microanalysis, and, for the diamagnetic $[CoF_3(L)]$, using ^{1}H, ^{19}F{^{1}H} and ^{59}Co NMR spectroscopy. Single crystal X-ray analyses are reported for $[MF_3(Me_3\text{-tacn})]$ (M = Mn, Co). Stability tests on $[MF_3(Me_3\text{-tacn})]$ (M = Cr, Mn, Fe, Co) and $[CrF_3(terpy)]$ were performed and the Cl/^{19}F halide exchange reactions using $[CrCl_3(Me_3\text{-tacn})]$ and $[FeCl_3(Me_3\text{-tacn})]$ were also carried out with added $[Me_4N]F$. The halide exchange reactions allowed partial Cl/F exchange for the Cr(III) systems, and proved to be successful in forming $[FeF_3(Me_3\text{-tacn})]$ cleanly.

Table of Contents

List of Tables

List of Figures

DECLARATION OF AUTHORSHIP

I, Francesco Matteo Monzittu declare that this thesis entitled "Main group and transition metal-based chelates for PET applications" and the work presented in it, are my own and has been generated by me as the result of my own original research.

I confirm that:

1. This work was done wholly or mainly while in candidature for a research degree at this University;
2. Where any part of this thesis has previously been submitted for a degree or any other qualification at this University or any other institution, this has been clearly stated;
3. Where I have consulted the published work of others, this is always clearly attributed;
4. Where I have quoted from the work of others, the source is always given. With the exception of such quotations, this thesis is entirely my own work;
5. I have acknowledged all main sources of help;
6. Where the thesis is based on work done by myself jointly with others, I have made clear exactly what was done by others and what I have contributed myself;
7. Parts of this work have been published as:

"Group 3 Metal Trihalides Complexes with Neutral-Donor Ligands – Exploring Their Affinity Towards Fluoride", E. Curnock, W. Levason, M. E. Light, S. K. Luthra, G. McRobbie, F. M. Monzittu, G. Reid, R. N. Williams, *Dalton Transactions*, 2018, **47**, 6059.

"Complexes of aluminium, gallium and indium trifluorides with neutral oxygen donor ligands: synthesis, properties and reactions", R. Bhalla, J. Burt, A. H. Hector, W. Levason, S. K. Luthra, G. McRobbie, F. M. Monzittu, G. Reid, *Polyhedron*, 2016, **106**, 65.

"[$AlCl_3$($BnMe_2$-tacn)] – a new metal chelate scaffold for radiofluorination by Cl/F exchange", W. Levason, S. K. Luthra, G. McRobbie, F. M. Monzittu, G. Reid, *Dalton Transactions*, 2017, **46**, 14519.

"Rapid Aqueous Late-Stage Radiolabelling of [GaF_3($BnMe_2$-tacn)] by $^{18}F/^{19}F$ Isotopic Exchange – Towards New PET Imaging Probes", F. M. Monzittu, I. Khan, W. Levason, S. K. Luthra, G. McRobbie, G. Reid, *Angewandte Chemie International Edition*, 2018, **57**, 6658.

Signed: .....

Date: .....

Acknowledgements

The work in this thesis is the result of 3.5 years of work that I could not have done without the help and support of my supervisors, here in Southampton and GE, previous and current members of the group and the love of my family.

In particular, I would like to thank Gill and Bill not only for the help with the scientific aspects of my PhD but also for always having a positive attitude towards the science and their support, making me believe in my abilities and that I could reach the end of the PhD even when the project was not going as I had expected. I would also like to thank Graeme for all his help during my PhD, from the comments on reports, abstracts or presentations to his help during the radiolabelling experiments at KCL. You've been "super patient" with me and hopefully you think it was worth it! Thanks to Immi as well for his advice on handling radioactivity and for coming up with a lot of ideas to improve the way the experiments were run. I really enjoyed my time at KCL and all the chats over lunch about football or sport in general with you. Many thanks to Dr. Sajinder Luthra for the really useful scientific discussions and advice for the development of the project. Thanks to Dr. Mark Light for his help with solving particularly nasty crystallographic problems.

Thanks to all the current and past members of the Reid Group, it's been a pleasure share my time in the lab with you! Specifically, I would like to thank Wenjian for his help with the synthesis of the macrocyclic ligands at the beginning of my PhD and for his help when the crystal structures required the intervention of a more experienced researcher.

Thanks to the four project/summer students I looked after during these years, your work has been very useful and it is part of this thesis. Emily Curnock and Nathan Williams carried out preliminary work on the Group 3 and lanthanide chemistry, while Nadeem Subhan and Tom Mules had their projects on the transition metal fluoride chemistry.

Thanks to Prof. Phil Blower and Dr. Michelle Ma for giving me the opportunity to work in the radiochemistry laboratories at St. Thomas' Hospital in London.

Thanks to EPSRC and GE for funding and the University of Southampton for providing excellent X-ray, NMR and MS facilities.

I ringraziamenti piú importanti vanno peró a Michela e alla mia Famiglia. So benissimo che non è stato facile per voi ma mi avete fatto sempre sentire la vostra vicinanza e mi avete aiutato in ogni situazione, che fosse facile, difficile, bella o brutta.

List of accompanying materials

Appendix 1 General experimental techniques

Appendix 2 Crystallographic information files (cif) for structures discussed in this thesis

Definitions and Abbreviations

PET	positron emission tomography
^{18}F	fluorine-18
RCY	radiochemical yield
RCP	radiochemical purity
SPE	Solid-Phase Extraction
HLB	Hydrophilic-Lipophilic-Balanced
HSA	Human Serum Albumin
Terpy	2,2',2''-terpyridine
Bipy	2,2'-bipyridine
Phen	1,10-phenantroline
Bn	benzyl
Tacn	1,4,7-triazacyclononane
fac	facial
mer	meridional
efg	electric field gradient
PBS	phosphate buffer solution
IR	infra-red
Bu	butyl
br	broad
NMR	nuclear magnetic resonance
pmdta	N,N,N',N'',N''-pentamethyldiethylenetriamine
thf	tetrahydrofuran
s	singlet
d	doublet
q	quartet
m	multiplet
ORTEP	Oak Ridge thermal ellipsoid plot
DMSO	dimethyl sulfoxide

MeCN	acetonitrile
MeOH	methanol
py	pyridine
py-NO	pyridine N-oxide
$\{^1H\}$	proton decoupled NMR spectroscopy
PXRD	Powder X-ray diffraction
HPLC	High Performance Liquid Chromatography
NOTA	1,4,7-triazacyclononane-1,4,7-triacetic acid
SiFA	Silicon-based Fluoride Acceptor
RGD	Arginylglycylaspartic acid
NHC	N-heterocyclic carbene
TBAF	Tetrabutylammonium fluoride
TMAF	Tetramethylammonium fluoride
[18]aneO_4S_2	1,10-dithia-18-crown-6
[18]aneO_4Se_2	1,10-diselena-18-crown-6
[15]aneO_3S_2	1,4-dithia-15-crown-5
Kryptofix2.2.2	4,7,13,16,21,24-hexaoxa-1,10-diazabicyclo[8.8.8]hexacosane
Cyclen	1,4,7,10-tetraazacyclododecane
Cyclam	1,4,8,11-tetraazacyclotetradecane

Chapter 1: **INTRODUCTION**

This thesis explores the synthesis and possible application of metal-based inorganic systems for the development of new positron emission tomography (PET) agents. The latest developments on the ^{18}F-radiolabelling experiments on the Group 13 metal fluoride complexes (Al^{3+}, Ga^{3+}) with $BnMe_2$-tacn as ligand are presented, as well as the preliminary investigation and assessment of new systems, such as the Group 3 (Sc^{3+}, Y^{3+}), La^{3+} and Lu^{3+}, and first row of transition metal (Cr^{3+}, Mn^{3+}, Fe^{3+} and Co^{3+}) fluorides coordinated to triazacyclononane derivatives or terpy.

This introductory Chapter discusses how PET works and why alternative systems to C-^{18}F bond formation reactions on organic molecules have been investigated and developed in the last 10- 15 years. The rationale behind the choice of the metals used in this work, the reason macrocyclic ligands are employed to coordinate these metals and a brief overview on the coordination chemistry of the Group 13 metal fluorides are also reported.

1.1 Positron Emission Tomography (PET)

PET is a non-invasive, whole body medical imaging technique, which provides diagnostic and clinical information. It has been used in oncology, cardiology, neurology and in drug development.[1] It requires the injection of a molecule (radiotracer) bearing a radioactive element which accumulates at the target tissue or enters metabolism processes. The radioactive element decays emitting a positron, which will travel for a few mm into the tissue until it interacts with an electron. The collision between a positron and an electron (annihilation) produces two gamma rays at almost exactly 180° each other (in a coincidence line) which can be detected by a PET camera, enabling an image of the body to be reconstructed (Figure 1.1).[2,3]

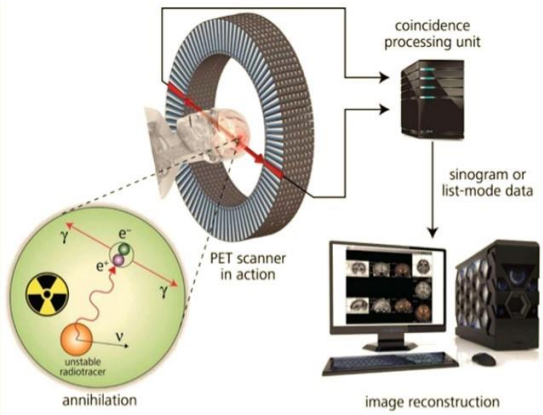

Figure 1.1. Schematic of the annihilation of positron and electron and image reconstruction. Image taken from the internet (https://www.slideshare.net/mustafaalbayati923/positron-emissions-tomography-pet-scan).

PET has a high sensitivity (allowing for quantities as low as fmol of radiotracer to be used) and high resolution (typically 4-10 mm, but depends on the energy of the emitted positron, the higher the energy of the positron the longer the distance it will travel before annihilation and the lower the spatial resolution).[4] Examples of positron emitting radioisotopes and their nuclear characteristic are shown in Table 1.1.

Isotope	Half-life (min)	Positron decay (%)	Energy of positron emitted (Mev)
^{11}C	20	99	0.97
^{18}F	110	97	0.64
^{44}Sc	238	94	0.63
^{68}Ga	68	89	1.90
^{89}Zr	4710	23	0.40

Table 1.1. Properties of radioisotopes used in PET.[5]

Thanks to its almost ideal chemical and nuclear characteristics, fluorine-18 (^{18}F) is the most widely utilised radioisotope.[1,6] ^{18}F has a short, but manageable half-life ($t_{½}$ = 110 min), high positron emission yield (97 %), low positron energy ($E_{\beta max}$ = 635 keV) and is readily available as it is produced in medical cyclotrons (note that ^{18}F half-life allows for the ^{18}F-pharmaceutical to be transported to hospitals without on-site cyclotrons).[7,8] Fluorine-18 can be produced *via* several nuclear reactions and using different targets depending on the form of ^{18}F required. However, the most common way of producing ^{18}F is by irradiation of oxygen-18 enriched water according to the ^{18}O(p,n)^{18}F reaction to obtain the nucleophilic [^{18}F]F$^-$ in water. In this way, activities of up to 100 GBq can be obtained in around 1 hour of irradiation.[5] Alternatively, the electrophilic [^{18}F]F_2 has also been employed, but with less success (see below).

The radiolabelling of target molecules should ideally satisfy the following conditions:

- The radio-product is obtained in high radiochemical yields (RCY) and high molar activity (amount of radioactivity per mole of radiolabelled compound; radiotracers used in the clinic have molar activity in the order of 100- 1000 GBq/µmol);
- The radiolabelling reaction is performed in aqueous solution and mild conditions (neutral pH and room temperature);
- The final step of the synthesis of the radiotracer should involve the introduction of [^{18}F]F$^-$ into the substrate, not only to maximise the amount of radioactivity, but also to limit the time operators are exposed to it;
- Minimal requirement for purification pre- and post-labelling;
- The target molecule should be radiolabelled at nM concentration or lower.

Organofluorine molecules are the most common radiotracers employed for a PET scan, but they have not achieved these "ideal conditions". The reactions to form C-^{18}F bonds are usually nucleophilic substitution involving the use of [^{18}F]F$^-$ and require multi-step and time consuming syntheses.[5,7] While a couple of examples of C-^{18}F bond formation reactions are reported in this chapter, the literature surveys of this thesis focuses on non C-^{18}F molecules (Chapter 2 and 3). The synthesis of the two most widely utilised radiotracers and the problems associated with their synthesis are briefly described: [^{18}F]FDOPA (6-fluoro-3,4-dihydroxyphenylalanine), which is used for probing cerebral dopamine metabolism[9,10] and neuroendocrine tumours[11] (made using the electrophilic [^{18}F]F$_2$), and [^{18}F]FDG (2-fluoro-2-deoxy-D-glucose), used for studying glucose metabolism[12] and made using the nucleophilic [^{18}F]F$^-$ (Figure 1.2).

Figure 1.2. [^{18}F]FDOPA (left) and [^{18}F]FDG (right).

1.1.1 [^{18}F]FDOPA: electrophilic radiofluorination

[^{18}F]F$_2$ can be produced by the ^{18}O(p,n)^{18}F nuclear reaction employing enriched ^{18}O$_2$ as target.[13] The maximum achievable RCY using [^{18}F]F$_2$ can only be 50 %, since only one fluorine atom in F$_2$ is radioactive.[5] This leads to products with low molar activity. Moreover, the highly reactive nature of [^{18}F]F$_2$ requires the use of specialised equipment and can lead to a mixture of by-products, due to poor selectivity.[7] For these reasons, [^{18}F]F$_2$ is usually converted into less reactive and more selective forms, such as acetyl hypofluorite,[14] xenon difluoride[15] or fluorosulfonamides.[16] Despite these difficulties, [^{18}F]FDOPA is produced by a regioselective demetallation reaction on an aryltrimethyltin precursor in 25 % RCY after a deprotection step with HBr and an HPLC purification (Scheme 1.1).[17]

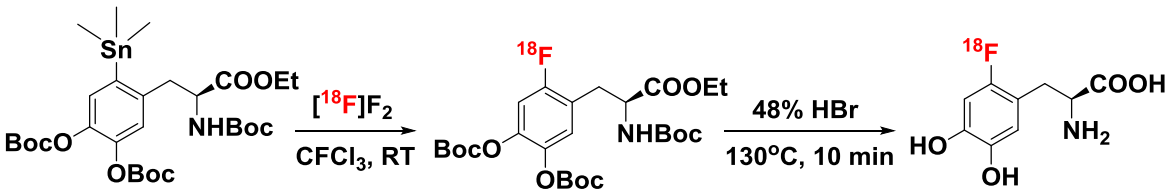

Scheme 1.1. Synthesis of [^{18}F]FDOPA.

Given the low RCY and molar activity achievable, as well as the difficulty of handling F$_2$, reactions employing nucleophilic [^{18}F]F$^-$ are preferred for the synthesis of ^{18}F-radiolabelled compounds.

1.1.2 [^{18}F]FDG: nucleophilic radiofluorination

As mentioned above, [^{18}F]F$^-$ is obtained in water from bombardment of oxygen-18 enriched water through the nuclear reaction ^{18}O(p,n)^{18}F. The [^{18}F]F$^-$ is easier to handle compared to [^{18}F]F$_2$ and can lead to higher molar activities. However, [^{18}F]F$^-$ is a poor nucleophile in the presence of water, since it is highly hydrated and forms strong hydrogen bonds, greatly reducing its tendency to act as a nucleophile.[18] To increase its nucleophilicity, the water must be strictly excluded.[5] This aspect has been the main challenge in ^{18}F-radiolabelling chemistry of C-^{18}F based radiotracers.[7] The synthesis of [^{18}F]FDG[19,20,21] proceeds through an S_N2 mechanism and is reported in scheme 1.2. This is used as a representative example of the challenges involved in the radiolabelling of organic molecules through C-^{18}F bond formation.

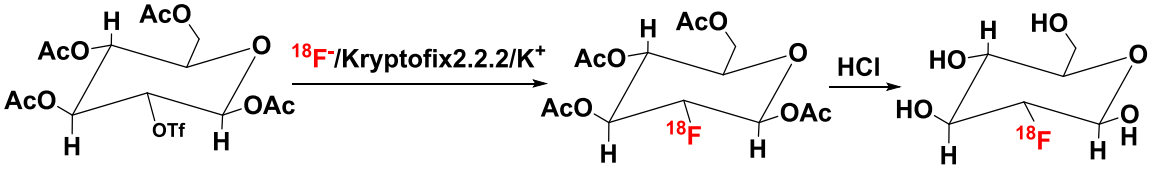

Scheme 1.2. Synthesis of [^{18}F]FDG.

The problem of the low nucleophilicity of [^{18}F]F$^-$ in water is partially resolved by including a drying step and subsequent transfer of [^{18}F]F$^-$ in an aprotic solvent, such as MeCN. This is achieved by passing the target water through an anion exchange cartridge which is able to trap [^{18}F]F$^-$; the radioactive fluoride anions are then eluted from the cartridge using a phase transfer catalyst such as a solution of kryptofix2.2.2 (4,7,13,16,21,24-hexaoxa-1,10-diazabicyclo[8.8.8]hexacosane) and K_2CO_3 in MeCN (Scheme 1.3).

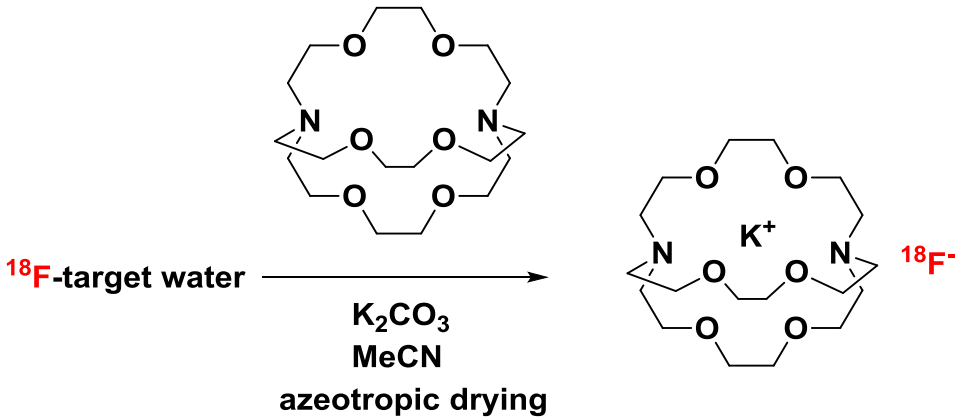

Scheme 1.3. Method to obtain a dry source of "naked" fluoride.

The MeCN solution is then azeotropically dried under a stream of nitrogen at ~ 100 °C several times in order to remove the water.[21] This method enhances the ability of [^{18}F]F$^-$ to act as a nucleophile, but even in this form the substrate must contain an excellent leaving group for efficient labelling.

In the [^{18}F]FDG radiosynthesis, the leaving group is triflate, but sulfonic acid esters, mesylate or tosylate have also been employed. The presence of other functional groups in the substrate that can interfere during the reaction, further complicate the system and introduce the need of protection and, more importantly, deprotection steps post-labelling (Scheme 1.2). Moreover, the basicity of fluoride ions in aprotic solvents could lead to competitive elimination reactions.[5] A final HPLC or solid-phase extraction (SPE) purification step is also required, further increasing the total reaction time. Similar (or more complex) conditions are required for the synthesis of other C-^{18}F based radiotracers.[5,7]

It is clear that these multi-step and time consuming syntheses to form C-^{18}F based tracers do not satisfy all the criteria reported above, but the clinical importance of [^{18}F]FDG has made it worthwhile and economically profitable.

Moreover, the reaction conditions for C-^{18}F bond formation are not compatible for bioconjugation to more complex molecules, such as peptides or proteins, since the functional groups present in the biomolecules can interact with the leaving groups and are denaturated in non-aqueous media (hence, it would be ideal to use directly the target water as received from the cyclotron[22]). It is not a surprise, therefore, that improvements and alternatives have been developed and explored over the years. Transition metal complexes have been used as catalysts in direct C-^{18}F bond formation reactions in small molecules in the final step[23,24,25] and, more relevant to this work, exploitation of the strong bonds B-^{18}F, Al-^{18}F[26] and Si-^{18}F[27] have been used in several systems as alternatives to C-^{18}F based molecules (See Chapter 2 and Chapter 3 for a more detailed discussion of these systems).

1.2 Choice of the metals and general properties of the complexes

A PET scan involves the injection of a radiotracer into the patient. The stability of the radiotracer in the time scale of the experiment and until it is cleared from the body, is therefore of paramount importance. On the other hand, the reaction to incorporate [^{18}F]F$^-$ into the precursor should be fast and ideally in the last stage of the synthesis. For the development of inorganic systems based on coordination complexes, the choice of the metal is a key aspect in order to achieve these conditions and therefore, the following criteria have been identified:

- The metal should have high affinity for F$^-$ in water, at room temperature and medium pH. Suitable metals are hard Lewis acids with high bond dissociation energies associated with the M-F bond;
- It should have a fixed coordination number and limited redox chemistry. The formation of other species during the radiolabelling reaction and degradation of the radiotracer as a

result of competitive reactions (i.e. redox, ligand exchange, etc.) must be avoided in order to obtain a well-defined, stable product in high yield;

- The kinetic properties of the metal should allow for fast $[^{18}F]F^-$ uptake through Cl/^{18}F halide exchange or ^{18}F/^{19}F isotopic exchange reactions;
- Once $[^{18}F]F^-$ is incorporated into the precursor, it should be resistant to substitution during purification and stable *in vivo*.

The Group 13 (Al, Ga), Group 3 (Sc, Y), La and Lu metals were identified as suitable candidates. They all have high affinity for fluoride (Table 1.2) and the closed shell configuration of the 3+ oxidation state means their chemistry is dominated by M^{3+} species.

Bond	Bond dissociation enthalpy (KJ mol^{-1})
Al-F	664
Al-Cl	494
Ga-F	577
Ga-Cl	481
Sc-F	589
Sc-Cl	318
Y-F	605
Y-Cl	527
Cr-F	437
Cr-Cl	366
Mn-F	423
Mn-Cl	361
Fe-F	447
Fe-Cl	352
Co-F	435
Co-Cl	398
La-F	598
Lu-F	569

Table 1.2. M-F and M-Cl bond dissociation energies of the metal used in this work.[28]

Al(I) and Ga(I) species are known, but they are accessible only in particular conditions and are very readily oxidised.[29,30,31] The most common coordination number of the complexes of these metals is six, although lower or higher coordination numbers become more important depending on the ionic radii of the metal. For example, coordination numbers of four are often seen in Al(III) chemistry and coordination numbers > 6 are likely to be observed in Y(III) or La(III) systems.[32,30] The kinetics of these metal ions allow for fast reactions and for the Cl/^{18}F halide exchange reactions the higher affinity towards fluoride than chloride provides an extra driving force to obtain a well-defined product rapidly, in mild conditions and with high stability. Obviously, the co-ligands are also very important to satisfy these aspects and can greatly influence the properties of the complex. The ligand should be strongly bound to the metal and should be retained in the coordination sphere not only during the radiolabelling experiments, but also over pH and temperature variations and in the presence of competitive species in solution (preferentially water). For this reason, the macrocyclic triazacyclononane derivatives have been chosen as ligands, since they give extra stability to the complexes thanks to the macrocyclic effect and can coordinate many metal ions across the periodic table (the origin of the macrocyclic effect is discussed in the next section), allowing for scoping different systems. Previous work in the Reid group has shown that triazacyclononane derivatives form very stable complexes with the Group 13 metal fluorides and that [$GaCl_3$($BnMe_2$-tacn)] ($BnMe_2$-tacn = 1-benzyl-4,7-dimethyl-triazacyclonane) can be successfully ^{18}F-radiofluorinated in mild reaction conditions (see introduction of Chapter 2 for more details). Additionally, the use of the tacn derivative, $BnMe_2$-tacn provides a chromophore group which allows the radiolabelling reactions to be analysed by UV-vis spectroscopy. The benzyl group also has the potential to be used as functionalisation group for bioconjugation reactions. Moreover, the rigid, linear ligand terpy has also been employed in this work as the aromatic rings can be in principle easily functionalised for bioconjugation reactions and the complexes formed have *meridional* geometries instead of the *facial* geometry in the case of complexes with tacn derivatives, providing a comparison between the two systems. However, it was shown that acyclic ligands such as terpy are less stable than the macrocyclic complexes.[33,34,4] The properties of the complexes employed in this work for ^{18}F-radiolabelling reactions are summarised in Figure 1.3.

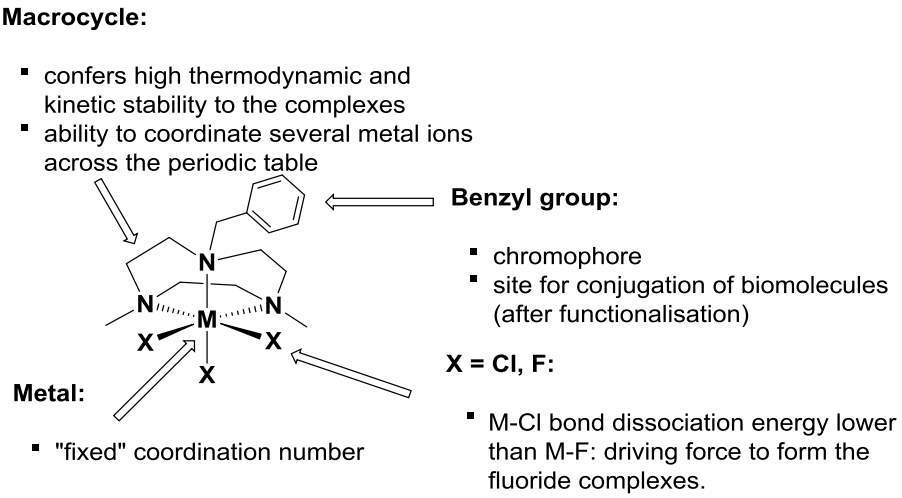

Figure 1.3. General properties of a complex of the type [MX_3($BnMe_2$-tacn)].

The transition metal ions Cr(III), Mn(III), Fe(III) and Co(III) were also explored. These metals have high or moderately high affinity with fluoride (Table 1.2), but do not have a closed shell configuration, allowing other oxidation states to be accessible in some cases. The d^3 Cr(III) complexes are expected to be thermodynamically stable, but the kinetics might be slow as well as for d^6 Co(III) system, whereas the d^5 Fe(III) complexes should allow faster reaction times, although species in different oxidation states may be formed under some conditions. The d^4 Mn(III) is expected to be the least stable of these systems as it is more labile and prone to disproportionation.

1.3 Stability of complexes with macrocyclic ligands

The chemistry of macrocycles is incredibly diverse and has a large number of applications, from medicinal chemistry and catalysis to supramolecular chemistry, cation and anion extraction/recognition, magnetic resonance imaging and single molecule magnets.[35,36,37,38,39,40,41,42,43] Common classes of macrocycles are: crown ethers, aza-macrocycles, aza-crowns, Schiff base macrocycles and porphyrins. Macrocycles can be synthesised with different ring sizes, degree of rigidity of the ring and bearing different donor atoms, all of which influence their electronic and structural properties and make them versatile systems able to coordinate many main group and transition metals.[44, 45] The functionalisation of the donor atoms can further tailor their properties for the application of interest.[46,47,48] Common macrocyclic donor atoms include nitrogen, oxygen and sulfur, but also phosphorus, arsenic, selenium and tellurium macrocycles have been prepared.[45,44] The macrocycles employed in this work are triazacyclononane derivatives (Me_3-tacn and $BnMe_2$-tacn), whose synthesis and functionalisation methodologies are reported in a comprehensive review by Chaudhuri and Wieghardt[49] and in Scheme 1.4. Triazacyclononane derivatives have been employed to coordinate many main group and transition metal ions.[33,50,51,52,53,54]

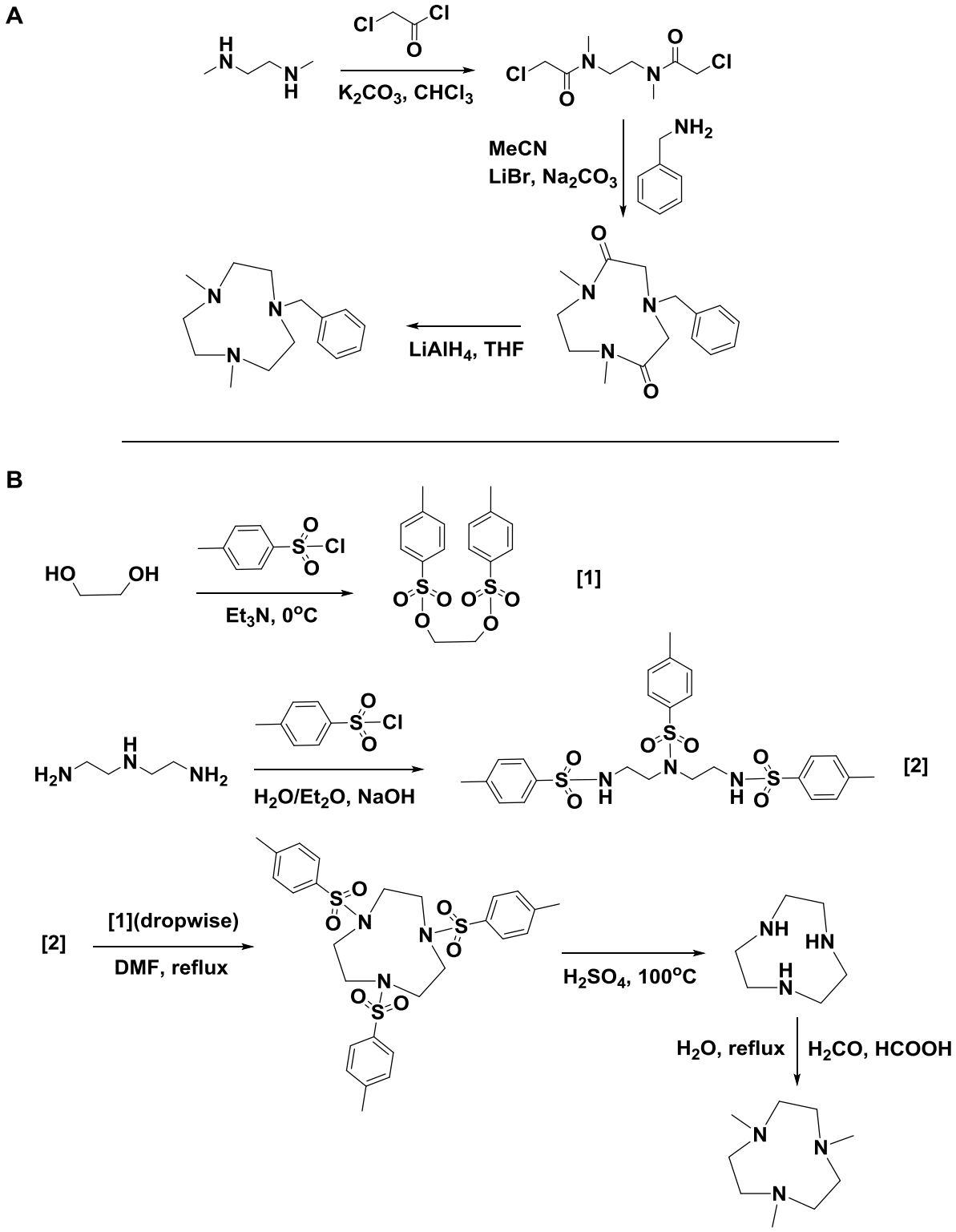

Scheme 1.4. Syntheses of $BnMe_2$-tacn (A) and Me_3-tacn (B).

Macrocyclic complexes are very robust and more thermodynamically stable and kinetically inert than those of the analogous open chain ligands, thanks to the macrocyclic effect.[55] This extra stability of the complexes derived from entropic and enthalpic contributions as well as kinetic effects.[56]

- Entropic contribution: a macrocyclic ligand and its open chain analogue have different degrees of freedom in their 'free' form and the flexibility of the ligands diminishes upon complexation in both cases. However, the net gain in entropy in releasing the open chain ligand is greater than the one of the macrocyclic analogue.
- Enthalpic contribution: this contribution arises from the difference in solvation for the open chain and macrocyclic ligand and greatly varies from system to system as it depends on the ring size, donor atoms and the metal ion coordinated. Open chain ligands are usually more readily solvated than the macrocyclic parent due to greater flexibility in the 'free' forms (considering systems with the same donor atoms).
- Kinetic effect: macrocyclic complexes are more difficult to form than the open chain complex analogues but once formed, they are very robust and resistant to dissociation. Considering the follow reaction:

  $M^{2+} + L \leftrightarrows ML^{2+}$ $\qquad K = \frac{[ML^{2+}]}{[M^{2+}][L]} = \frac{k_f}{k_d}$

  Both the formation (k_f) and dissociation (k_d) rate constant are lower in the macrocyclic complex than those of the analogue open chain system, due to the difference in flexibility of the coordinated bonds. This means that dissociation requires elongation and cleavage of the M-L bond, but in a macrocyclic complex this is inhibited as it would lead to a distortion throughout the whole ring.

In some cases the macrocyclic effect may be slightly enhanced by a preorganisation effect. On the contrary, a rearrangement of the ligand upon complexation can lead to a diminished macrocyclic effect. For example, thioether macrocycles adopt an *exo* conformation in the free form (lone pairs on the S atoms are directed away to minimise repulsion), but there is a conformational rearrangement to the *endo* form upon coordination to the metal, which requires the input of energy.

1.4 Overview of the Group 13 metal fluoride coordination chemistry with neutral nitrogen-donor ligands

Chapters 2 and 3 discuss the radiolabelling experiments performed on the complexes [MX_3($BnMe_2$-tacn)] (M = Al, Ga; X = Cl, F), however, only the background related to PET applications is reported. For completeness, this section focuses on the coordination chemistry of the Group 13 metal fluorides towards neutral N-donor ligands (the coordination chemistry of this group towards O-donor ligands is discussed in the introduction to Chapter 4, whereas Chapter 5 and 6 discuss the coordination chemistry of Group 3, La(III), Lu(III) and some of the first row transition metal fluorides towards nitrogen donor ligands).

While the anhydrous Group 13 metal fluorides MF_3 (M = Al, Ga, In) are inert polymeric solids and unreactive, the hydrates, $MF_3 \cdot 3H_2O$, are more reactive.[32,57] They mainly exist in two forms, the α-form with discrete molecules of $[AlF_3(OH_2)_3]$, or the polymeric β-form, $[\{MF_2(OH_2)_2(\mu\text{-}F)\}_n] \cdot nH_2O$ (M = Al, Ga, In)[58,59] (see Chapter 4 for further details). Although the $MF_3 \cdot 3H_2O$ are more reactive compared to the anhydrous MF_3, they still are very poorly soluble in organic solvents or water and require harsh reaction conditions in order to react with neutral ligands. The reaction of $GaF_3 \cdot 3H_2O$ with pyridine in thf under reflux gave the *meridional* octahedral complex $[GaF_3(py)_3]$,[60] while reacting $GaF_3 \cdot 3H_2O$ with 1,4,7-tris(2-amino-3,5-di-*tert*-butyl-benzyl)-1,4,7-triazacyclononane (L) in ethanol under reflux, followed by recrystallization from MeOH, afforded $[GaF_3(L)] \cdot 6MeOH$ (Figure 1.4 A).[61] Interestingly, the structure crystallises with 6 MeOH molecules connected by H-bonding in a cyclic S_6-symmetry hexamer.

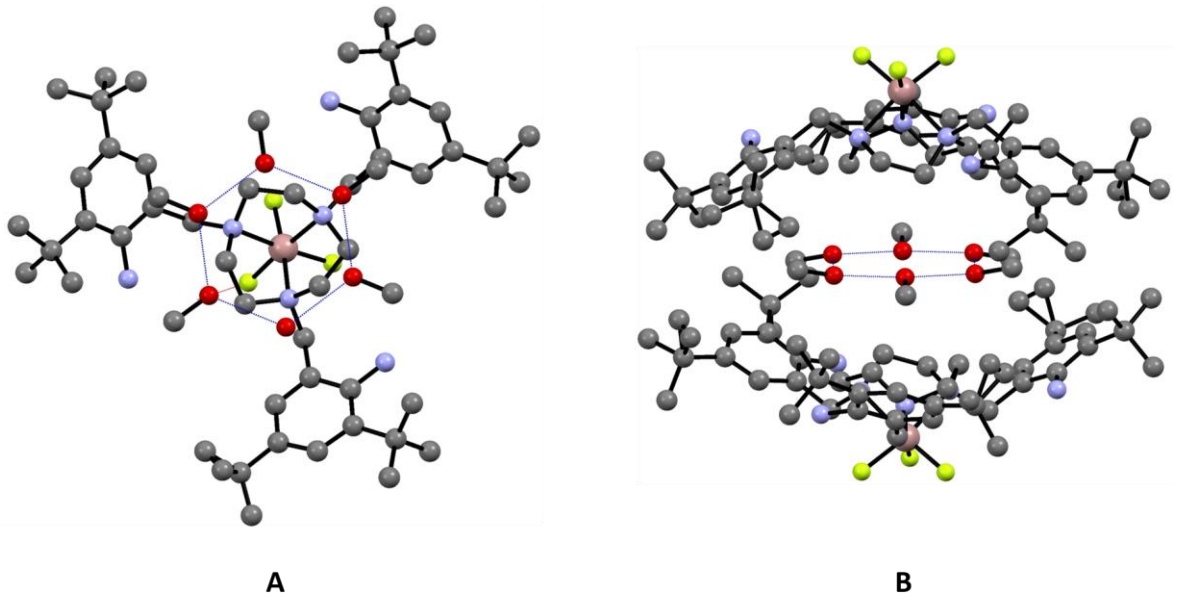

Figure 1.4. A: Crystal structure of $[GaF_3(L)] \cdot 6MeOH \cdot CH_2Cl_2$ (L = 1,4,7-tris(2-amino-3,5-di-*tert*-butyl-benzyl)-1,4,7-triazacyclononane) showing the cyclic S_6-symmetric hexamer of methanol. B: cyclic S_6-symmetric hexamer inside the "hydrophobic pocket" (blue dotted lines represent the H-bonding interactions). H atoms and solvated CH_2Cl_2 are omitted for clarity. Ga = pink, F = green, N = blue, O = red, C = grey. Image redrawn from CCDC number 1220143.[61]

The crystal structure of the neutral species $[GaF_3(L)] \cdot 6MeOH \cdot CH_2Cl_2$ shows a distorted octahedral geometry around the metal. The three 2-amino-3,5-di-*tert*-butylbenzyl arms are not coordinated and are folded upwards on the side of the macrocyclic ring, resulting in a "bowl-shaped" hydrophobic cavity. The adjacent $[GaF_3(L)] \cdot 6MeOH \cdot CH_2Cl_2$ molecule has the three 2-amino-3,5-di-*tert*-butylbenzyl arms facing the ones of the other molecule resulting in the arms staggered each other and in a "hydrophobic pocket". Inside this pocket there are 6 MeOH molecules forming a cyclic structure held by O-H···O H-bonding in a S_6 symmetry (Figure 1.4 B).[61]

Hydrothermal conditions (180 °C, 15 hours) were employed for a systematic study of the reactions of $MF_3 \cdot 3H_2O$ (M = Al, Ga, In) with neutral N-donor ligands to form the species $[MF_3(L)]$ (L = Me_3-tacn, $BnMe_2$-tacn, terpy) and $[MF_3(OH_2)(L)]$ (L = bipy, phen) (Figure 1.5). When bi-dentate ligands were used, a water molecule coordinates to the metal, completing the octahedral geometry.[62,33] The species $[InF_3(OH_2)(bipy)]$ (Figure 1.5D) and $[InF_3(OH_2)(phen)]$ have also been reported.[63,64,65]

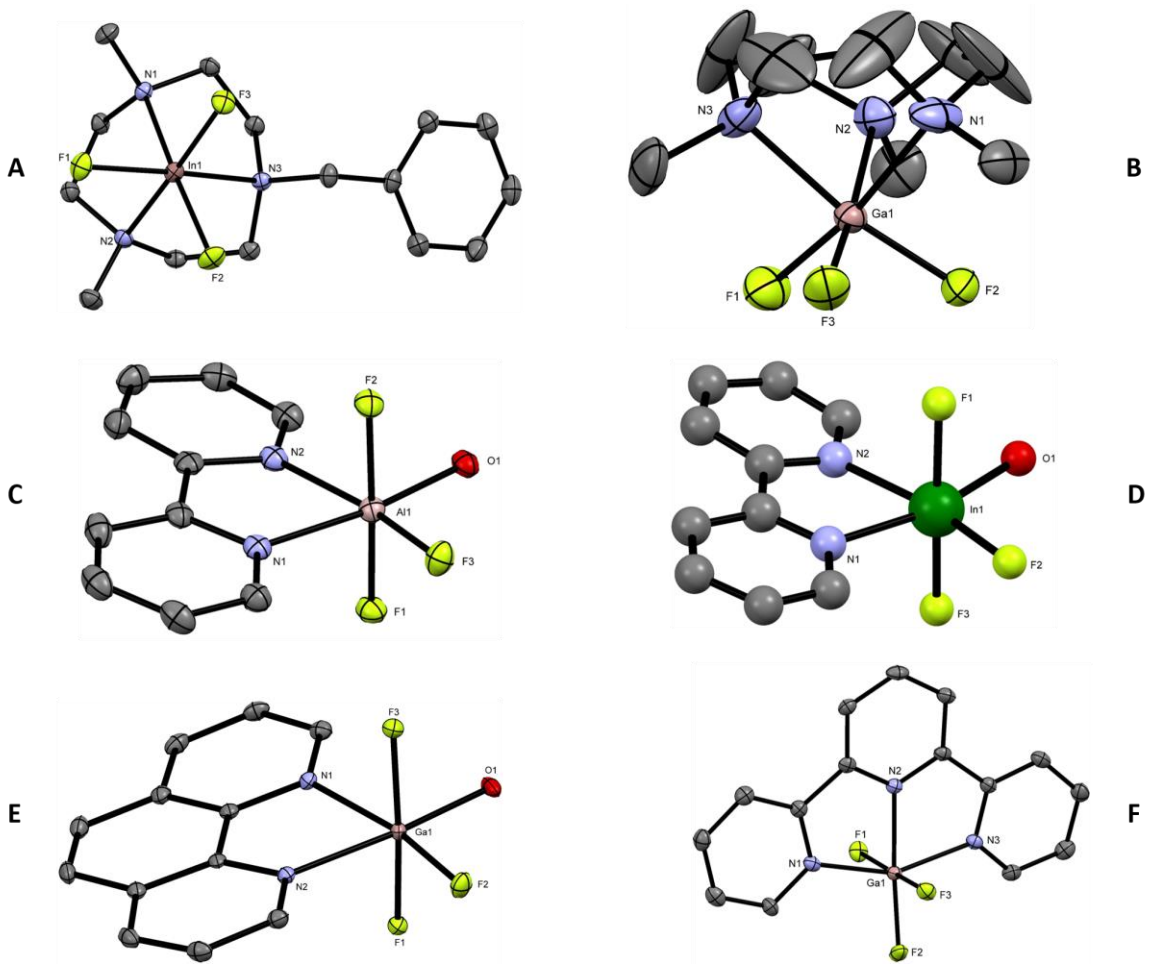

Figure 1.5. Crystal structures of (A) $[InF_3(BnMe_2\text{-tacn})] \cdot 2H_2O$, (B) $[GaF_3(Me_3\text{-tacn})] \cdot 4H_2O$, (C) $[AlF_3(OH_2)(bipy)] \cdot 2H_2O$, (D) $[InF_3(OH_2)(bipy)] \cdot 2H_2O$, (E) $[GaF_3(OH_2)(phen)]$ and (F) $[GaF_3(terpy)] \cdot 3H_2O$. Ellipsoids are drawn at 50 % probability level (excluding D) and H atoms and solvated H_2O are omitted for clarity. Image redrawn from CCDC numbers 926506 and 926504,[33] 1053153, 1053158 and 1053047[62] and 1299072.[63]

Other examples of Group 13 metal fluorides with neutral N-donor ligands have been formed from the reaction of AlN or InN with NH_4F in supercritical ammonia at 400 °C, from NH_4F or NH_4HF_2 and elemental Ga, and from $[NH_4]_3[MF_6]$ and gaseous NH_3, or $MF_3 \cdot 3H_2O$ and liquid NH_3.[66,67,68,69,70,71] The polymeric $[MF_3(4,4'\text{-bipy})]$ (M = Ga, In) were obtained by reaction of $MF_3 \cdot 3H_2O$ and 4,4'-bipy in aqueous HF at 180 °C.[72] Studies in aqueous solution of various ethylenediamine derivatives of Al and Ga have also been reported.[73,74]

The coordination chemistry of the $MF_3 \cdot 3H_2O$ (M = Al, Ga, In) with neutral O-donor ligands is less developed and it is discussed in Chapter 4.

1.5 General consideration regarding radiolabelling experiments and characterisation of radio-products

The radiolabelling experiments were carried out in London at the St. Thomas' Hospital in which King's College London have their radiochemistry laboratories. The hospital has an on-site cyclotron for the production of aqueous $[^{18}F]F^-$ (target water) through the nuclear reaction $^{18}O(p,n)^{18}F$. The $[^{18}F]F^-$ produced is used in the clinic (production of [^{18}F]FDG) and for research purposes. Although the quantity of radioactivity per mL of solution can be modified during the bombardment step in the production of $[^{18}F]F^-$, the radioactivity concentration (RAC) of the solution used for research applications is usually in the order of 200-300 MBq/mL (0.25 mL were used in a typical experiment in this work). This low activity available will have implications for the molar activity obtained in the radiolabelling experiments (see Chapter 3), and is considerably lower than the amount of radioactivity employed during the radiolabelling experiments carried out previously in the Reid group (these experiments were performed in GE Healthcare's laboratories in Amersham) with the possibility of achieving activity of up to 100 GBq in 3-4 mL. In term of actual quantities, the amount of $[^{18}F]F^-$ in the ^{18}F-target water is low, with approximatively 0.2 nmol of $[^{18}F]F^-$ in 13 GBq.[75]

The target water produced in the cyclotron is contained in a lead pot and delivered to the radiochemistry lab where it is kept in lead shielded workstations and shared between the researchers as appropriate. Everyone handling radioactivity must wear body and finger dosimeters which are replaced every month and record the amount of radioactivity a person has been exposed to during that period. If someone receives a particularly high monthly dose, she or he might be asked to stop radioactive work for a period of time. Working with care and with all the precautions and safety rules in place is important not only for your own safety and that of others in the laboratory, but also for your work.

The amount of radioactivity a person is exposed to and the manipulation time of radioactive materials should be as low as possible, whereas the distance from a radioactive source should be maximised when possible using tongs. The radiolabelling experiments are carried out in shielded workstations or in fume hood where the equipment (for example, stirrer hot plates) is inside lead bricks enclosures. Tongs, syringes, vials and lead pots are used to transport and transfer radioactive solutions in order to minimise the exposure to radioactivity. Any radioactive waste is collected in sharps bins for solid waste (contaminated syringes, needles, vials etc.) and designed containers for liquid waste. There are several radiation counters in the lab to constantly monitor the radioactivity.

1.5.1 Typical radiolabelling experiment procedure

A schematic of a typical radiolabelling experiment can be seen in Figure 1.6.

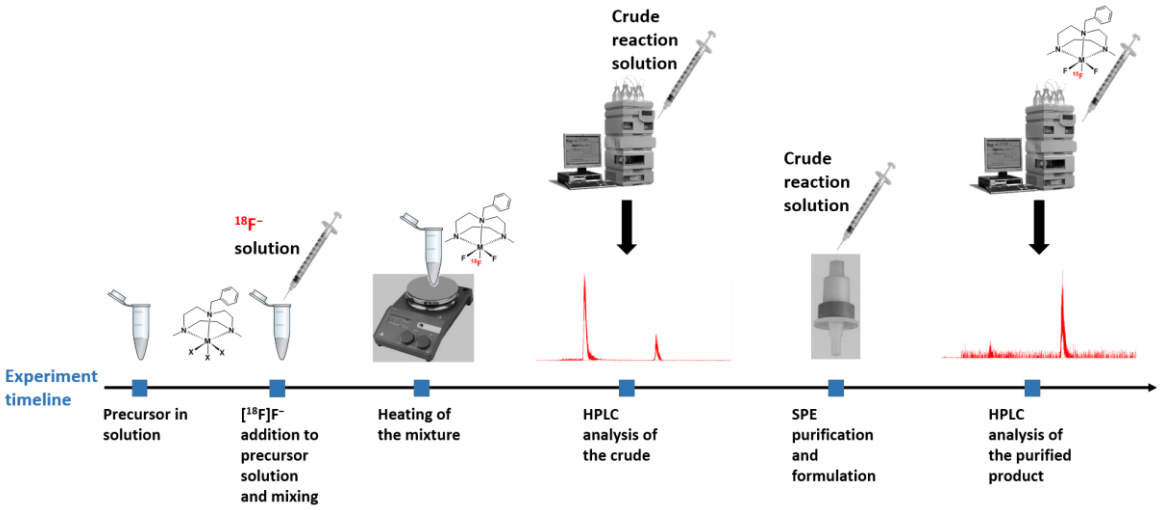

Figure 1.6. Schematic of a radiolabelling experiment.

The radiolabelling reactions were carried out in Eppendorf vials. The precursor (1, 0.1, 0.01 mg) was dissolved in the appropriate solvent (MeCN, EtOH or pH 4 sodium acetate buffer solution in this work) and a solution of target water were added using a syringe. All the manipulation were carried out in lead shielded workstation and the vials containing radioactive solutions were further shielded by lead pots. The reaction mixture was mixed by drawing up the solution into the syringe and expelling it back into the vial. The amount of radioactivity in solution was measured (MBq) and the vial was placed in a hot stirrer plate and heated to the appropriate temperature for a time between 10 and 90 minutes (for further experimental details see experimental sections in Chapters 2 and 3). Once the reaction was completed, an aliquot of the mixture was diluted with water (in order to have a water ratio which is comparable with the aqueous ratio present in the mobile phase in the HPLC system) and it was injected onto the analytical HPLC system to analyse the crude product. The HPLC has a UV-vis and radio-detector which allow for the identification of non-radioactive (if a chromophore is present in the molecule) and radioactive species, respectively. In a radio-HPLC chromatogram of the crude, there will almost always be a peak in the void volume which corresponds to unreacted [^{18}F]F$^-$. The product peak (if only one radioproduct is formed during the reaction) will typically have a higher retention time (Rt) that depends on the nature of the compound and its interaction with the column. The radiochemical yield (RCY) of the reaction is hence obtained by integration of the two peaks. The identification of the desired product is made by comparison with the UV-chromatogram of the non-active product (reference standard) and the UV- and radio-chromatogram of the crude reaction: the Rt of the product should be the same in all the chromatograms. If the desired product is formed, a purification step is carried out. This involved

either a preparative HPLC purification or a solid-phase extraction (SPE) purification. During this work a SPE purification was developed; a diluted solution of the crude was passed through a cartridge where the product was trapped. The product was washed by passing water through the cartridge in order to remove any unreacted $[^{18}F]F^-$ and then the product was eluted using an organic solvent (typically 1 mL of EtOH in this work, but other organic solvents can be used). This organic solution was formulated in water or pH 7.4 phosphate buffer solution (PBS). Alternatively, human serum albumin (HSA) can be used to mimic human blood conditions. The radiochemical purity (RCP) of the purified product formulated in this conditions was checked by injecting an aliquot onto the analytical HPLC system at different time intervals (from t = 0 to t = 2-4 hours since the ^{18}F half-life is 110 minutes) and ideally the RCP should be > 90 % over this period (the RCP is measured by integrating the free $[^{18}F]F^-$ and product peaks).

If the product is unstable and loses $[^{18}F]F^-$, there might be a variety of reasons, but radiolysis is one of the most common. Radiolysis is the degradation process of the radiolabelled compound induced by radicals produced by interaction of ionising radiation (β particles produced during the decay of ^{18}F in this case) and water. Radicals, such as $OH^\bullet$, $H^\bullet$ and $O_2^{\bullet-}$, can interact with the radiolabelled compound and induce $[^{18}F]F^-$ liberation from the radiolabelled complex. In some cases, this can be prevented adding a radiostabiliser (e.g. ascorbic acid) into the formulated solution of the product.[76] The radiostabiliser is a radical scavenging antioxidant which should not interfere with the radiolabelled compound and have no toxicity.[77] If radiolysis is the cause of the instability of the radiolabelled compound, the addition of the radiostabiliser should maintain the RCP constant over time.

The stability tests and the $Cl/^{19}F$ halide exchange reactions on the precursors were carried out in a preparative scale (15-50 mg of precursor). However, during a radiolabelling experiment very small quantities of precursor are employed and the amount of $[^{18}F]F^-$ in the target water is also extremely low. This is a really important aspect to consider, since the reactivity and/or stability of the precursor could be different when small quantities are employed. Trace impurities, such as the anions Cl^- or OH^-, but also the vast excess of water and $[^{19}F]F^-$ present in the mixture can compete with $[^{18}F]F^-$ or disrupt the coordination around the metal, resulting in low RCY or a decrease in the RCP over time. The low quantities employed also affect the methods for the characterisation of the compounds in solution and the purification of the product. Typically, the identification or purification of the species in the system is achieved through analytical and preparative HPLC systems. Alternatively, SPE protocols can be used for the purification of the product.

1.5.2 High performance liquid chromatography (HPLC)

HPLC is a technique which allows the identification, quantification and purification of species in a reaction mixture, and it is particularly useful when small quantities are employed. It is extensively used in radiochemistry. During this work the analytical HPLC system was mainly utilised.

The experiment consists of a sample dissolved in a suitable solvent, an automated arm for injection, a pump, solvent or mixture of solvents (mobile phase), a column (stationary phase) and a UV-vis and radiation detector. The pump pushes the mobile phase and the sample onto the column where the species are separated depending on the nature of the interaction of the species in the mixture with the column. The separated fractions elute off the column at different retention times (Rt) are detected by a UV-vis and/or radio-detector and the signals reprocessed and displayed in a monitor (Scheme 1.5).

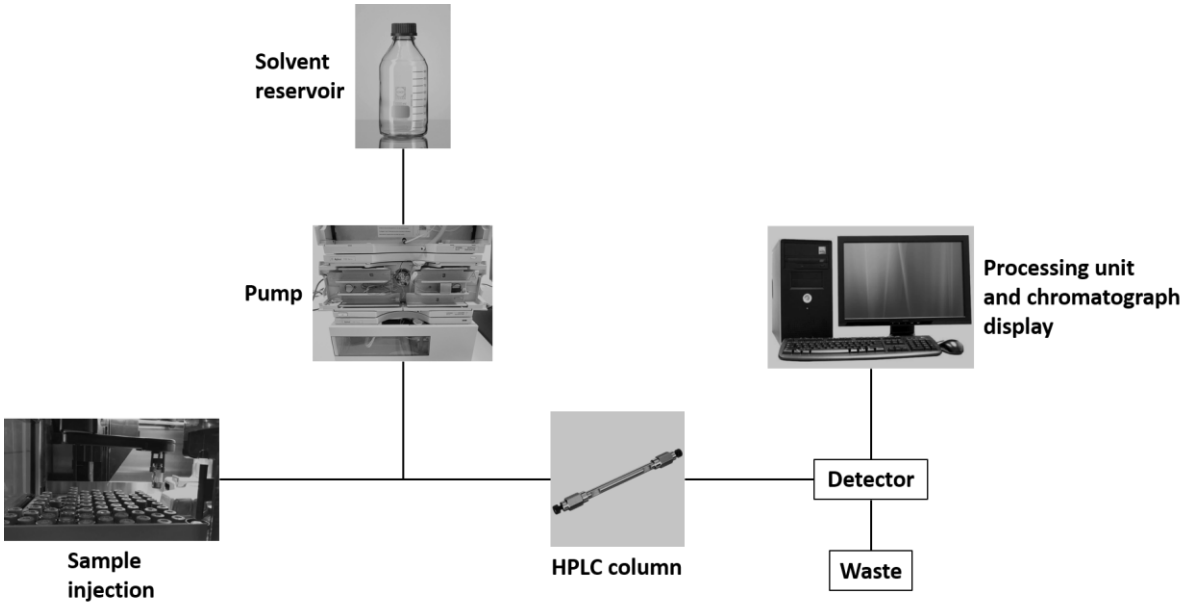

Scheme 1.5. Schematic of HPLC apparatus.

During this work a reverse phase HPLC was employed: a polar mobile phase and a silica column were utilised, meaning that hydrophilic species are eluted off the column at shorter Rt (little interaction with the column, i.e. unreacted $[^{18}F]F^-$), while species containing organic moieties will elute at longer Rt (i.e. products, more interaction with the column). A UV-vis detector and a radiation detector allow the identification (based on Rt) and quantification of the species in the mixture. HPLC is a very sensitive technique where only small quantities of sample are required and the species eluted from the column can be detected at very low concentration (nanomolar or picomolar).

1.6 Characterisation methods

A series of techniques have been utilised to characterise the compounds synthesised in this work. Solid state techniques, such as X-ray diffraction and IR spectroscopy, and solution state techniques, such as multinuclear NMR spectroscopy ^{1}H, $^{13}C\{^{1}H\}$, $^{19}F\{^{1}H\}$, $^{31}P\{^{1}H\}$, ^{27}Al, ^{71}Ga, ^{45}Sc, ^{59}Co, were utilised to fully characterise the compounds in solution and solid state. Microanalysis (C, H and N elemental analysis) has also been performed to confirm the molecular formulae and verify the purity of the bulk compounds.

1.6.1 NMR spectroscopy

Nuclear magnetic resonance (NMR) spectroscopy, is a technique that exploits the magnetic properties of the atomic nuclei. It can provide detailed information about the structure, reaction state, and chemical environment of the molecules in which the NMR active nuclei are contained.

The properties of the nuclei utilised during this work are summarised in Table 1.3.

NMR nucleus	Nuclear Spin (I)	Natural Abundance (%)	Quadrupole Moment (10^{-28} m^2) (Q)	Resonance frequency (MHz)	Reference standard
^{1}H	1/2	99.9	n/a	100.0	TMS and Residual solvent resonance
^{19}F	1/2	100	n/a	94.1	$CFCl_3$
^{31}P	1/2	100	n/a	40.5	H_3PO_4, 85% aq
^{27}Al	5/2	100	0.15	26.1	$[Al(H_2O)_6]^{3+}$
^{71}Ga	3/2	39.6	0.11	30.6	$[Ga(H_2O)_6]^{3+}$
^{45}Sc	7/2	100	−0.22	24.3	$[Sc(H_2O)_7]^{3+}$
^{59}Co	7/2	100	0.42	23.7	$[Co(CN)_6]^{3-}$

Table 1.3. Selected properties of the NMR nuclei utilised in this work.[78]

All the parameters reported affect an NMR spectrum. In a molecule there is an electric field gradient (efg) at the nucleus due to asymmetry in the local charge distribution caused by the electrons and other nuclei. The nucleus orients itself to the lowest energy. While this is possible for nuclei with I = 1/2, the ones having I > 1/2 are constantly moving to try to orientate themselves to the lowest possible energy level. This is due to the quadrupole moment associated with those nuclei. Indeed, ^{27}Al, ^{71}Ga, ^{45}Sc and ^{59}Co nuclei have quadrupole moments (I > 1/2) that cause line broadening in NMR spectra and only when these nuclei are in a highly symmetric environment (for example in the

C_{3v} symmetry which has an efg close to zero), coupling can be observed. On the contrary, if low symmetry species are present, they are not observed in the NMR spectrum so this is an aspect that must be considered (although the combination with other characterisation techniques should confirm/exclude this possibility). Resonances of nuclei close to a quadrupolar nucleus are also expected to be broadened and sometimes this can prevent the observation of coupling when coupling constant are small.

^{27}Al, ^{71}Ga, ^{45}Sc, ^{59}Co but also ^{19}F and ^{31}P have large chemical shift ranges and the donor set of the ligand, coordination geometry, temperature and the solvent in which the experiment is run can influence it. This, for example, allows for information regarding the coordination around the metal to be obtained.

NMR spectroscopy was employed to test the stability of the precursors used in the radiolabelling experiments (in case of paramagnetic systems UV-vis spectroscopy was utilised). In a typical experiment ~ 15-50 mg of compound was dissolved in ~ 4 mL of a mixture deuterated/non-deuterated solvent giving a concentration between 3 and 6 order of magnitude higher than the concentration used in the radiolabelling experiments. As a result, the stability of a compound can be different at the high concentration in which an NMR experiment is performed compared to the much lower concentration of a radiolabelling experiment in which the presence of trace species in solution (at a concentration comparable to the one of precursor) can disrupt the coordination around the metal.

1.6.2 Infra-red spectroscopy

Infrared spectroscopy was performed as Nujol mulls over the range 4000-200 cm^{-1}. IR spectroscopy is a technique used to identify the types of bonds or functional groups present in the species. Each bond has definite vibrational energies and definite vibrational transitions; when the sample is irradiated with a specific energy that matches with the vibrational transition, that energy is absorbed. Subtraction of these absorbed energies from a pre-recorded background, gives an IR spectrum characteristic of the compound. IR spectroscopy is particularly powerful when functional groups such as P=O or S=O are present, because they have characteristic absorptions and significantly shift upon coordination, hence they can be used as diagnostic features. Moreover, Group Theory can be used to determine the molecular symmetry of the compound from the number of stretches corresponding to a bond type observed: for example from the number of the M-F stretching frequencies in an octahedral complex of the type MF_3L_3, it is possible to determine if the geometry of the complex is *facial* (C_{3v} symmetry, two bands a_1 + e) or *meridional* (C_{2v} symmetry, three bands $2a_1 + b_1$). It is also worth bearing in mind that the Group Theory is based on

molecular species and does not take into account, for example, intermolecular interactions. These interactions can cause broadening of the peaks and fewer bands than predicted are observed. This technique is also useful to verify if water is present in the compound: the broad *v* O-H band at 3500-3300 cm^{-1} and δ H-O-H band at 1650 cm^{-1} provide evidence of water being present.

1.6.3 Single crystal X-ray diffraction

Single crystal X-ray diffraction is a powerful technique which allows the determination of the structure of a compound, hence locating the position of the atoms or ions that make up a crystalline solid. This technique requires a single crystal of suitable size to be grown; crystals may be obtained from different methods, such as slow evaporation of a solution of a compound at ambient temperature and pressure, or by vapour diffusion. The crystal of a compound can be regarded as constructed of regularly repeating structural elements, which may be atoms, molecules, or ions. The crystal lattice is the geometrical pattern formed by the points that represent the positions of these repeating structural elements. A unit cell of a crystal is an imaginary parallelepiped from which the entire crystal can be made up by simple translational displacements. The relationship between the unit cell parameters in three dimensions (three side *a*, *b* and *c* and three angles α, β and γ that define the unit cell) gives rise to the seven crystal systems (Table 1.4).

System	Unit cell parameters
Triclinic	$a \neq b \neq c$, $\alpha \neq \beta \neq \gamma \neq 90°$
Monoclinic	$a \neq b \neq c$, $\alpha = \gamma = 90°$, $\beta \neq 90°$
Orthorhombic	$a \neq b \neq c$, $\alpha = \beta = \gamma = 90°$
Rhombohedral	$a = b = c$, $\alpha = \beta = \gamma \neq 90°$
Tetragonal	$a = b \neq c$, $\alpha = \beta = \gamma = 90°$
Hexagonal	$a = b \neq c$, $\alpha = \beta = 90°$, $\gamma \neq 120°$
Cubic	$a = b = c$, $\alpha = \beta = \gamma = 90°$

Table 1.4. Crystal systems.

The asymmetric unit of a crystal is a portion of the unit cell that contains all the structural and symmetry information. The unit cell can be obtained by applying the symmetry operations on the asymmetric unit while the packing of a crystal can be obtained by applying translational operation on the unit cell. The asymmetric unit may consist of one molecule, more than one molecule, or a fraction of a molecule

During a single crystal X-ray experiment, an image is produced for each position in which the crystal is hit by an X-ray beam. Each image shows several spots of varied intensity which represents a set

of parallel planes in the crystal. Each set of planes give rise to a spot when the Bragg equation (Equation 1.1) is satisfied:

$$\lambda = 2d_{\mathrm{hkl}} \sin\theta$$

Equation 1.1. Bragg equation.

Where λ is the wavelength of the X-ray beam, d is the distance between successive planes, *hkl* are three integer numbers which define the orientation of the planes with respect to the three unit cell sides, and θ is the angle between the plane and the incoming and outgoing beam.

The diffraction conditions represented by the Bragg equation are severe, and will be satisfied by only few reflections of a randomly orientated crystal in an X-ray beam. In order to bring more lattice planes into a reflection position, the crystal must be rotated in the X-ray beam.

From the position of the spots in the pattern it is possible to find the unit cell parameters while from the intensities of the spots it is possible to extract information about the positions of the atoms in the unit cell of the crystal structure.

Crystals are mounted on a support and the structural information is acquired at 100 K, in order to minimise the thermal motion of the atoms in the crystal. The thermal motion of the atoms in the structure is quantified graphically using an Oak Ridge Thermal Ellipsoid Plot (ORTEP) image.

The technique gives information about the types and the positions of the atoms, bond lengths and angles between them, and intra- and inter-molecular interactions. It is always appropriate to bear in mind that the crystal structure obtained may not be representative of the bulk solid or of the species in solution.

1.6.4 Elemental Analysis

Elemental analysis is a technique where a sample is analysed for its elemental composition. During this work the CHN analysis were performed off site. The sample is burned in an excess of oxygen and the species CO_2, H_2O and N_2 formed are trapped and used to calculate the percentage amounts of C, H and N present in the sample. Elemental analysis is particularly useful to confirm the molecular formula of the bulk, check the purity of the compound and whether the complexes formed are solvent free, or if not, what degree of solvation is present (in this case other techniques should confirm the presence of solvent in the bulk).

1.6.5 UV-vis spectroscopy

During a UV-vis experiment the transitions of valance electron of a molecule are investigated. For the transition metal complexes the bands observed are due to d-d or ligand-to-metal or metal-to-

ligand charge transfer transitions. The former are usually in the visible region of the electromagnetic spectrum whereas the latter are more energetic and are typically in the ultraviolet region. This technique is hence particularly useful, for example, to investigate the oxidation state of the metal. During this work, the experiments were acquired *via* diffuse reflectance on the solid or transmission on the aqueous solutions of the complexes. Absorbance and molar absorption are related in the Lambert-Beer Law (Equation 1.2):

$$A = -\log\left(\frac{I}{I_0}\right) = \varepsilon l c$$

Equation 1.2. Lambert-Beer Law. A = absorbance, I = intensity, I_0 = intensity, ε = extinction coefficient (mol^{-1} dm^3 cm^{-1}), *c* = concentration (mol dm^{-3}), *l* = pathlengths (cm).

During this work, the UV-vis experiments were performed on complexes of Cr(III), Mn(III), Fe(III) and Co(III) metals, d^3, d^4, d^5, d^6 respectively. The complexes are all octahedral with *meridional* or *facial* geometry (C_{2v} and C_{3v}) but further distortions and therefore even lower symmetry compared to the regular octahedron O_h symmetry, are expected. This further complicates the systems and in addition to this, more bands can be observed as a result of Jahn-Teller distortions and spin-forbidden transitions.

The ground state term in an octahedral field for a d^3 metal is $^4A_{2g}$ and three spin-allowed transitions are predicted: $^4T_{2g} \leftarrow {}^4A_{2g}$, $^4T_{1g} \leftarrow {}^4A_{2g}$, $^4T_{1g} \leftarrow {}^4A_{2g}$ (Figure 1.7). The ground state term in a high spin octahedral field for a d^4 metal is ^5E_g and only one transition is predicted: $^5T_{2g} \leftarrow {}^5E_g$ (Figure 1.7). While for a d^5 high spin system there are no spin-allowed transitions (ground state $^6A_{1g}$), for a d^6 low spin metal two transitions are allowed: $^1T_{1g} \leftarrow {}^1A_{1g}$ and $^1T_{2g} \leftarrow {}^1A_{1g}$ (Figure 1.7).

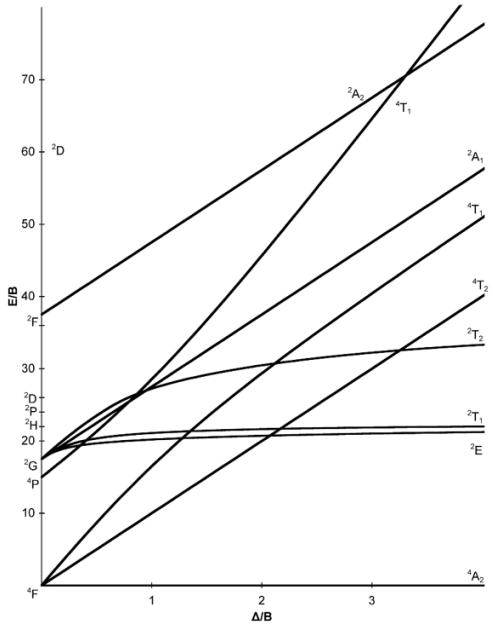

***d*³**

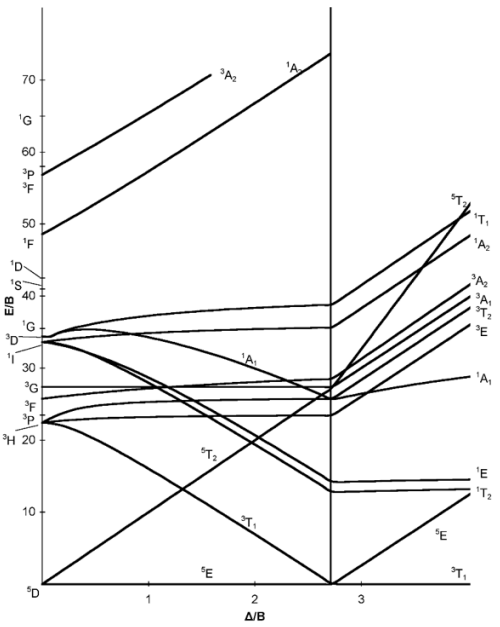

***d*⁴**

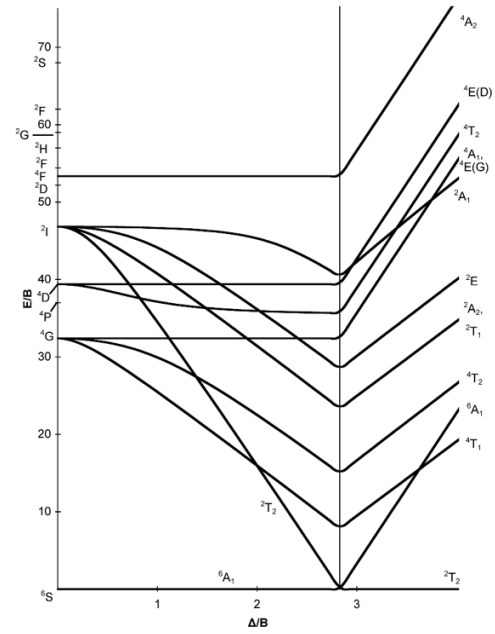

***d*⁵**

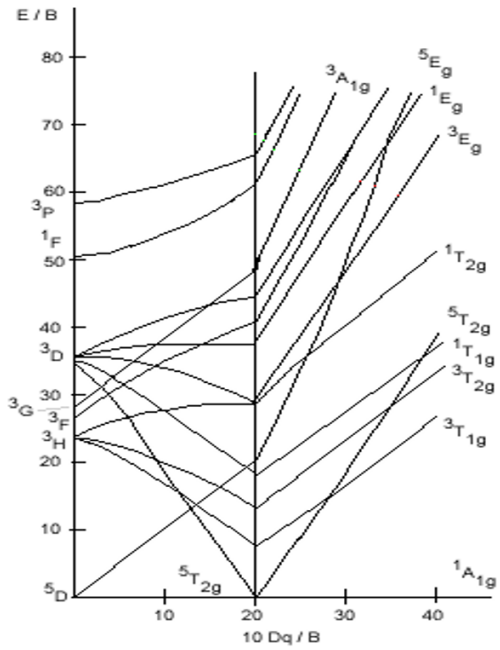

***d*⁶**

Figure 1.7 Tanabe-Sugano diagrams for a d^3 (top left), d^4 (top right), d^5 (bottom left) and d^6 (bottom right) metal.

1.7 Aims

The objectives of this Thesis can be summarised in four main points:

- To further investigate the radiochemistry of the Group 13 metal halide complexes of the type $[MX_3(BnMe_2\text{-tacn})]$ (M = Al, Ga; X = Cl, F) towards the identification of the best systems for bioconjugation reactions and eventually *in vivo* studies. Previous work using $[GaCl_3(BnMe_2\text{-tacn})]$ and $[GaCl(Bn(CH_2COO)_2\text{-tacn})]$ has shown that these systems can be successfully radiofluorinated under mild conditions (aqueous solution and room temperature for the former and pH 4 sodium acetate solution and 80 °C for the latter), however, they could only be radiolabelled at μM concentration of precursor. In order to have a real prospects for possible PET applications, there is the need to perform the radiolabelling reactions using less precursor (nM or lower). Moreover, there is also a need to better understand the factors affecting the ^{18}F-radiolabelling and the stability of these ^{18}F-radiolabelled systems, such as choice of the metal ion, its Lewis acidity and the specific ligand donor set. The ^{18}F-radiolabelling of $[AlCl_3(BnMe_2\text{-tacn})]$ through Cl/^{18}F halide exchange reactions (Chapter 2) and $[GaF_3(BnMe_2\text{-tacn})]$ through ^{18}F/^{19}F isotopic exchange reactions (Chapter 3) will provide an insight into these aspects.
- To develop the coordination chemistry of the Group 13 metal trifluorides towards neutral O-donor ligands and hence to establish whether promising systems with potential applications in PET imaging can be identified (Chapter 4).
- To identify other promising systems for future ^{18}F-radiolabelling studies. This part of the work focuses on the synthesis and assessment of the stability of new metal trifluoride complexes with Me_3-tacn, $BnMe_2$-tacn or terpy as ligands, similarly to the Group 13 metal fluoride chemistry that had been developed. The Group 3 metal fluorides of Sc and Y, as well as La and Lu (Chapter 5) and the first row of transition metal trifluorides of Cr, Mn, Fe and Co (Chapter 6) are explored.
- To investigate halide exchange reactions with the chloride complexes, $[MCl_3(Me_3\text{-tacn})]$ or $[MCl_3(terpy)]$, using $[Me_4N]F$, $[Bu_4N]F$ or Me_3SnF as the source of fluoride, on a preparative scale in order to assess the possibility of introducing the radioactive $[^{18}F]F^-$ in a radiolabelling experiment (Chapter 5 and Chapter 6).

1.8 References

1. Miller, P. W.; Long, N. J.; Vilar, R.; Gee, A. D., *Angew. Chem. Int. Ed.* **2008**, *47*, 8998.

2. Cherry, S. R.; Dahlbom, M., *Pet: Physics, Instrumentation, and Scanners,* Phelps, Michael E., **2006**.

3. Levin, C. S., *Eur. J. Nucl. Med. Mol. Imaging* **2005**, *32 Suppl 2*, S325.

4. McBride, W. J.; Sharkey, R. M.; Karacay, H.; D'Souza, C. A.; Rossi, E. A.; Laverman, P.; Chang, C. H.; Boerman, O. C.; Goldenberg, D. M., *J. Nucl. Med.* **2009**, *50*, 991.

5. Ametamey, S. M.; Honer, M.; Schubiger, P. A., *Chem. Rev.* **2008**, *108*, 1501.

6. Cai, L.; Lu, S.; Pike, V. W., *Eur. J. Org. Chem.* **2008**, *2008*, 2853.

7. Smith, G. E.; Sladen, H. L.; Biagini, S. C.; Blower, P. J., *Dalton Trans.* **2011**, *40*, 6196.

8. Varagnolo, L.; Stokkel, M. P. M.; Mazzi, U.; Pauwels, E. K. J., *Nucl. Med. Biol.* **2000**, *27*, 103.

9. Garnett, E. S.; Firnau, G.; Nahmias, C., *Nature* **1983**, *305*, 137.

10. Volkow, N. D.; Fowler, J. S.; Gatley, S. J.; Logan, J.; Wang, G.-J.; Ding, Y.-S.; Dewey, S., *J. Nucl. Med.* **1996**, *37*, 1242.

11. Becherer, A.; Szabo, M.; Karanikas, G.; Wunderbaldinger, P.; Angelberger, P.; Raderer, M.; Kurtaran, A.; Dudczak, R.; Kletter, K., *J. Nucl. Med.* **2004**, *45*, 1161.

12. Reivich, M.; Kuhl, D.; Wolf, A.; Greenberg, J.; Phelps, M.; Ido, T.; Casella, V.; Fowler, J.; Hoffman, E.; Alavi, A.; Som, P.; Sokoloff, L., *Circ. Res.* **1979**, *44*, 127.

13. Bishop, A.; Satyamurthy, N.; Bida, G.; Hendry, G.; Phelps, M.; Barrio, J. R., *Nucl. Med. Biol.* **1996**, *23*, 189.

14. Fowler, J. S.; Shiue, C. Y.; Wolf, A. P.; Salvador, A. P.; MacGregor, R. R., *J. Label. Compd. Radiopharm.* **1982**, *19*, 1634.

15. Chirakal, R.; Firnau, G.; Schrobilgen, G. J.; McKay, J.; Garnett, E. S., *The International Journal of Applied Radiation and Isotopes* **1984**, *35*, 401.

16. Satyamurthy, N.; Bida, G. T.; Phelps, M. E.; Barrio, J. R., *Int. J. Rad. Appl. Instrum. A* **1990**, *41*, 733.

17. Namavari, M.; Bishop, A.; Satyamurthy, N.; Bida, G.; Barrio, J. R., *Int. J. Rad. Appl. Instrum. A* **1992**, *43*, 989.

18. Zhan, C. G.; Dixon, D. A., *J. Phys. Chem.* **2004**, *108*, 2020.

19. Levy, S.; Elmaleh, D. R.; Livni, E., *J. Nucl. Med.* **1982**, *23*, 918.

20. Tewson, T. J., *J. Nucl. Med.* **1983**, *24*, 718.

21. Hamacher, K.; Coenen, H. H.; Stocklin, G., *J. Nucl. Med.* **1986**, *27*, 235.

22. Liu, Z.; Pourghiasian, M.; Radtke, M. A.; Lau, J.; Pan, J.; Dias, G. M.; Yapp, D.; Lin, K. S.; Benard, F.; Perrin, D. M., *Angew. Chem. Int. Ed.* **2014**, *53*, 11876.

23. Watson, D. A.; Su, M.; Teverovskiy, G.; Zhang, Y.; Garcia-Fortanet, J.; Kinzel, T.; Buchwald, S. L., *Science* **2009**, *325*, 1661.

24. Lee, E.; Kamlet, A. S.; Powers, D. C.; Neumann, C. N.; Boursalian, G. B.; Furuya, T.; Choi, D. C.; Hooker, J. M.; Ritter, T., *Science* **2011**, *334*, 639.

25. Teare, H.; Robins, E. G.; Kirjavainen, A.; Forsback, S.; Sandford, G.; Solin, O.; Luthra, S. K.; Gouverneur, V., *Angew. Chem. Int. Ed.* **2010**, *49*, 6821.

26. Chansaenpak, K.; Vabre, B.; Gabbai, F. P., *Chem. Soc. Rev.* **2016**, *45*, 954.

27. Bernard-Gauthier, V.; Bailey, J. J.; Liu, Z.; Wangler, B.; Wangler, C.; Jurkschat, K.; Perrin, D. M.; Schirrmacher, R., *Bioconjugate Chem.* **2016**, *27*, 267.

28. Speight, J. G., *Lange's Handbook of Chemistry, 17th Edition; Section 1,* **2017**.

29. McCleverty, J. A.; Meyer, T. J., *Comprehensive Coordination Chemistry II,* Pergamon, Oxford, **2004**, Vol. *3*.

30. McCleverty, J. A.; Meyer, T. J., *Comprehensive Coordination Chemistry II,* Pergamon, Oxford, **2004**, Vol. *6*.

31. Wilkinson, G.; Gillard, R. D.; McCleverty, J. A., *Comprehensive Coordination Chemistry I,* Pergamon, Oxford, **1987**, Vol. *3*, 1060.

32. Downs, A. J., *Chemistry of Aluminium, Gallium, Indium and Thallium,* Blackie Academic & Professional, **1993**.

33. Bhalla, R.; Darby, C.; Levason, W.; Luthra, S. K.; McRobbie, G.; Reid, G.; Sanderson, G.; Zhang, W., *Chem. Sci.* **2014**, *5*, 381.

34. Bhalla, R.; Levason, W.; Luthra, S. K.; McRobbie, G.; Sanderson, G.; Reid, G., *Chem. Eur. J.* **2015**, *21*, 4688.

35. Patil, S. A.; Patil, S. A.; Patil, R., *Chem. Biol. Drug. Des.* **2017**, *89*, 639.

36. Pedersen, K. S.; Sigrist, M.; Weihe, H.; Bond, A. D.; Thuesen, C. A.; Simonsen, K. P.; Birk, T.; Mutka, H.; Barra, A. L.; Bendix, J., *Inorg. Chem.* **2014**, *53*, 5013.

37. Raimondi, A. C.; Evans, D. J.; Hasegawa, T.; Drechsel, S. M.; Nunes, F. S., *Spectrochim. Acta A: Mol. Biomol. Spectrosc.* **2007**, *67*, 145.

38. Murthy, N. N.; Mahroof-Tahir, M.; Karlin, K. D., *Inorg. Chem.* **2001**, *40*, 628.

39. Redshaw, C., *Catalysts* **2017**, *7*, 165.

40. Whitty, A.; Viarengo, L. A.; Zhong, M., *Org. Biomol. Chem.* **2017**, *15*, 7729.

41. Titov, A. A.; Filippov, O. A.; Epstein, L. M.; Belkova, N. V.; Shubina, E. S., *Inorg. Chim. Acta* **2018**, *470*, 22.

42. Stasiuk, G. J.; Long, N. J., *Chem. Commun.* **2013**, *49*, 2732.

43. Aime, S.; Crich, S. G.; Gianolio, E.; Giovenzana, G. B.; Tei, L.; Terreno, E., *Coord. Chem. Rev.* **2006**, *250*, 1562.

44. Levason, W.; Reid, G., *Comprehensive Coordination Chemistry II, Meyer, T.J.; McCleverty, J.A.,* Pergamon, Oxford, **2003**, Vol. *1*.

45. Levason, W.; Reid, G., *Comprehensive Coordination Chemistry II, Meyer, T.J; McCleverty, J.A.,* Pergamon, Oxford, **2003**, Vol. *1*.

46. Wainwright, K. P., *Coord. Chem. Rev.* **1997**, *166*, 35.

47. Donald, J. R.; Unsworth, W. P., *Chem. Eur. J.* **2017**, *23*, 8780.

48. Borisova, N. E.; Reshetova, M. D.; Ustynyuk, Y. A., *Chem. Rev.* **2007**, *107*, 46.

49. Chaudhuri, P.; Wieghardt, K., *Prog. Inorg. Chem.* **1987**, *35*, 329.

50. Cheng, F.; Hector, A. L.; Levason, W.; Reid, G.; Webster, M.; Zhang, W., *Chem. Commun.* **2009**, 1334.

51. Knopp, P.; Wieghardt, K., *Z. Naturforsch.* **1991**, *46b*, 1077.

52. Wieghardt, K.; Chaudhuri, P.; Nuber, B.; Weiss, J., *Inorg. Chem.* **1982**, *21*, 3086.

53. Hajela, S.; Schaefer, P. W.; Bercaw, E. J., *J. Organomet. Chem.* **1997**, *532*, 45.

54. Everett, M.; Jolleys, A.; Levason, W.; Light, M. E.; Pugh, D.; Reid, G., *Dalton Trans.* **2015**, *44*, 20898.

55. Cabbiness, D. K.; Margerum, D. W., *J. Am. Chem. Soc.* **1969**, *91*, 6540.

56. Dei, A.; Gori, R., *Inorg. Chim. Acta* **1975**, *14*, 157.

57. Benjamin, S. L.; Levason, W.; Reid, G., *Chem. Soc. Rev.* **2013**, *42*, 1460.

58. Kemnitz, E.; Groß, U.; Rüdiger, S.; Scholz, G.; Heidemann, D.; Troyanov, S. I.; Morosov, I. V.; Lemée-Cailleau, M. H., *Solid State Sci.* **2006**, *8*, 1443.

59. Bukovec, P.; Kaucic, V., *Inorg. Nucl. Chem. Lett.* **1978**, *14*, 79.

60. Petricek, S.; Demsar, A.; Bukovec, P.; Golic, L.; Brencic, J. V., *Acta Chimica Slovenica* **1997**, *44*, 317.

61. Weyhermüller, T.; Wieghardt, K., *Chem. Commun.* **1998**, 557.

62. Bhalla, R.; Levason, W.; Luthra, S. K.; McRobbie, G.; Monzittu, F. M.; Palmer, J.; Reid, G.; Sanderson, G.; Zhang, W., *Dalton Trans.* **2015**, *44*, 9569.

63. Malyarik, M. A.; Petrosyants, S. P.; Ilyukhin, A. B.; Buslaev, Y. A., *Russ. J. Inorg. Chem.* **1991**, *36*, 2816.

64. Ilyukhin, A. B.; Malyarik, M. A., *Koord. Khim.* **1999**, *4*, 1511.

65. Ilyukhin, A. B.; Malyarik, M. A., *Kristallographiya* **1994**, *39*, 439.

66. Ketchum, D. R.; Schimek, G. L.; Pennington, W. T.; Kolis, J. W., *Inorg. Chim. Acta* **1999**, *294*, 200.

67. Roos, M.; Meyer, G., *Z. Anorg. Allg. Chem.* **1999**, *625*, 1129.

68. Roos, M.; Meyer, G., *Z. Anorg. Allg. Chem.* **1999**, *625*, 1843.

69. Roos, M.; Wittrock, J.; Meyer, G.; Fritz, S.; Strähle, J., *Z. Anorg. Allg. Chem.* **2000**, *626*, 1179.

70. Kozerenko, S. P.; Polyshchuk, S. A.; Sigula, N. I., *Russ. J. Inorg. Chem.* **1972**, *17*, 954.

71. Polyshchuk, S. A.; Kozerenko, S. P.; Gagarisnky, Y. V., *J. Less-Common Met.* **1972**, *17*, 954.

72. Petrosyants, S. P.; Ilyukhin, A. B., *Russ. J. Inorg. Chem.* **2010**, *55*, 30.

73. Petrosyants, S. P.; Buslaeva, E. R., *Russ. J. Inorg. Chem.* **1989**, *34*, 932.

74. Polyshchuk, S. A.; Krysenko, G. F., *Koord. Khim.* **1977**, *3*, 816.

75. Cleeren, F.; Lecina, J.; Billaud, E. M.; Ahamed, M.; Verbruggen, A.; Bormans, G. M., *Bioconjugate Chem.* **2016**, *27*, 790.

76. Chen, J.; Linder, K. E.; Cagnolini, A.; Metcalfe, E.; Raju, N.; Tweedle, M. F.; Swenson, R. E., *Appl. Radiat. Isot.* **2008**, *66*, 497.

77. Liu, S.; Ellars, C. E.; Edwards, D. S., *Bioconjugate Chem.* **2003**, *14*, 1052.

78. Mason, J., *Multinuclear NMR,* ed. Plenum, New York, **1987**.

Chapter 2: **Cl/^{18}F halide exchange reactions on [AlCl$_3$(BnMe$_2$tacn)]**

2.1 Introduction

The ^{18}F-radiolabelling of small molecules conjugated to biomolecules (e.g. peptides) is typically achieved by binding [^{18}F]F$^-$ covalently to a carbon atom. Typically, small organic molecules, called prosthetic groups, are ^{18}F-radiolabelled in a 2- or 3-step process and subsequently conjugated to the biomolecule and purified. However, C-F bond formation usually requires multistep syntheses, which are time-consuming and inefficient, and often need to be performed under conditions that result in degradation of the peptide itself (see Chapter 1 for a discussion of the challenges associated with C-^{18}F bond formation). Overcoming these problems was the reason several research groups started looking into alternatives to C-^{18}F bond formation. Main group elements such as those from Group 13 as well as silicon, have been investigated on the basis of their high bond dissociation energies with fluoride in an effort to obtain a radiofluorinated species in high yield and with minimal purification required post radiolabelling that would be stable *in vivo*. Some of the aspects reported in the introduction of this chapter are illustrated in a recent review on the development of ^{18}F-Group 13 fluoride derivatives as radiotracers for PET. The review discusses how the compounds can be converted into their ^{18}F-analogues and how they can be incorporated into bioconjugates.[1]

2.1.1 Overview of the "Al-^{18}F" radiolabelling methodology developed by McBride

Inorganic PET radiotracers, where ^{18}F is attached directly to a main group element, gained momentum after McBride and his co-workers investigated the possibility of attaching ^{18}F to the Group 13 metal aluminium. The idea was to exploit the high bond dissociation energy between Al(III) and the fluoride anion (664 KJ mol^{-1})[2] to allow incorporation of ^{18}F into the metal complex rapidly and without the need for lengthy purification and drying steps prior and following radiolabelling. A general scheme illustrating this method is reported in Scheme 2.1.

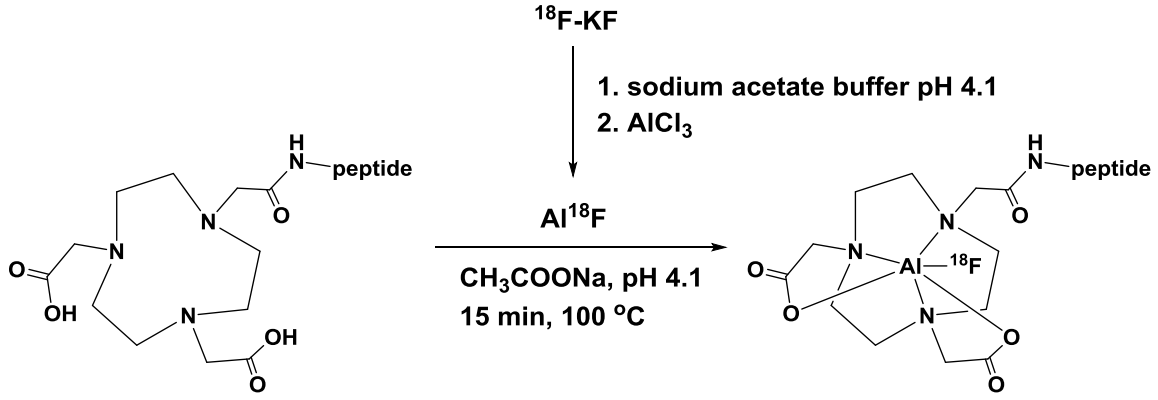

Scheme 2.1. McBride Radiolabelling method for the incorporation of ^{18}F into an Al-chelate conjugated to a peptide.[3]

This is a 2-step, 1-pot reaction where "$Al^{18}F$" is first obtained by mixing [^{18}F]KF and $AlCl_3$ in sodium acetate buffer pH 4.1 and then adding this mixture to a pH 4.1 solution of a NOTA derivative (NOTA = 1,4,7-triazacyclononane-1,4,7-triacetic acid) attached to a peptide.[4] This mixture is heated to 100-110 °C for 15-30 minutes, starting with an amount of precursor as low as 10- 30 nM concentration, giving an optimised radiochemical yield (RCY) between 50- 95 %, depending on the system. In most cases (when RCY is lower than 95 %), HPLC and SPE purification steps were performed after the radiolabelling reaction to remove unreacted "$Al^{18}F$" or unreacted ligand. Moreover, the aqueous [^{18}F]F^- solution received from the cyclotron was washed with water prior to mixing with $AlCl_3$ in order to remove any metal, which could interfere with the radiolabelling reaction. Given the pH conditions employed, although it has not been confirmed, it seems likely that the species [^{18}F]$AlF(AcO)_2$, or an aquo adduct of this, is formed *via* the first step. The formation of an aluminium species with three ^{18}F is excluded as the concentration of ^{18}F in solution is very low and even if ^{18}F was present in the ratio 3:1, [^{18}F]AlF_3 would almost certainly precipitate out of solution and be unable to react with the ligand. The NOTA derivative has been attached to several peptides in order to target different tumour types in the body. Examples of peptides attached to the chelate are: octreotide,[3] antagonist of gastrin-releasing peptide receptors (GRPR) for targeting prostate cancer[5] and bombesin (Figure 2.1).[6]

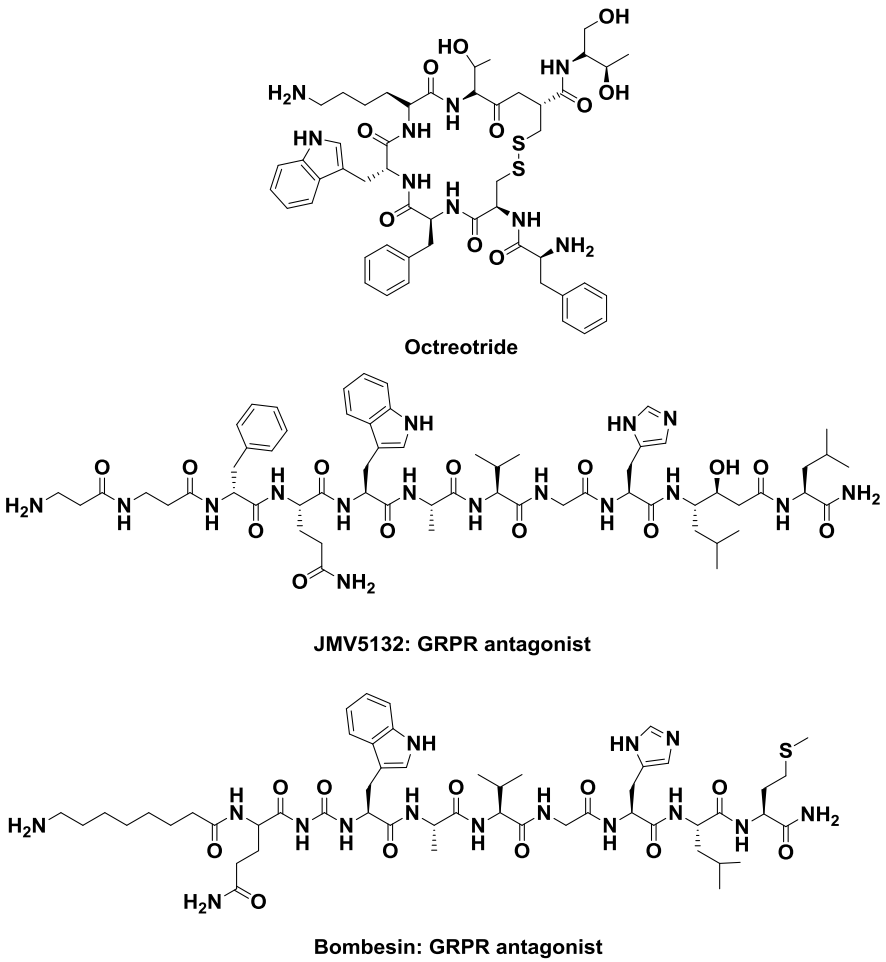

Figure 2.1. Structure of octreotride and the GRPR antagonists JMV5132 and bombesin.

Modifications of the linker between the macrocyclic ring and the peptide were also explored.[7, 8] A crystal structure with a methyl-phenylacetic acid linker is shown in Figure 2.2.[8]

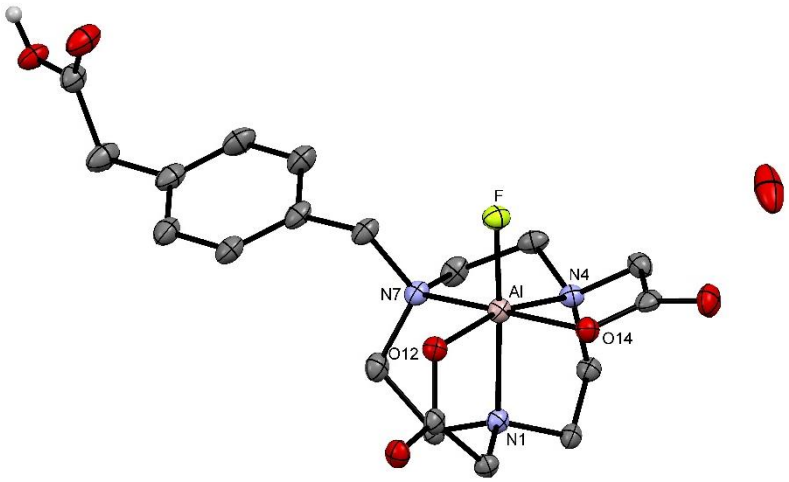

Figure 2.2. Crystal structure of [AlF(NODA-MPAA)]·H_2O (MPAA = methyl-phenylacetic acid).[8] Selected bond lengths (Å) and angles (°): Al-F 1.7143(16), Al-O12 1.8542(19), Al-O14 1.8748(19), Al-N4 2.036(2), Al-N1 2.074(2), Al-N7 2.080 (2), F Al O12 97.71(8), F Al O14 93.28(8), O12 Al O14 95.64(8), F Al N4 96.85(9), O12 Al N4 165.44(9), O14 Al N4 83.35(8), F Al N1 176.25(8).

The structure shows a distorted octahedron where the N_3O_2 donor set of the ligand and one fluoride complete the coordination sphere around the aluminium centre. The fluoride atom is in an axial position with a N-donor atom from the ring lying *trans* to it. The other two N atoms and the two O atoms of the pendant carboxylate groups occupy the equatorial positions of the octahedron.

McBride's method was an important breakthrough, providing the first example of metal-based chelate that could be radiofluorinated in water. The key aspects of this chemistry are summarised in two reviews.[9,10] The major drawbacks of the system are the high temperature (> 100 °C) and the low pH required for the radiofluorination reaction. These conditions are unlikely to be compatible with sensitive peptide-based biomolecules.

2.1.2 ^{18}F-radiolabelling reactions on Al-systems developed by other workers

After the publication of the "Al-F" method by McBride, other research groups began looking into the system with the aim of either targeting other biomolecules for imaging other tumour types or developing a method in which the ^{18}F-radiolabelling could be performed at lower temperature.

Examples of biomolecules conjugated to the Al-NOTA chelate are: HER3 (a human epidermal growth factor receptor whose overexpression has been found in a wide variety of cancers including breast, ovary, lung, head and neck cancers),[11] serum albumin (the most abundant plasma protein which is used to transport the radioactivity in the blood and study, for example, cardiac function after myocardial infraction), [12] and the amino acid A20FMDV2 that selectively targets $\alpha_v\beta_6$ ($\alpha_v\beta_6$ is a cell surface receptor detected in a range of cancers, such as breast, cervix, colon and gastric cancer).[13] In all of these examples, the incorporation of [^{18}F]AlF^{2+} into the ligand was performed at 100 °C and pH 4. Fewer studies in which the radiolabelling conditions are milder can be found in the literature and those usually require the use of flexible open chain polydentate ligands instead of macrocycles. Malik *et al.* reported the radiofluorination of [^{18}F]AlF^{2+} with HBED (HBED = N,N'-Bis(2-hydroxybenzyl)ethylenediamine-N,N'-diacetic acid) conjugated to PSMA (prostate specific membrane antigen): parameters such as T, amount of precursor and pH were investigated and it was found that a higher RCY was obtained at 35 °C, sodium acetate buffer pH 5 and 0.026 μmol of precursor.[14] The same principle was utilised in another study where polydentate ligands allow coordination of [^{18}F]AlF^{2+} at moderate temperature (40 °C) and slightly less acidic (pH 5) conditions. This method was employed for the radiolabelling of thermally sensitive biomolecules (Scheme 2.2).[15] The use of open chain ligands allows for lower temperature reactions at the expense of the added stability provided by the macrocyclic effect; the authors claim good stability of the radiolabelled compound in PBS, but *in vitro* incubation in rat plasma showed slow decomposition. Nonetheless, biodistribution studies showed the absence of bone uptake, indicating that *in vivo* defluorination or demetallation is limited. In both these latter examples, in contrast to the

macrocyclic ligands, increasing the temperature of the reaction leads to a decrease in RCY. Moreover, the donor set of the ligand is N_2O_3 (instead of the N_3O_2 set in the NOTA derivatives) but the coordination environment around the metal is not discussed in depth in the studies and there is no comment on the additional oxygen atom in the coordination sphere around the aluminium that makes the overall charge of the system −1.

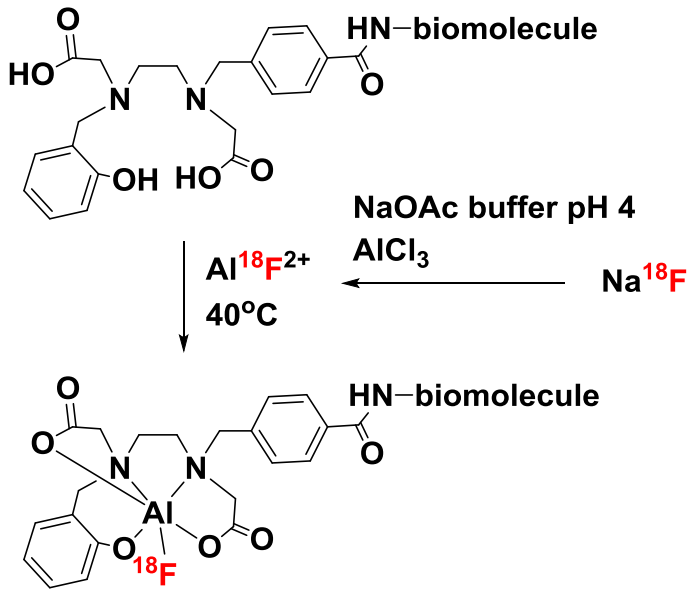

Scheme 2.2 ^{18}F-radiolabelling scheme as reported in reference 15.

An automated "Al-F" radiolabelling procedure has also been reported aiming at the clinical translation of this methodology.[16] The radioconjugates employed in the study were obtained with RCY between 48 and 56 % and a RCP after purification > 98%. The total reaction times were within 26-35 minutes.

2.1.3 ^{18}F-radiolabelling of boron systems

Within the Group 13 elements, boron has the highest bond dissociation energy with fluorine (>730 kJ mol^{-1})[17] and, after carbon, has been the most studied element for PET applications. Several different types of molecules have been successfully radiolabelled with ^{18}F, including, aryl-trifluoroborates,[18,19,20] zwitterionic onium-trifluoroborates,[21,22,23] and BODIPY-based dyes (BODIPY = boron-dipyrromethene).[24,25] Typically, radiofluorination is achieved by either converting a boronic ester moiety into a fluoroborate species or by an isotopic exchange reaction. Very recently, [^{18}F]BF_4^- as a PET probe for imaging the sodium-iodide symporter has been radiolabelled through an isotopic exchange reaction.[26] A discussion of ^{18}F-radiolabelled systems by isotopic exchange reactions is reported in Chapter 3, here the other methods will be briefly discussed.

The first ^{18}F-radiolabelled aryl-trifluoroborate compound was developed by Perrin and co-workers.[27] They observed that, in organic chemistry,[28] the high stability of the B-F bond had been exploited for the formation of aryl-trifluoroborates from aryl boronic acids or esters. These reactions were performed in partially aqueous media showing fast kinetics, and hence, making them attractive for PET applications. Indeed, biotinylated boronic ester was converted into the radiolabelled trifluoroborate using an aqueous $[^{18}F]F^-$ solution and KHF_2 as a carrier added fluoride anion source (Scheme 2.3).[27]

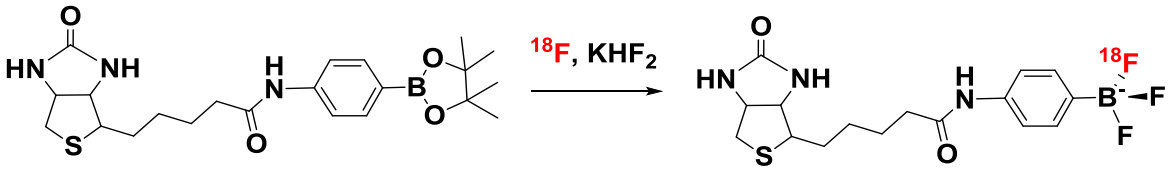

Scheme 2.3 Radiolabelling of biotinylated boronic ester.

Nonetheless, the stability of these species in water is limited, forming the corresponding boronic acid by hydrolysis. Modifications to the aryl groups were explored hoping to improve this aspect. Electron-withdrawing groups, such as F^- or Br^- were introduced, conferring stabilisation to the trifluoroborate moiety in aqueous solution.[18,29]

The zwitterionic onium-trifluoroborates chemistry were developed by the Gabbaï group. Examples of these compounds are reported in Figure 2.3[22,30,31]

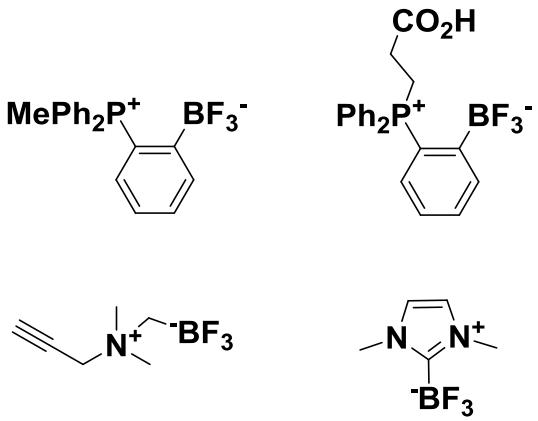

Figure 2.3. Zwitterionic organotrifluoroborates.

The presence of a cationic group greatly enhances the fluoride ion affinity of the borates. This was attributed to coulombic forces, with the cationic group acting as an electrostatic anchor for the oppositely charged anion. ^{18}F-radiolabelling of these species was achieved either starting with the boronic ester with KHF_2 in the presence of $[^{18}F]F^-$ or by isotopic exchange reactions.

The use of BODIPY dyes, a chromophore used in biology as a fluorescent tag, conjugated to a ^{18}F-boron fluoride moiety allows the combination of PET with fluorescence imaging techniques in order

to improve the low spatial resolution of the latter. Since the B-F bond of this compound is very stable, ^{18}F-radiolabelling is usually achieved by first removing an F^- ion from the compound in the presence of an anion abstractor and then reacting it with $[^{18}F]F^-$, as reported in the representative example in Scheme 2.4.[32] Alternatively, isotopic exchange reactions can be employed, but the reaction conditions are harsher as they usually require the presence of a Brønsted or a Lewis acid and non-aqueous solvents (Chapter 3).

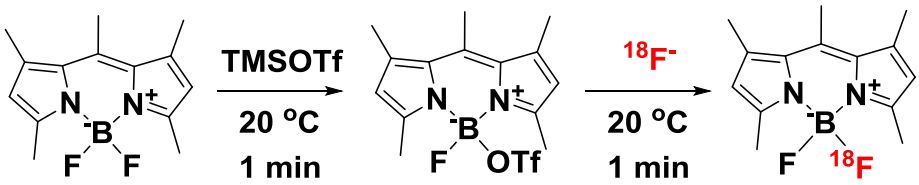

Scheme 2.4. Radiosynthesis of a difluoro BODIPY dye using trimethylsilyltriflate (TMSOTf) as fluoride abstractor.

2.1.4 "Ga-^{18}F" systems reported by the Southampton group

The complexation of the Al-F systems is achieved using anionic NOTA-based ligands having oxygen atoms in the donor set (typically acetate pendant arms). The Reid group investigated a similar approach, but with gallium in place of aluminium, [GaF(Bn($CH_2COO)_2$-tacn)] (Bn($CH_2COO)_2$-tacn = 1-benzyl-4,7-diacetate-1,4,7-triazacyclononane), (Scheme 2.5 B).

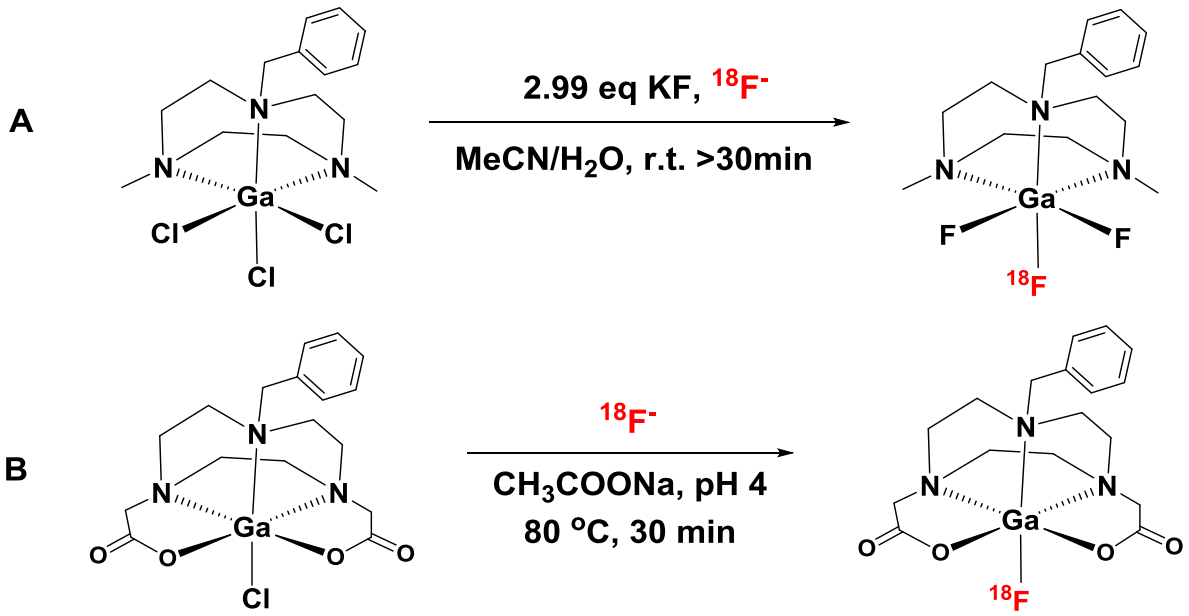

Scheme 2.5. ^{18}F radiolabelling conditions for (A) [$GaCl_3$($BnMe_2$-tacn)] and (B) [GaCl(Bn($CH_2COO)_2$-tacn)].

Successful radiofluorination, starting with the preformed chloride analogue in Scheme 2.5 B, was achieved through Cl/^{18}F halide exchange at pH 4 in a sodium acetate buffer solution using ^{18}F-target

water as received from the cyclotron and keeping the mixture at 80 °C for at least 30 minutes.[33] The RCY of the reaction was *ca.* 70 %. The radiochemical product showed good stability at pH 6 (10 % EtOH/NaOAc) for at least 3 hours, however, when formulated at pH 7.5 (10 % EtOH/PBS), the RCP decreased to 40 % after 20 minutes with release of fluoride. The compound was also unstable when formulated in human serum albumin. This instability at higher pH was attributed, at least in part, to the lower stability of the carboxylate bonds to the less Lewis acidic Ga(III) *cf.* Al(III).

With the aim of improving this aspect, the neutral ligand $BnMe_2$-tacn was investigated.[34] It is a neutral triazacyclononane derivative in which two nitrogen atoms are functionalised with methyl groups and the third one bears a benzyl group (allowing for identification of the species *via* UV-vis). The coordination chemistry of the Ga(III) metal chloride and fluoride complexes of this ligand was developed and the reference complexes fully characterised, yielding complexes of the type $[MX_3(BnMe_2\text{-tacn})]$ (M = Al, Ga, In; X = Cl, F).[34] Fluorination through halide exchange reactions from the chloride complexes of the three metals using "cold" $^{19}F^-$ (as KF in MeCN aqueous solution and $[Me_4N]F$ in organic solvents), identified the gallium systems as the most promising candidate for ^{18}F-radiofluorination, hence the reactions with radioactive $[^{18}F]F^-$ on $[GaCl_3(BnMe_2\text{-tacn})]$ were explored. ^{18}F-radiofluorination on the preformed $[GaCl_3(BnMe_2\text{-tacn})]$ was achieved in mild conditions (room temperature, MeCN aqueous solution) in the presence of ^{18}F-target water doped with 2.99 equivalents of KF (Scheme 2.5 A). The approximatively 2.99 equivalents were added to ensure complete substitution of Cl for F, and allowing incorporation of just one $^{18}F^-$ into the complex (considering also the low concentration of $^{18}F^-$ in target water solution). The RCY was *ca*. 30 % and the HPLC purified radio-product showed high stability when formulated in 10 % EtOH/PBS solution (pH 7.2) with an RCP of 98 % after 120 minutes (Figure 2.4).

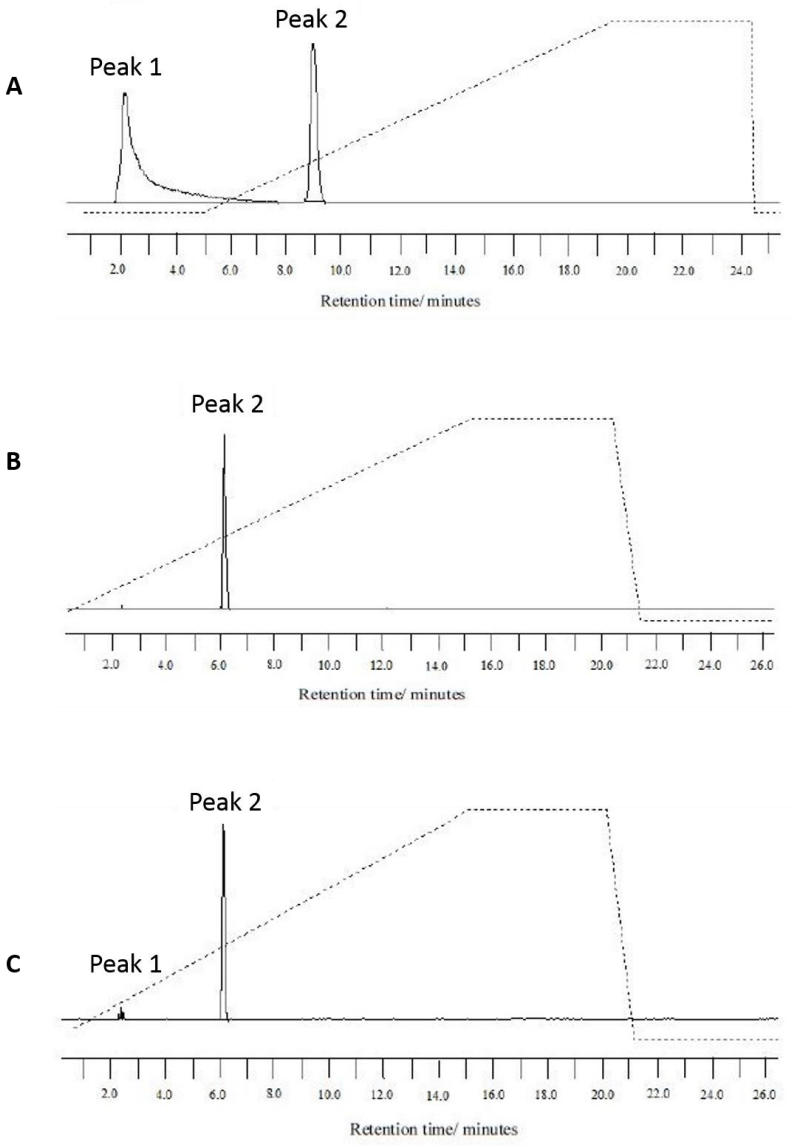

Figure 2.4. A: preparative radio-HPLC chromatogram of the crude product reaction mixture. Peak 1: Rt = 2.16 min 70 % ($^{18}F^-$). Peak 2: Rt = 9.02 min 30 % ([$Ga^{18}F^{19}F_2$(BnMe$_2$tacn)]); B: analytical radio-HPLC chromatogram of the purified product formulated in 10 % EtOH/PBS at t = 0. Peak 2: Rt = 6.23 min >99% ([$Ga^{18}F^{19}F_2$(BnMe$_2$tacn)]); C: Analytical radio-HPLC chromatogram of the purified product in 10 % EtOH/PBS. Peak 1: Rt = 2.15 min 1% ($^{18}F^-$). Peak 2: Rt = 6.13 min 98% ([$Ga^{18}F^{19}F_2$(BnMe$_2$tacn)]).

In both reactions shown in Scheme 2.5, the higher bond energy of Ga-F over Ga-Cl is the major thermodynamic driving force for the fluorination reaction.

Since these reactions were performed on Ga(III) systems, it was thought that the investigation of radiofluorination reactions on the Al(III) analogue would give an insight into the differences between the Group 13 metals. This chapter discusses the radiofluorination conditions of [$AlCl_3$(BnMe$_2$-tacn)] through Cl/^{18}F halide exchange reactions and compares it with the Ga(III) analogue[34] and also with McBride's 'Al-F' systems.[4,3]

2.2 Results and discussion

As mentioned in Chapter 1 section 1.5, the radiolabelling experiments were performed at the St. Thomas' Hospital in London. Given that the complex [$GaCl_3$($BnMe_2$-tacn)] was originally radiolabelled by a previous member of the Reid group in the GE radiochemistry laboratories in Amersham,[34] the same radiolabelling reaction (Scheme 2.5 A) was repeated in the radiochemistry labs at the St. Thomas' Hospital in order to familiarise with the equipment in a radiochemistry laboratory and to establish whether the result were reproducible when using [^{18}F]F^- produced in a different cyclotron (see Chapter 1, section 1.5 for the difference in activity of the ^{18}F-target water between the two cyclotrons). [$GaCl_3$($BnMe_2$-tacn)] (1 mg, 2.68 µM) was dissolved in 0.6 mL of a 5:1 MeCN:H_2O mixture and radiolabelled using ^{18}F-target water (0.4 mL) doped with 2.99 mol. equiv. of KF at room temperature. The desired radiolabelled product, [Ga^{18}F$^{19}F_2$($BnMe_2$-tacn)], was obtained in 27 % RCY (Figure 2.5) replicating the result obtained previously (30 % RCY).[34] The mobile phase conditions of the analytical HPLC systems were the same as the original experiment and the identification of the radioproduct was made by comparison of the retention times (Rt).

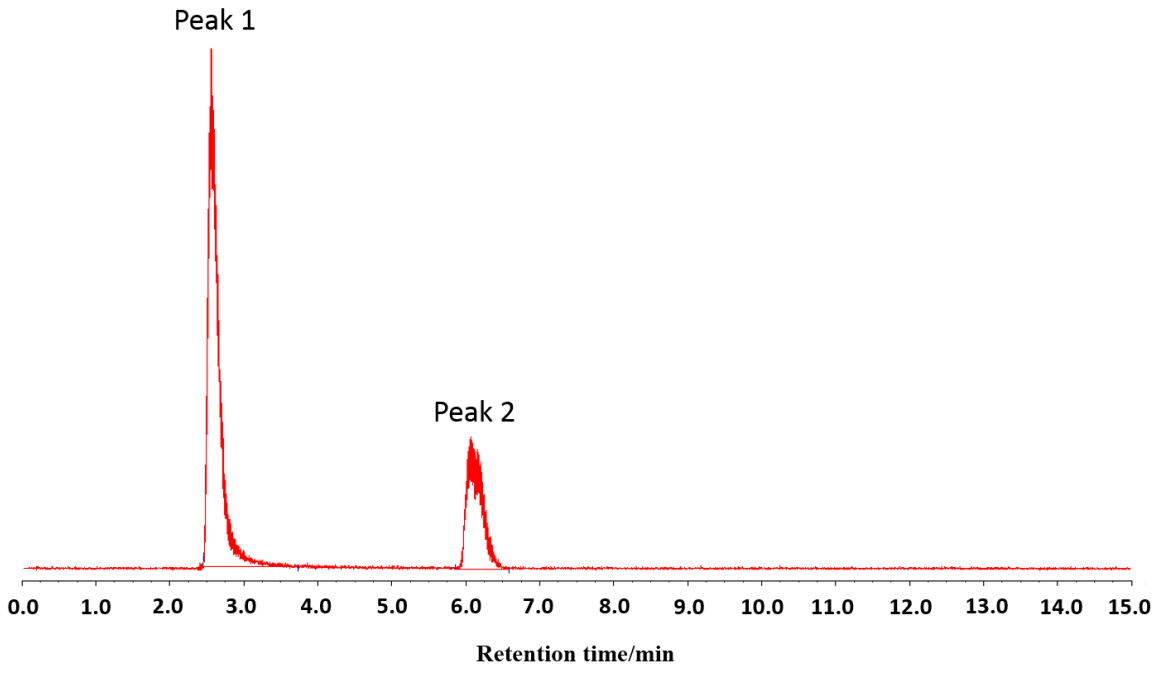

Figure 2.5. Analytical radio-HPLC chromatogram of the crude product from reaction of [$GaCl_3$($BnMe_2$-tacn)] (1 mg, 2.68 µmol) in MeCN (0.6 mL) with 2.99 eq of KF doped with 0.4 mL of aqueous [^{18}F]F^- at room temperature for 120 mins. Peak 1: Rt = 2.56 min 73 % ($^{18}F^-$). Peak 2: Rt = 6.07 min 27 % ([Ga^{18}F$^{19}F_2$($BnMe_2$tacn)]).

The product was purified through a hydrophilic-lipophilic-balanced (HLB) solid-phase extraction (SPE) cartridge whereas the previous experiment was purified through a preparative HPLC system. The product was formulated in a 20 % EtOH/PBS solution (10 % EtOH/PBS for the other experiment)

in order to have a sufficient radioactivity concentration (RAC) in solution for the analysis (as a result of the low activity of the ^{18}F-target water available at the St. Thomas' Hospital). The SPE purification did not work as well as the HPLC one (81 % *vs.* >99 % RCP), but the RCP remained constant over at least 2 hours, with a RCP of 79 % at t = 120 minutes.

Having established that the radiolabelling of [$GaCl_3$(BnMe$_2$-tacn)] could be replicated, we then moved on exploring the radiolabelling of new systems. [$AlCl_3$(BnMe$_2$-tacn)] was investigated as a potential scaffold for next-generation PET imaging agents through radiofluorination by Cl/^{18}F halide exchange reactions. [$AlCl_3$(BnMe$_2$-tacn)] was made as reported in the literature[34] and described in the experimental section. The radiofluorination reactions were performed on a 1 mg scale (2.63 µM concentration).

Preparative scale experiments on the complexes [$AlCl_3$(RMe$_2$-tacn)] (R = Bn, Me) showed that ^{19}F-fluorination could be achieved upon addition of aqueous KF to an MeCN suspension of the [$AlCl_3$(BnMe$_2$-tacn)] at room temperature. It is notable that, unlike the gallium analogues, the aluminium complexes did not undergo Cl/^{19}F exchange with [Bu_4N]F or [Me_4N]F in anhydrous MeCN at room temperature or on heating (which displaces the macrocycle forming the species $[AlF_4]^-$, easily identified in the ^{19}F{^{1}H} NMR spectrum).[34] The different reactivity between the two metals suggested that the radiofluorination conditions of [$AlCl_3$(BnMe$_2$-tacn)] would be different from those of [$GaCl_3$(BnMe$_2$-tacn)]. Indeed, treatment of a 2.63 µM (MeCN) solution of [$AlCl_3$(BnMe$_2$-tacn)] (1.0 mg) with 2.99 mol. equiv. of [^{19}F]KF doped with $[^{18}F]F^-$ (50 MBq) in unbuffered water with heating to 80 °C for 30 min resulted in very low ^{18}F incorporation (<10%, determined by radio-HPLC) (Figure 2.6).

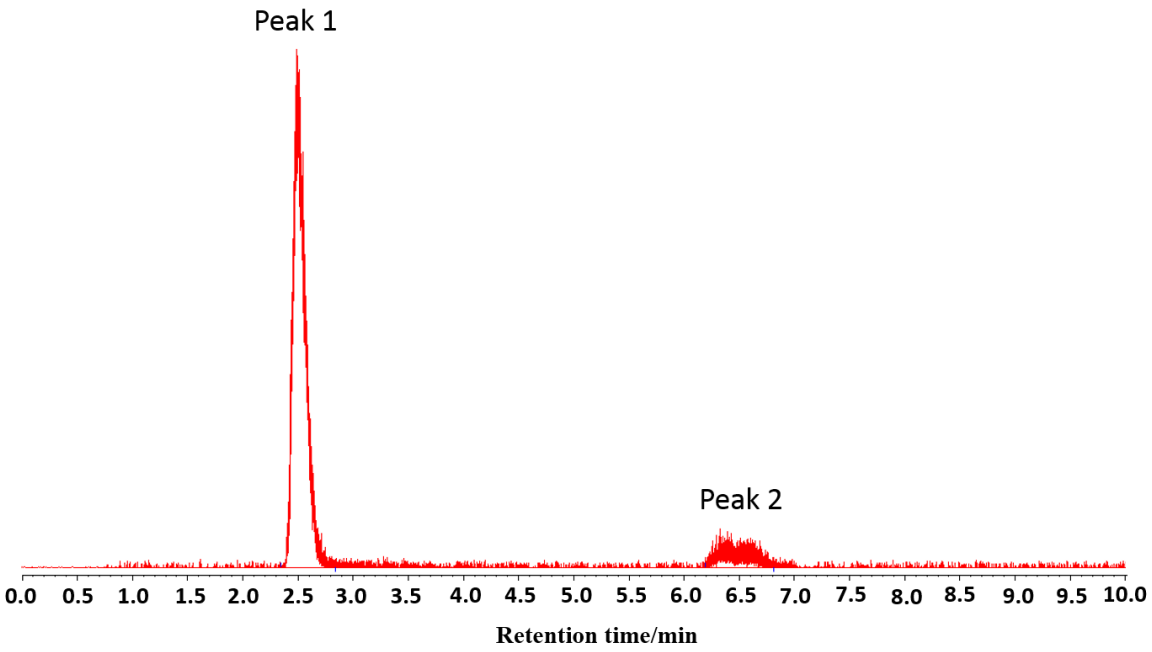

Figure 2.6. Analytical radio-HPLC chromatogram of the crude product from reaction of [$AlCl_3$($BnMe_2$-tacn)] (1 mg, 2.63 µmol) in MeCN (0.6 mL) with 2.99 eq of KF doped with 0.4 mL of aqueous [^{18}F]F^- at 80 °C for 30 mins. Peak 1: Rt = 2.54 min 91% ($^{18}F^-$). Peak 2: Rt = 6.68 min 9% ([$Al^{18}F^{19}F_2$($BnMe_2$tacn)]).

However, the radiochemical yield was significantly increased when the labelling experiments were performed in an aqueous sodium acetate buffered solution at pH 4 with heating (80-100 °C, 60-90 min), leading up to 24 % incorporation (Scheme 2.6).

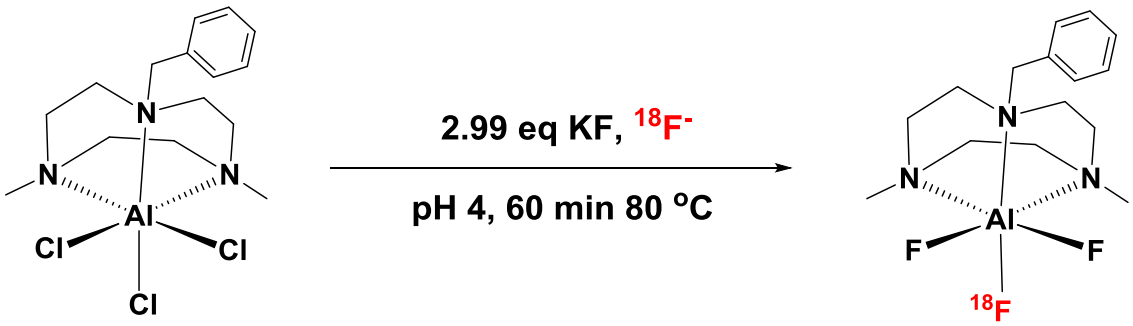

Scheme 2.6. ^{18}F radiolabelling protocol employed for [$AlCl_3$($BnMe_2$-tacn)] (Method 2).

The analytical HPLC chromatogram of the crude reaction is shown in Figure 2.7.

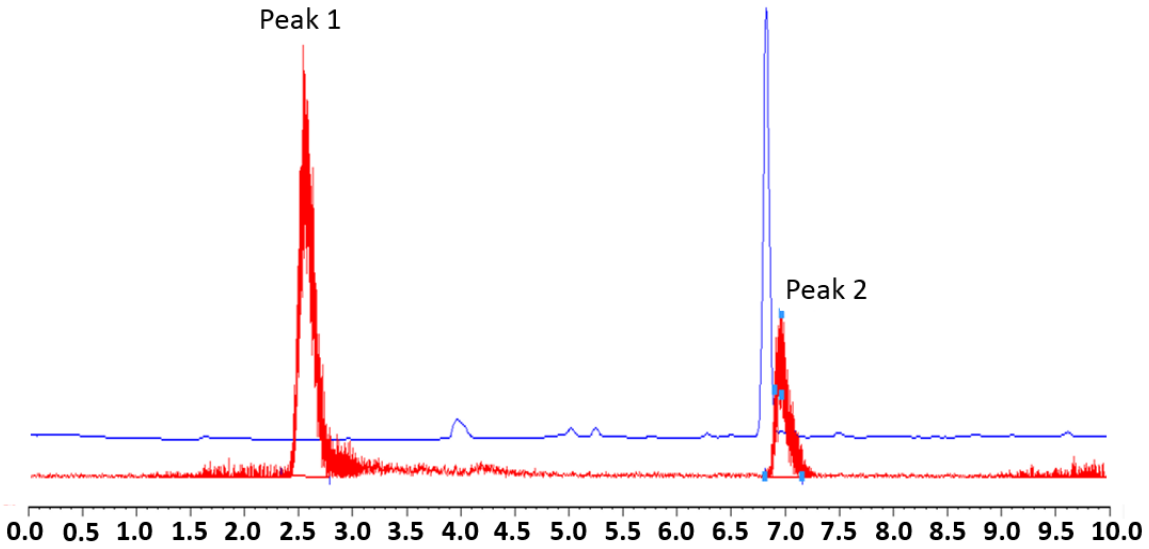

Figure 2.7. Analytical HPLC chromatogram of the crude product from reaction of [$AlCl_3$($BnMe_2$-tacn)] (1 mg, 2.63 µmol) at pH 4 (sodium acetate buffered solution) with 2.99 eq of KF doped with 0.1 mL of aqueous [^{18}F]F^- at 80 °C for 90 mins. Radio (red) and UV (blue). Peak 1: Rt = 2.51 min 76% ($^{18}F^-$). Peak 2: Rt = 6.95 min 24% ([$Al^{18}F^{19}F_2$($BnMe_2$tacn)]). Peak 2 matches the UV-vis peak of [AlF_3($BnMe_2$-tacn)].

The identity of the radio-product as the distorted octahedral *fac*-[AlF_3($BnMe_2$-tacn)] was confirmed by comparison of its UV-trace against that of the inactive reference compound [$Al^{19}F_3$($BnMe_2$-tacn)] (same Rt in both experiments). In order to incorporate one ^{18}F atom per molecule in the final product, the radiolabelling experiments were performed in the presence of 2.99 mol. equiv. of [^{19}F]KF (per one mole of [$AlCl_3$($BnMe_2$-tacn)]) doped with [^{18}F]F^- (20-280 MBq). The ^{18}F-target water was used as received from the cyclotron without the need of any drying or purification steps. Figure 2.7 shows the analytical HPLC chromatogram of the crude product, along with the UV trace, confirming that [$Al^{18}F^{19}F_2$($BnMe_2$-tacn)] was the only radio-product present, in addition to unreacted [^{18}F]F^-. A simple purification protocol was also established, allowing purification of the product from unreacted [^{18}F]F^- anions. Thus, [$Al^{18}F^{19}F_2$($BnMe_2$-tacn)] was successfully purified to leave the metal chelate as the single product, Rt = 6.92 min., in the radio-chromatogram (Figure 2.8 A). SPE cartridges allow for the simple and rapid purification of the crude reaction mixture. In the method we have developed, the crude is passed through the cartridge and the radio-product is trapped allowing for the solution containing unreacted [^{18}F]F^- to pass through. Several washes with water ensure that the remaining trace [^{18}F]F^- anions are completely removed from the cartridge. Finally, the purified radio-product is eluted off the cartridge with an organic solvent (EtOH in this case) and formulated in water or PBS, for example (Chapter 1, section 1.5). [$Al^{18}F^{19}F_2$($BnMe_2$-tacn)] was formulated in a 50% EtOH/phosphate buffered saline (PBS) solution at pH 7.4, showing very high stability for at least 180 mins., with the RCP being >99% over this period (Figure 2.8). The

radioproduct was formulated in a 50 % EtOH/PBS solution to ensure a suitable radioactive concentration (RAC) for analytical HPLC analysis over the period of 2-3 hours.

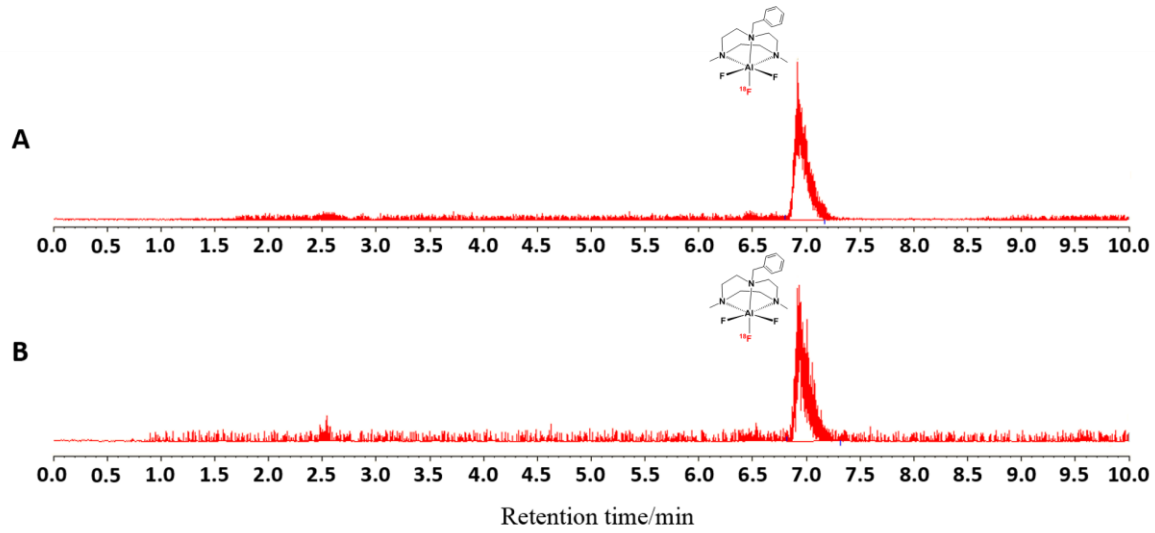

Figure 2.8. Analytical radio-HPLC chromatogram of: A: SPE purified product at t = 20 min. Peak: Rt = 6.92 min >99% ([$Al^{18}F^{19}F_2$(BnMe2tacn)]); B: SPE purified product at t = 180 min. Peak: Rt = 6.92 min >99% ([$Al^{18}F^{19}F_2$(BnMe2tacn)]).

Several attempts to reduce the amount of precursor (to 0.1 mg, 0.26 µmol of [$AlCl_3$($BnMe_2$-tacn)]) failed to produce the desired radio-product, [$Al^{18}F^{19}F_2$($BnMe_2$-tacn)], with [$^{18}F]F^-$ as the only species present in the radio-HPLC chromatogram.

2.2.1 Stability tests on [AlF_3($BnMe_2$-tacn)] by NMR spectroscopy

The stability of the inactive [$Al^{19}F_3$($BnMe_2$-tacn)] complex was tested in the presence of a 10-fold excess of biologically relevant competitive anions (Cl^-, CO_3^{2-}, PO_4^{3-}, F^-, AcO^-) by $^{19}F\{^1H\}$ and ^{27}Al NMR spectroscopy. Figure 2.9 shows the $^{19}F\{^1H\}$ and ^{27}Al NMR of the complex in D_2O solution.

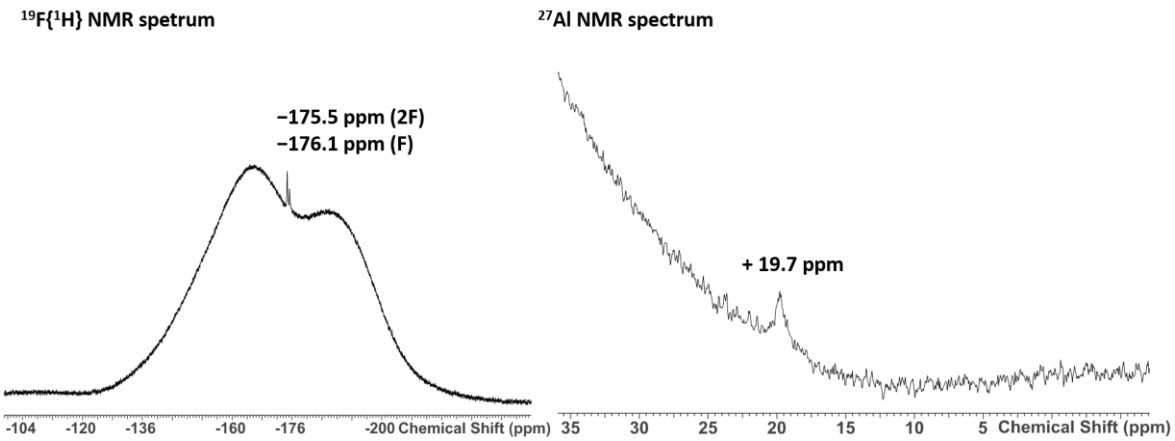

Figure 2.9. $^{19}F\{^{1}H\}$ (left) and ^{27}Al (right) NMR spectra of [AlF_3($BnMe_2$-tacn)]. The rolling baseline in the $^{19}F\{^{1}H\}$ is due to the Teflon in the probe whereas the rising baseline in the ^{27}Al spectrum is due to the presence of aluminium in the probe.

The $^{19}F\{^{1}H\}$ NMR spectrum of the complex shows two resonances in a 2:1 ratio at −175.5 and −176.1 ppm respectively. Although the complex shows a distorted octahedral coordination environment at Al, with the three fluorides in a *facial* geometry, the presence of the benzyl group in one of the nitrogen atoms reduces the symmetry, leading to two fluoride resonances, with similar chemical shifts. The ^{27}Al NMR spectrum shows a broad singlet at +19.7 ppm with no resolved $^{1}J_{AlF}$ coupling (although the moderate quadrupole moment associated with the ^{27}Al nuclei and the efg close to zero in C_{3v} symmetry allow for relatively sharp lines, coupling are rarely observed) in the range expected for six-coordinated aluminium.[35]

The presence of a 10-fold excess of NaCl, NaOAc, or KF did not affect the NMR spectra even after several days. The pH of the solutions was close to 7. However, [$Al^{19}F_3$($BnMe_2$-tacn)] is completely decomposed by addition of a 10-fold excess of Na_2CO_3 or Na_3PO_4. The pH of these solutions was more basic (pH 10) than the solutions containing the other salts and the instability of the complex might be a consequence of the high pH rather than the presence of the anions themselves. Figure 2.10 shows the $^{19}F\{^{1}H\}$ and ^{27}Al NMR spectra of the sample containing a 10-fold excess of Na_2CO_3 in solution. The complex decomposes to $[Al(OH)_4]^-$ (^{27}Al = +80 ppm)[35] and F^- and HF_2^- (−122.5 and −158.6 ppm) (major products).

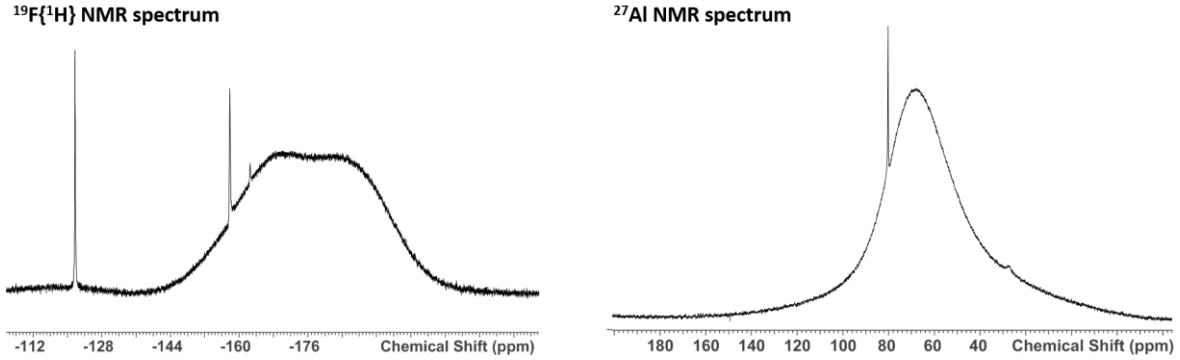

Figure 2.10. $^{19}F\{^{1}H\}$ (left) and ^{27}Al (right) NMR spectra of [AlF_3(BnMe$_2$-tacn)] in the presence of a 10-fold excess of Na_2CO_3 showing the decomposition products. The rolling baseline in the $^{19}F\{^{1}H\}$ NMR spectrum is due to the Teflon in the probe whereas the broad feature in the ^{27}Al NMR spectrum is due to the presence of aluminium in the probe.

Other considerations regarding the stability of the complex can be made. Since the [AlF_3(BnMe$_2$-tacn)] was originally prepared under hydrothermal conditions (15 h at 180 °C in water),[34] and the radiolabelling experiments are performed at pH 4 in sodium acetate buffer solution, the complex is extremely stable in water and in acidic conditions (although it should be noted that the stability of the inactive and active forms may be different due to radiolysis pathways).

2.2.2 Attempted $^{18}F/^{19}F$ isotopic exchange reactions

The Cl/F halide exchange reaction on [$AlCl_3$(BnMe$_2$-tacn)] discussed in this Chapter is successful using 1 mg (2.63 µmol) of precursor, whereas all the attempts to scale down the reaction were unsuccessful. We propose that the reason for the failure of the experiment starting with 0.1 mg of chelate may be attributed to the moisture sensitivity of the chloride complex, with hydrolysis competing with the Cl/^{18}F exchange. Ideally a compound should be radiolabelled using less material in order to be really promising for PET applications, hence isotopic exchange reactions on the preformed [AlF_3(BnMe$_2$-tacn)] were investigated. In the stability tests, [AlF_3(BnMe$_2$-tacn)] showed very good stability in water, suggesting that the isotopic exchange reaction might be very attractive. However, in practice no $^{18}F/^{19}F$ exchange occurred in any of the conditions that were explored. Using 1 mg of [$AlCl_3$(BnMe$_2$-tacn)] at pH 4, or in unbuffered solution, heating to 80 °C and changing the amount of organic solvent in solution (from 10 % to 75 % MeCN) had no effect (Scheme 2.7), with no evidence for the formation of the target radio-product in the radio-HPLC chromatogram. The high Lewis acidity of Al(III) and the high bond dissociation energy of the Al-F bond may be the reasons for the failure of this reaction. The use of a Lewis acid promoter (for example $SnCl_4$) to activate the Al-F bond towards isotopic exchange is an option that will be explored in the future.

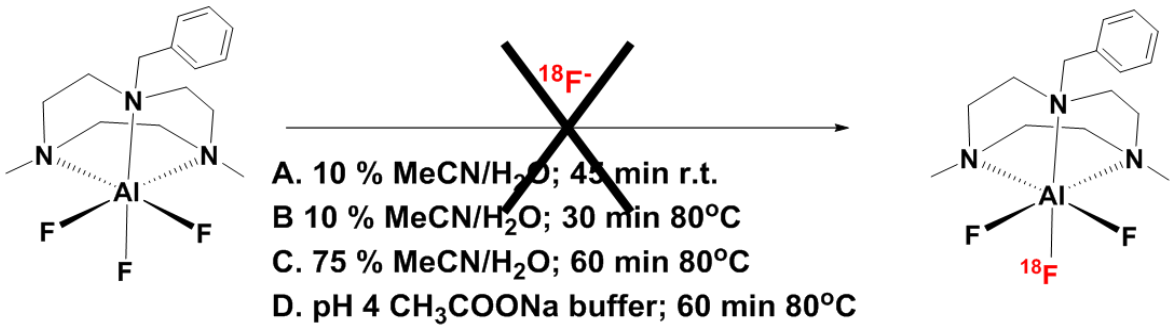

Scheme 2.7. Attempted $^{18}F/^{19}F$ isotopic exchange reactions on [AlF_3($BnMe_2$-tacn)].

The only radiospecies present was unreacted [^{18}F]F^- (Figure 2.11).

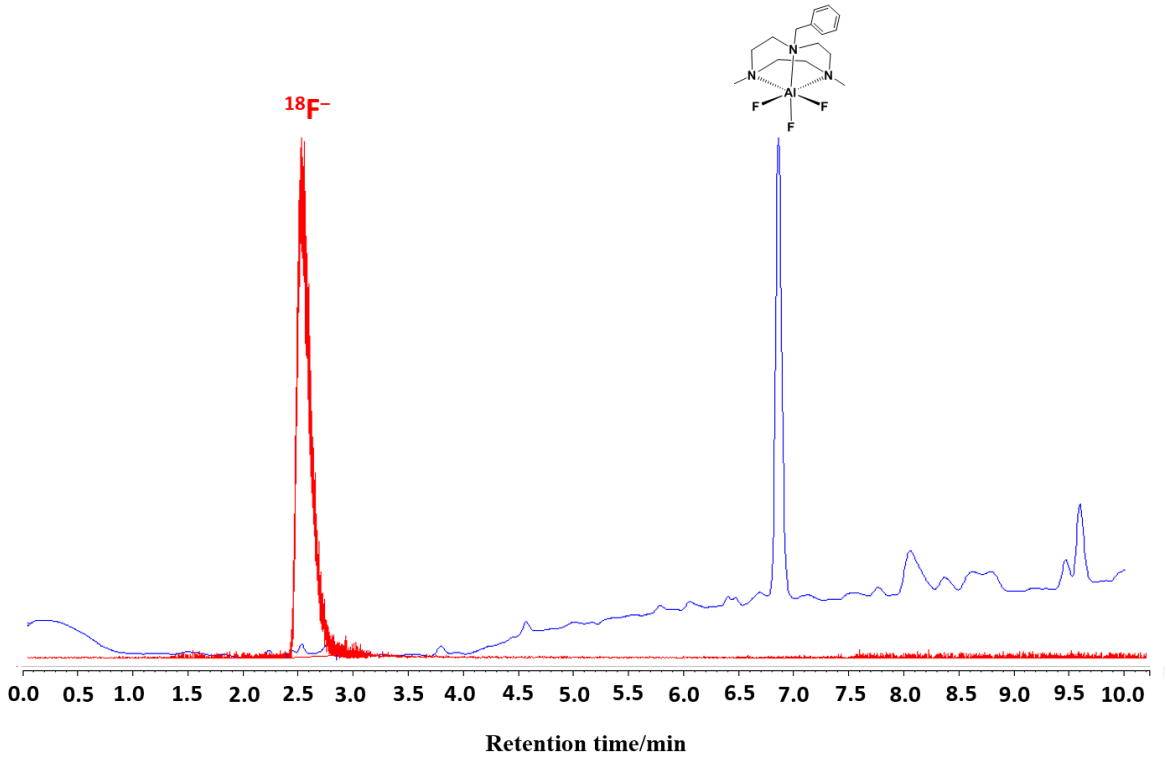

Figure 2.11. Radio-HPLC chromatogram and the corresponding UV-trace (blue) of the crude product of the attempted $^{18}F/^{19}F$ isotopic exchange reaction using [AlF_3($BnMe_2$-tacn)] (1 mg, 2.63 µmol) in 8 % MeCN/water at 80 °C for 30 min. Radio-HPLC chromatogram: Rt = 2.51 min 100% ($^{18}F^-$); UV-trace: [$Al^{19}F_3$($BnMe_2$-tacn)] (Rt 6.90 min).

Confirmation that the complex is not exchanging [^{19}F]F^- for [^{18}F]F^- but that [$Al^{19}F_3$($BnMe_2$-tacn)] is eluting off the column intact is given by the UV trace associated with the HPLC-radio chromatogram of the crude product, in which the inactive complex peak is present (Rt = 6.90 min) (Figure 2.11).

2.3 Conclusions

This chapter has demonstrated that the preformed neutral complex, [$AlCl_3$($BnMe_2$-tacn)], can be ^{18}F-radiolabelled readily in buffered pH 4 solution in the presence of 2.99 equiv. of [^{19}F]KF doped with [^{18}F]F^- at 80 °C in 60 minutes and that cyclotron-produced [^{18}F]F^- target water can be added directly to the buffered solution. An SPE purification protocol, without the need for an HPLC purification step, was established for the radiolabelled Al(III) complex. The resulting [$Al^{18}F^{19}F_2$($BnMe_2$-tacn)] shows excellent stability in PBS pH 7.4 ethanolic solution over several hours. However, in unbuffered MeCN solution and heating to 80 °C the RCY was much lower (< 10%). Stability tests on [AlF_3($BnMe_2$-tacn)] shows that the chelate is stable to the presence of a 10-fold excess of NaOAc, NaCl and KF, but that it is not stable to a 10-fold excess of Na_2CO_3 and Na_3PO_4, forming $[Al(OH)_4]^-$ (the pH of these solutions was ~ 10). These results suggest that the pH is an important factor for the radiolabelling of this system: the radiolabelling reaction is more efficient at pH 4 and the trifluoride-complex is stable (in contrast to its instability in basic conditions).

Section 2.1.4 discusses the radiolabelling conditions of the gallium analogue [$GaCl_3$($BnMe_2$-tacn)] (the experiment was replicated during this work and presented in the results and discussion section of this Chapter). This complex undergoes radiofluorination (with *ca.* 30% RCY) at room temperature in unbuffered aqueous MeCN.[34] Thus, a significant difference in the behaviour of the Al(III) *vs.* Ga(III) analogues is evident. Likely factors contributing to the differences observed are the higher Al-F bond dissociation energy (664 KJ mol^{-1}) compared to Ga-F (577 KJ mol^{-1})[2] and the higher Lewis acidity of the Al system.[36] The Lewis acidity of Al(III) and the high affinity toward oxygen atoms as a result, may also be a factor in explaining the instability of the complex at basic pH and for the less efficient radiolabelling in unbuffered MeCN solution as the hydroxide ions may be competing with the fluoride anions.

Comparing [AlF_3($BnMe_2$-tacn)] with [GaF_3($BnMe_2$-tacn)] and the "Al-F" system reported by McBride *et al.* (section 2.1.1), in the McBride system the pH of the radiolabelling reaction needs to be 4 and the mixture heated to 100 °C, whereas [$GaCl_3$($BnMe_2$-tacn)] can be ^{18}F-radiolabelled in unbuffered MeCN solution and at room temperature. This difference suggests that the size of the metal ion, its Lewis acidity and the specific ligand donor set are important considerations in determining the conditions necessary for effective radiofluorination at micromolar concentration or lower. In this regard, unlike McBride *et al.*, who were able to radiofluorinate their "Al-F" system at nM concentration, for [$AlCl_3$($BnMe_2$-tacn)] radiofluorination was not observed at concentrations below 2.63 μM. No evidence for the formation of [$Al^{18}F^{19}F_2$($BnMe_2$-tacn)] was observed using 0.1 mg of the metal precursor through Cl/^{18}F halide exchange or through ^{18}F/^{19}F isotopic exchange reactions,

contrasting with the gallium analogue (see Chapter 3). The use of a Lewis acid promoter in order to activate the Al-F bond will be explored in the future.

2.4 Experimental

$AlCl_3$, $GaCl_3$ and KF were obtained from Sigma-Aldrich, $NaOOCCH_3$ from Alfa Aesar and acetic acid from Fisher Scientific. The syntheses of $[MCl_3(BnMe_2\text{-tacn})]$ (M = Al, Ga) were carried out using standard Schlenk and vacuum line techniques. 1,4-dimethyl-7-benzyl-1,4,7-triazacyclononane was prepared as described previously.[37] For further details regarding the instrumentation see Appendix 1.

2.4.1 $[GaCl_3(BnMe_2\text{-tacn})]$

The compound was prepared as reported in the literature.[34] A solution of $BnMe_2$-tacn (0.025 g, 0.10 mmol) in CH_2Cl_2 was added to a solution of $GaCl_3$ (0.016 g, 0.09 mmol) in the same solvent. After 2 hours a white precipitate had formed. The white solid was filtered and dried *in vacuo* (0.021 g, 49 %). ^{1}H NMR (CD_3CN, 298 K): δ = 7.35 (m, [5H], ArH), 4.48 (s, [2H], Ar-CH_2), 3.46-3.41 (m, [2H], tacn-CH_2), 3.21-3.15 (m, [4H], tacn-CH_2), 2.87 (s, [6H], CH_3), 2.75-2.68 (m, [4H], tacn-CH_2), 2.49-2.40 (m, [2H], tacn-CH_2). ^{71}Ga NMR (CD_3CN/CH_3CN, 298 K): δ = 92.5 (br).

2.4.2 $[AlCl_3(BnMe_2\text{-tacn})]$

The compound was prepared as reported in the literature.[34] A solution of $BnMe_2$-tacn (0.029 g, 0.12 mmol) in CH_3CN was added to a solution of $AlCl_3$ (0.015 g, 0.011 mmol) in the same solvent, causing the precipitation of a white solid. The solid was filtered, washed with hexane and dried *in vacuo* (0.021 g, 49 %). IR (Nujol, ν/cm^{-1}): 398, 385 (Al-Cl). ^{1}H NMR (CD_2Cl_2, 298 K): δ = 7.39 (m, [5H], ArH), 4.65 (s, [2H], Ar-CH_2), 3.64-3.57 (m, [2H], tacn-CH_2), 3.36-3.30 (m, [4H], tacn-CH_2), 3.00 (s, [6H], CH_3), 2.75-2.69 (m, [4H], tacn-CH_2), 2.52-2.44 (m, [2H], tacn-CH_2). ^{27}Al NMR (CD_2Cl_2/CH_2Cl_2, 298 K): δ = 36.4 (s).

2.4.3 Cl/^{18}F exchange radiolabelling procedure

2.4.3.1 $[GaCl_3(BnMe_2\text{-tacn})]$

$[GaCl_3(BnMe_2\text{-tacn})]$ (0.001 g, 2.68 µmol) was dissolved in 0.6 mL of a 1:5 H_2O/MeCN mixture. 2.99 eq. of KF in cyclotron target $[^{18}F]F^-$ water (0.4 mL, 107.4 MBq) was added. The mixture was left at room temperature for 2 hours. Analytical HPLC analysis of the crude reaction solution showed 27 % ^{18}F incorporation. Peak 1: Rt = 2.56 min ($^{18}F^-$). Peak 2: Rt = 6.07 min ($[Ga^{18}F^{19}F_2(BnMe_2\text{-tacn})]$ complex). The product was purified through a SPE protocol using an HLB cartridge and formulated in 20 % EtOH/PBS.

2.4.3.2 [$AlCl_3$(BnMe_2-tacn)]

Method 1: [$AlCl_3$(BnMe_2-tacn)] (0.001 g, 2.63 µmol) was dissolved in MeCN (0.6 mL). 2.99 equiv. of KF in cyclotron target [^{18}F]F^- water (0.4 mL, 50 MBq) was added. The mixture was heated to 80 °C for 30 min. Analytical HPLC analysis of the crude reaction solution showed ca. 9 % ^{18}F incorporation. Method 2: In a typical experiment, [$AlCl_3$(BnMe_2-tacn)] (0.001 g, 2.63 µmol) was dissolved in pH 4 sodium acetate buffer solution (1 mL). 2.99 eq. of KF in cyclotron target [^{18}F]F^- water (0.1–1 mL, 20–280 MBq) was added. The mixture was heated to 80–100 °C for 60–90 min. Analytical HPLC analysis of the crude reaction solution showed up to 24 % ^{18}F incorporation (n = 7). Peak 1: Rt = 2.51 min ($^{18}F^-$). Peak 2: Rt = 6.95 min ([$Al^{18}F^{19}F_2$(BnMe_2-tacn)] complex).

2.4.4 Analytical HPLC system

Experiments were analysed on an Agilent 1290 HPLC system with an Agilent 1260 DAD UV detector (G4212B). Dionex Chromeleon 6.8 Chromatography data recording software was used to integrate the UV and radiochemical peak areas. Analytical HPLC method Column: Phenomenex Luna 5 µm C18(2) 250 × 4.6 mm. Mobile phase A: 10 mM ammonium acetate. B: MeCN. Flow rate: 1 mL min−1. Gradient: 0–15 min (10–90% B), 15–20 min (90% B), 20–21 min (90–10% B), 21–26.5 min (10% B).

2.4.5 SPE purification procedure for [$Al^{18}F^{19}F_2$(BnMe_2-tacn)]

The crude product was trapped on a HLB cartridge, washed with water (5 mL) to remove the [^{18}F]F^- and eluted from the cartridge with 1 mL of ethanol. pH 7.4 PBS solution was used to dilute the product to give a 50 % ethanolic formulation. The purified product was analysed by analytical HPLC, giving a pure product with an Rt of 6.92 min (RCP >99%). The product was stable for at least three hours (RCP = >99% at t = 180 min).

2.5 References

1. Chansaenpak, K.; Vabre, B.; Gabbai, F. P., *Chem. Soc. Rev.* **2016**, *45*, 954.

2. Speight, J. G., *Lange's Handbook of Chemistry, 17th Edition; Section 1,* **2017**.

3. Laverman, P.; McBride, W. J.; Sharkey, R. M.; Eek, A.; Joosten, L.; Oyen, W. J.; Goldenberg, D. M.; Boerman, O. C., *J. Nucl. Med.* **2010**, *51*, 454.

4. McBride, W. J.; Sharkey, R. M.; Karacay, H.; D'Souza, C. A.; Rossi, E. A.; Laverman, P.; Chang, C. H.; Boerman, O. C.; Goldenberg, D. M., *J. Nucl. Med.* **2009**, *50*, 991.

5. Chatalic, K. L.; Franssen, G. M.; van Weerden, W. M.; McBride, W. J.; Laverman, P.; de Blois, E.; Hajjaj, B.; Brunel, L.; Goldenberg, D. M.; Fehrentz, J. A.; Martinez, J.; Boerman, O. C.; de Jong, M., *J. Nucl. Med.* **2014**, *55*, 2050.

6. Dijkgraaf, I.; Franssen, G. M.; McBride, W. J.; D'Souza, C. A.; Laverman, P.; Smith, C. J.; Goldenberg, D. M.; Oyen, W. J.; Boerman, O. C., *J. Nucl. Med.* **2012**, *53*, 947.

7. McBride, W. J.; D'Souza, C. A.; Karacay, H.; Sharkey, R. M.; Goldenberg, D. M., *Bioconjugate Chem.* **2012**, *23*, 538.

8. D'Souza, C. A.; McBride, W. J.; Sharkey, R. M.; Todaro, L. J.; Goldenberg, D. M., *Bioconjugate Chem.* **2011**, *22*, 1793.

9. McBride, W. J.; Sharkey, R. M.; Goldenberg, D. M., *EJNMMI* **2013**, *3*, 36.

10. Laverman, P.; McBride, W. J.; Sharkey, R. M.; Goldenberg, D. M.; Boerman, O. C., *J. Label. Compd. Radiopharm.* **2014**, *57*, 219.

11. Da Pieve, C.; Allott, L.; Martins, C. D.; Vardon, A.; Ciobota, D. M.; Kramer-Marek, G.; Smith, G., *Bioconjugate Chem.* **2016**, *27*, 1839.

12. Niu, G.; Lang, L.; Kiesewetter, D. O.; Ma, Y.; Sun, Z.; Guo, N.; Guo, J.; Wu, C.; Chen, X., *J. Nucl. Med.* **2014**, *55*, 1150.

13. Hausner, S. H.; Bauer, N.; Sutcliffe, J. L., *Nucl. Med. Biol.* **2014**, *41*, 43.

14. Malik, N.; Baur, B.; Winter, G.; Reske, S. N.; Beer, A. J.; Solbach, C., *Mol. Imaging Biol.* **2015**, *17*, 777.

15. Cleeren, F.; Lecina, J.; Billaud, E. M.; Ahamed, M.; Verbruggen, A.; Bormans, G. M., *Bioconjugate Chem.* **2016**, *27*, 790.

16. Allott, L.; Da Pieve, C.; Turton, D. R.; Smith, G., *React. Chem. Eng.* **2017**, *2*, 68.

17. Smith, G. E.; Sladen, H. L.; Biagini, S. C.; Blower, P. J., *Dalton Trans.* **2011**, *40*, 6196.

18. Harwig, C. W.; Ting, R.; Adam, M. J.; Ruth, T. J.; Perrin, D. M., *Tetrahedron Lett.* **2008**, *49*, 3152.

19. Ting, R.; Harwig, C.; auf dem Keller, U.; McCormick, S.; Austin, P.; Overall, C. M.; Adam, M. J.; Ruth, T. J.; Perrin, D. M., *J. Am. Chem. Soc.* **2008**, *130*, 12045.

20. Li, Y.; Ting, R.; Harwig, C. W.; auf dem Keller, U.; Bellac, C. L.; Lange, P. F.; Inkster, J. A. H.; Schaffer, P.; Adam, M. J.; Ruth, T. J.; Overall, C. M.; Perrin, D. M., *Med. Chem. Commun.* **2011**, *2*, 942.

21. Chansaenpak, K.; Wang, M.; Wu, Z.; Zaman, R.; Li, Z.; Gabbai, F. P., *Chem Commun.* **2015**, *51*, 12439.

22. Li, Z.; Chansaenpak, K.; Liu, S.; Wade, C. R.; Conti, P. S.; Gabbaï, F. P., *Med. Chem. Commun.* **2012**, *3*, 1305.

23. Bernard, J.; Malacea-Kabbara, R.; Clemente, G. S.; Burke, B. P.; Eymin, M. J.; Archibald, S. J.; Juge, S., *J. Org. Chem.* **2015**, *80*, 4289.

24. Hendricks, J. A.; Keliher, E. J.; Wan, D.; Hilderbrand, S. A.; Weissleder, R.; Mazitschek, R., *Angew. Chem. Int. Ed.* **2012**, *51*, 4603.

25. Liu, S.; Lin, T. P.; Li, D.; Leamer, L.; Shan, H.; Li, Z.; Gabbai, F. P.; Conti, P. S., *Theranostics* **2013**, *3*, 181.

26. Khoshnevisan, A.; Jauregui-Osoro, M.; Shaw, K.; Torres, J. B.; Young, J. D.; Ramakrishnan, N. K.; Jackson, A.; Smith, G. E.; Gee, A. D.; Blower, P. J., *EJNMMI* **2016**, *6*, 34.

27. Ting, R.; Adam, M. J.; Ruth, T. J.; Perrin, D. M., *J. Am. Chem. Soc.* **2005**, *127*, 13094.

28. Vedejs, E.; Chapman, R. W.; Fields, S. C.; Lin, S.; Schrimpf, M. R., *J. Org. Chem.* **1995**, *60*, 3020.

29. Liu, Z.; Hundal-Jabal, N.; Wong, M.; Yapp, D.; Lin, K. S.; Bénard, F.; Perrin, D. M., *Med. Chem. Commun.* **2014**, *5*, 171.

30. Wade, C. R.; Zhao, H.; Gabbai, F. P., *Chem Commun.* **2010**, *46*, 6380.

31. Hudnall, T. W.; Gabbai, F. P., *J. Am. Chem. Soc.* **2007**, *129*, 11978.

32. Hudnall, T. W.; Gabbai, F. P., *Chem Commun.* **2008**, 4596.

33. Bhalla, R.; Levason, W.; Luthra, S. K.; McRobbie, G.; Sanderson, G.; Reid, G., *Chem. Eur. J.* **2015**, *21*, 4688.

34. Bhalla, R.; Darby, C.; Levason, W.; Luthra, S. K.; McRobbie, G.; Reid, G.; Sanderson, G.; Zhang, W., *Chem. Sci.* **2014**, *5*, 381.

35. Mason, J., *Multinuclear NMR,* ed. Plenum, New York, **1987**.

36. A. J. Downs; H. Himmel, *The Group 13 Metals Aluminium, Gallium, Indium and Thallium: Chemical Patterns and Peculiarities,* ed. S. Aldridge and A. J. Downs Wiley, **2011**.

37. Belousoff, M. J.; Duriska, M. B.; Graham, B.; Batten, S. R.; Moubaraki, B.; Murray, K. S.; Spiccia, L., *Inorg. Chem.* **2006**, *45*, 3746.

Chapter 3: $^{18}F/^{19}F$ isotopic exchange reactions on $[GaF_3(RMe_2\text{-tacn})]$ (R = Me, Bn)

3.1 Introduction

The ^{18}F-radiofluorination conditions required for $[AlCl_3(BnMe_2\text{-tacn})]$ and a comparison with its gallium analogue are discussed in Chapter 2. Despite requiring very different reaction conditions for effective $[^{18}F]F^-$ incorporation, to-date neither precursor has been shown to be radiolabelled below ca. 2 μM concentration. This could present a limitation on these systems for PET application (the ideal criteria for a PET agent are set out in Section 1.1). In both cases, the hydrolytic sensitivity of the metal trichloride complexes may result in competition between slow hydrolysis and Cl/F exchange under the labelling conditions.[1] Therefore, an alternative approach to overcome this apparent limitation was sought.

This Chapter focuses particularly on obtaining $[Ga^{18}F^{19}F_2(BnMe_2\text{-tacn})]$ in good RCY and using mild reaction conditions, while specifically starting with a lower concentration of the gallium precursor. Since the metal-fluoride complexes, $[MF_3(BnMe_2\text{-tacn})]$ (M = Al, Ga, In), are very stable in water, isotopic exchange reactions were considered as an alternative method to achieve ^{18}F-radiofluorination at nmol precursor concentration. However, it was shown in Chapter 2 that $[AlF_3(BnMe_2\text{-tacn})]$ did not exchange with $[^{18}F]F^-$, but given the considerably higher bond dissociation energy of Al-F compared to Ga-F (664 *vs.* 577 KJ/mol,[2] Table 1.2) the isotopic exchange may be successful when using $[GaF_3(BnMe_2\text{-tacn})]$.

This Chapter discusses the experiments undertaken to explore the ^{18}F-radiofluorination of $[GaF_3(BnMe_2\text{-tacn})]$ through $^{18}F/^{19}F$ isotopic exchange reactions, including the effects of varying the reaction parameters (temperature, organic solvent, organic solvent ratio and concentration of precursor) on the radiochemical yield, as well as other relevant aspects of the system, such as the effect of F^-, Cl^- and OH^- on the radiochemical purity of the formulated radio-product (see Chapter 1 section 1.5 for further details on stability requirements of the radiolabelled product).

Among the alternatives to C-^{18}F bond formation, and the challenges associated with it (Chapter 1, Section 1.1), Al-^{18}F, B-^{18}F (Chapter 2) and Si-^{18}F have all been established and proven to be successful as viable labelling strategies for the conjugation of peptides and imaging of many tumour types *in vivo*. With the exception of the "Al-F" system, which is based on a metal-chelate complex as the prosthetic group, the boron and silicon systems are mainly based on organo-BF_3 and organo-silicon fluoride compounds (also named silicon-based fluoride acceptors, SiFA).[3,4] The ^{18}F-radiolabelled version of the boron and silicon systems can be obtained through $^{18}F/^{19}F$ isotopic exchange

reactions. The use of isotopic exchange reactions to form the inorganic compounds [^{18}F]Me_2SiF_6,[5] [^{18}F]Me_3SiF[6] and [^{18}F]KBF_4[7,8] has been known since the late 1950s and early 1960s, but it was only a decade ago when isotopic exchange reactions on B-F and Si-F systems started to be developed towards ^{18}F-PET radiotracers and *in vivo* PET imaging.[9,10]

The use of isotopic exchange reactions for the synthesis of ^{18}F-PET radiotracers introduce some advantages compared to the other methodologies for C-^{18}F, Al-^{18}F, B-^{18}F and Si-^{18}F bond formation:

- Potential by-product formation is minimal; there are only two species present in the crude reaction mixture and they are chemically identical: the unlabelled molecule, bearing ^{19}F, and the ^{18}F-labelled version of it. This greatly simplifies the purification steps of the process, as typically the only purification required is a solid-phase extraction (SPE) to remove unreacted [^{18}F]F^-. The more time-consuming HPLC purifications procedures, which lead to a decreased RCY and need trained radiochemists, are not required.
- The radiosynthesis is usually performed in a single (often rapid) step.

On the other hand, some disadvantages could also arise:

- The concentration of the ^{19}F-precursor needed could be high (10- 100 µM), leading to low molar activity values.[4,10]
- If the ^{18}F/^{19}F exchange rate is slow, the reaction time is too long relative to the moderately short ^{18}F half-life (110 min.) (this exchange rate can be improved by increasing the temperature).
- In case of systems conjugated to peptides, high temperatures (> 100 °C) could result in degradation of the biomolecules.

The isotopic exchange reactions on the organo-BF_3 and SiFA systems, along with some other systems that have been published recently, will be discussed briefly in the following sections.

3.1.1 Isotopic exchange reactions on organotrifluoroborate systems

The revival of [^{18}F]BF_4^- for PET imaging applications was reported by the Blower group.[11,12,13] The small inorganic molecule was utilised for imaging the sodium/iodide symporter (target molecule in thyroid disease) and it is now in clinical trials. [^{18}F]BF_4^- was prepared by ^{18}F/^{19}F isotopic exchange of BF_4^- in hot hydrochloric acid (120 °C, 10 min) (Scheme 3.1). The RCY of the reaction was *ca.* 10 %.

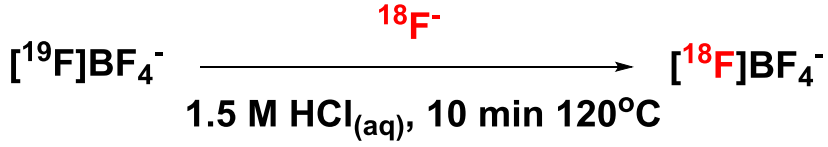

Scheme 3.1. ^{18}F/^{19}F isotopic exchange reaction conditions of BF_4^-.

Other more elaborate "B-F" systems, based on organoboron moieties have also been ^{18}F-radiofluorinated. Aryl trifluoroborates, zwitterionic onium-trifluoroborates, N-heterocyclic carbene-trifluoroborates (NHC-BF_3) and boron-based BODIPY dyes have all been radiolabelled through ^{18}F/^{19}F isotopic exchange reactions, conjugated to biomolecules and investigated *in vivo*.

Although the ^{18}F-radiolabelled aryl trifluoroborates are usually obtained from the aryl boronic acids or esters through nucleophilic substitution reactions, ^{18}F/^{19}F isotopic exchange reactions have also been used. A heteroaryltrifluoroborate (50 nmol), conjugated to RGD (arginylglycylaspartic acid), was radiofluorinated in a kit-like approach in a 50 % DMF/water solution with mild heating (45 °C) at pH 2 (Scheme 3.2).[14]

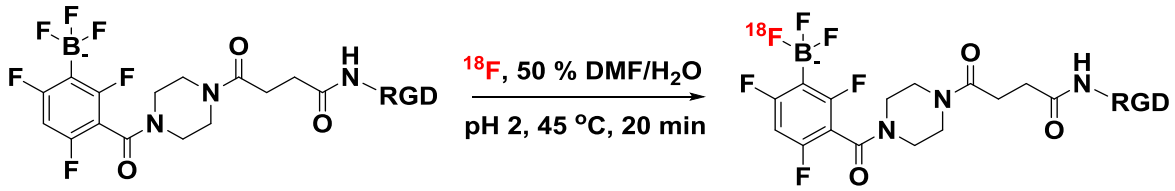

Scheme 3.2. ^{18}F/^{19}F isotopic exchange reaction conditions of RGD-ArBF_3^-.

The RCY of the reaction was 65 %, but *ca.* 40 % of the precursor was converted to the corresponding boronic acid during the radiofluorination reaction due to competitive hydrolysis.

The zwitterionic N-heterocyclic carbene-trifluoroborates are considered in the same category as the onium-trifluoroborates. In this species, the cationic moiety increases the stability against hydrolysis, on condition that the cation is close to the BF_3^- group. The aryltrifluoroborate (4.5 mM) in Scheme 3.3 was ^{18}F-radiofluorinated simply by stirring with [^{18}F]F^- in water at pH 1.5, giving the target product in very good RCY (87 %).[15]

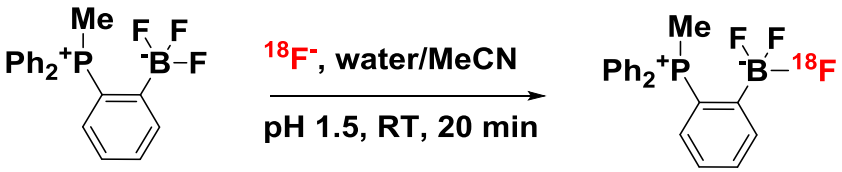

Scheme 3.3. ^{18}F/^{19}F isotopic exchange reaction conditions of an aryltrifluoroborate with an *ortho*-phosphonium group.

The ^{18}F/^{19}F isotopic exchange reactions on NHC-BF_3 systems proved to be more challenging. These compounds do not undergo exchange in mild conditions due to the lack of lability of the BF_3^- group. As a result, the radiofluorination reactions are performed in anhydrous conditions, with heating and in the presence of a Lewis acid promoter such as $SnCl_4$. Although the effect of a Lewis acid promoter is not entirely clear, they are able to activate the B-F bond and promote the isotopic exchange presumably through coordination to F^- to form an F^- bridge transition state. 1,3-

dimethylimidazolium-2-trifluoroborate (7 mM) was ^{18}F-radiofluorinated in dry MeCN at 60 °C with [^{18}F]TBAF (TBAF = tetrabutylammonium fluoride) as radioactive source, in the presence of 5 equiv. of $SnCl_4$ as Lewis acid promoter (Scheme 3.4).[16]

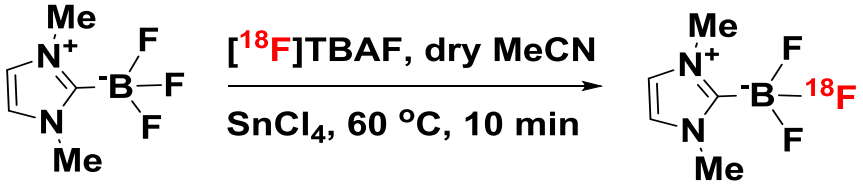

Scheme 3.4. ^{18}F/^{19}F isotopic exchange reaction conditions of 1,3-dimethylimidazolium-2-trifluoroborate.

Leaving the mixture at 60 °C for 10 min gave the highest RCY of 53 %. The same method was employed for a similar system bearing a maleimide group for peptide conjugation.[16]

Boron-based BODIPY dyes suffer from the same problem as the NHC-BF_3 carbene systems: the stability of the B-F bond makes the ^{18}F/^{19}F isotopic exchange reaction poorly suited to mild reaction conditions. As reported in Chapter 2 (section 2.1.3), these systems are usually ^{18}F-fluorinated by initially treating the boron compound with a fluoride abstractor, which allows the formation of a much more reactive intermediate, that can be radiolabelled subsequently. ^{18}F/^{19}F isotopic exchange reactions avoid the formation of a reactive intermediate in a two steps process, but are usually performed in the presence of a Brønsted or a Lewis acid promoter. The cationic BODIPY dye (0.37 µmol) (Scheme 3.5) was converted into the ^{18}F-analogue, under acidic conditions in aqueous solution (pH 2, HCl). However, the radio-product was obtained in very poor RCY (2 %).[17]

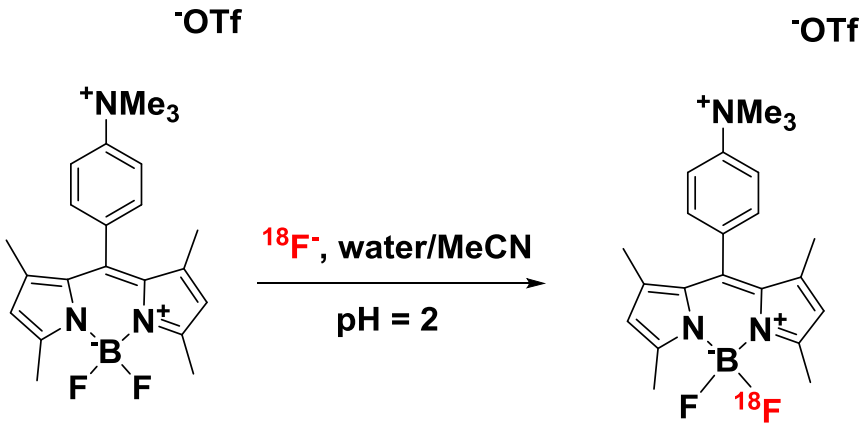

Scheme 3.5. ^{18}F/^{19}F isotopic exchange reaction conditions of the cationic BODIPY dye in in the presence of a Brønsted acid promoter.

However, the same molecule could be successfully radiofluorinated in much higher RCY (> 95 %) in the presence of a Lewis acid promoter (Scheme 3.6). Several Lewis acids were tested, with the best results obtained using $SnCl_4$ in 13-fold excess at room temperature.[17,18]

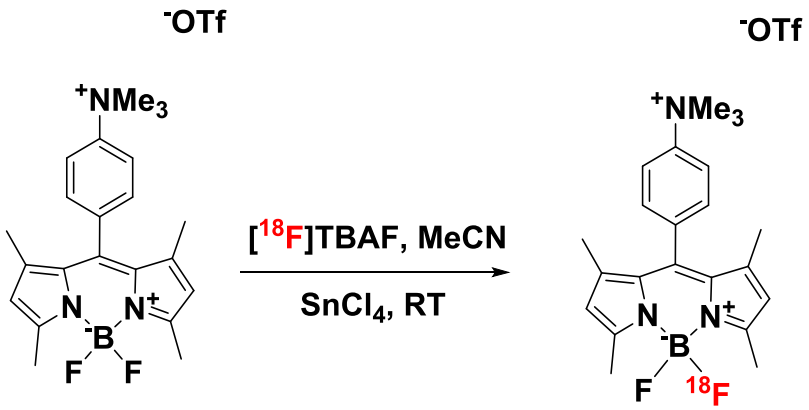

Scheme 3.6. $^{18}F/^{19}F$ isotopic exchange reaction conditions of the cationic BODIPY dye in in the presence of a Lewis acid promoter.

To-date, the most stable "B-F" systems, in terms of resistance to hydrolysis, are the zwitterionic onium-trifluoroborates species. The hydrolysis rate constant of aryl-phosphonium, -ammonium and -sulfonium trifluoroborate were measured in PBS (pH 7.5), showing that the phosphonium compound is the most stable to hydrolysis.[19] Subsequently, the zwitterionic alkylammoniumtrifluoroborate ($AMBF_3$) species also showed very good stability *in vitro* and *in vivo*.[20]

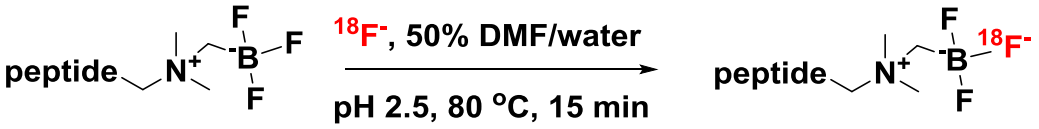

Scheme 3.7. $^{18}F/^{19}F$ isotopic exchange reaction conditions of $AMBF_3$.

The peptide-conjugated alkylammonium trifluoroborate compound shown in Scheme 3.7 (~ 50 nmol) was labelled through a $^{18}F/^{19}F$ isotopic exchange reaction in a 50 % dmf/water solution at pH 2.5, using quaternary methyl ammonium (QMA) purified $[^{18}F]F^-$ target water with heating (80 °C) for 15 min. The RCY of the reaction was 25 %.[20]

3.1.2 Isotopic exchange on SiFA systems

In the same way as for boron and aluminium, silicon has attracted the interest of radiochemists, thanks to its high bond dissociation energy with fluoride (> 570 KJ mol^{-1}).[21] Early works explored this aspect and proved that silicon fluoride-based radiotracers could be utilised in radiochemistry and for PET applications; the formation of $[^{18}F]SiF_4$ has been known since 1958[5,6,22] and $[^{18}F]Me_3SiF$ was firstly hypothesised as an intermediate in the reaction of hexamethyldisiloxane with [^{18}F]HF in 1978.[23] The first *in vivo* evaluation was reported in 1985 by the Rosenthal group who radiofluorinated Me_3SiF from the chloride analogue through a $Cl/^{18}F$ halide exchange reaction in aqueous MeCN.[24] Ten years later, Pilcher and co-workers fluorinated organosilanoles with non-

radioactive HF in high yields.[25] However, the research into silicon-based PET radiotracers developed after Perrin *et al.* published the first efficient ^{18}F labelling of an alkyl triethoxysilane in aqueous solution (Scheme 3.8).[9]

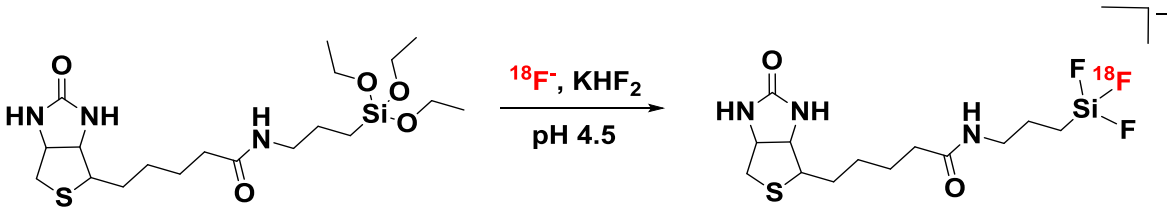

Scheme 3.8. ^{18}F-fluorination conditions to obtain the alkyl trifluorosilicate.

The alkyl triethoxysilane is mixed with a solution of ^{18}F-target water with KHF_2 as carrier, added in a sodium acetate solution at pH 4.5. The poor kinetic stability of the organofluorosilane led to hydrolytic release of fluoride to give the silanol analogue, and poor *in vitro* and *in vivo* stability, as a result.[24] It was suggested that bulky groups at the silicon atom may confer higher resistance to hydrolysis. This suggestion was confirmed by density functional theory models and experimental data.[26,27] An important aspect to mention is that the reactions discussed so far all proceed through nucleophilic substitution at the silicon centre in which the leaving group (e.g. alkoxy, hydroxy etc.) is replaced by the fluoride anion. These reactions often required elevated temperature (~ 100 °C in DMSO solution), and hence require the formation of the radiolabelled compound conjugated to a peptide in a two steps process (bioconjugation after radiolabelling reaction).[26]

As an alternative to the leaving group approach, the Schirrmacher group proposed the first example of a [^{18}F]SiFA system obtained by an isotopic exchange reaction.[10] The reaction was performed on the compound di-*tert*-butylphenyl-fluorosilane conjugated to the peptide tyr^3-octreotate (74 µmol) either in anhydrous conditions (dry MeCN, $^{18}F^-$/kryprofix 2.2.2/K^+) at room temperature or aqueous MeCN solution with heating (95 °C), forming the product in high RCY (70- 90 %) (Scheme 3.9).

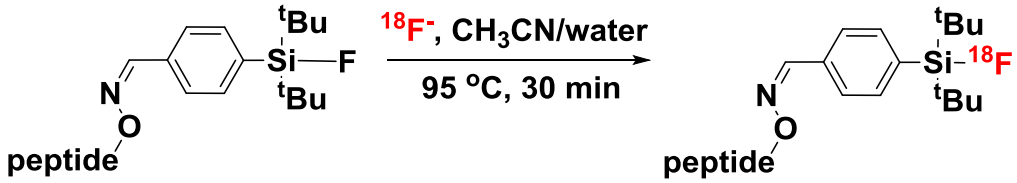

Scheme 3.9. $^{18}F/^{19}F$ isotopic exchange reaction conditions of di-*tert*-butylphenyl-fluorosilane.

The phenyl group was functionalised with an aldehyde group in the *para* position in order to conjugate the peptide through the formation of an oxime group. This was a breakthrough as the peptide-conjugated ^{18}F-labelled fluorosilane was obtained efficiently in a single-step, with heating, in aqueous solution through an isotopic exchange reaction. The non-conjugated radio-product was formed in moderate molar activity (~ 200 GBq/µmol) without the need of a post-labelling HPLC

purification step and showed good stability. Since the publication of this work, the SiFA moiety has been conveniently functionalised to conjugate to different peptides for imaging of several tumour types.[28,29,30,31] Hydrolysis of the Si-F was satisfactorily reduced by the bulky *tert*-butyl groups. However, the stability brought by the alkyl groups comes with a significant increase in lipophilicity, which substantially influences the pharmacokinetics and biodistribuition profiles, resulting in a significant non-specific binding and therefore poor PET imaging quality.[10] This issue has been addressed by the introduction of lipophilicity-reducing auxiliaries such as carbohydrate/polyethylene glycol (PEG) groups (Scheme 3.10).[32] The reaction proceeds in "anhydrous conditions" in DMSO using ~ 20 nmol of precursor and dried [^{18}F]F$^-$ with a RCY of 38 ± 4 %.

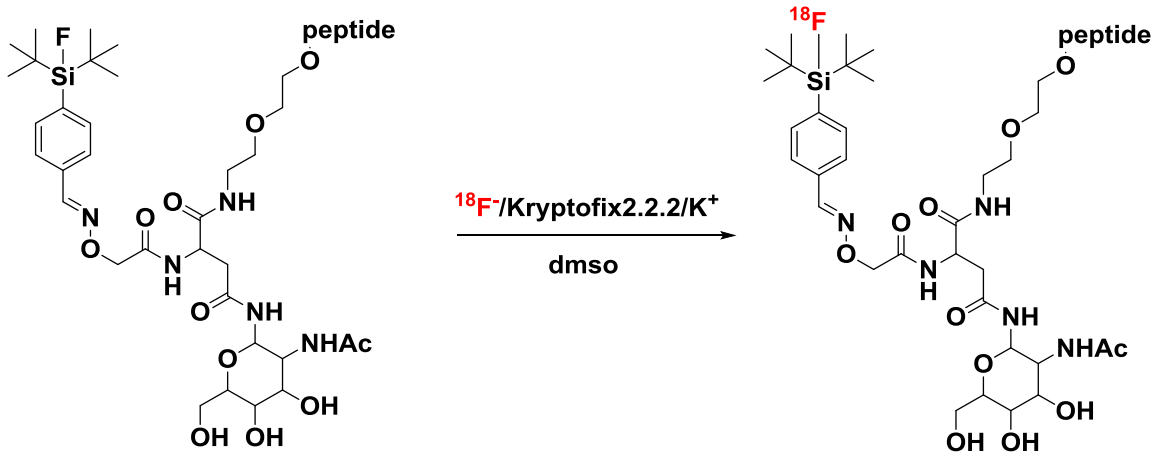

Scheme 3.10. ^{18}F/^{19}F isotopic exchange reaction conditions of SiFA-Asn(AcNH-β-Glc)PEG-Tyr3-octreotate. (Peptide = Tyr3-octreotate).

This work demonstrated the feasibility of tuning the lipophilicity of the compound by modification of the groups between the biomolecule and the SiFA moiety in order to improve the biodistribution profiles and obtain higher resolution images. This led to the introduction of permanently charged auxiliaries (Scheme 3.11)[33] in order to further increase the hydrophilicity of the system (it is worth noting that the AMBF$_3$ systems also bear a positively charged ammonium group, section 3.1.1).

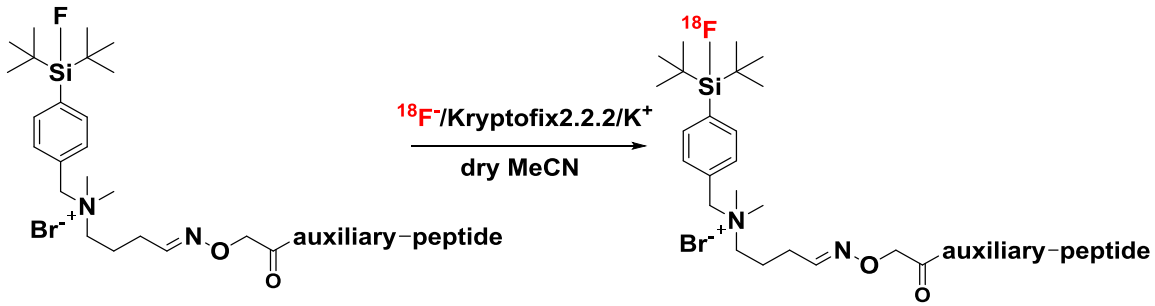

Scheme 3.11. ^{18}F/^{19}F isotopic exchange reaction conditions of the SiFA compound (25 nmol). Auxiliary = Glc-Asp$_2$-PEG$_1$; Peptide = Tyr3-octreotate.

The compound showed comparable pharmacokinetics and higher tumour accumulation in somatostatin receptor-bearing tumours than ^{68}Ga-DOTATE (current clinical "gold standard"). The ^{18}F/^{19}F isotopic exchange is performed in anhydrous conditions in MeCN at room temperature, forming the target ^{18}F-radioproduct with a RCY between 70- 90 % within 5 minutes.

3.1.3 Other related systems

Very recently, Gabbaï, Li and co-workers reported successful isotopic exchange reactions on an NHC-PF_5 system, the phosphorus analogue of the NHC-BF_3 chemistry developed previously.[34] IMe-PF_5 (IMe = 1,3-dimethylimidazol-2-ylidene) undergoes a Lewis acid promoted ($SnCl_4$) ^{18}F/^{19}F isotopic exchange reaction in MeCN solution with [^{18}F]TBAF, giving low RCY (4-6 %) (Scheme 3.12). The reaction was performed in the presence of 5 mol. equiv. of $SnCl_4$ and the best RCY was obtained at 80 °C. It was also found that when the reaction temperature is further increased, the radiolabelled compound decomposes. The target compound showed good stability in PBS pH 7 solution for at least 3 hours and no bone uptake was observed *in vivo*.

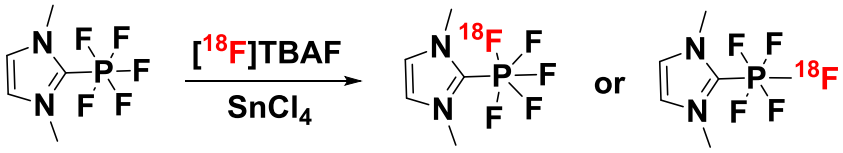

Scheme 3.12. ^{18}F/^{19}F isotopic exchange reaction conditions of IMe-PF_5.

The lower RCY obtained, in comparison to the NHC-BF_3 analogue, was attributed to the stronger P-F bond (380 KJ mol^{-1} for PF_5 *vs.* 346 KJ mol^{-1} for BF_3, based on computed gas phase fluoride ion affinity data)[35] which hinders the ^{18}F/^{19}F exchange process.

The Schirrmacher group also developed the ^{18}F-labelling strategy of the SiFA coupled to nanomaterials. An ^{18}F-SiFA moiety, previously ^{18}F-radiolabelled through isotopic exchange reactions, was attached to maleimide-terminated PEGylated gold nanoparticles *via* a Michael addition. *In vivo* studies showed detectable brain uptake.[36] In a more recent study, the SiFA moieties were ^{18}F-radiolabelled through isotopic exchange reactions when already attached to the nanoparticles. The isotopic exchange reaction was performed in EtOH solution with azeotropically dried [^{18}F]F$^-$ and heating the mixture to 65 °C for 30 minutes (Scheme 3.13).[37]

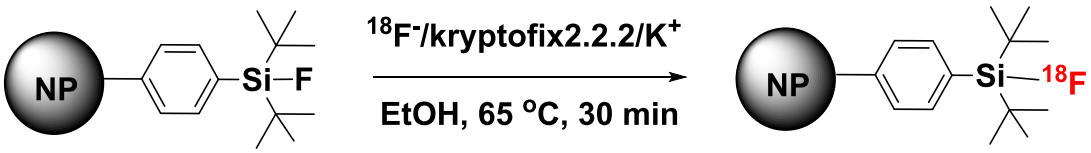

Scheme 3.13. ^{18}F/^{19}F isotopic exchange reaction conditions of di-*tert*-butylphenyl fluorosilane attached to a nanoparticle. NP = nanoparticle.

The aspects discussed in this introduction on boron- and silicon-fluoride systems for PET applications, are also illustrated in several reviews.[38,3,39,4,40]

3.2 Results and discussion

The $^{18}F/^{19}F$ isotopic exchange reaction on [GaF_3($BnMe_2$-tacn)] was investigated in order to establish whether this system could be ^{18}F-radiofluorinated at lower concentration than the chloride analogue, for which the current lower limit is reported as 2.63 µmol (1 mg/mL). The reaction conditions in which the [$Ga^{19}F_3$($BnMe_2$-tacn)] was originally synthesised (hydrothermal conditions, 180 °C for 15 hours)[1] suggested that this chelate has a high stability in water and hence, competitive hydrolysis should not interfere during the radiolabelling. Moreover, the trifluoro-complex should be a more convenient precursor due to its ease of handling, together with its much longer shelf-life, compared to [$GaCl_3$($BnMe_2$-tacn)]. A more convenient synthesis of [GaF_3($BnMe_2$-tacn)] was also established, as an alternative to the hydrothermal method, *via* the direct reaction of the molecular [GaF_3(DMSO)$(OH_2)_2$] complex with $BnMe_2$-tacn in CH_2Cl_2 at room temperature[41] (see Chapter 4 for further details, including experimental conditions and spectroscopic data). The product, obtained in 87 % isolated yield, gave the characteristic IR and ^{1}H, ^{19}F and ^{71}Ga NMR spectroscopic signatures; ES^+ MS (MeCN/H_2O) shows *m/z* consistent with [GaF_3($BnMe_2$-tacn)+Li]$^+$ and [GaF_2($BnMe_2$-tacn)]$^+$. The strong affinity of [GaF_3($BnMe_2$-tacn)] to alkali metal cations has been demonstrated previously.[42]

The method for the ^{18}F-radiofluorination of [GaF_3($BnMe_2$-tacn)] developed successfully in this work is illustrated in Scheme 3.14.

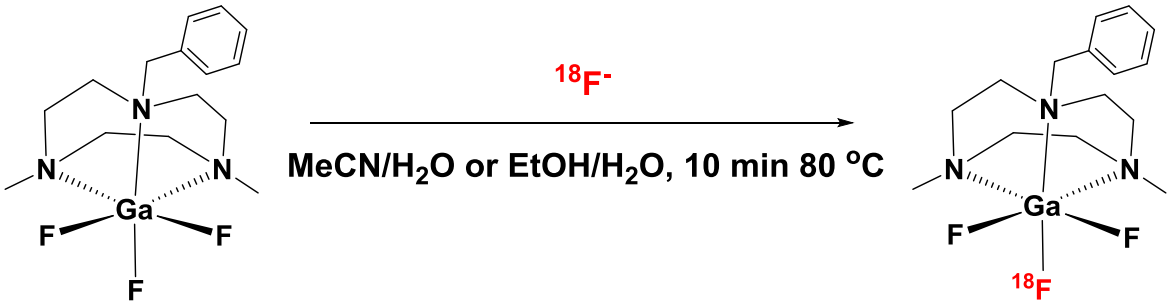

Scheme 3.14. Radiofluorination method for [GaF_3($BnMe_2$-tacn)].

Initial $^{18}F/^{19}F$ isotopic exchange reactions were performed at 2.6 µM concentration of [GaF_3($BnMe_2$-tacn)] (1 mg/mL) in 8 % MeCN/H_2O solution at room temperature, using [^{18}F]F^- target water directly from the cyclotron (i.e. without any purification or drying steps). The activity of the target water used during this work is considerably lower compared to that used to radiolabel [$GaCl_3$($BnMe_2$-tacn)] at GE (up to 100 GBq in 3-4 mL but ~ 500 MBq in a typical experiment using 0.4 mL of ^{18}F-target water). The target product, [$Ga^{18}F^{19}F_2$($BnMe_2$-tacn)], was obtained in poor RCY (4±2 %), but

an improved ^{18}F-incorporation was observed when the sample was heated to 80 °C, giving 18 ± 4 % RCY (Figures 3.1 and 3.2). The identification of the radioactive product, [$Ga^{18}F^{19}F_2$(BnMe$_2$-tacn)], was made by comparison with the retention time of the product obtained from the Cl/^{18}F halide exchange reaction on [$GaCl_3$(BnMe$_2$-tacn)].[1] (Note that the same reaction was also successfully repeated in the radiochemistry laboratories at the St. Thomas' Hospital (Chapter 2)).

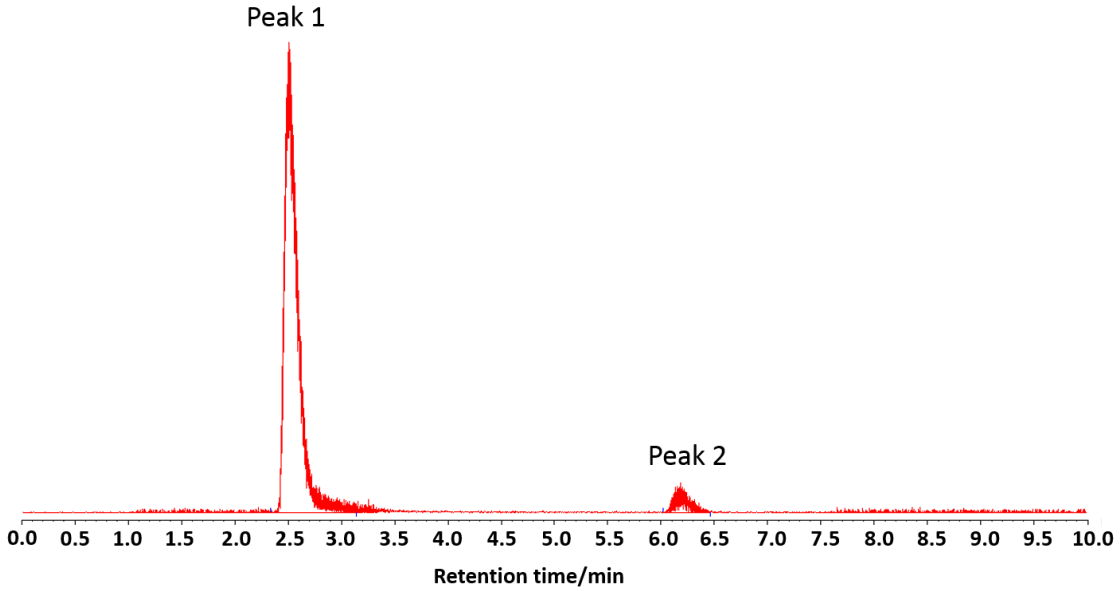

Figure 3.1. Radio-HPLC chromatogram of the crude product from radiofluorination of [GaF_3(BnMe$_2$-tacn)] (1 mg, 2.68 µmol) in 8%/92% CH_3CN/H_2O at 25 °C for 45 min. Peak 1: Rt = 2.51 min 96% ($^{18}F^-$). Peak 2: Rt = 6.18 min 4% ([$Ga^{18}F^{19}F_2$(BnMe$_2$-tacn)]).

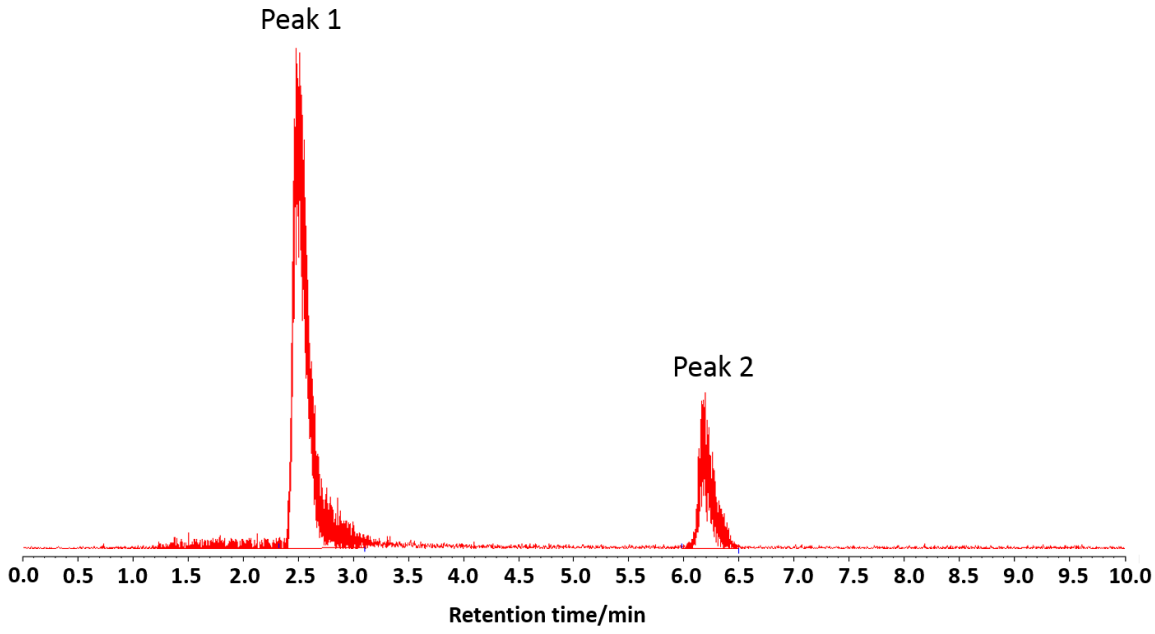

Figure 3.2. Radio-HPLC chromatogram of the crude product from radiofluorination of [GaF_3(BnMe$_2$-tacn)] (1 mg, 2.68 µmol) in 8%/92% CH_3CN/H_2O at 80 °C for 30 min. Peak 1: Rt = 2.49 min 82% ($^{18}F^-$). Peak 2: Rt = 6.20 min 18% ([$Ga^{18}F^{19}F_2$(BnMe$_2$-tacn)]).

Encouraged by these preliminary results, a range of experimental conditions were explored to improve the ^{18}F incorporation, including the choice of the labelling solvent, the solvent ratio, temperature and amount of precursor, to establish the effect on the $[^{18}F]F^-$ incorporation (Table 3.1).

Table 3.1. Reaction conditions used for the $^{18}F/^{19}F$ radiofluorination experiments using $[GaF_3(BnMe_2\text{-tacn})]$. All experiments were performed at least three times.

$[GaF_3(BnMe_2\text{-tacn})]$ (mass/mg)	Scale (nmol)	Organic solvent/H_2O ratio	Organic solvent	T/°C (time/min)	RCY* (%)
1	2680	8:92	MeCN	25 (45)	4±2
1	2680	8:92	MeCN	80 (30)	18±4
1	2680	50:50	MeCN	80 (60)	23±4
1	2680	75:25	MeCN	80 (10)	73±4
0.1	268	75:25	MeCN	25 (80)	8±4
0.1	268	75:25	MeCN	80 (10)	66±4
0.01	27	75:25	MeCN	80 (10)	37±5
1	2680	75:25	EtOH	80 (10)	81±1
0.1	268	75:25	EtOH	80 (10)	50±4

*determined from analytical HPLC chromatograms.

The results (Table 3.1) show that the isotopic exchange is very efficient when employing the 75 % organic solvent / 25 % water (80 °C) conditions (Figure 3.3, 2680 µmol). The high RCY were obtained without the need of a Lewis acid promoter, making it a very simple and rapid method, with little need for post-labelling purification. The target $[Ga^{18}F^{19}F_2(BnMe_2\text{-tacn})]$ was obtained as the only radio-product (along with unreacted $[^{18}F]F^-$), as shown in the radio-HPLC chromatogram, and this peak matches the only peak present in the UV-vis trace due to the benzyl group present in the complex. The Rt of the product, $[Ga^{18}F^{19}F_2(BnMe_2\text{-tacn})]$, in the radio-HPLC chromatogram and UV-trace match the Rt of the product obtained from the $Cl/^{18}F$ halide exchange reaction of $[GaCl_3(BnMe_2\text{-tacn})]$[1] (Chapter 2).

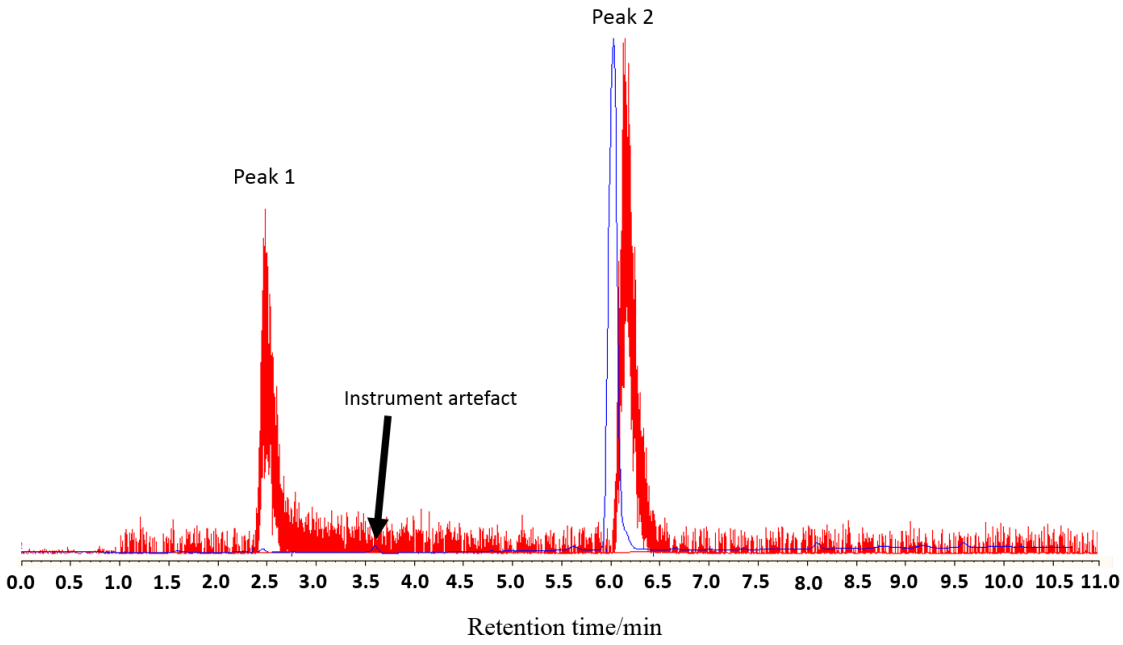

Figure 3.3. Radio-HPLC chromatogram (red) and the corresponding UV-trace (blue) of the crude product from radiofluorination of [GaF_3($BnMe_2$-tacn)] (1 mg, 2.68 µmol) in 75%/25% MeCN/H_2O at 80 °C for 10 mins. Peak 1: Rt = 2.51 min 33% ($^{18}F^-$). Peak 2: Rt = 6.14 min 67% ([$Ga^{18}F^{19}F_2$($BnMe_2$tacn)]). Peak 2 matches the UV-vis peak of [GaF_3($BnMe_2$-tacn)].

Very importantly, high RCYs were obtained at much lower concentration of precursor, i.e. 66 ± 4 % at 268 nM (Figures 3.4) and 37 ± 5 (Figures 3.5) at 27 nM.

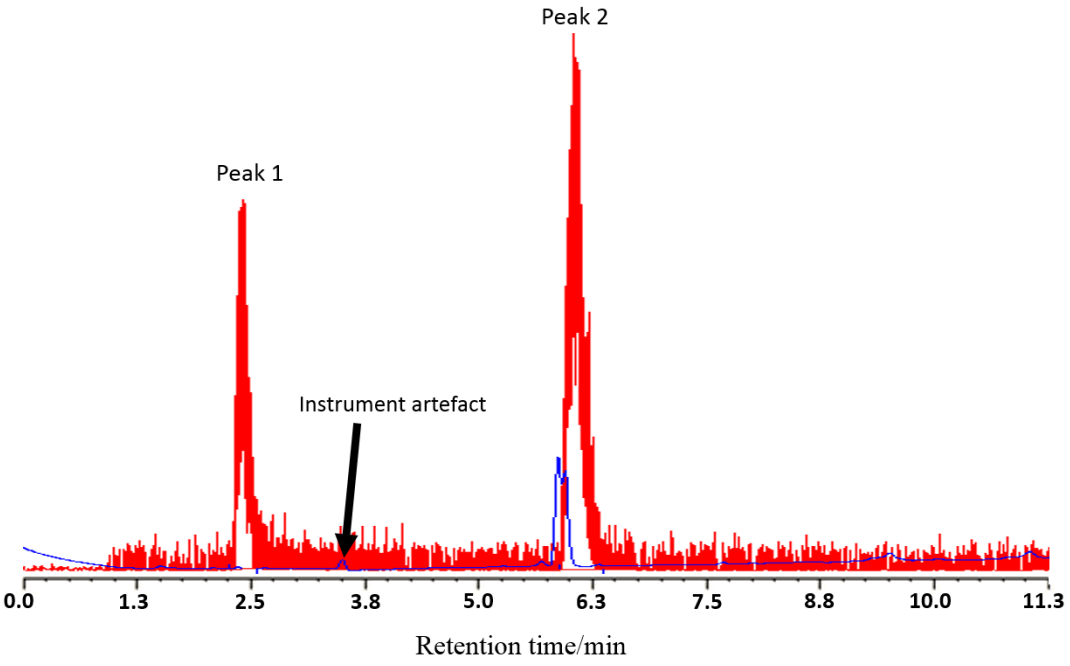

Figure 3.4. Radio-HPLC chromatogram (red) and the corresponding UV-trace (blue) of the crude product from radiofluorination of [GaF_3($BnMe_2$-tacn)] (0.1 mg, 268 nmol) in 75%/25% MeCN/H_2O at 80 °C for 10 mins. Peak

1: Rt = 2.52 min 32 % ($^{18}F^-$). Peak 2: Rt = 6.13 min 68 % ([$Ga^{18}F^{19}F_2$(BnMe$_2$-tacn)]). Peak 2 matches the UV-vis peak of [GaF_3(BnMe$_2$-tacn)].

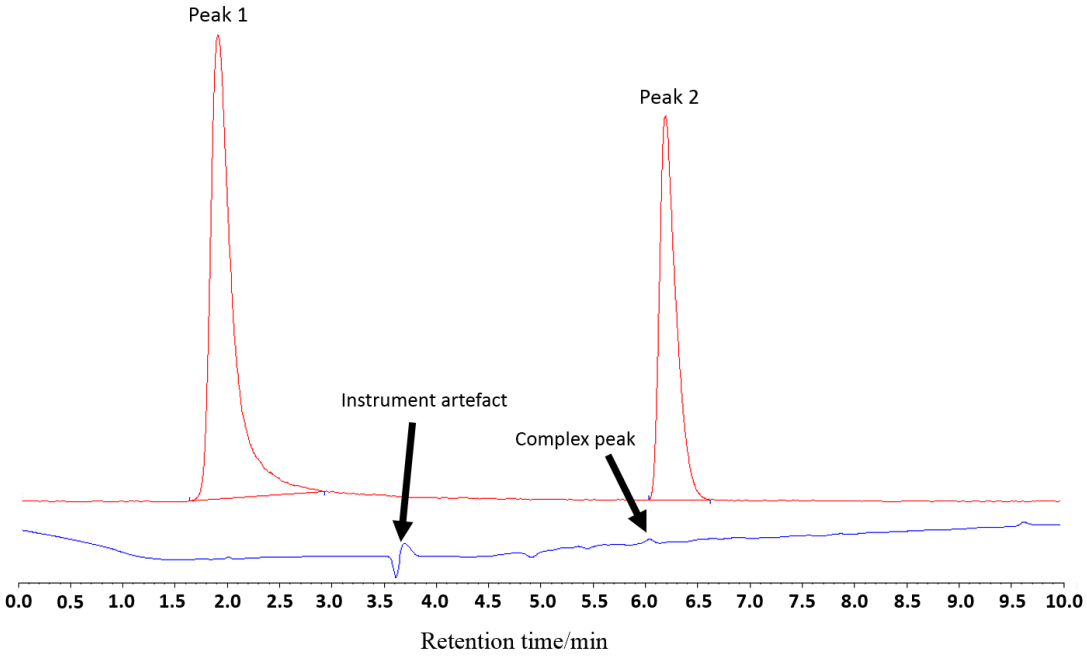

Figure 3.5. Radio-HPLC chromatogram (red) and the corresponding UV-trace (blue) of the crude product from radiofluorination of [GaF_3(BnMe$_2$-tacn)] (0.01 mg, 27 nmol) in 75%/25% MeCN/H_2O at 80 °C for 10 mins. Peak 1: Rt = 2.11 min 62% ($^{18}F^-$). Peak 2: Rt = 6.19 min 38% ([$Ga^{18}F^{19}F_2$(BnMe$_2$tacn)]).

The UV-trace shown in Figures 3.3-3.5 show only one species present and this matches the radioproduct peak. The ^{18}F-radiofluorination at 27 nM concentration of precursor (0.01 mg/mL) is a remarkable decrease of two orders of magnitude compared to the radiofluorination of [MCl_3(BnMe$_2$-tacn)] (M = Al, Ga) by Cl/^{18}F halide exchange reactions[1,43] (Chapter 2). Using the relatively low activity [^{18}F]F^- employed in these experiments (*ca*. 150 MBq), the molar activity determined for the 27 nanomolar precursor concentration was *ca.* 675 MBq/µmol (molar activity is discussed in Chapter 1, sections 1.1 and 1.5). This number is quite low if compared to the molar activity of the radiotracers used in the clinic (100-1000 GBq/µmol) but given the low activity available from the cyclotron (typically 50- 150 MBq in 0.25 mL of ^{18}F-target water) and the possibility of optimised the method, this value could be greatly improved.

Table 3.1 allows us to make other observations: when starting with the same amount of precursor, increasing the amount of organic solvent or the temperature, the RCY increases: from 4 ± 2 % at room temperature to 18 ± 4 % at 80 °C in the mixture 8 % MeCN/H_2O and from 23 ± 4 % in 50 % MeCN/H_2O to 73 ± 4 % in 75 % MeCN/H_2O at 80 °C. Moreover, changing the organic solvent to EtOH slightly increases the RCY.

It is likely that the F/F exchange reaction at the distorted octahedral Ga(III) complex proceeds via a dissociative mechanism, involving a five-coordinate intermediate, [GaF_2(BnMe$_2$-tacn)]$^+$. In order to

test this, the $^{18}F/^{19}F$ isotopic exchange reaction was also performed in the strongly coordinating solvent DMSO. It was expected that the DMSO might quench the intermediate and therefore reduce the RCY. The precursor was dissolved in 0.75 mL of DMSO and 0.25 mL of ^{18}F-target water were added. The mixture was left at 80 °C for 10 minutes and the crude analysed by analytical HPLC (Figure 3.6). The RCY was rather poor (14 %), providing supporting evidence for the dissociative mechanism proposed.

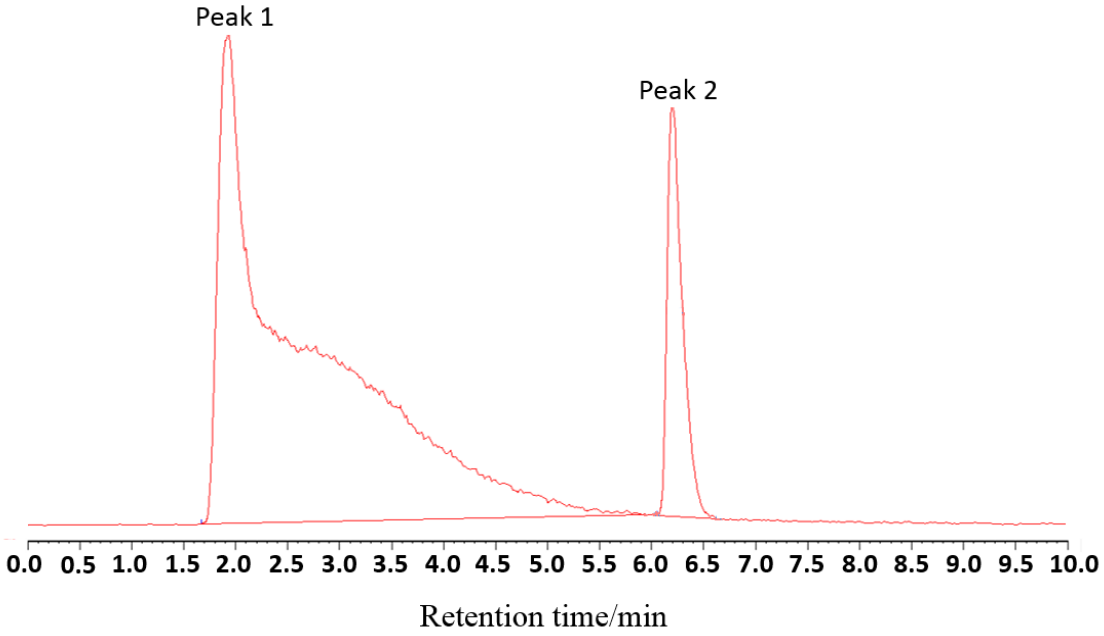

Figure 3.6. Radio-HPLC chromatogram of the crude product from radiofluorination of [GaF_3($BnMe_2$-tacn)] (0.1 mg, 268 nmol) in 75%/25% DMSO/H_2O at 80 °C for 10 mins. Peak 1: Rt = 2.57 min 86% ($^{18}F^-$). Peak 2: Rt = 6.16 min 14% ([$Ga^{18}F^{19}F_2$($BnMe_2$tacn)]). The broad $[^{18}F]F^-$ peak is due to the relatively large amount of $[^{18}F]F^-$ present in solution.

A simple purification protocol was established for the 75 % MeCN(or EtOH)/H_2O system, using a hydrophilic-lipophilic-balanced (HLB) solid-phase extraction (SPE) cartridge (see Experimental Section). The target radio-product was formulated in a mixture of 20 % EtOH/H_2O giving a radiochemical purity (RCP) of ~99% at t = 0. The RCP was monitored over time (typically 2-3 hours) (Figure 3.7).

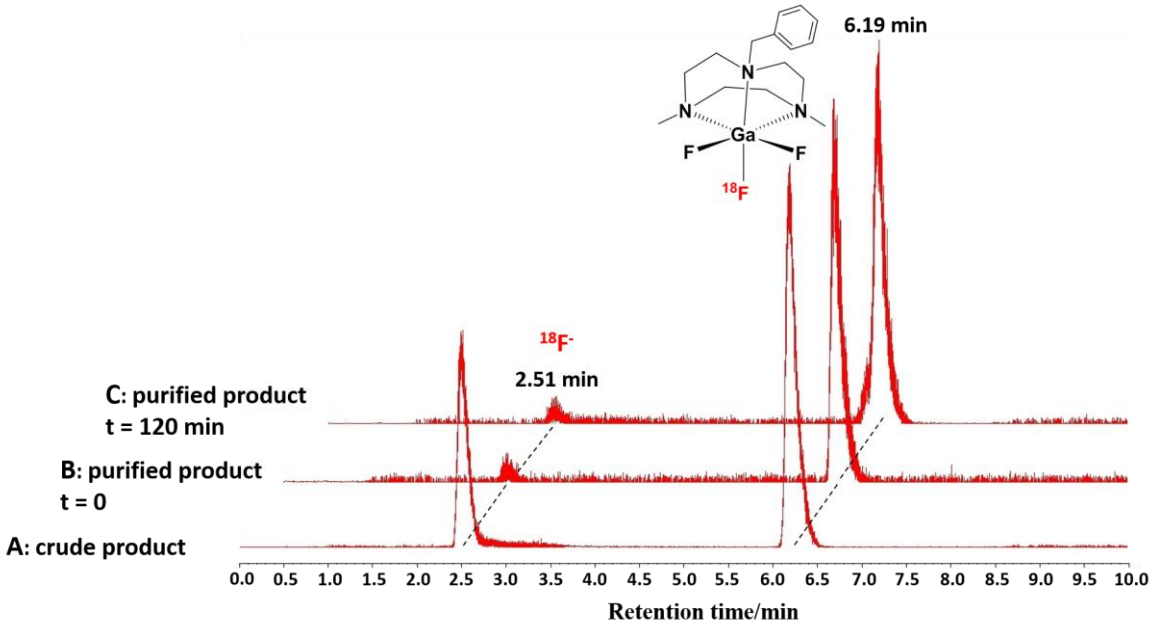

Figure 3.7. A: radio-HPLC chromatogram of the crude product. Peak 1: Rt = 2.51 min 35% ($^{18}F^-$). Peak 2: Rt = 6.19 min 65% ([$Ga^{18}F^{19}F_2$(BnMe$_2$tacn)]); B: radio-HPLC chromatogram of the purified product eluted from a HLB cartridge (in 20% EtOH/H_2O). Peak 1: Rt = 2.49 min 1% ($^{18}F^-$). Peak 2: Rt = 6.18 min 99% ([$Ga^{18}F^{19}F_2$(BnMe$_2$tacn)]); C: radio-HPLC chromatogram of the purified product after 120 minutes (in 20% EtOH/H_2O). Peak 1: Rt = 2.53 min 12% ($^{18}F^-$). Peak 2: Rt = 6.20 min 88% ([$Ga^{18}F^{19}F_2$(BnMe$_2$tacn)]).

It was found that the RCP decreases to between 88% and 77% after 120 min at room temperature, apparently through partial loss of $[^{18}F]F^-$ from the radio-product. The stability of the radioproduct was also tested in 90 % human serum albumin (HSA)/ 10 % EtOH showing a similar behaviour (RCP = 97 % at t = 0; RCP = 83 % at t = 120 min).

3.2.1 Effect of various conditions on the RCP of the formulated [$Ga^{18}F^{19}F_2$(BnMe$_2$-tacn)]

The gradual decrease in the RCP of [$Ga^{18}F^{19}F_2$(BnMe$_2$-tacn)] over time was unexpected. The ^{18}F-radio-product obtained from the Cl/^{18}F halide exchange reaction of [$GaCl_3$(BnMe$_2$-tacn)] showed high stability over time, with a RCP >98 % after 2 hours when formulated in 10 % EtOH/PBS pH 7.4 solution.[1] The radio-product of this reaction, which was also repeated during this work and showed that the complex was stable over at least 2 hours (Chapter 2), is chemically identical to the one obtained from the $^{18}F/^{19}F$ isotopic exchange reaction, i.e. [$Ga^{18}F^{19}F_2$(BnMe$_2$-tacn)]. Since ΔG for the isotopic exchange is ~ 0, and some (~ 8 %) $[^{18}F]F^-$ incorporation is seen at room temperature (with much higher incorporation at 80 °C over a similar time-scale), the following equilibrium reaction must apply:

$$[Ga^{18}F^{19}F_2(BnMe_2\text{-tacn})] + {}^{19}F^- \leftrightarrows [Ga^{19}F_3(BnMe_2\text{-tacn})] + {}^{18}F^-$$

This means that some of the $[^{18}F]F^-$ incorporated into the complex is exchanging back with $[^{19}F]F^-$ or other species present in solution. Another possibility for the decrease in RCP might be instability due to radiolysis.

In order to probe these aspects and find a possible explanation for the lower RCP over time from the isotopic exchange reaction compared to the Cl/F exchange, the effect on the RCP of T, pH, excess of anions in solution (F^-, Cl^- and OH^-), and presence of ascorbic acid (this is used as a stabiliser since it can absorb possible radicals present in solution, see Chapter 1 section 1.5 and below for further details) or $Ca(NO_3)_2$ (in an attempt to remove excess $[^{19}F]F^-$ from the solution forming CaF_2) was investigated.

- **Effect of temperature**

Since the isotopic exchange is an equilibrium reaction (equation above), a decrease in the temperature should lead to a decrease in the exchange rate. Indeed, it was observed that the RCP could be maintained above 93 % over 240 minutes when the formulated product (20 % EtOH/water) was kept at −20 °C (Figure 3.8).

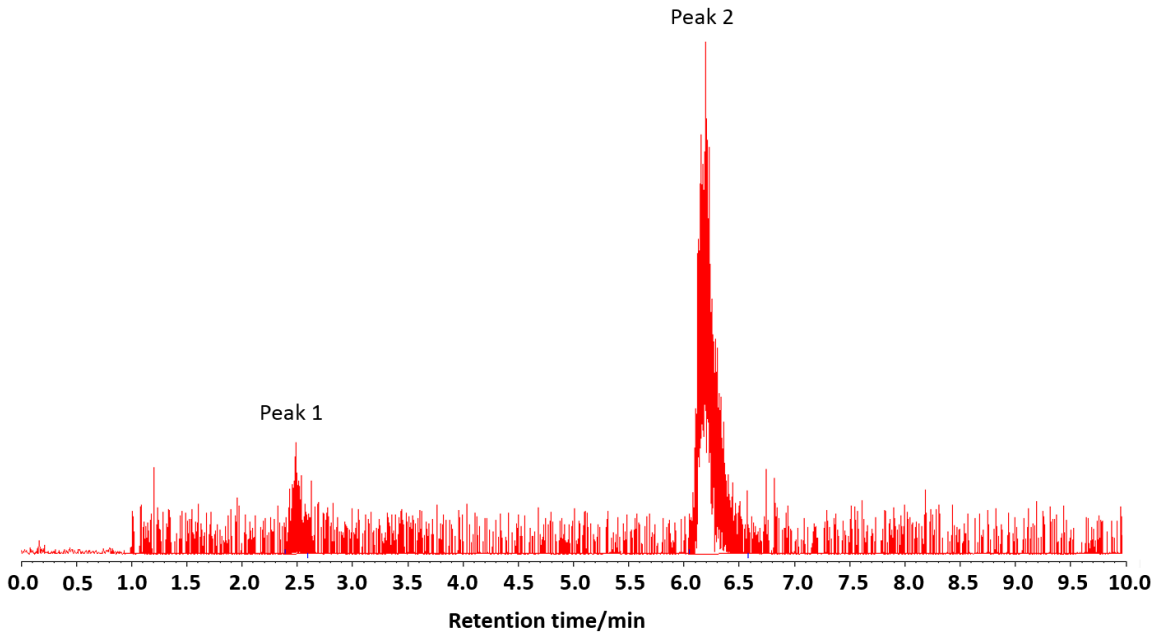

Figure 3.8. radio-HPLC chromatogram of the purified product after storing at −20 °C for 240 minutes (in 20% EtOH/H_2O). Peak 1: Rt = 2.51 min 6% ($^{18}F^-$). Peak 2: Rt = 6.21 min 94% ($[Ga^{18}F^{19}F_2(BnMe_2\text{-tacn})]$).

- **Effect of anions present in solution**

If the $[^{18}F]F^-$ incorporated into the radio-product is replaced by other competitive anions in solution, an excess of them should lead to a further decrease in the RCP. It is also worth noting that the $[^{18}F]F^-$ concentration in the target water is already negligible compared to the concentration of $[^{19}F]F^-$ (13 GBq corresponds to 0.2 nmol of $[^{18}F]F^-$,[44] with the main source of inactive fluoride being the tubing

system in the loading and delivery of [^{18}O]water in the cyclotron, which is often made of Teflon[45]). The effect of an excess of competitive anions fluoride, chloride and hydroxide, was tested. Samples of [Ga^{18}F^{19}F$_2$(BnMe$_2$-tacn)], after elution from the cartridge (EtOH), were formulated in a 10 % KF solution, 0.9 % saline or a 20 % NaOH solution as they are common impurities in the ^{18}F-target water and may be exchanging with the [^{18}F]F$^-$ of the complex (see experimental section). The RCP measured after 2 hours for these solutions was 82 (Figure 3.9), 80 and 83 %, respectively, hence no significant effect on the RCP was observed in comparison with the RCP of the product formulated in 20 % EtOH/water.

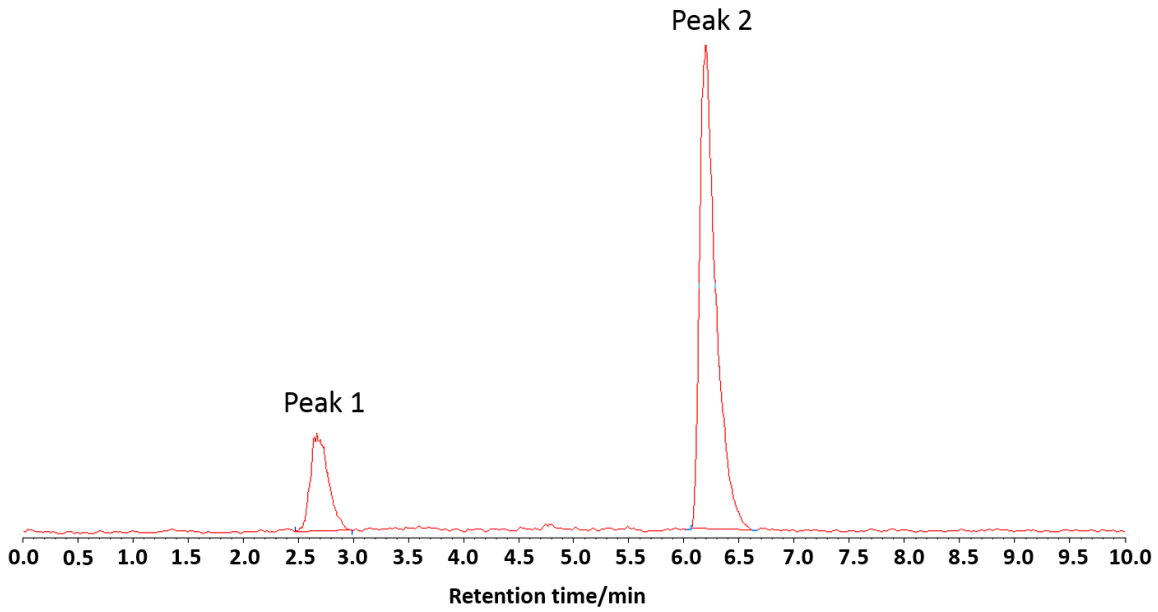

Figure 3.9. radio-HPLC chromatogram of the purified product eluted from a HLB cartridge and formulated in EtOH/10% KF solution. Peak 1: Rt = 2.68 min 18% (^{18}F$^-$). Peak 2: Rt = 6.20 min 82% ([Ga^{18}F^{19}F$_2$(BnMe$_2$tacn)]).

- **Effect of pH**

Since previous work showed that the ^{18}F-radiofluorinated complex [GaF(Bn(CH$_2$COO)$_2$-tacn)] was stable at pH 6 and unstable at pH 7.5,[46] the effect of the pH on [Ga^{18}F^{19}F$_2$(BnMe$_2$-tacn)] produced via F/F exchange was also tested. The purified [Ga^{18}F^{19}F$_2$(BnMe$_2$-tacn)] was formulated at two pH conditions: pH 4 (NaOAc buffer) and pH 7.4 (PBS buffer). The RCP of the sample at neutral pH was similar after 2 hours to the values obtained in normal conditions (77 %, Figure 3.10) whereas the RCP of the sample at pH 4 was significantly lower (55 %, Figure 3.11).

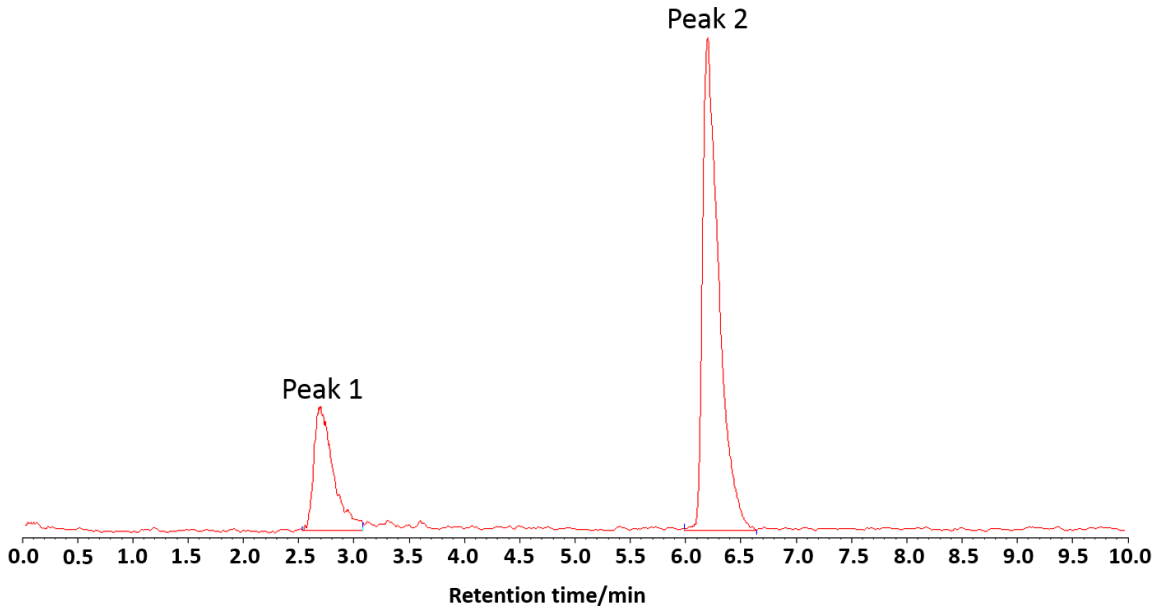

Figure 3.10. radio-HPLC chromatogram of the purified product eluted from a HLB cartridge and formulated in EtOH/PBS pH 7.4 solution. Peak 1: Rt = 2.69 min 23% ($^{18}F^-$). Peak 2: Rt = 6.20 min 77% ([$Ga^{18}F^{19}F_2$(BnMe$_2$tacn)]).

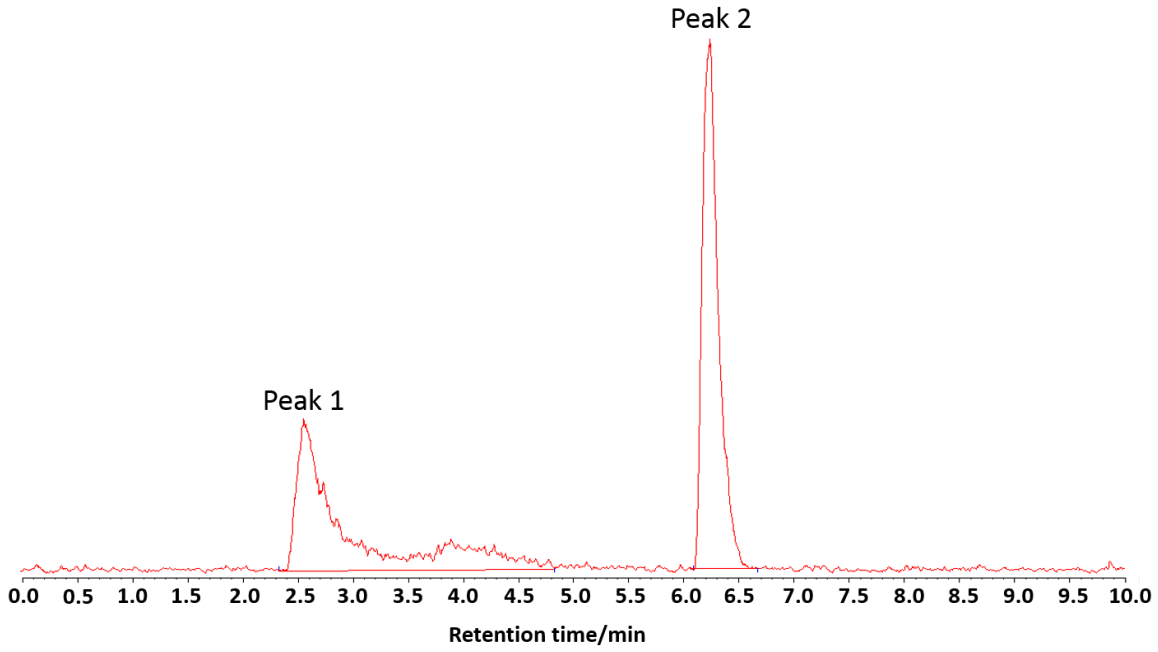

Figure 3.11. radio-HPLC chromatogram of the purified product eluted from a HLB cartridge and formulated in EtOH/pH 4 solution. Peak 1: Rt = 2.58 min 45% ($^{18}F^-$). Peak 2: Rt = 6.24 min 55% ([$Ga^{18}F^{19}F_2$(BnMe$_2$tacn)]).

The radio-product is more stable at neutral pH, whereas the acidic conditions destabilises the radio-product.

- **Effect of ascorbic acid and $Ca(NO_3)_2$**

$Ca(NO_3)_2$ was added in an attempt to reduce the amount of $[^{19}F]F^-$ in solution (*via* precipitation of the very poorly soluble CaF_2 which has a solubility product of 3.9×10^{-11}). The salt was added either before or after formulation of the product (20 % EtOH/water), but in both cases it had no effect on the RCP, with values between 76 and 88 % observed.

Ascorbic acid is a known stabiliser in case of instability of the radio-product due to radiolysis (see Chapter 1 section 1.5).[47,48,49] If radiolysis were the problem in this systems, the RCP of $[Ga^{18}F^{19}F_2(BnMe_2\text{-tacn})]$ formulated in ascorbic acid would not be expected to decrease over time. On the contrary, the observed RCP was 48 % after 2 hours (Figure 3.12).

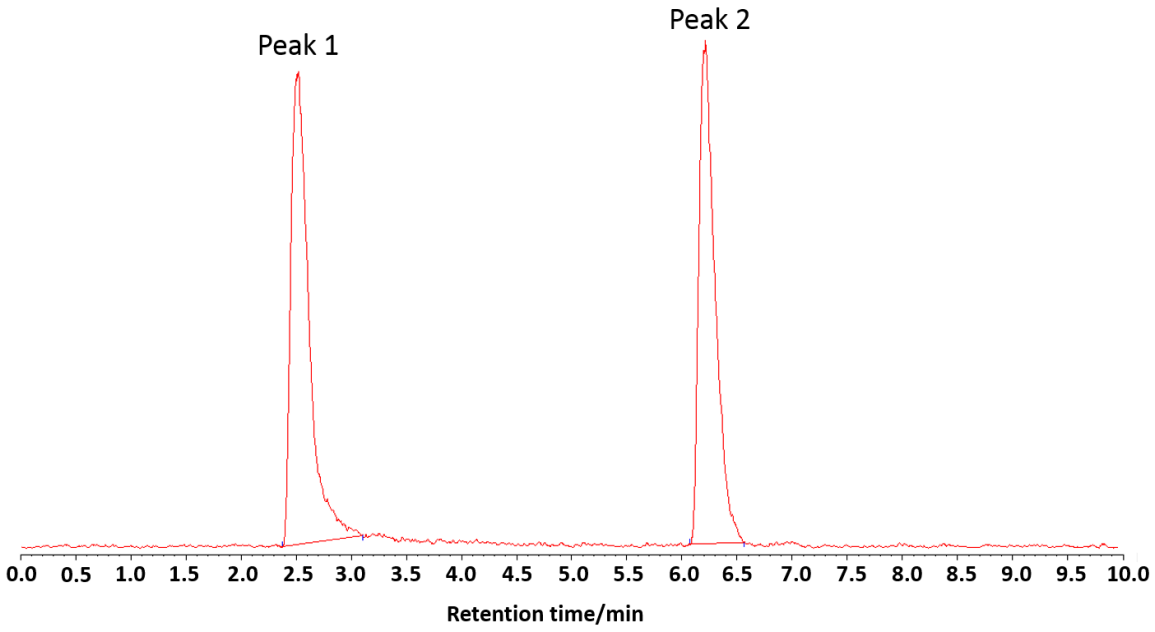

Figure 3.12. radio-HPLC chromatogram of the purified product eluted from a HLB cartridge and formulated in 50% EtOH/ascorbic acid solution. Peak 1: Rt = 2.58 min 45% ($^{18}F^-$). Peak 2: Rt = 6.24 min 55% ($[Ga^{18}F^{19}F_2(BnMe_2tacn)]$).

3.2.2 Stability tests on $[Ga^{19}F_3(Me_3\text{-tacn})]$ via $^{19}F\{^1H\}$ NMR spectroscopy

The stability of the inactive complex $[GaF_3(Me_3\text{-tacn})]$ was challenged in the presence of various competitive anions, from pH 4 to pH 11, at elevated temperature and against time on a preparative scale. The experiments were carried out in D_2O and followed by $^{19}F\{^1H\}$ NMR spectroscopy. The stability tests were performed on $[GaF_3(Me_3\text{-tacn})]$, as the ligand can be synthesised in higher yields compared to $BnMe_2$-tacn and it is likely to behave in the same way as the benzyl analogue. The $^{19}F\{^1H\}$ NMR spectrum for $[GaF_3(Me_3\text{-tacn})]$ was acquired and used as reference (Figure 3.13)

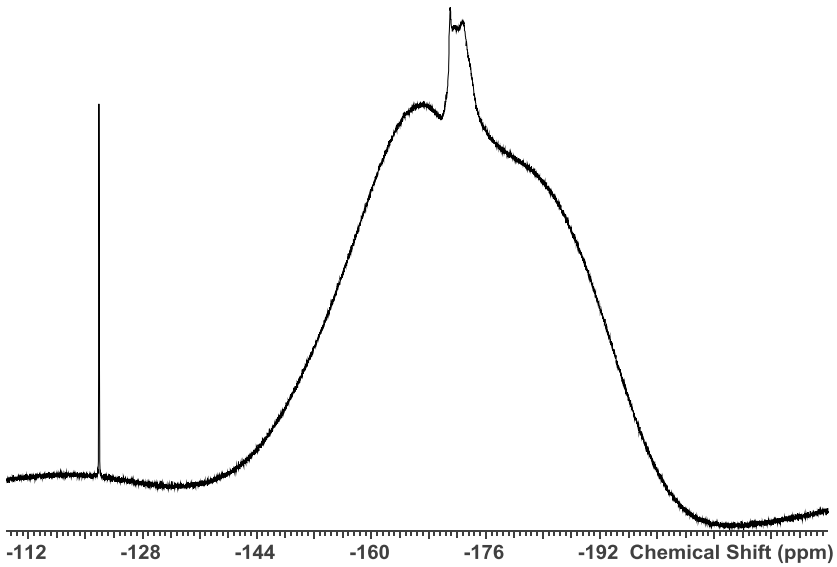

Figure 3.13. $^{19}F\{^{1}H\}$ NMR spectra of $[GaF_3(Me_3\text{-tacn})]$ in D_2O. The rolling baseline is due to the Teflon in the probe.

Figure 3.13 shows the resonance of $[GaF_3(Me_3\text{-tacn})]$ as a broad peak at −172.6 ppm (which matches the value reported in the literature[1]) with no resolved $^{1}J_{Ga\text{-}F}$ coupling. The resonance is broad as the fluorine nuclei are interacting with the two NMR active nuclei ^{69}Ga and ^{71}Ga (both have I = 3/2) and each should give a four-line pattern if coupling were observed. The sharp resonance at −122.7 ppm is due to F^-, a feature often seen in fluorine chemistry. The stability of the complex to competitive anions was tested in the presence of a 10-fold excess of CO_3^{2-}, PO_4^{3-}, $CH_3CO_2^-$, F^-, Cl^-, which were added as sodium salts or potassium (KF). The $^{19}F\{^{1}H\}$ NMR spectra were unchanged upon addition of the salts (Figure 3.14).

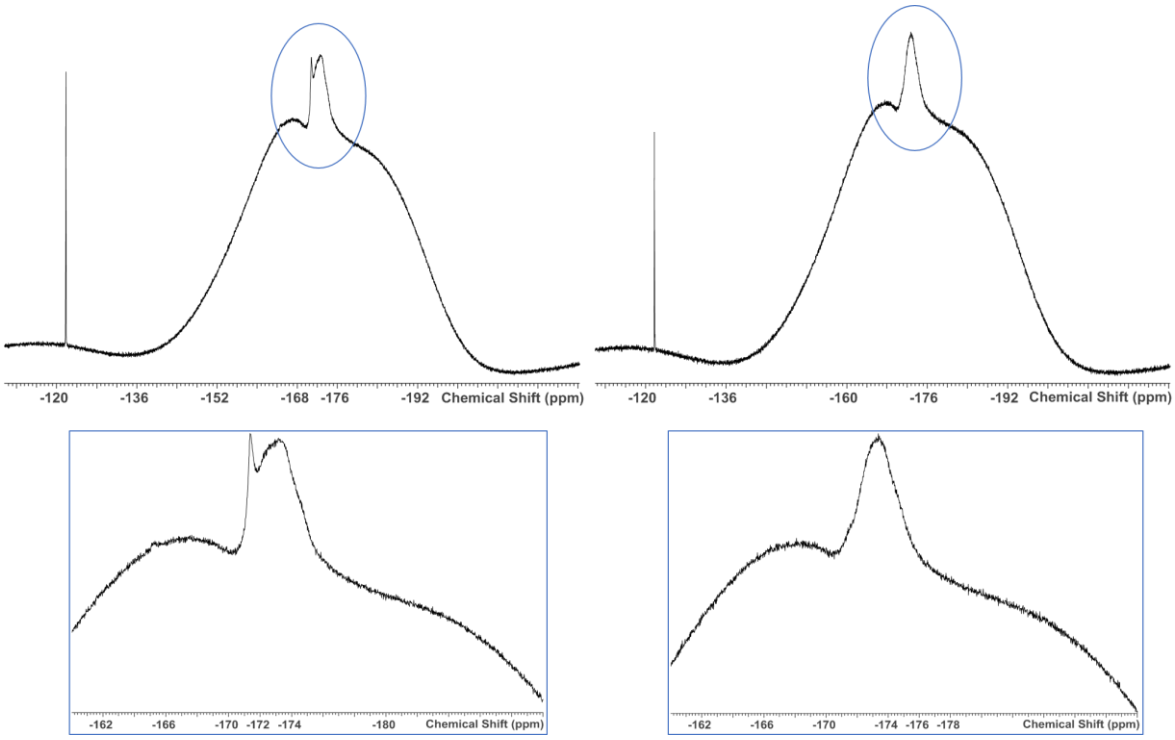

Figure 3.14. Top: $^{19}F\{^{1}H\}$ NMR spectra of $[GaF_3(Me_3\text{-tacn})]$ in the presence of a 10-fold excess of NaCl (left) and in the presence of a 10-fold excess of Na_3PO_4 (right). Bottom: Enlargement of the $^{19}F\{^{1}H\}$ NMR spectra of $[GaF_3(Me_3\text{-tacn})]$ in the presence of a 10-fold excess of NaCl (left) and in the presence of a 10-fold excess of Na_3PO_4 (right).

The stability of the complex in the presence of excess KF was also tested at higher temperatures (40 °C, 60 °C and 80 °C). $[GaF_3(Me_3\text{-tacn})]$ proved to be stable, not only in the presence of a large excess of fluoride anions at room temperature, but also at higher temperature (up to 80 °C). The relative intensity of the F^- and complex peak obviously changes upon addition of KF, but their chemical shifts remain the same throughout the experiment. The appearance of another unidentified small peak at −166.3 ppm is also observed (~ 10-15 %, from integration of the peak against the complex peak, [although the presence of the broad feature due to the Teflon in the probe makes the integration unreliable]). Interestingly, increasing the temperature the resonance of the complex resolves, showing a *pseudo*-quartet at 80 °C (Figure 3.15) due to the coupling to the two NMR active gallium isotopes (^{69}Ga and ^{71}Ga, both I = 3/2 and 60.1 and 30.6 % abundance, respectively) from the overlapping of the two very close four-line patterns, which result in a broad quartet. The *pseudo*-quartet is also observed at room temperature when the experiment is carried out in CD_3CN instead of D_2O,[1] indicating that the system is solvent dependant (this is also very common in fluorine chemistry).

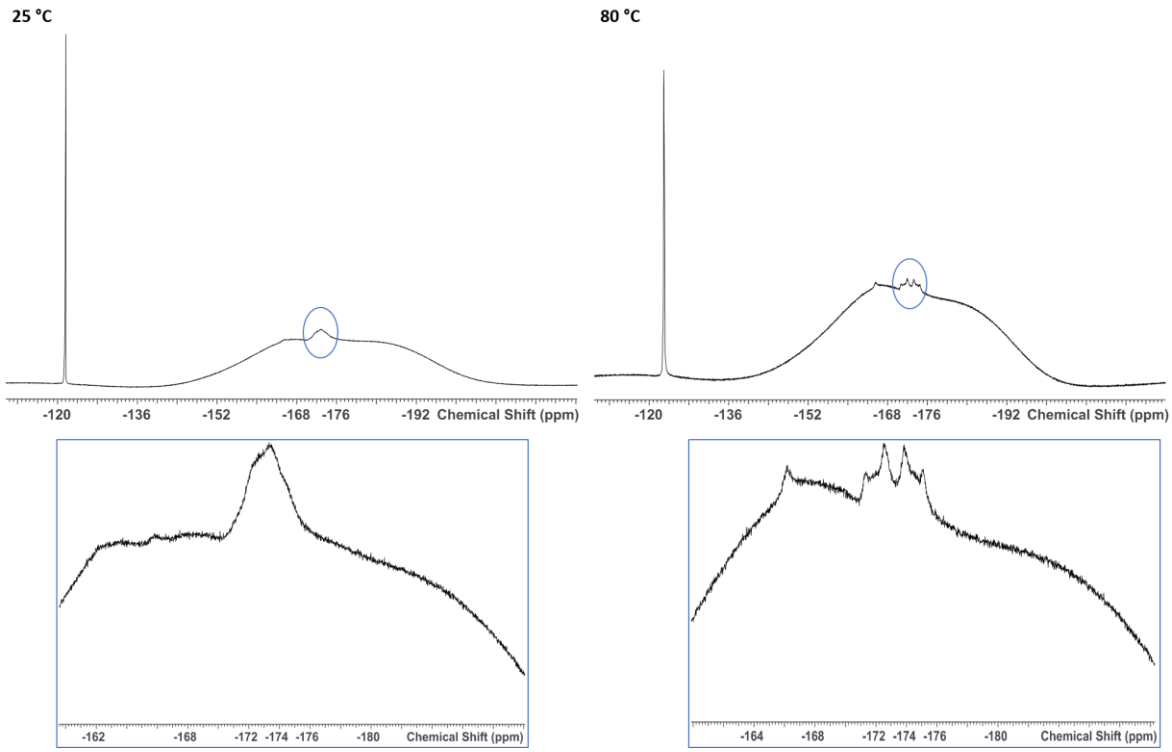

Figure 3.15. Top: $^{19}F\{^{1}H\}$ NMR spectra of [GaF_3(Me_3-tacn)] in the presence of a 10-fold excess of KF (left) at 25 °C and at 80 °C (right). Bottom: Enlargement of the [GaF_3(Me_3-tacn)] peak at 25 °C (left) and at 80 °C (right).

The trifluoro-complex also shows a very good pH tolerance, with no detectable degradation between pH 4-11 (Figure 3.16).

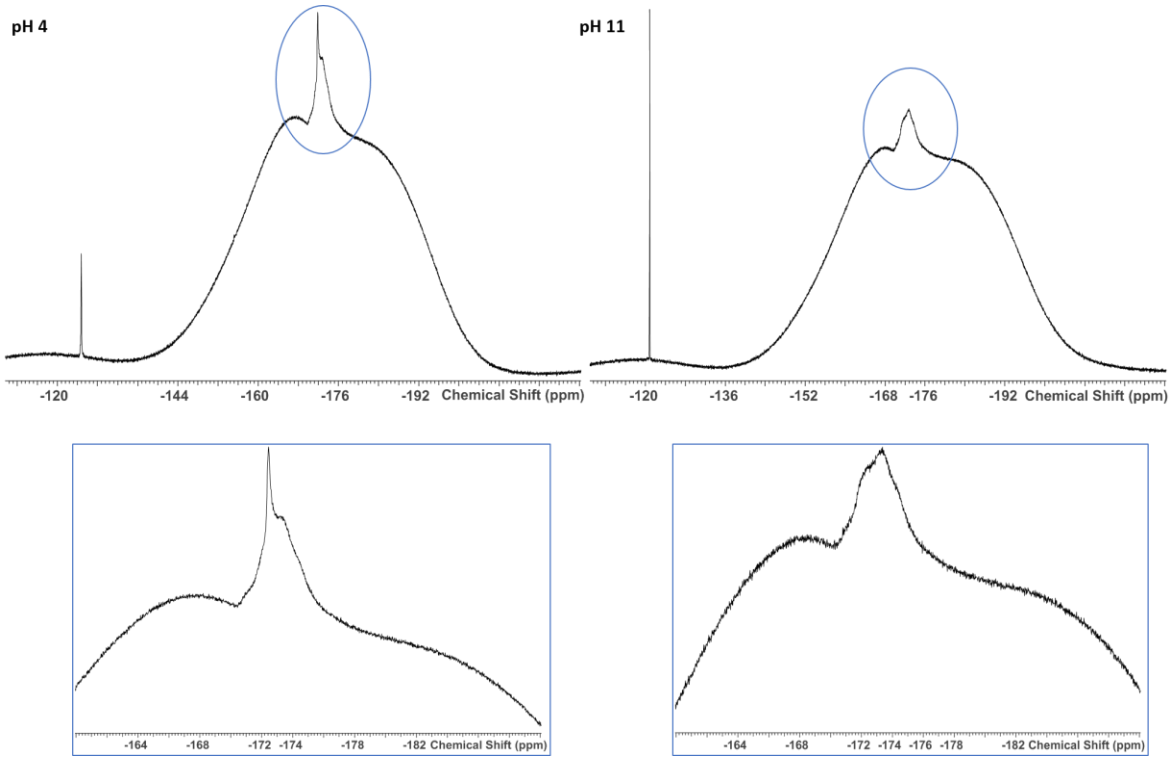

Figure 3.16. Top: $^{19}F\{^{1}H\}$ NMR spectra of [GaF_3(Me_3-tacn)] at pH 4 (left) and pH 11 (right). Bottom: Enlargement of the $^{19}F\{^{1}H\}$ NMR of [GaF_3(Me_3-tacn)] at pH 4 (left) and pH 11 (right).

[$GaF_3(Me_3$-tacn)] proved to be stable after heating at 80 °C for 2 hours as well as in D_2O solution for 1 week, with the $^{19}F\{^1H\}$ NMR spectrum unchanged (Figure 3.17).

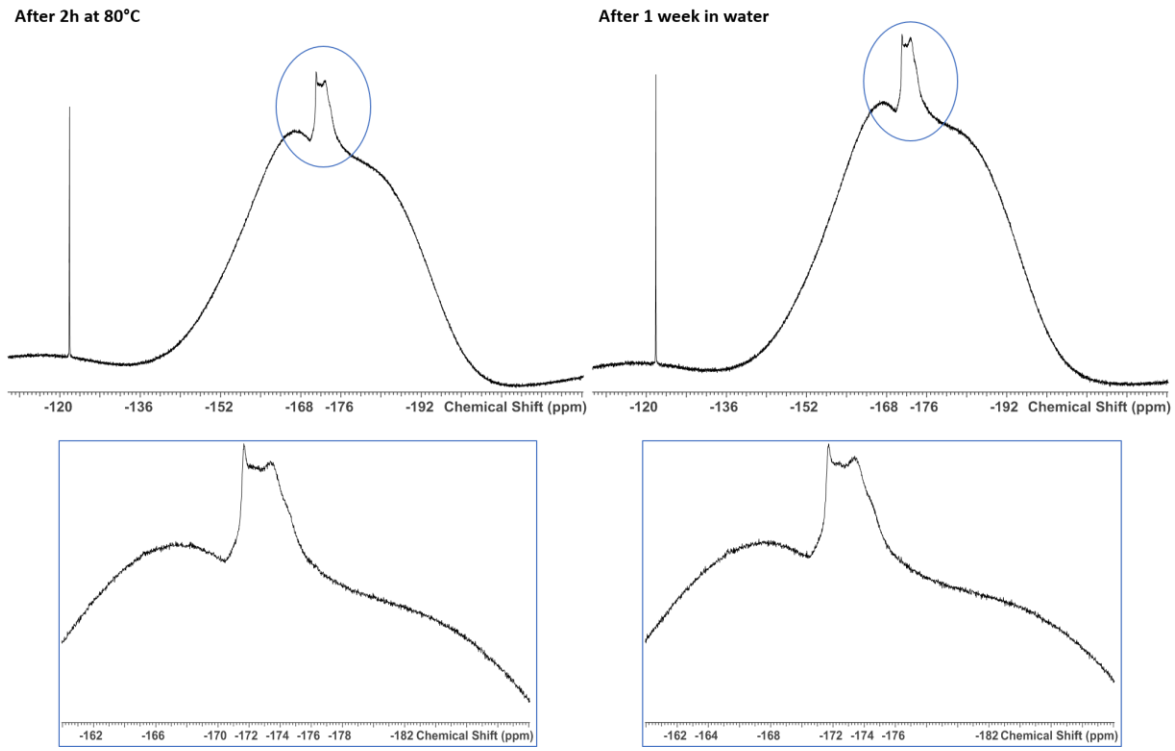

Figure 3.17. $^{19}F\{^1H\}$ NMR spectra of [$GaF_3(Me_3$-tacn)] acquired after the sample was kept at 80 °C for 2 hours (left) and after 1 week in water solution (right).

The line width and resolution of the complex peak changed in some of the spectra. This is almost certainly due to different effects of the solvents (secondary coordination sphere) broadening the resonances rather than any chemical change. Solvent effects of this type are common in polar M-F bond systems. Moreover, the presence of other minor species which are not detectable due to broadness of the complex resonance or underlying the Teflon very broad feature, should not be excluded.

3.3 Conclusions and future work

[GaF_3($BnMe_2$-tacn)] was successfully ^{18}F-labelled through $^{18}F/^{19}F$ isotopic exchange reactions. This is the first example of an isotopic exchange reaction on a metal-chelate based system. The precursor can be radiolabelled rapidly in high radiochemical yields (66-77 %) in 75 % MeCN aqueous solution and with moderate heating (80 °C), using directly $[^{18}F]F^-$ target water from the cyclotron. The reaction does not need a Lewis acid promoter. It was shown that the method allows the concentration of the precursor used for the radiofluorination to be scaled down by at least two orders of magnitude (27 nM, 0.01 mg), representing a very significant decrease in the quantity of material needed compared to the $Cl/^{18}F$ exchange reaction on [$GaCl_3$($BnMe_2$-tacn)]. These aspects suggest that [GaF_3($BnMe_2$-tacn)] offers a promising basis for the development of PET probes.

The $^{18}F/^{19}F$ isotopic exchange in 75 % DMSO/water solution lead to the formation of the target product in a much lower RCY (14 *vs.* ~70 %). This suggests some quenching of the reaction due to the more competitive (strongly coordinating) solvent, and is consistent with the isotopic exchange occurring via a dissociative mechanism involving a five-coordinate Ga(III) intermediate. A dissociative mechanism also explains why the RCP of the purified complex, [$Ga^{18}F^{19}F_2$($BnMe_2$-tacn)], is not effected by the presence of an excess of $^{19}F^-$ anions or other competitive anions such as Cl^- or OH^- (dissociative mechanisms proceed through first-order kinetics and hence, independent of the entering group).

A simple and effective solid-phase extraction (SPE) purification method using an HLB cartridge was established allowing the target product [$Ga^{18}F^{19}F_2$($BnMe_2$-tacn)] (formulated in a 20 % EtOH/water solution) to be obtained in 99 % RCP. However, in contrast to the chemically identical radio-product obtained from the $Cl/^{18}F$ halide exchange using [$GaCl_3$($BnMe_2$-tacn)], a noticeable decrease in the RCP over time was observed, leading to values between 88 and 77 % after 120 minutes at room temperature. Several experiments were carried out in order to try to investigate this further. The RCP was maintained >90 % when the purified product was kept at −20 °C; however, an excess of fluoride, hydroxide or chloride anions did not affect the RCP. Formulating the purified radio-product in EtOH/NaOAc pH 4 solution caused a further decrease in the RCP. Moreover, the possibility of radiolysis was also explored, both by formulating the purified product in 10 % EtOH/PBS (pH 7.4) and by addition of ascorbic acid: neither had any appreciable effect.

The stability tests performed on [GaF_3(Me_3-tacn)] confirmed that the complex is very robust. Solution $^{19}F\{^1H\}$ NMR studies demonstrated that [GaF_3(Me_3-tacn)] is very stable in water over time (at least a week in solution) and at elevated temperature (2 hours at 80 °C). This is in contrast to the [$GaCl_3$(RMe_2-tacn)] (R = Bn, Me) complexes which hydrolyse within minutes when small amounts of water are added to a solution of the complex in MeCN at room temperature. The

trifluoro-complex is also tolerant to a wide pH range (4-11) and stable to the presence of a 10-fold excess of several physiologically relevant anions added as their sodium salts (CO_3^{2-}, PO_4^{3-}, $CH_3CO_2^-$, F^-, Cl^-).

Considering all the experiments performed, the explanation for the RCP decay remains unclear and will need further study. Ultimately, the complex will be conjugated to a biomolecule, which may also affect the properties and lead to a more stable system. In this regard, as part of the future work, the conjugation of peptide such as PSMA (prostate-specific membrane antigen, overexpressed in prostate cancer) or folate (overexpressed on the surface of ovarian cancers) to [$Ga^{18}F^{19}F_2$(BnMe_2-tacn)] will be explored. These biomolecules will be attached to the metal-based complex through the benzyl group, which can be conveniently functionalised for this purpose using standard methods, and the *in vitro* and *in vivo* stability of the systems will be studied. The use of more sterically bulky tacn derivatives will be also considered to provide protection around the Ga(III) centre.

3.4 Experimental

Details regarding the instrumentation used are reported in Appendix 1.

3.4.1 $[GaF_3(OH_2)_2(DMSO)]$

The complex was prepared as reported in Chapter 4 (section 4.4.5) and in the literature.[50]

3.4.2 $[GaF_3(BnMe_2\text{-tacn})]$

$[GaF_3(OH_2)_2(DMSO)]$ (0.040 g, 0.16 mmol) was suspended in 5 mL of CH_2Cl_2. A solution of $BnMe_2$-tacn (0.041 g; 0.016 mmol) in 3 mL of CH_2Cl_2 was added. After 10 min the solution became clear. The reaction mixture was left stirring for a further hour at room temperature. The solvent was then reduced to ~ 4 mL and 15 mL of hexane was added, causing the precipitation of a white solid, which was filtered, washed with hexane (5 mL) and dried *in vacuo* (0.054 g; 87 %). Spectroscopic data match that reported.[1] ^{1}H NMR (D_2O, 298 K): 7.52-7.45 (m, [5H], ArH), 4.16 (s, [2H], Ar-CH_2), 3.30-3.22 (m, [2H], tacn-CH_2), 3.06-2.90 (m, [8H], tacn-CH_2), 2.72 (s, [6H], CH_3), 2.60-2.53 (m, [2H], tacn-CH_2). $^{19}F\{^1H\}$ NMR (D_2O, 298 K): −172.5 (br). ^{71}Ga NMR (D_2O, 298 K): +44.3 (br). ES^+ MS (MeCN/H_2O): *m/z* = 380 ($[GaF_3(BnMe_2\text{-tacn})+Li]^+$), 354 ($[GaF_2(BnMe_2\text{-tacn})]^+$).

HPLC purification: Column: Waters XBridge Prep Shield RP18, 5 um, 10 x 100 mm (p/n 186003258, s/n 115/123411KK01); Dionex Ultimate 3000 pump; Knauer Smartline 2500 UV detector. $[GaF_3(BnMe_2\text{-tacn})]$ (7.3 mg) was dissolved in 4 mL of water and injected onto the prep. HPLC loop (mobile phase A = 100% water; B = 100% MeCN). Flow rate 3 mL min^{-1}. Gradient 0 to 10 min (0-10% B), 10-15 min (10-90% B), 15-20 min (90% B), 20-25 min (90-2% B). 6.0 mg of purified $[GaF_3(BnMe_2\text{-tacn})]$ was obtained.

3.4.3 $^{18}F/^{19}F$ Isotopic exchange radiolabelling procedure

In a typical experiment, $[GaF_3(BnMe_2\text{-tacn})]$ (1 mg, 2.68 μM, 0.1 mg, 268 nM or 0.01 mg, 27 nM) was dissolved in MeCN (n = 18) or EtOH (n = 5) (0.75 mL). To this solution was added 0.25 mL of an aqueous solution containing $[^{18}F]F^-$ (10-200 MBq) and the vial was heated to 80 °C for 10 mins. The crude reaction solution was diluted with water (20 mL) so that approximately 10% of the solvent composition was organic. A small sample (~ 100 uL) of the diluted crude reaction solution was removed for analysis by analytical HPLC, which confirmed the percentage incorporation of ^{18}F into the metal complex (based upon integration of the radio peaks). [Note that 8 % ^{18}F incorporation was observed when the radiolabelling experiment was performed at 2.36 μM concentration in MeCN/H_2O (75:25) at room temperature.

3.4.4 $^{18}F/^{19}F$ Isotopic exchange radiolabelling procedure in DMSO

[GaF_3($BnMe_2$-tacn)] (0.1 mg, 268 nmol) was dissolved in DMSO (0.75 mL). To this solution was added 0.25 mL of an aqueous solution containing [^{18}F]F^- (62 MBq) and the vial was heated to 80 °C for 10 mins. The crude reaction was diluted with 1 mL of water. A small sample (~ 100 uL) of the diluted crude reaction solution was removed for analysis by analytical HPLC, giving a RCY of 14 %.

3.4.5 SPE purification protocol

The diluted reaction mixture was then trapped on a HLB cartridge, washed with water (5 mL x 3) to remove the $^{18}F^-$ and residual MeCN and eluted from the cartridge with ethanol (1 mL) into water or pH 7.4 PBS (4 mL) to result in a formulated product in 80:20 water (or pH 7.4 PBS):EtOH. The formulated product was analysed by HPLC at t = 0 and various time intervals up to 240 mins.

3.4.6 Analytical HPLC method

Column: Phenomenex Luna 5 um C18(2) 250 x 4.6 mm. Mobile phase A = 10 mM ammonium acetate, B = MeCN. Flow rate 1 mL min^{-1}. Gradient 0-15 min (10-90 % B), 15-20 min (90 % B), 20-21 min (90-10 % B), 21-26.5 min (10 % B).

3.4.7 Addition of saline, KF, OH^- solutions to the SPE purified radiolabelled product

Radiolabelling experiment and SPE purification protocol performed as reported above (0.1 mg of [GaF_3($BnMe_2$-tacn)], MeCN). The product was eluted from the cartridge with 1.6 mL of EtOH and this volume divided into three vials. A 0.9 % saline solution, a 10 % KF solution and a 20 % NaOH solution were added (one for each vial). The RCP of the solutions was checked after 120 minutes by analytical HPLC giving a RCP value of 80, 82 and 83 % respectively.

3.5 References

1. Bhalla, R.; Darby, C.; Levason, W.; Luthra, S. K.; McRobbie, G.; Reid, G.; Sanderson, G.; Zhang, W., *Chem. Sci.* **2014**, *5*, 381.

2. Speight, J. G., *Lange's Handbook of Chemistry, 17th Edition; Section 1,* **2017**.

3. Chansaenpak, K.; Vabre, B.; Gabbai, F. P., *Chem. Soc. Rev.* **2016**, *45*, 954.

4. Bernard-Gauthier, V.; Bailey, J. J.; Liu, Z.; Wangler, B.; Wangler, C.; Jurkschat, K.; Perrin, D. M.; Schirrmacher, R., *Bioconjugate Chem.* **2016**, *27*, 267.

5. Gens, T. A.; Wethington Jr., J. A.; Brosi, A. R., *J. Phys. Chem.* **1958**, *62*, 1593.

6. Poole, R. T.; Winfield, J. M., *J. Chem. Soc., Dalton Trans.* **1976**, 1557.

7. Entzian, W.; Aronow, S.; Soloway, A. H.; Sweet, W. H., *J. Nucl. Med.* **1964**, *5*, 542.

8. Askenasy, H. M.; Anbar, M.; Laor, Y.; Lewitus, Z.; Kosay, I. Z.; Guttmann, S., *Am. J. Roentgenol.* **1962**, *88*, 350.

9. Ting, R.; Adam, M. J.; Ruth, T. J.; Perrin, D. M., *J. Am. Chem. Soc.* **2005**, *127*, 13094.

10. Schirrmacher, R.; Bradtmoller, G.; Schirrmacher, E.; Thews, O.; Tillmanns, J.; Siessmeier, T.; Buchholz, H. G.; Bartenstein, P.; Wangler, B.; Niemeyer, C. M.; Jurkschat, K., *Angew. Chem. Int. Ed.* **2006**, *45*, 6047.

11. Jauregui-Osoro, M.; Sunassee, K.; Weeks, A. J.; Berry, D. J.; Paul, R. L.; Cleij, M.; Banga, J. P.; O'Doherty, M. J.; Marsden, P. K.; Clarke, S. E.; Ballinger, J. R.; Szanda, I.; Cheng, S. Y.; Blower, P. J., *EJNMMI* **2010**, *37*, 2108.

12. Khoshnevisan, A.; Jauregui-Osoro, M.; Shaw, K.; Torres, J. B.; Young, J. D.; Ramakrishnan, N. K.; Jackson, A.; Smith, G. E.; Gee, A. D.; Blower, P. J., *EJNMMI* **2016**, *6*, 34.

13. O'Doherty, J.; Jauregui-Osoro, M.; Brothwood, T.; Szyszko, T.; Marsden, P. K.; O'Doherty, M. J.; Cook, G. J. R.; Blower, P. J.; Lewington, V., *J. Nucl. Med.* **2017**, *58*, 1666.

14. Liu, Z.; Li, Y.; Lozada, J.; Wong, M. Q.; Greene, J.; Lin, K. S.; Yapp, D.; Perrin, D. M., *Nucl. Med. Biol.* **2013**, *40*, 841.

15. Li, Z.; Chansaenpak, K.; Liu, S.; Wade, C. R.; Conti, P. S.; Gabbaï, F. P., *Med. Chem. Commun.* **2012**, *3*, 1305.

16. Chansaenpak, K.; Wang, M.; Wu, Z.; Zaman, R.; Li, Z.; Gabbai, F. P., *Chem Commun.* **2015**, *51*, 12439.

17. Liu, S.; Lin, T. P.; Li, D.; Leamer, L.; Shan, H.; Li, Z.; Gabbai, F. P.; Conti, P. S., *Theranostics* **2013**, *3*, 181.

18. Liu, S.; Li, D.; Shan, H.; Gabbai, F. P.; Li, Z.; Conti, P. S., *Nucl. Med. Biol.* **2014**, *41*, 120.

19. Wade, C. R.; Zhao, H.; Gabbai, F. P., *Chem Commun.* **2010**, *46*, 6380.

20. Liu, Z.; Pourghiasian, M.; Radtke, M. A.; Lau, J.; Pan, J.; Dias, G. M.; Yapp, D.; Lin, K. S.; Benard, F.; Perrin, D. M., *Angew. Chem. Int. Ed.* **2014**, *53*, 11876.

21. Luo, Y. R., *Handbook of Chemical Bond Energies,* CRC Press, **2007**.

22. Winfield, J. M., *J. Fluorine Chem.* **1980**, *16*, 1.

23. Fry, B. W.; Whitford, G. M.; Pashley, D. H., *The International Journal of Applied Radiation and Isotopes* **1978**, *29*, 123.

24. Rosenthal, M. S.; Bosch, A. L.; Nickles, R. J.; Gatley, S. J., *The international Journal of Applied Radiation and Isotopes* **1985**, *36*, 318.

25. Pilcher, A. S.; Ammon, H. L.; DeShong, P., *J. Am. Chem. Soc.* **1995**, *117*, 5166.

26. Mu, L.; Hohne, A.; Schubiger, P. A.; Ametamey, S. M.; Graham, K.; Cyr, J. E.; Dinkelborg, L.; Stellfeld, T.; Srinivasan, A.; Voigtmann, U.; Klar, U., *Angew. Chem. Int. Ed.* **2008**, *47*, 4922.

27. Hohne, A.; Yu, L.; Mu, L.; Reiher, M.; Voigtmann, U.; Klar, U.; Graham, K.; Schubiger, P. A.; Ametamey, S. M., *Chem. Eur. J.* **2009**, *15*, 3736.

28. Kostikov, A. P.; Iovkova, L.; Chin, J.; Schirrmacher, E.; Wängler, B.; Wängler, C.; Jurkschat, K.; Cosa, G.; Schirrmacher, R., *J. Fluorine Chem.* **2011**, *132*, 27.

29. Rosa-Neto, P.; Wangler, B.; Iovkova, L.; Boening, G.; Reader, A.; Jurkschat, K.; Schirrmacher, E., *Chembiochem* **2009**, *10*, 1321.

30. Iovkova, L.; Könning, D.; Wängler, B.; Schirrmacher, R.; Schoof, S.; Arndt, H.-D.; Jurkschat, K., *Eur. J. Inorg. Chem.* **2011**, *2011*, 2238.

31. Kostikov, A. P.; Chin, J.; Orchowski, K.; Niedermoser, S.; Kovacevic, M. M.; Aliaga, A.; Jurkschat, K.; Wangler, B.; Wangler, C.; Wester, H. J.; Schirrmacher, R., *Bioconjugate Chem.* **2012**, *23*, 106.

32. Wangler, C.; Waser, B.; Alke, A.; Iovkova, L.; Buchholz, H. G.; Niedermoser, S.; Jurkschat, K.; Fottner, C.; Bartenstein, P.; Schirrmacher, R.; Reubi, J. C.; Wester, H. J.; Wangler, B., *Bioconjugate Chem.* **2010**, *21*, 2289.

33. Niedermoser, S.; Chin, J.; Wangler, C.; Kostikov, A.; Bernard-Gauthier, V.; Vogler, N.; Soucy, J. P.; McEwan, A. J.; Schirrmacher, R.; Wangler, B., *J. Nucl. Med.* **2015**, *56*, 1100.

34. Vabre, B.; Chansaenpak, K.; Wang, M.; Wang, H.; Li, Z.; Gabbai, F. P., *Chem Commun.* **2017**, *53*, 8657.

35. Bayne, J. M.; Stephan, D. W., *Chem. Soc. Rev.* **2016**, *45*, 765.

36. Zhu, J.; Chin, J.; Wangler, C.; Wangler, B.; Lennox, R. B.; Schirrmacher, R., *Bioconjugate Chem.* **2014**, *25*, 1143.

37. Berke, S.; Kampmann, A. L.; Wuest, M.; Bailey, J. J.; Glowacki, B.; Wuest, F.; Jurkschat, K.; Weberskirch, R.; Schirrmacher, R., *Bioconjugate Chem.* **2018**, *29*, 89.

38. Bernard-Gauthier, V.; Wangler, C.; Schirrmacher, E.; Kostikov, A.; Jurkschat, K.; Wangler, B.; Schirrmacher, R., *Biomed. Res. Int.* **2014**, *2014*, 1.

39. Smith, G. E.; Sladen, H. L.; Biagini, S. C.; Blower, P. J., *Dalton Trans.* **2011**, *40*, 6196.

40. Zeng, J. L.; Wang, J.; Ma, J. A., *Bioconjugate Chem.* **2015**, *26*, 1000.

41. Levason, W.; Monzittu, F. M.; Reid, G.; Zhang, W. J.; Hope, E. G., *J. Fluorine Chem.* **2017**, *200*, 190.

42. Bhalla, R.; Levason, W.; Luthra, S. K.; McRobbie, G.; Reid, G.; Sanderson, G.; Zhang, W., *Chem Commun.* **2014**, *50*, 12673.

43. Levason, W.; Luthra, S. K.; McRobbie, G.; Monzittu, F. M.; Reid, G., *Dalton Trans.* **2017**, *46*, 14519.

44. Cleeren, F.; Lecina, J.; Billaud, E. M.; Ahamed, M.; Verbruggen, A.; Bormans, G. M., *Bioconjugate Chem.* **2016**, *27*, 790.

45. Fuchtner, F.; Preusche, S.; Mading, P.; Zessin, J.; Steinbach, J., *Nuklearmedizin* **2008**, *47*, 116.

46. Bhalla, R.; Levason, W.; Luthra, S. K.; McRobbie, G.; Sanderson, G.; Reid, G., *Chem. Eur. J.* **2015**, *21*, 4688.

47. Liu, S.; Ellars, C. E.; Edwards, D. S., *Bioconjugate Chem.* **2003**, *14*, 1052.

48. Chen, J.; Linder, K. E.; Cagnolini, A.; Metcalfe, E.; Raju, N.; Tweedle, M. F.; Swenson, R. E., *Appl. Radiat. Isot.* **2008**, *66*, 497.

49. de Blois, E.; Chan, H. S.; de Zanger, R.; Konijnenberg, M.; Breeman, W. A., *Appl. Radiat. Isot.* **2014**, *85*, 28.

50. Bhalla, R.; Burt, J.; Hector, A. L.; Levason, W.; Luthra, S. K.; McRobbie, G.; Monzittu, F. M.; Reid, G., *Polyhedron* **2016**, *106*, 65.

Chapter 4: Group 13 coordination chemistry: exploring reactions of $MF_3 \cdot 3H_2O$ with neutral O- and N-donor ligands

4.1 Introduction

Chapters 2 and 3 discussed the ^{18}F radiolabelling reaction conditions for the complexes [$AlCl_3$($BnMe_2$-tacn)] and [GaF_3($BnMe_2$-tacn)] through $Cl/^{18}F$ halide and $^{18}F/^{19}F$ isotopic exchange reactions, respectively. The co-ligands used in these complexes are tacn derivatives, where the macrocyclic amine N-donor atoms bind strongly to the metal, resulting in *facial* octahedral coordination geometries for the complexes. The chemistry of the Group 13 trifluorides had been very little explored prior to the Reid group developing their chemistry with nitrogen-donor ligands.[1,2] The reason for this may be due to the very low reactivity of the anhydrous and highly polymerised metal trifluorides towards neutral ligands[3] and the poor solubility of the metal trifluoride hydrates.[4] As a result, the reported complexes were obtained by reaction of the metal trifluoride hydrate, $MF_3 \cdot 3H_2O$ (M = Al, Ga, In) with the appropriate neutral N-donor ligand in hydrothermal conditions (180 °C, 15 h) or by halide exchange reactions from the chloride analogues (Scheme 4.1). The crystal structures of these complexes are all hydrates and show extensive H-bonding (a feature also shared by the new complexes reported in this Chapter).

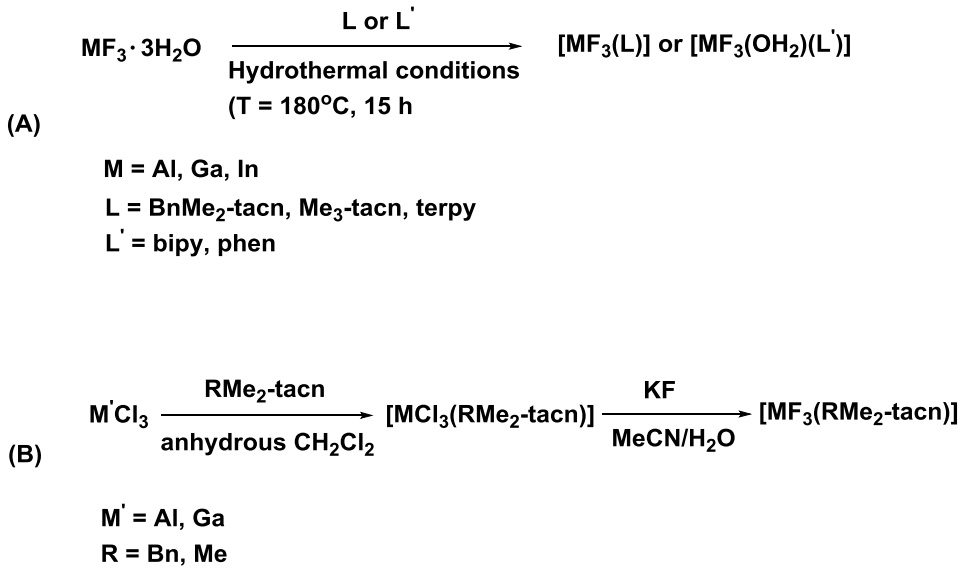

Scheme 4.1. Reaction conditions reported for the synthesis of the Group 13 metal fluoride complexes with neutral ligands in (A) hydrothermal conditions from the $MF_3 \cdot 3H_2O$ and (B) from the chloride analogues by halide exchange reactions.

This Chapter develops this work further, discussing the reactions of the metal trifluoride hydrates, $MF_3{\cdot}3H_2O$, with a range of neutral O-donor ligands. These reactions were explored in order to develop the coordination chemistry of the trifluorides, to consider whether these systems might form a potential basis to develop future PET agents and also with a view to preparing a soluble molecular synthon, more reactive than the $MF_3{\cdot}3H_2O$, that could be used under milder conditions and utilised as an entry point for the $[MF_3(RMe_2\text{-tacn})]$ chemistry. This would be useful not only for the development of the chemistry with O-donor ligands, but also for the tacn complexes, providing a more readily accessible route to the syntheses of the complexes, (the $[GaF_3(BnMe_2\text{-tacn})]$ utilised in Chapter 2 was prepared through the improved, milder route developed in this work).

Excluding the aquo-fluoro-anions,[4,5,1,6,7] such as $[Al_2F_8(OH_2)_2]^{2-}$ or $[GaF_4(OH_2)_2]^-$, and the aquo-imine complexes, *mer*-$[MF_3(bipy)(OH_2)]{\cdot}2H_2O$, *mer*-$[MF_3(phen)(OH_2)]$,[2] other examples of complexes of the Group 13 metal fluorides with neutral O-donor ligands are limited to the cation in $[AlF_2(thf)_4][\{(SiMe_3)_3C\}_2Al_2F_5]$[8] (Figure 4.1).

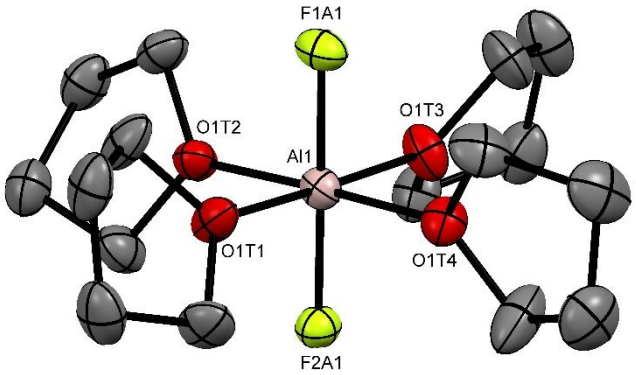

Figure 4.1. Crystal structure of the cation in $[AlF_2(thf)_4][\{(SiMe_3)_3C\}_2Al_2F_5]$. Image redrawn from CCDC 116810.[8] Selected bond lengths (Å) and angles (°): Al1-F2A1 1.7006(14), Al1-O1T3 1.9435(17), F2A2-Al1-F1A1 179.33(8), O1T4-Al1-O1T3 90.37(8), F1A1-Al1-O1T2 90.49(7).

The structure shows a *trans*-octahedron in which the metal is bound to four tetrahydrofuran ligands with two fluoride ligands in axial positions. The compound was obtained by treating an insoluble solid from the reaction of $[(SiMe_3)_3CAlF_2]_3$ with AgF and NH_4F in thf solution.

During the Southampton group's earlier work with N-donor ligands, it was observed that different batches of the commercial $MF_3{\cdot}3H_2O$ had different reactivity, reflecting different structural forms, particle size and the drying method used in their synthesis. This Chapter also attempts to address these aspects.

4.2 Results and discussion

4.2.1 Synthesis of $MF_3 \cdot 3H_2O$ and $[MF_3(OH_2)_2(DMSO)]$ (M = Al, Ga, In)

The $MF_3 \cdot 3H_2O$ (M = Al, Ga, In) exist in several structural forms. $AlF_3 \cdot 3H_2O$ has two forms, the α-form with discrete $[AlF_3(OH_2)_3]$ (R-3) octahedral molecules and the polymeric and more stable β-form, $[\{AlF_2(OH_2)_2(\mu\text{-}F)\}_n] \cdot nH_2O$ (P4/n) in which bridging fluorides connect each octahedron to form infinite chains, (Figure 4.2).[9]

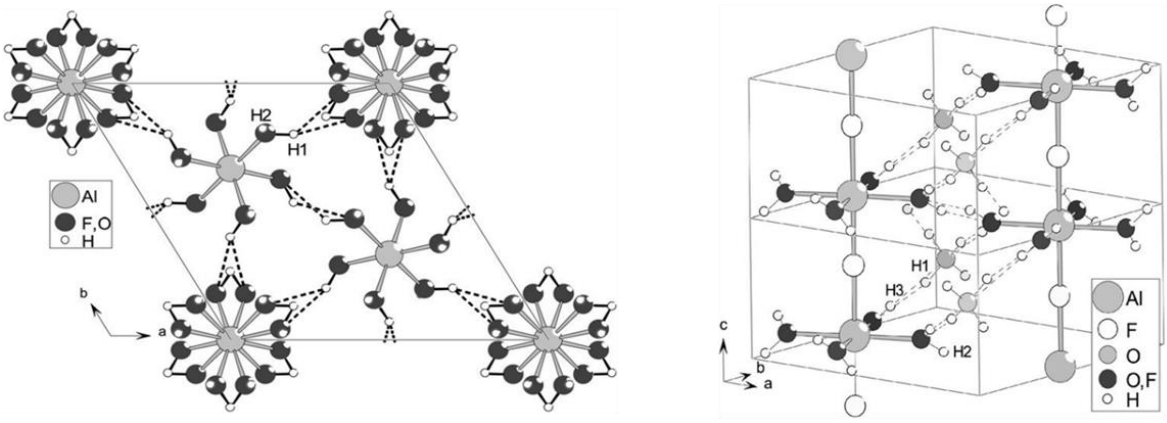

Figure 4.2. α-$AlF_3 \cdot 3H_2O$ (left) and β-$AlF_3 \cdot 3H_2O$ (right). Images taken from reference 9.

The crystal structure of the α-form shows the aluminium centre to be coordinated by either a fluoride or a water molecule in each position (due to disorder), whereas the β-form shows the same behaviour in the equatorial positions and only fluoride ions in axial positions through which each octahedron is connected. Whilst the structure of $GaF_3 \cdot 3H_2O$ has not been studied in detail and its structure is not entirely clear, $InF_3 \cdot 3H_2O$ shows the same polymeric structure as the β-form of $AlF_3 \cdot 3H_2O$ (P4/n).

The commercially available $MF_3 \cdot 3H_2O$ samples were analysed by PXRD and were shown to be the polymeric form for $AlF_3 \cdot 3H_2O$ and $InF_3 \cdot 3H_2O$ and the molecular form in the case of $GaF_3 \cdot 3H_2O$.

In order to obtain more reactive and reliable samples, the $MF_3 \cdot 3H_2O$ were therefore synthesised freshly. $AlF_3 \cdot 3H_2O$ was prepared by precipitation of cold aqueous aluminium sulfate solution with 10 % HF, while $GaF_3 \cdot 3H_2O$ and $InF_3 \cdot 3H_2O$ were prepared by dissolving freshly precipitated $M(OH)_3$ in aqueous HF and drying the white powders *in vacuo* at ambient temperature (Scheme 4.2).

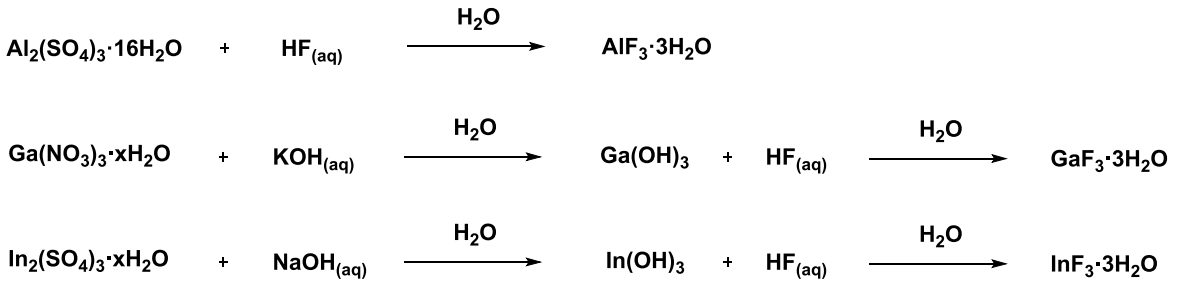

Scheme 4.2. Synthesis of $MF_3 \cdot 3H_2O$.

PXRD data on the freshly prepared sample of $GaF_3 \cdot 3H_2O$ confirmed it to have the rhombohedral structure (R-3); the PXRD data and the Rietveld fit are shown in Figure 4.3.

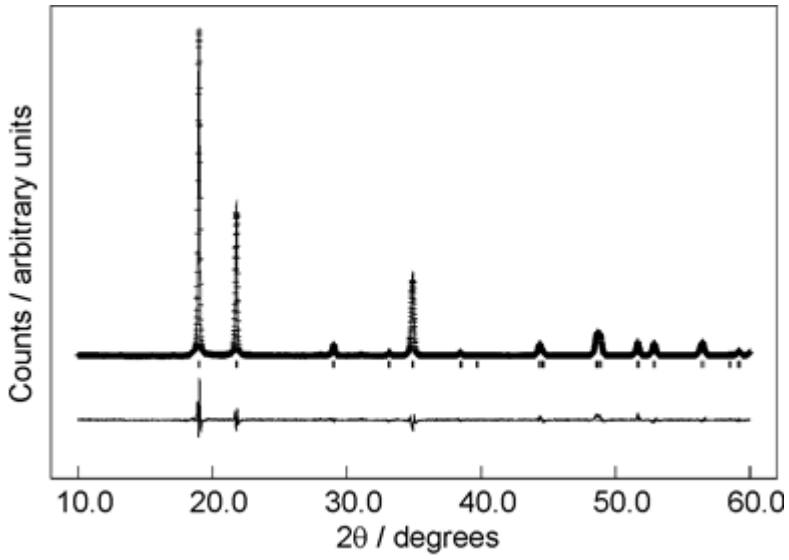

Figure 4.3. Fit to the PXRD pattern of $GaF_3 \cdot 3H_2O$ (Rw_p = 13.4 %, R_p = 10.3 %). Crosses mark the data point, upper continuous line the fit, and lower continuous line the difference. Tick marks show the positions of allowed reflections in R−3. Cell dimensions: a = 9.3812(3) and c = 4.73971(19) Å, with F and O disordered on a single site; no attempt was made to model H positions. The Ga-F/O distance is 1.845(3) Å.

The PXRD of the precipitated indium fluoride hydrate confirmed it was the chain polymer $[\{InF_2(OH_2)_2(\mu\text{-}F)_2\}n] \cdot nH_2O$.[10] Unlike the commercial samples of $AlF_3 \cdot 3H_2O$, the PXRD of the synthesised $AlF_3 \cdot 3H_2O$ revealed its structure to be the molecular α-form (Figure 4.4).

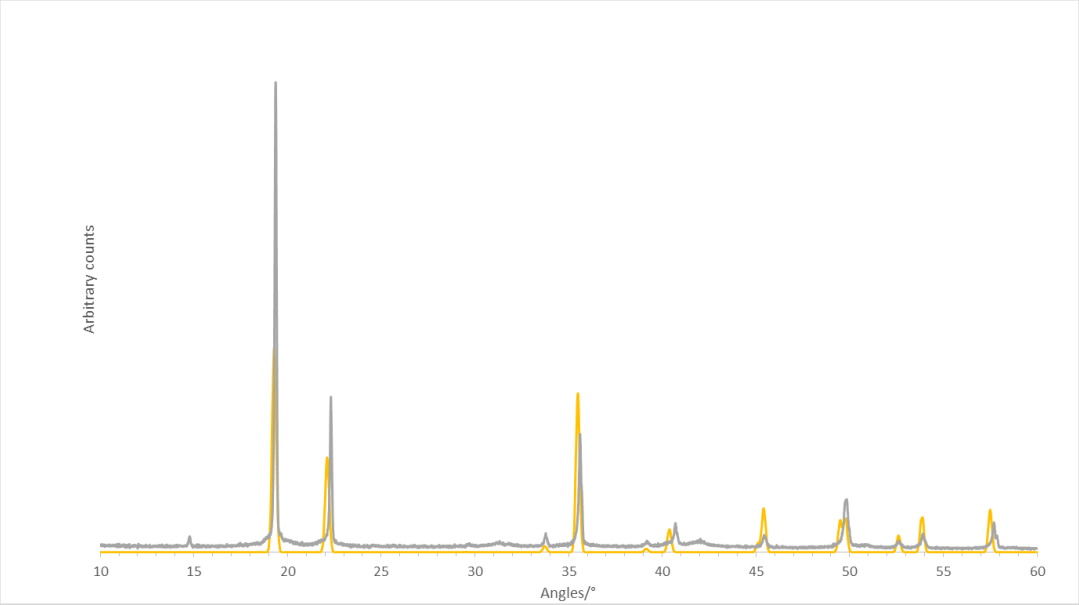

Figure 4.4. PXRD Comparison between α-$AlF_3 \cdot 3H_2O$ (grey, from reference 9) and $AlF_3 \cdot 3H_2O$ of this work (yellow).

The freshly prepared $MF_3 \cdot 3H_2O$ were in general found to be more reactive than the commercial samples and their use was therefore preferred for the work described in this Chapter. For aluminium, the lower reactivity of the commercial samples may be due to the polymeric β-form, but for the Ga and In compounds, which have the same structures as the freshly made samples, it most likely reflects particle size or surface properties.

The reactions of the $MF_3 \cdot 3H_2O$ (Al, Ga) with the ligands Ph_3PO, Me_3PO, $Ph_2P(O)CH_2P(O)Ph_2$ were undertaken in refluxing alcoholic solutions (MeOH, EtOH, ^{i}PrOH) or CH_2Cl_2, as well as hydrothermal conditions (180 °C, 15 h). In all cases the unchanged reactants were recovered. It was concluded that these ligands cannot compete for the metal with the large excess of water in hydrothermal conditions and that the $MF_3 \cdot 3H_2O$ do not have enough solubility in alcoholic solutions or CH_2Cl_2 to react with the weakly basic phosphine oxides. In an attempt to synthesise a more reactive species, the $MF_3 \cdot 3H_2O$ were reacted in the presence of strongly coordinating solvents such as N,N-dimethylformamide (dmf) (M = Al, Ga) and dimethylsulfoxide (DMSO) (M = Al, Ga, In). Refluxing $GaF_3 \cdot 3H_2O$ with dmf produced some colourless crystals, which were identified by single crystal X-ray diffraction to be $[Me_2NH_2][trans\text{-}GaF_4(OH_2)_2]$ (Figure 4.5), resulting from cleavage of the solvent (a behaviour often observed, especially in metal-organic frameworks (MOFs) syntheses[11,12,13]), along with a white solid containing a mixture of species; this reaction was not pursued further.

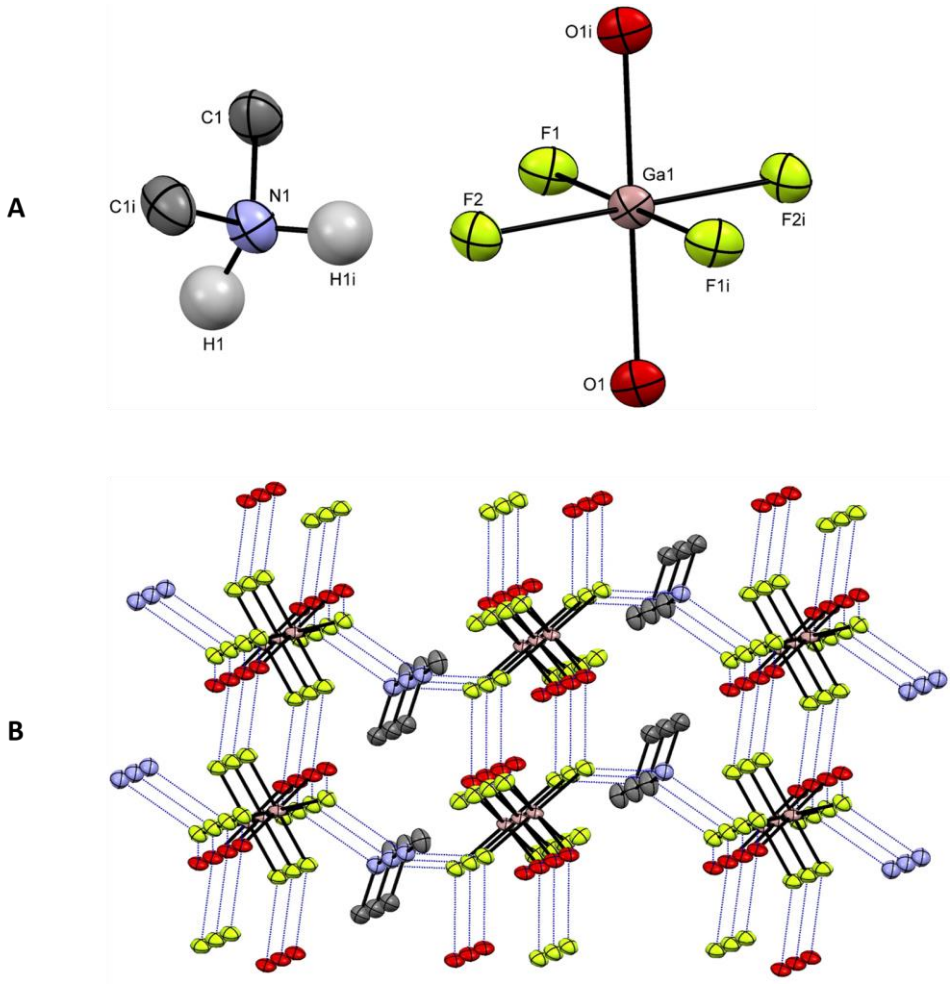

Figure 4.5. (A) The structure of $[Me_2NH_2][trans\text{-}GaF_4(OH_2)_2]$ with ellipsoids drawn at the 50% probability level. Hydrogen atoms on the water ligands and methyl carbons are omitted. Selected bond lengths (Å) and angles (°): Ga1–F1 = 1.8595(18), Ga1–F2 = 1.8974(18), Ga1–O1 = 1.987(2), F1–Ga1–F2 = 90.18(8), F1–Ga1–F2^{i} = 89.82(8), F1–Ga1–O1 = 91.35(8), F1–Ga1–O1^{i} = 88.65(8), F2–Ga1–O1 = 89.92(8), F2–Ga1–O1^{i} = 90.08(8). Symmetry codes: –x, y+1/2, –z+1/2. (B) View of the H-bonding network (blue) between the cations and anions present in the crystal structure of $[NMe_2H_2][GaF_4(OH_2)_2]$.

Figure 4.5A shows a centrosymmetric anion in which the metal is coordinated in an octahedral fashion by four fluorides in the equatorial plane and two water molecules in axial positions, with N-H···F (2.72 Å) and O-H···F (2.64 Å) hydrogen bonding linking the cations and anions in a chain and parallel chains into a 3D network (Figure 4.5 B). NMR analysis in CD_3OD show that the anion has a broad singlet at δ = −174.8 in the $^{19}F\{^{1}H\}$ NMR spectrum, while the $[NMe_2H_2]^+$ cation has δ(^{1}H) = 2.67 (s, Me). The structure of $[LH_2][cis\text{-}GaF_4(OH_2)_2]\cdot H_2O$ (L = 4,4′-trimethylenedipyridine) has been reported,[6] with bond lengths of Ga–F = 1.853(2)–1.882(2) Å and Ga–O = 2.017(2), 2.026(2) Å.

The reactions in DMSO proved much more successful, producing the species $[MF_3(OH_2)_2(DMSO)]$ (M = Al, Ga, In) as colourless powdered solids. The Al and Ga complexes were obtained in hot DMSO (70- 85 °C) in good yields, whilst $InF_3\cdot 3H_2O$ was only poorly soluble even at higher temperature, giving $[InF_3(OH_2)_2(DMSO)]$ in low yield (12 %) (Scheme 4.3).

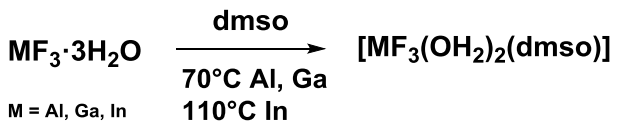

Scheme 4.3. Method for preparation of $[MF_3(OH_2)_2(DMSO)]$.

Interestingly, the water molecules remain coordinated to the metals even when DMSO is present in a vast excess, and using longer reaction times or adding dry molecular sieves. Crystals suitable for X-ray analysis were obtained by slowly cooling a concentrated solution of the Ga(III) complex in DMSO (Figure 4.6).

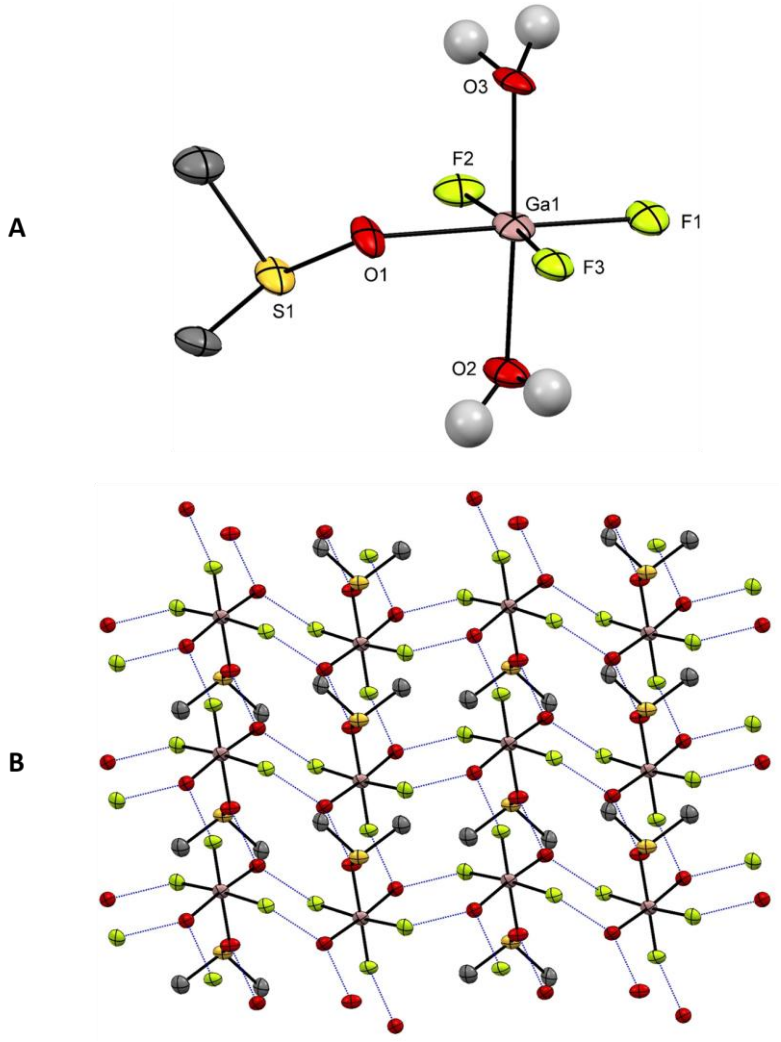

Figure 4.6. (A) The structure of *mer-trans*-$[GaF_3(OH_2)_2(DMSO)]$ with ellipsoids drawn at the 50% probability level. Methyl group hydrogen atoms are omitted. Selected bond lengths (Å) and angles (°) : Ga1–F1 = 1.865(7), Ga1–F2 = 1.870(5), Ga1–F3 = 1.876(5), Ga1–O3 = 1.993(6), Ga1–O1 = 2.042(8), Ga1–O2 = 1.972(7), S1–O1 = 1.549(8), F1–Ga1–F2 = 92.0(3), F1–Ga1–O3 = 92.7(3), F1–Ga1–F3 = 94.7(3), F1–Ga1–O2 = 90.9(3), F2–Ga1–O3 = 91.8(3), F2–Ga1–O1 = 88.5(3), F2–Ga1–O2 = 90.2(3), O3–Ga1–O1 = 87.7(3), F3–Ga1–O3 = 88.4(2), F3–Ga1–O1 = 84.8(3), F3–Ga1–O2 = 89.2(3), O2–Ga1–O1 = 88.7(3), S1–O1–Ga1 = 124.4(4); (B) The

H-bonding network (blue) in the crystal structure of $[GaF_3(OH_2)_2(DMSO)]$ (colour key: pink = Ga, yellow = S, green = F, red = O, grey = C).

The structure of $[GaF_3(OH_2)_2(DMSO)]$ shows a distorted octahedral coordination environment around the metal with the three fluoride atoms in a *meridional* configuration, the DMSO *trans* to a fluoride anion and the two water molecules *trans* to each other. The Ga-F and Ga-OH_2 bond lengths are typical of these systems and there is little difference between coordinated and free DMSO.[14] The crystal packing also shows extensive hydrogen bonding between water molecules and fluoride atoms of adjacent molecules. Each F or O atom coordinated to the metal is involved in O-H···F (2.56-2.61 Å) or O-H···O=S$(CH_3)_2$ (2.64 Å) H-bonding interactions with neighbour molecules. The IR spectra of the complexes $[MF_3(OH_2)_2(DMSO)]$ showed the presence of water, a shift towards lower frequency of the ν_{SO} of DMSO compared to "free" DMSO (1004 *vs.* 1044 cm^{-1}) and a broad feature assigned to the M-F stretches around 460- 525 cm^{-1}. The $^{19}F\{^1H\}$ NMR spectrum of $[AlF_3(OH_2)_2(DMSO)]$ in CD_3OD showed two resonances, with 2:1 ratio, and a singlet at δ = -10.1 in the ^{27}Al NMR consistent with a *mer*-MF_3 coordination and a six-coordinated Al species.[1] In CD_3OD solution, the $^{19}F\{^1H\}$ NMR spectrum of $[GaF_3(OH_2)_2(DMSO)]$ showed only a broad singlet at room temperature, which resolved on cooling the solution, into two resonances, suggesting that the complex is dynamic at room temperature (Figure 4.7). The complexes are soluble in MeOH and slightly soluble in CH_2Cl_2.

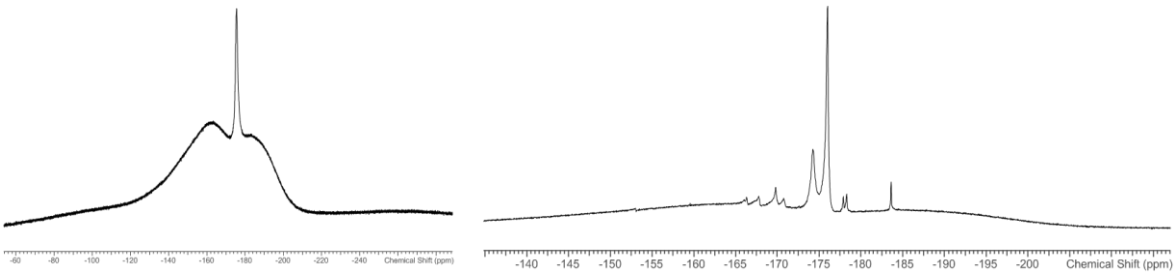

Figure 4.7. $^{19}F\{^1H\}$ NMR spectrum of $[GaF_3(OH_2)_2(DMSO)]$ at 298 K (left) and 183 K (right). Note that the rolling base-line in the spectra is due to the Teflon in the probe.

$[InF_3(OH_2)_2(DMSO)]$ did not exhibit a $^{19}F\{^1H\}$ NMR resonance at ambient temperature, but showed three resonances at low temperature, indicative of decomposition in solution and hence, it was not reacted with other ligands.

4.2.2 Reactions of $[MF_3(OH_2)_2(DMSO)]$ (M = Al, Ga) with neutral ligands

The new, soluble molecular synthons, $[MF_3(OH_2)_2(DMSO)]$, were reacted with other neutral ligands in order to develop the coordination chemistry of the MF_3 fragments further (Scheme 4.4).

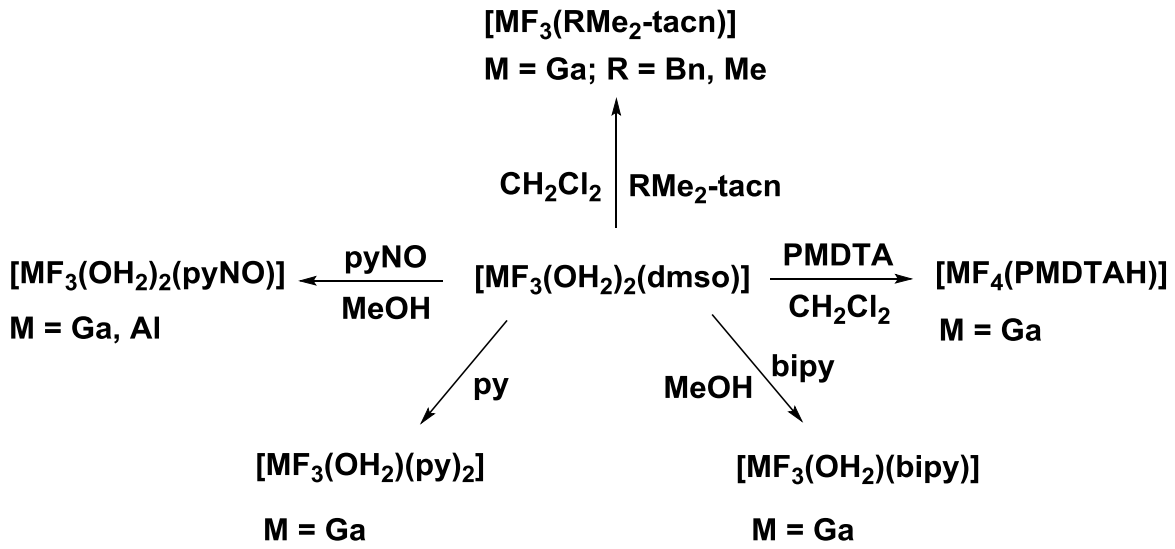

Scheme 4.4. Reactions of $[MF_3(OH_2)_2(DMSO)]$.

The reactions of $[GaF_3(OH_2)_2(DMSO)]$ with N-donor ligands, such as bipy and RMe_2-tacn (R = Bn, Me), are particularly relevant for the work in this thesis and the $[GaF_3(BnMe_2\text{-tacn})]$ used for the studies in Chapter 2 was made by this route. The reactions to obtain $[GaF_3(bipy)(OH_2)]\cdot 2H_2O$ and $[GaF_3(RMe_2\text{-tacn})]$ were performed at room temperature in MeOH and CH_2Cl_2, respectively, i.e. using much milder conditions than the hydrothermal method employed previously.[1, 2]

Phosphine oxides have been shown to form stable complexes with many p-block fluorides,[4] including SiF_4,[15] GeF_4,[16] SnF_4,[17] SnF_2,[18] TeF_4,[19] AsF_3[20] and SbF_3.[20] It was therefore somewhat unexpected that all attempts to form phosphine oxide complexes by refluxing $[MF_3(OH_2)_2(DMSO)]$ (M = Al or Ga) with Ph_3PO, Me_3PO or $R_2P(O)CH_2P(O)R_2$ (R = Me or Ph) in CH_2Cl_2, MeOH, or EtOH solution were unsuccessful, with only the starting materials being recovered after work-up of the reactions. Both H_2O and DMSO are strongly coordinating ligands and the water molecules in $[MF_3(OH_2)_2(DMSO)]$ are also involved in extensive H-bonding, possible contributory reasons why they are not replaced by the other O-donor, phosphine oxide ligands. It has been noted above that the reaction of $MF_3\cdot 3H_2O$ with Me_3PO and Ph_3PO in refluxing ROH (R = Me, Et, ^{i}Pr) or CH_2Cl_2 and in hydrothermal conditions were also unsuccessful.

The reactions with pyridine N-oxide (pyNO) were more successful, giving $[MF_3(OH_2)_2(pyNO)]$ (M = Al, Ga). $[AlF_3(OH_2)_2(PyNO)]$ was obtained as a white solid by reaction of $[AlF_3(OH_2)_2(DMSO)]$ with two mol. equivalents of pyNO in MeOH. The $^{19}F\{^1H\}$ NMR spectrum of the product in CD_3OD (Figure 4.8) showed two resonances (integrals 2:1) at 298 K (F-F coupling was not observed probably as a result of small coupling constant). In the IR spectrum the Al-F stretches appeared as a broad band at 564 cm^{-1}, whereas the ν_{NO} of coordinated pyNO observed at 1154 cm^{-1} is significantly lower than the value either for "free" pyNO (1265 cm^{-1}) or for $[AlX_3(pyNO)]$ (X = Cl, Br) (both 1204 cm^{-1}).[21]

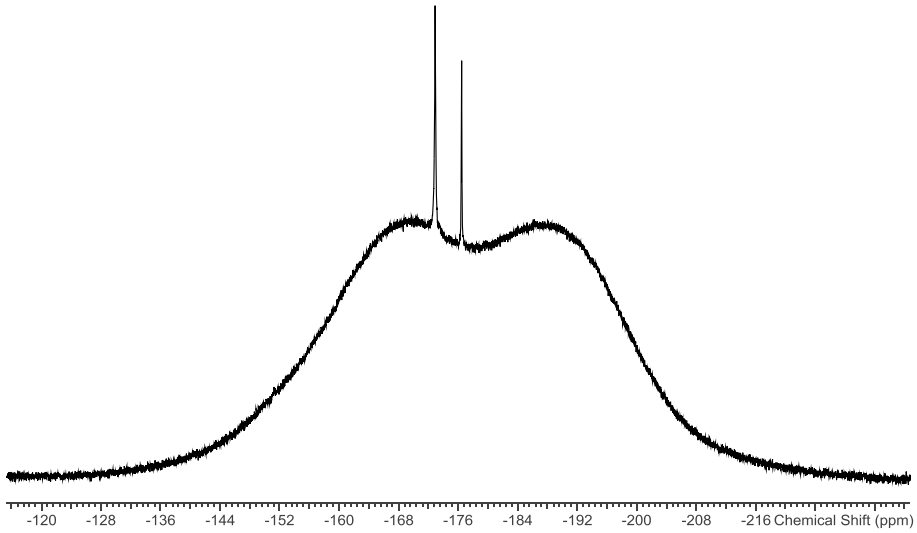

Figure 4.8. $^{19}F\{^{1}H\}$ NMR spectrum of $[AlF_3(OH_2)_2(pyNO)]$ at 298 K showing two resonances (2:1 integral), consistent with two fluoride environments in a *mer*-F_3 coordination. The rolling baseline is due to the Teflon in the probe.

The reaction of $[GaF_3(OH_2)_2(DMSO)]$ with three mol. equivalents of pyNO in MeOH produced a colourless oil which, over several days, deposited a quantity of colourless crystals suitable for X-ray analysis (Figure 4.9).

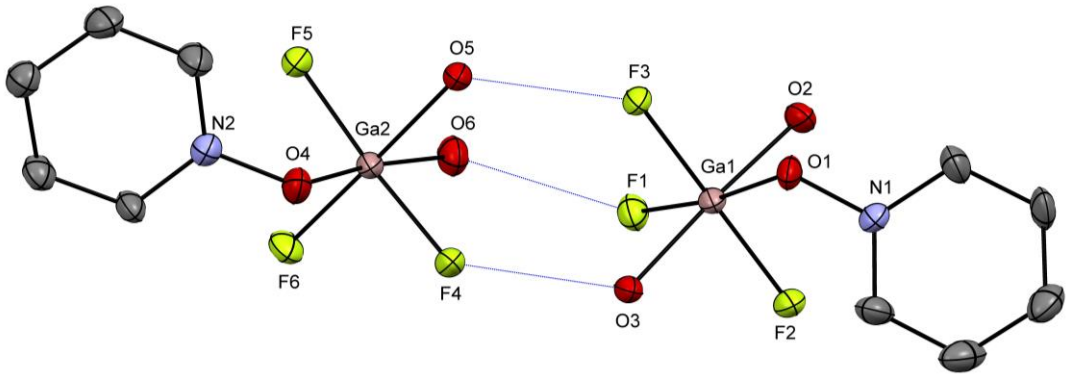

Figure 4.9. The structure of the two geometric isomers in $[GaF_3(OH_2)_2(pyNO)]\cdot pyNO\cdot H_2O$ showing the hydrogen bonding (blue dotted line) and with ellipsoids drawn at the 50% probability level. The lattice pyNO and H_2O are omitted for clarity. Hydrogen atoms on the coordinated water and pyNO are not shown. Selected bond lengths (Å) and angles (°): Ga1-centred molecule (*mer-trans)* Ga1–F1 = 1.879(4), Ga1–F2 =1.856(4), Ga1–F3 = 1.858(4), Ga1–O1 = 1.997(5), Ga1–O2 = 1.982(5), Ga1–O3 = 2.003(5), F1–Ga1–O2 = 89.3(2), F1–Ga1–O3 = 91.9(2), F2–Ga1–F1 = 93.86(19), F2–Ga1–O1 = 92.57(19), F2–Ga1–O2 = 88.9(2), F2–Ga1–O3 = 88.22(19), F3–Ga1–F1 = 91.11(19), F3–Ga1–O1 = 82.56(19), F3–Ga1–O2 = 94.1(2), F3–Ga1–O3 = 88.67(19), O1–Ga1–O3 = 90.0(2), O2–Ga1–O1 = 89.1(2); Ga2-centred molecule (*mer-cis*) Ga2–F4 = 1.855(4), Ga2–F5 = 1.863(4), Ga2–F6 = 1.866(4), Ga2–O4 = 1.985(5), Ga2–O5 = 1.995(5), Ga2–O6 = 2.013(6), F4–Ga2–F6 = 93.41(19), F4–Ga2–O4 = 86.0(2), F4–Ga2–O5 = 87.33(19), F4–Ga2–O6 = 88.0(2), F5–Ga2–F6 = 90.32(19), F5–Ga2–O4 = 95.6(2), F5–Ga2–O5 = 88.96(19), F5–Ga2–O6 = 90.3(2), F6–Ga2–O4 = 90.0(2), F6–Ga2–O6 = 90.1(2), O4–Ga2–O5 = 89.3(2), O5–Ga2–O6 = 90.7(2).

The structure of $[GaF_3(OH_2)_2(pyNO)]\cdot pyNO\cdot H_2O$ shows two geometrical isomers linked into dimers by F···H-O (2.53-2.61 Å) hydrogen bonding. The isomers are present in the structure in equal ratio and both show the fluorides arranged in a *meridional* configuration and only one pyNO molecule coordinated to the metal. pyNO is *trans* to a fluoride in one isomer and *trans* to a water molecule in the other, resulting in *trans*-OH_2 in the former and *cis*-OH_2 in the latter. The Ga-F, Ga-O and Ga-ONpy bond distances are similar in the two isomers and for Ga-F and Ga-O, comparable with the other structures reported in this chapter (1.865-1.876 Å for Ga-F and 1.972-2.042 Å for Ga-O in $[GaF_3(OH_2)_2(DMSO)]$ for example). PyNO and H_2O are also present in the lattice. The ^{1}H NMR spectrum of this complex in CD_3OD exhibited only three resonances associated with pyNO, while the corresponding $^{19}F\{^1H\}$ NMR spectrum was a broad singlet, suggesting that the complex is exchanging or dissociating the neutral ligands in solution. When the solution was cooled to 183 K, the ^{1}H NMR spectrum showed six broad resonances corresponding to coordinated and lattice pyNO and the $^{19}F\{^1H\}$ NMR spectrum contained three overlapping resonances at δ = −174.1, −175.0 and −176.5. This contrasts with $[AlF_3(OH_2)_2(PyNO)]$ which is stable in solution and shows only one isomer. The increasing lability of neutral ligands in the MF_3 complexes in descending Group 13 is also found in other systems.[1, 2] $[GaF_3(OH_2)_2(pyNO)]\cdot pyNO$ also exhibited ν(NO) at 1154 cm^{-1} for the coordinated ligand, and 1265 cm^{-1} for the lattice pyNO, which compare with values of 1198 and 1192 cm^{-1} for the $[GaX_3(pyNO)]$ (X = Cl or Br), respectively.[22]

The water molecules in $[MF_3(OH_2)_2(DMSO)]$ proved to be difficult to displace by other O-donor ligands, whereas Me_3-tacn and BnM_2tacn were successful in this respect. The structure of *mer*-$[GaF_3(py)_3]$ has also been reported.[23] In an effort to replace the water molecules coordinated to the metal, the reactions with other nitrogen donor ligands were explored. $[GaF_3(OH_2)_2(DMSO)]$ partially dissolved in pyridine, and after filtration to remove the solid (which contained a mixture of products by ^{1}H and $^{19}F\{^1H\}$ NMR spectroscopy), some crystals formed from the mother liquor after a few days. The crystal structure is shown in Figure 4.10.

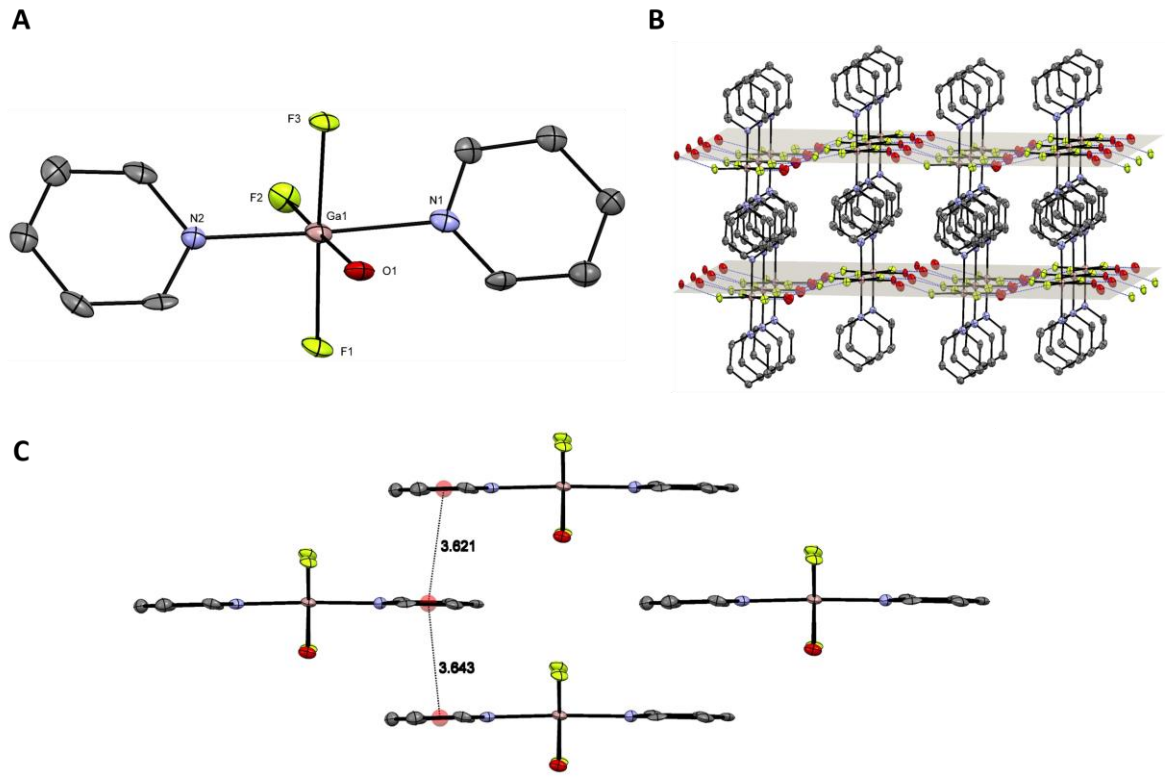

Figure 4.10. (A) The structure of *mer-trans*-[$GaF_3(OH_2)(py)_2$] with ellipsoids drawn at the 50% level. Selected bond lengths (Å) and angles (°): Ga1–N2 = 2.074(7), Ga1–N1 = 2.093(7), Ga1–F2 = 1.889(6), Ga1–F3 = 1.867(6), Ga1–F1 = 1.854(6), Ga1–O1 = 2.014(7), F2–Ga1–N2 = 90.8(4), F2–Ga1–N1 = 89.2(4), F3–Ga1–N2 = 88.8(3), F3–Ga1–N1 = 88.2(3), F3–Ga1–F2 = 93.0(3), F3–Ga1–O1 = 87.4(3), F1–Ga1–N2 = 91.2(3), F1–Ga1–N1 = 91.8(3), F1–Ga1–F2 = 94.2(3), F1–Ga1–O1 = 85.5(3); (B) View of the hydrogen bonding in [$Ga(F_3(OH_2)(py)_2$] shown in grey; (C) view of the π-stacking.

The structure shows a six-coordinated gallium centre with GaF_3 in *meridional* configuration and the pyridine molecules lie *trans* to each other. The bond distances are similar to those reported in [$GaF_3(py)_3$].[23] Moreover, extensive H-bonding (Figure 4.10 B), between the fluoride and the water molecule, and π-stacking of the pyridine rings (Figure 4.10 C), are present in the structure. As can be seen, one water molecule is retained in the first coordination sphere. The same reaction was also attempted in MeOH solution with two mol. equivalents of pyridine, in order to obtain a pure sample. However, ^{1}H and $^{19}F\{^{1}H\}$ NMR spectra of the product after work-up showed a similar complicated mixture of species present. Hence, this was not pursued further.

The reaction of [$GaF_3(OH_2)_2(DMSO)$] with the tridentate, open chain ligand N,N,N',N'',N''-pentamethyldiethylenetriamine (pmdta) was also investigated. It was reported previously that the reaction of $GaF_3{\cdot}3H_2O$ with pmdta under hydrothermal conditions, produced the species [$\subset Me_2N(CH_2)_2NMe(CH_2)_2]_2[Ga_2F_8(OH_2)_2]{\cdot}2H_2O$, with the 1,1,4-trimethylpiperazinium cation resulting from cleavage of the triamine.[2] Its structure was postulated on the basis of analytical and spectroscopic data and by analogy with the crystallographically characterised

$[\subset Me_2N(CH_2)_2NMe(CH_2)_2]_2[Al_2F_8(OH_2)_2]\cdot 2H_2O$. In this case, the reaction of $[GaF_3(OH_2)_2(DMSO)]$ with pmdta at room temperature in CH_2Cl_2 solution formed the zwitterionic species, $[GaF_4(pmdtaH)]\cdot 2H_2O$ (Scheme 4.4 and Figure 4.11).

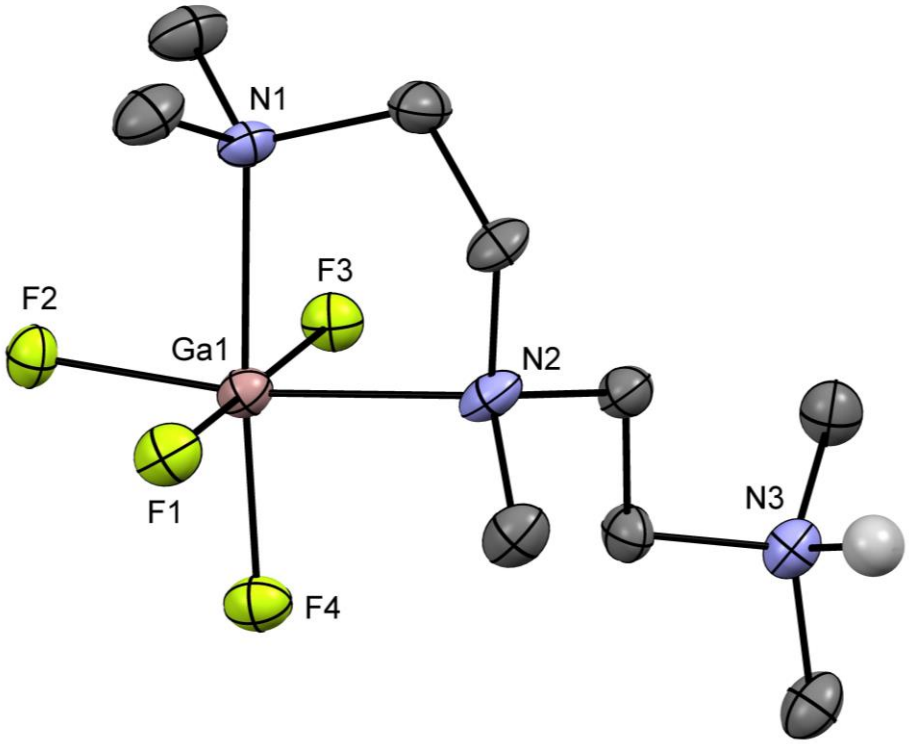

Figure 4.11. The structure of $[GaF_4(pmdtaH)]\cdot 2H_2O$ with ellipsoids drawn at the 50% level. Selected bond lengths (Å) and angles (°): Ga1–F1 = 1.8641(16), Ga1–F2 = 1.8850(15), Ga1–F3 = 1.8687(15), Ga1–F4 = 1.8417(17), Ga1–N1 = 2.153(2), Ga1–N2 = 2.192(2), F1–Ga1–F2 = 91.14(6), F1–Ga1–N1 = 90.00(7), F1–Ga1–N2 = 88.16(6), F2–Ga1–N1 = 87.11(8), F3–Ga1–F2 = 91.55(6), F3–Ga1–N1 = 87.32(7), F3–Ga1–N2 = 88.73(6), F4–Ga1–F1 = 92.26(6), F4–Ga1–F2 = 95.96(7), F4–Ga1–F3 = 90.27(6), F4–Ga1–N2 = 93.08(8), N1–Ga1–N2 = 83.87(8).

The crystal structure shows *cis* κ^2 coordinated triamine, with a free protonated NMe_2 group to balance the charge of the $[GaF_4]^-$ unit. Diffusion of hexane into a concentrated CH_2Cl_2 solution of $[GaF_4(pmdtaH)]$ over several weeks, formed the dianion $[\subset Me_2N(CH_2)_2NMe(CH_2)_2]_2[Ga_2F_8(OH_2)_2]\cdot 2H_2O$ (Figure 4.12), confirming its postulated structure.

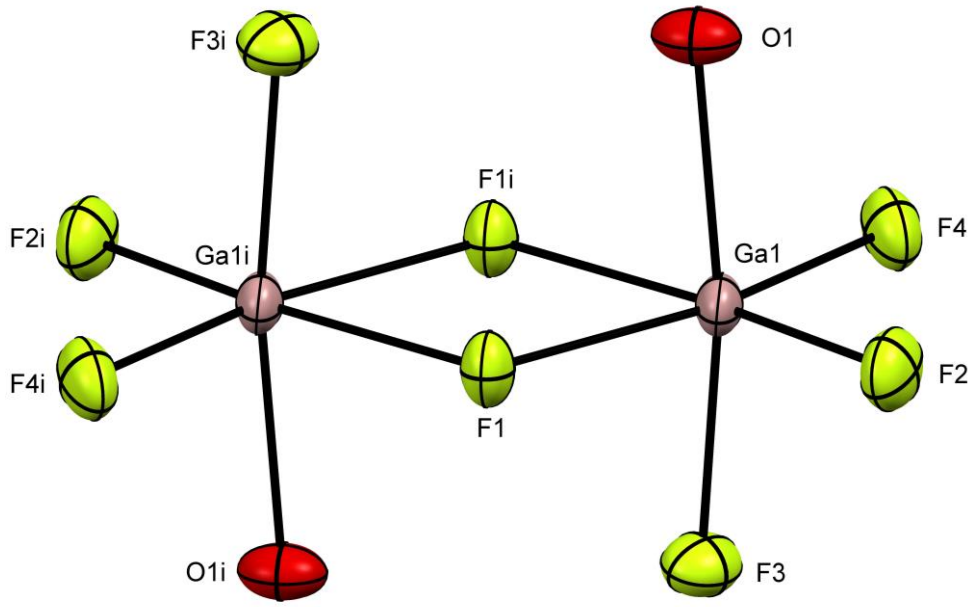

Figure 4.12. The anion in $[\subset Me_2N(CH_2)_2NMe(CH_2)_2]_2[Ga_2F_8(OH_2)_2]\cdot 2H_2O$ with ellipsoids drawn at the 50% probability level. The H-atoms on the water molecules were not located in the difference map. Selected bond lengths (Å) and angles (°): Ga1–F1 = 2.002(2), Ga1–F1 = 1.965(2), Ga1–F2 = 1.832(2), Ga1–F3 = 1.856(3), Ga1–F4 = 1.833(2), Ga1–F1^{i} = 1.965(2), Ga1–O1 = 1.946(3), F1–Ga1–F1^{i} = 76.37(12), F2–Ga1–F1 = 91.34(11), F2–Ga1–F3 = 93.37(12), F2–Ga1–F4 = 100.65(12), F2–Ga1–O1 = 90.74(13), F3–Ga1–F1^{i} = 88.59(11), F3–Ga1–F1 = 86.34(11), F4–Ga1–F1^{i} = 91.60(11), F4–Ga1–F3 = 94.05(12), F4–Ga1–O1 = 92.47(12), O1–Ga1–F1^{i} 85.81(12), O1–Ga1–F1 = 86.16(12), Ga1–F1–Ga1^{i} = 103.63(12). Symmetry codes: –x, y+1/2, –z+1/2.

The geometry is similar to that of the aluminium analogue,[2] although the crystals are not isomorphous. The Ga–O and Ga–F bonds are ~ 0.07–0.08 Å longer than the corresponding bonds to aluminium. The anion appears to be unstable in solution (as is the aluminium analogue[2]) since in CD_3OD solution only a broad singlet $^{19}F\{^1H\}$ NMR resonance is observed at δ = –162 ppm.

4.2.3 Attempted Cl/F halide exchange reactions from $[MCl_3(OPMe_3)]$ (M = Al, Ga)

A further possible entry to fluoro-Group 13 complexes containing other O-donor ligands is via Cl^-/F^- exchange using a fluoride source, such as $[Me_4N]F$, and the corresponding chloro-complexes.[1, 2, 5] In order to explore this with Group 13 fluoride complexes bearing phosphine oxide ligands, the distorted tetrahedral $[AlCl_3(OPMe_3)]$ and $[GaCl_3(OPMe_3)]$ complexes were prepared from the appropriate MCl_3 and $OPMe_3$ in anhydrous CH_2Cl_2 solution according to the reported method.[24, 25] Treatment of a solution of either $[GaCl_3(OPMe_3)]$ or $[AlCl_3(OPMe_3)]$ with three molar equivalents of $[NMe_4]F$ in dry CH_2Cl_2 instantly produced white precipitates (most probably GaF_3 and AlF_3), and the phosphine oxide was liberated from the metal (confirmed by ^{31}P NMR spectroscopy). This suggests that the chlorides are being replaced by fluorides but this is followed by dissociation of the neutral

co-ligands and subsequent polymerisation/precipitation of MF_3. Thus, halide exchange also fails to generate phosphine oxide complexes of these metal ions.

4.2.4 Stability tests on $[GaF_3(OH_2)(DMSO)]$ for evaluation as a precursor for ^{18}F radiolabelling reactions

$[GaF_3(OH_2)_2(DMSO)]$ was identified as possible precursor for $^{18}F/^{19}F$ isotopic exchange reactions. In order to assess its feasibility in this regard, its stability was investigated in the presence of an excess of chloride and fluoride anions. Specifically, a 1:1 molar ratio and a 10-fold excess of chloride or fluoride anions were added to a solution of the complex in d^6-DMSO. $^{19}F\{^1H\}$ NMR spectroscopy was used as a probe to follow the experiments. The $^{19}F\{^1H\}$ NMR spectrum of the complex shows two singlets very close in chemical shift (δ = −148.3, −148.4 ppm) reflecting the two fluoride environments in the structure (It should be noted that the spectrum in CD_3OD at room temperature of the same complex gives only one broad peak, shifted by 30 ppm at lower frequency, which resolves at 183 K, suggesting that the exchange in DMSO is slower or not present at all). When one mol. equiv. of KCl was added to this solution the peaks of the complex were lost and another unidentified, much more intense resonance at δ = −151.1 ppm appeared (most likely to be HF_2^- or F^- although the peak is very broad). This resonance broadened in the presence of a 10-fold excess of Cl^-, and the complex peak disappeared completely (Figure 4.13).

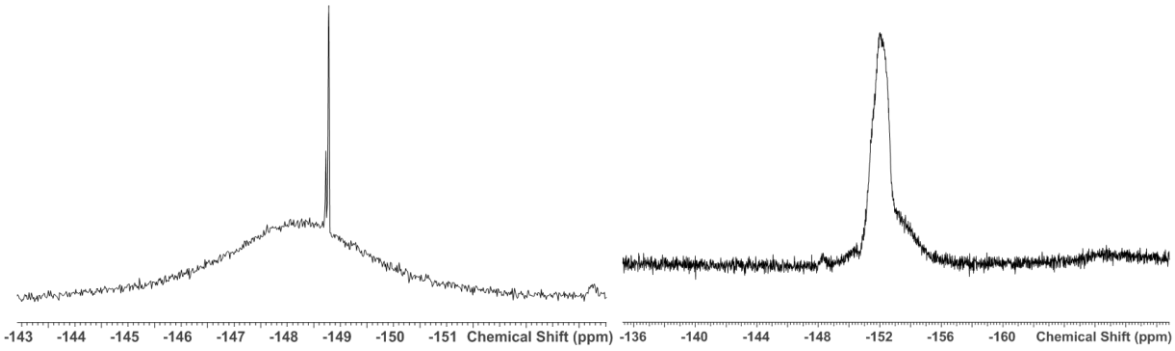

Figure 4.13. $^{19}F\{^1H\}$ NMR spectrum of $[GaF_3(OH_2)_2(DMSO)]$ in d^6-DMSO (left) and in the presence of 10 mol. equiv. (right) of KCl.

As a result of the instability of the complex in the presence of chloride anions, it was concluded that even though the ^{18}F radiolabelling might prove to be possible, the application as a PET agent would not be possible due to the inherent instability of the complex to Cl^-.

In contrast, when $[GaF_3(OH_2)_2(DMSO)]$ was challenged by fluoride anions, the $^{19}F\{^1H\}$ NMR spectrum showed that the complex was stable even in the presence of a 10-fold excess of F^-.

4.3 Conclusions

The work in this Chapter has demonstrated that $MF_3 \cdot 3H_2O$ and $[MF_3(OH_2)_2(DMSO)]$ (M = Al, Ga, In) do not react directly with phosphine oxide ligands in alcoholic and CH_2Cl_2 solutions. However, the DMSO adduct proved more successful and was used as a synthon for reactions with other O-donor ligands, producing several new complexes, which were characterised in solution and in the solid state. These O-donor complexes are generally significantly less stable than those with N-donor ligands and are partially dissociated in solution (the dissociation increases down the group). The complexes show high affinity for coordinated water, which was partially retained at the metal centre even in the presence of excess ligand or molecular sieves. The strong donor properties of H_2O and DMSO, along with the extensive H-bonding shown in the crystal structures, may confer stabilisation to the complexes and hence disfavour the substitution of all coordinated water molecules by the ligand. Although the failure to obtain complexes with soft donor ligands, such as phosphines or thioethers,[26] directly or via Cl^-/F^- exchange has parallels in other metal fluoride systems,[27] the failure to obtain complexes with phosphine oxides (O-donors) was somewhat unexpected.

Having noticed that different batches of the commercial $MF_3 \cdot 3H_2O$ show different reactivity, the use of the freshly synthesised $MF_3 \cdot 3H_2O$ hydrates was preferred during this work. The fresh samples of $AlF_3 \cdot 3H_2O$ and $GaF_3 \cdot 3H_2O$ have the molecular α-form (R−3), whereas $InF_3 \cdot 3H_2O$ has the polymeric β-form (P4/n). In all cases the hydrated metal trifluoride species were produced, in contrast with the synthesis of the Group 3 metal fluorides and LaF_3 discussed in Chapter 5, in which the MF_3 polymers are produced with no water coordinated to metal and are completely unreactive with neutral ligands.

Considering the PET aspect of this work, the synthesis of the complex $[GaF_3(OH_2)_2(DMSO)]$ was particularly important. It provides an alternative method to obtain the complexes $[GaF_3(RMe_2\text{-}tacn)]$ (R = Me, Bn) under much milder conditions (CH_2Cl_2 solution, room temperature) than the hydrothermal synthesis or without the need to perform halide exchange reactions from the chloride analogues. Moreover, the stability of $[GaF_3(OH_2)_2(DMSO)]$ was tested in the presence of an excess of chloride and fluoride anions. It turned out that although the complexes is stable in the presence of a 10-fold excess F^-, it starts decomposing in a 1:1 KCl solution and completely decomposes in a 10-fold excess KCl solution. Therefore, the possibility of performing an $^{18}F/^{19}F$ isotopic exchange reaction on this complex was discarded.

4.4 Experimental

The $MF_3 \cdot 3H_2O$ (M = Al, Ga or In), 2,2′-bipyridyl, 1,4,7-trimethyl-1,4,7-triazacyclononane (Me_3-tacn), N,N,N′,N′,N″-pentamethyldiethylenetriamine (pmdta), Ph_3PO, Me_3PO and pyNO were obtained from Sigma-Aldrich or Alfa-Aesar. Hydrothermal preparations were conducted in a 23 mL Teflon reactor vessel placed in a Parr stainless steel autoclave and heated to 180 °C overnight. For further details regarding the instrumentation used see Appendix 1.

4.4.1 $AlF_3 \cdot 3H_2O$

In a Teflon beaker, $Al_2(SO_4)_3 \cdot 16H2O$ (4.05 g, 6.42 mmol) was dissolved in freshly distilled water (15 mL). After adding $HF_{(aq)}$ 40 % (2 mL, 46.0 mmol), a white precipitate formed immediately. The white solid was filtered off, rinsed with water (20 mL) and dried in vacuo. Yield: 1.58 g, 89 %. IR (Nujol/cm^{-1}): 3500 (vbr) (O–H, H_2O), 1670 (br) (H–O–H), 585 (m), 545 (m) (Al–F).

4.4.2 $GaF_3 \cdot 3H_2O$

$Ga(NO_3)_3 \cdot 8H_2O$ (4.08 g, 10.2 mmol) was dissolved in freshly distilled water (15 mL). A solution of KOH (5 M) in water (10 mL) was added, giving a white precipitate of $Ga(OH)_3$. The precipitate was filtered off, rinsed with water and suspended in HF 40 % (10 mL, 230 mmol) in a Teflon beaker. The mixture was heated to 100 °C giving a clear solution, which was cooled to ambient temperature. Ethanol (20 mL) was added to the mixture, causing the precipitation of $GaF_3 \cdot 3H_2O$. The product was filtered off and dried *in vacuo*. Yield: 1.61 g, 56 %. IR (Nujol/cm^{-1}) 3500 (br), 3180 (br) (O–H, H_2O), 1659 (m) (H–O–H), 450 (vbr) (Ga–F).

4.4.3 $InF_3 \cdot 3H_2O$

$In_2(SO_4)_3 \cdot 9H_2O$ (3.3 g, 4.9 mmol) was dissolved in hot freshly distilled water (50 mL). A concentrated solution of NaOH (5 mL of 10 M) was added until a white solid precipitated. The solid was filtered off and washed with water. The solid was then suspended again in water (10 mL) in a Teflon beaker and HF 40 % (5 mL, 115 mmol) were added, giving a clear solution. After several minutes a white solid started to precipitate and the mixture was allowed to stand overnight. The solvent was decanted off and the solid dried *in vacuo*. Yield: 0.89 g, 62 %. IR (Nujol/cm^{-1}): 3350 (br) (O–H, H_2O), 1640 (m) (H–O–H), 452 (vbr) (In–F).

4.4.4 $[AlF_3(OH_2)_2(DMSO)]$

$AlF_3{\cdot}3H_2O$ (0.10 g, 0.72 mmol) was added to DMSO (30 mL) and stirred. The mixture was gradually heated to 75 °C and left at this temperature for 10 min, causing complete dissolution to give a colourless solution. After cooling, the solution was filtered to remove any solid deposited, and the solvent was removed *in vacuo*, giving a white solid. Yield: 0.104 g, 72 %. Required for $C_2H_{10}AlF_3O_3S$: C, 12.1; H, 5.1. Found: C, 12.1; H, 4.9 %. IR (Nujol/cm^{-1}): 3410 (br) (O–H, H_2O), 1660 (m) (H–O–H),1010 (br) (S=O), 524 (br) (Al–F). ^{1}H NMR (CD_3OD, 298 K): δ = 2.66 (s, Me). 4.85 (s, H_2O). $^{19}F\{^1H\}$ NMR (CD_3OD, 298 K): δ = −173.6 (s, [2F]), −177.2 (s [F]); (183 K): −171.8 (br s, [2F]), −176.5 (s, [F]). ^{27}Al NMR (CD_3OD, 298 K): δ = −10.1 (s).

4.4.5 $[GaF_3(OH_2)_2(DMSO)]$

$GaF_3{\cdot}3H_2O$ (0.290 g, 1.6 mmol) was added to DMSO (40 mL) and stirred. The mixture was gradually heated to 85 °C and left at this temperature for 10 min, causing almost complete dissolution of the solid. After cooling, the solvent was removed *in vacuo* giving a white solid. The solid was dissolved in methanol (10 mL), the solution was filtered to remove the unreacted $GaF_3{\cdot}3H_2O$ and the solvent removed again, giving a white solid. Yield: 0.278 g, 72 %. Required for $C_2H_{10}F_3GaO_3S$: C, 10.0; H, 4.2. Found: C, 10.1; H, 4.1 %. IR (Nujol/cm^{-1}): 3400 (vbr) (O–H, H_2O), 3180 (sh) (O–H, H_2O), 1605 (br) (H–O–H), 1004 (br) (S=O), 496 (br) (Ga–F). ^{1}H NMR (CD_3OD, 298 K): δ = 2.66 (s, Me), 4.92 (s, H2O). $^{19}F\{^1H\}$ NMR (CD_3OD, 298 K): δ = −177.4 (br s); (183 K): −175.0 (br s [2F]), −176.6 (s, [F]).

4.4.6 $[InF_3(OH_2)_2(DMSO)]$

$InF_3{\cdot}3H_2O$ (0.21 g, 0.92 mmol) was added to DMSO (40 mL) and stirred. The mixture was gradually heated to 110 °C, leading to partial dissolution. The mother liquor was decanted off and, after cooling, the solvent was removed *in vacuo* giving a white solid. Yield: 0.032 g, 12 %. Required for $C_2H_{10}F_3InO_3S$: C, 8.4; H, 3.5. Found: C, 8.5; H, 3.3 %. IR (Nujol/cm^{-1}): 3320 (br) (O–H, H_2O), 1643 (m, H–O–H), 1001 (br) (S=O), 464 (br) (In–F). ^{1}H NMR (CD_3OD, 298 K): δ = 2.66 (s, Me), 4.86 (s, H_2O) $^{19}F\{^1H\}$ NMR (CD_3OD, 298 K): not observed; (183 K): δ = −133.5 (s), −136.7 (br), −187.65 (s).

4.4.7 $[AlF_3(OH_2)_2(pyNO)]$

$[AlF_3(OH_2)_2(DMSO)]$ (0.05 g, 0.25 mmol)) was suspended in MeOH (5 mL). A solution of pyNO (0.05 g, 0.57 mmol) in MeOH (5 mL) was added. After 2 h the solvent was removed *in vacuo* and the resulting white solid was washed with CH_2Cl_2 (5 mL) and dried *in vacuo*. Yield: 0.049 g, 90 %. Required for$C_5H_9AlF_3NO_3$: C, 27.9; H, 4.2; N, 6.6. Found: C, 28.0; H, 4.1; N, 6.6 %. IR (Nujol/cm^{-1}): 3606 (vb) (O–H, H_2O), 1605 (br) (H–O–H), 1154 (br) (N–O), 565 (br) (Al–F). ^{1}H NMR (CD_3OD, 298 K):

δ = 4.85 (s, H_2O), 7.57 (s, [2H]), 7.65 (s, [H]), 8.36 (s, [2H]). $^{19}F\{^1H\}$ NMR (CD_3OD, 298 K): δ = −173.7 (s, [2F]), −177.3 (s, [F]).

4.4.8 $[GaF_3(OH_2)_2(pyNO)]\cdot pyNO\cdot H_2O$

$GaF_3(OH_2)_2(DMSO)]$ (0.05 g, 0.21 mmol) was dissolved in MeOH (15 mL). pyNO (0.08 g, 0.62 mmol) was added, giving a colourless solution. After 7 h the solvent was removed *in vacuo* giving a colourless oil. After several days the oil partially solidified into crystals, which were manually separated from the oil and dried *in vacuo*. Yield: 0.043 g, 56 %. Required for $C_{10}H_{16}GaF_3N_2O_5$: C, 32.4; H, 4.3; N, 7.6. Found: C, 32.3; H, 4.2; N, 7.4 %. IR (Nujol/cm^{-1}): 3616 (br) (O–H, H_2O), 1605 (br, H–O–H), 1265, 1154, (br) (N–O), 565, 555 (Ga–F). 1H NMR (CD_3OD, 298 K): δ = 4.86 (s, H_2O), 7.57 (s, [2H]), 7.65 (s, [H]), 8.36 (s, [2H]); (183 K): 7.65 (s), 7.75 (s), 7.77 (br s), 8.06 (br s), 8.46 (s), 8.73 (br s). $^{19}F\{^1H\}$ NMR (CD_3OD, 298 K): δ = −176.9 (s); (183 K): −174.1, −175.0, −176.5.

4.4.9 $[GaF_4(pmdtaH)]$

$[GaF_3(OH_2)_2(DMSO)]$ (0.06 g, 0.25mmol) was suspended in CH_2Cl_2 (5 mL). pmdta (0.06 mL, 0.30 mmol) was added giving a clear solution after few minutes. After 2 h the solvent was removed *in vacuo* and the resulting solid washed with hexane, giving a white solid which was dried *in vacuo*. Yield: 0.04 g, 50 %. Required for $C_9H_{24}F_4GaN_3$: C, 33.8; H, 7.6; N, 13.1. Found: C, 33.8; H, 7.7; N, 13.0 %. IR (Nujol/cm^{-1}): 536, 524, 504 (Ga–F). ^1H NMR (CD_2Cl_2, 298 K): δ = 2.42 (s, [3H]), 2.57 (s, [6H]), 2.60 (s, [6H]), 2.95 (td, [4H]), 3.44 (td, [4H]), 3.46 (s, H). $^{13}C\{^1H\}$ NMR (CD_2Cl_2, 298 K): δ = 40.80 ([C]), 44.82 ([C]), 48.57 ([C]), 49.71 ([C]), 54.78 ([2C]), 56.23 ([2C]), 56.74 ([C]). $^{19}F\{^1H\}$ NMR (CD_2Cl_2, 298 K): δ = −156.1 (br s, [F]), −168.2 (br s, [2F]), −194.6 (br s, [F]). Evaporation of a CD_2Cl_2 solution gave crystals of $[GaF_4(pmdtaH)]\cdot 2H_2O$ suitable for X-ray diffraction. Diffusion of hexane into a solution of the product in CH_2Cl_2 gave a few crystals after several weeks, which were shown to be $[\subset Me_2N(CH_2)_2NMe(CH_2)_2]_2[Ga_2F_8(OH_2)_2]\cdot 2H_2O$.

4.4.10 $[GaF_3(Me_3\text{-tacn})]\cdot 4H_2O$

The reaction was carried out using Schlenk techniques and under an atmosphere of dry N_2 and with anhydrous CH_2Cl_2. $[GaF_3(OH_2)_2DMSO]$ (0.07 g, 0.29 mmol) was suspended in 8 mL of CH_2Cl_2. Me_3tacn (0.07 mL, 0.36 mmol) was added, giving a clear solution after ~ 2 minutes. After 2 h hexane was added and a white solid precipitated. The solid was filtered, washed with hexane and dried *in vacuo*. Yield: 0.08 g, 81 %. Required for $C_9H_{23}F_3GaN_3O$: C, 34.2; H, 7.3; N, 13.3. Found: C, 33.9; H, 8.4; N, 12.7 %. IR (Nujol/cm^{-1}): 3425 (br) (O–H), 1666 (br) (H–O–H), 520, 485 (Ga–F). ^1H NMR (CD_3CN, 298 K): δ = 2.63 (s, [9H]), 2.72 (m, [6H],), 2.85 (m, [6H]). $^{19}F\{^1H\}$ NMR (CD_2Cl_2, 298 K): δ = –181.6 (br q).

Colourless crystals whose unit cell matched the one reported in the literature[1] were grown adding hexane into a CH_2Cl_2 solution of the product and cooling in a freezer.

4.4.11 $[GaF_3(OH_2)(bipy)]\cdot 2H_2O$

$[GaF_3(OH_2)_2(DMSO)]$ (0.050 g, 0.21 mmol) was added to 10 mL of MeOH giving a colourless solution. A solution of bipy in 10 mL of MeOH was added. After 4 h the solvent was removed *in vacuo* giving a white solid. The solid was dissolved in the minimum amount of MeOH and left in the fridge overnight, causing the formation of crystals suitable for X-ray diffraction. Yield: 0.042 g, 60 %. Required for $C_{10}H_{14}F_3GaN_2O_3$: C, 35.7; H, 4.2; N, 8.3. Found: C, 35.6; H, 4.1; N, 8.2 %. IR (Nujol, ν/cm^{-1}): 3500, 3380 (br) (O–H, H_2O), 1660 (br) (O–H), 576, 539 (Ga–F). ^1H NMR (CD_3OD, 298 K): δ = 9.08 (br, [2H], ArH), 8.67 (br d, J_{HH} 8 Hz, [2H], ArH), 8.40 (br t, J_{HH} 7 Hz, [2H], ArH), 7.91 (br t, J_{HH} 6 Hz, [2H], ArH). $^{19}F\{^1H\}$ NMR (CD_2Cl_2, 298 K): δ = –176.5.

4.4.12 X-ray experimental

The crystal quality for $[GaF_4(pmdtaH)]\cdot 2H_2O$ and $[GaF_3(OH_2)_2(pyNO)]\cdot pyNO\cdot H_2O$ was rather poor, leading to higher than normal residuals, hence detailed comparisons of bond lengths and angles require caution. Except for $[NMe_2H_2][GaF_4(OH_2)_2]$ and $[GaF_3(OH_2)_2(DMSO)]$, the H atoms on the water molecules were not located in the difference map.

Table 4.1. Crystal data and structural refinement details. [a]

Compound	$[Me_2NH_2][trans\text{-}GaF_4(OH_2)_2]$	$[GaF_3(OH_2)_2(DMSO)]$	$[GaF_3(OH_2)_2(pyNO)]\cdot pyNO\cdot H_2O$
Formula	$C_2H_{12}F_4GaNO_2$	$C_2H_{10}F_3GaO_3S$	$C_{20}H_{32}F_6Ga_2N_4O_{10}$
M	227.85	240.87	741.94
Crystal system	Monoclinic	triclinic	triclinic
Space group	C2/c (no.15)	P-1 (no. 2)	P-1 (no. 2)
a /Å	6.8849(10)	4.951(3)	9.395(6)
b /Å	7.6680(10)	7.808(5)	11.274(8)
c /Å	14.5718(10)	9.556(6)	15.285(10)
α/ °	90	93.469(12)	95.773(18)
β /°	97.153(4)	93.421(15)	107.49(2)
γ/°	90	94.188(16)	109.552(15)
U /Å^3	763.31(16)	367.0(4)	1418.1(16)
Z	4	2	2
μ(Mo-K$_\alpha$)/mm^{-1}	3.627	4.040	1.997
F(000)	456	240	752
Total no. reflns	2641	4454	24366
R_{int}	0.043	0.128	0.112
Unique reflns	872	1427	5555
No. of params, restraints	50, 0	93, 2	397, 24
R_1, wR_2 [$I > 2\sigma(I)$][b]	0.031, 0.073	0.094, 0.240	0.087, 0.245
R_1, wR_2 (all data)	0.044, 0.078	0.120, 0.261	0.101, 0.254

Table 4.1 continued

Compound	$[GaF_4(pmdtaH)]\cdot 2H_2O$	$[Me_2N(CH_2)_2NMe(CH_2)_2]_2[Ga_2F_8(OH_2)_2]\cdot 2H_2O$	$[GaF_3(OH_2)(py)_2]\cdot H_2O$
Formula	$C_9H_{24}F_4GaN_3O_2$	$C_{14}H_{46}F_8Ga_2N_4O_6$	$C_{10}H_{14}F_3GaN_2O_2$
M	352.06	657.99	320.95
Crystal system	Monoclinic	monoclinic	monoclinic
Space group	$P2_1/n$ (no.14)	$P2_1/c$ (no. 14)	$P2_1$ (no. 4)
a /Å	11.819(7)	10.262(4)	7.220(2)
b /Å	9.993(6)	7.592(3)	11.123(3)
c /Å	12.973(8)	16.436(8)	8.111(2)
α/ °	90	90	90
β /°	97.800(10)	98.398(11)	115.353(5)
γ/°	90	90	90
U /Å^3	1518.0(16)	1266.7(9)	588.6(3)
Z	4	2	2
μ(Mo-K$_\alpha$)/mm^{-1}	1.857	2.226	2.372
F(000)	728	694	316
Total no. reflns	15289	11243	4940
R_{int}	0.221	0.047	0.051
Unique reflns	3491	2491	1959
No. of params, restraints	177, 2	175, 28	163, 15
R_1, wR_2 [$I > 2\sigma(I)$][b]	0.071, 0.137	0.046, 0.122	0.054, 0.140
R_1, wR_2 (all data)	0.154, 0.168	0.062, 0.134	0.062, 0.145

[a] Common items: T = 100 K; wavelength (Mo-Kα) = 0.71073 Å; ϑ(max) = 27.5°;

[b] $R_1 = \Sigma||F\sigma| - |Fc|| / \Sigma|Fo|$; $wR_2 = [\Sigma w(Fo^2 - Fc^2)^2 / \Sigma wFo^2]^{1/2}$.

4.5 References

1. Bhalla, R.; Darby, C.; Levason, W.; Luthra, S. K.; McRobbie, G.; Reid, G.; Sanderson, G.; Zhang, W., *Chem. Sci.* **2014**, *5*, 381.

2. Bhalla, R.; Levason, W.; Luthra, S. K.; McRobbie, G.; Monzittu, F. M.; Palmer, J.; Reid, G.; Sanderson, G.; Zhang, W., *Dalton Trans.* **2015**, *44*, 9569.

3. Downs, A. J., *Chemistry of Aluminium, Gallium, Indium and Thallium,* Blackie Academic & Professional, **1993**.

4. Benjamin, S. L.; Levason, W.; Reid, G., *Chem. Soc. Rev.* **2013**, *42*, 1460.

5. Bhalla, R.; Levason, W.; Luthra, S. K.; McRobbie, G.; Sanderson, G.; Reid, G., *Chem. Eur. J.* **2015**, *21*, 4688.

6. Petrosyants, S. P.; Ilyukhin, A. B., *Russ. J. Inorg. Chem.* **2011**, *56*, 1250.

7. Bodor, A.; Toth, I.; Banyai, I.; Szabo, Z.; Hefter, G. T., *Inorg. Chem.* **2000**, *39*, 2530.

8. Hagen, H.; Roesky, Herbert W.; Thomas, L.; Cord, R.; M, S. G.; Manish, B., *Organometallics* **1998**, *17*, 4326.

9. Kemnitz, E.; Groß, U.; Rüdiger, S.; Scholz, G.; Heidemann, D.; Troyanov, S. I.; Morosov, I. V.; Lemée-Cailleau, M. H., *Solid State Sci.* **2006**, *8*, 1443.

10. Bukovec, P.; Kaucic, V., *Inorg. Nucl. Chem. Letters* **1978**, *14*, 79.

11. Wei, Y.-S.; Hu, X.-P.; Han, Z.; Dong, X.-Y.; Zang, S.-Q.; Mak, T. C. W., *J. Am. Chem. Soc.* **2017**, *139*, 3505.

12. An, J.; Farha, O. K.; Hupp, J. T.; Pohl, E.; Yeh, J. I.; Rosi, N. L., *Nat. Commun.* **2012**, *3*, 604.

13. Verma, A.; De, D.; Tomar, K.; Bharadwaj, P. K., *Inorg. Chem.* **2017**, *56*, 9765.

14. Davies, A. J., *Adv. Inorg. Chem. Radiochem.* **1981**, *24*, 115.

15. George, K.; Hector, A. L.; Levason, W.; Reid, G.; Sanderson, G.; Webster, M.; Zhang, W., *Dalton Trans.* **2011**, *40*, 1584.

16. Cheng, F.; Davis, M. F.; Hector, A. L.; Levason, W.; Reid, G.; Webster, M.; Zhang, W., *Eur. J. Inorg. Chem.* **2007**, *2007*, 2488.

17. Davis, M. F.; Levason, W.; Reid, G.; Webster, M., *Polyhedron* **2006**, *25*, 930.

18. Gurnani, C.; Hector, A. L.; Jager, E.; Levason, W.; Pugh, D.; Reid, G., *Dalton Trans.* **2013**, *42*, 8364.

19. Hector, A. L.; Jolleys, A.; Levason, W.; Reid, G., *Dalton Trans.* **2012**, *41*, 10988.

20. Levason, W.; Light, M. E.; Maheshwari, S.; Reid, G.; Zhang, W., *Dalton Trans.* **2011**, *40*, 5291.

21. Brown, D. H.; Stewart, D. T.; Jones, D. E. H., *Spectrochim. Acta, Part A* **1972**, *29*, 213.

22. Masaguer, J. R.; Sanchez, A.; Casas, J. S.; Sordo, J.; Castineiras, A., *J. Inorg. Nucl. Chem.* **1978**, *40*, 355.

23. Petricek, S.; Demsar, A.; Bukovec, P.; Golic, L.; Brencic, J. V., *Acta Chimica Slovenica* **1997**, *44*, 317.

24. Cheng, F.; Codgbrook, H. L.; Hector, A. L.; Levason, W.; Reid, G.; Webster, M.; Zhang, W., *Polyhedron* **2007**, *26*, 4147.

25. Burford, N.; Royan, B. W.; Spence, R. E. v. H.; Cameron, T. S.; Linden, A.; Rogers, R. D., *J. Chem. Soc., Dalton Trans.* **1990**, 1521.

26. Bhalla, R.; Burt, J.; Hector, A. L.; Levason, W.; Luthra, S. K.; McRobbie, G.; Monzittu, F. M.; Reid, G., *Polyhedron* **2016**, *106*, 65.

27. Benjamin, S. L.; Levason, W.; Pugh, D.; Reid, G.; Zhang, W. J., *Dalton Trans.* **2012**, *41*, 12548.

Chapter 5: **Group 3 (Sc^{3+}, Y^{3+}) and lanthanide (La^{3+}, Lu^{3+}) coordination chemistry: exploring the synthesis of neutral metal trifluoride complexes**

5.1 Introduction

Chapters 2 and 3 (along with the works previously published[1,2]) have demonstrated that Group 13 metal fluorides are promising systems for the development of PET radiotracers. In this Chapter, the coordination chemistry of the trivalent Group 3 and lanthanide ions (Sc, Y, La, Lu) with the neutral N-donor ligands (terpy, Me_3-tacn) is explored in order to assess their feasibility as potential PET platforms. Scandium and yttrium were selected because they have some similarities with the Group 13 metals; they have a closed shell electronic configuration, their chemistry is dominated by the 3+ oxidation state and both groups are hard Lewis acids.[3] However, the larger ionic radius of Sc(III) and Y(III) (table 5.1) make the formation of complexes with higher coordination numbers (generally up to eight for Y) more likely, and their higher oxophilicity makes their chemistry with O-donor ligands predominant. Their oxophilicity, therefore, could potentially disrupt the coordination at the metal in aqueous solution, leading to higher coordination numbers.

M^{3+}	Ionic radius (Å)	Reference
Al(III)	0.54	4
Ga(III)	0.62	4
In(III)	0.80	4
Sc(III)	0.68	5
Y(III)	0.88	5
La(III)	1.22	6
Lu(III)	1.03	6

Table 5.1. Ionic radii of the M^{3+} cations in octahedral complexes.

The preferred coordination number for scandium is typically six, whereas the larger Y(III) often shows coordination numbers of seven and eight. The chemistry of the Group 3 metal ions has often been associated with and investigated along with the lanthanides ions, looking more into similarities rather than differences.[7] The La(III) and Lu(III) ions are also taken into consideration in this Chapter as they also have a closed shell configuration and their most common oxidation number is 3+ (as for all the lanthanides elements, apart from some that are relatively stable in the

oxidation state +2[8] and Ce(IV)[9]). Moreover, in contrast to the other Ln(III) ions, NMR spectroscopy can be used as a probe to investigate solution speciation in these diamagnetic systems. Similar considerations to the Group 3 can be made regarding their chemical behaviour; they are highly oxophilic and, due to their larger ionic radii (Table 5.1), the preferred coordination numbers are often higher (8-9) compared to scandium and yttrium, with examples of even higher coordination numbers in non-sterically demanding or macrocyclic systems.[10,11,12]

In consideration of the potential application of these systems as PET tracers, the stable oxidation state of the metals is certainly a positive aspect, but the range of coordination numbers in the complexes could lead to the formation of a wider range of species in aqueous solution. These systems are also often labile, so the choice of co-ligand is important in order to form kinetically inert complexes. This is particularly relevant for *in vivo* applications (e.g. PET), as these metals are usually toxic and the lability could lead to loss of $[^{18}F]F^-$.

The chemistry of Sc(III), Y(III), La(III) and Lu(III) is vast and diverse. For example, aluminium alloys containing scandium have applications in the aerospace industry, as a recrystallisation inhibitor and as an additive for superplastic materials.[13] Up to the 1990s, the chemistry of Sc(III) and Y(III) was dominated by organometallic compounds with cyclopentadienyl (Cp) derivatives.[14] These compounds have found applications in C-H bond activation (ethene, styrene and α-olefin polymerisation) and aromatic C-F bond activation.[15,16,17,18,14] The negative thermal expansion of ScF_3 has been exploited by optical, electronic and biomedical industries.[19,20,21] However, the coordination chemistry of the halides of these metals has been less developed, in particular with neutral ligands. Due to the high oxophilicity of these metals, O-donor ligands, such as crown ethers, have often been utilised.[5]

5.1.1 Overview of MX_3 (M = Sc, Y, La, Lu; X = Cl, Br, I) coordination chemistry with neutral ligands

The MX_3 (M = Sc, Y, La, Lu; X = Cl, Br, I) have poor or limited solubility in most solvents, with the exception of the iodides, which are slightly soluble in weakly coordinating solvents such as MeCN. The different solubility reflects the increasing lattice energy and the tendency to polymerise *via* halide bridges for the lighter halides. As a result, MI_3 can be used directly to react with neutral ligands but the bromides and chlorides usually require the synthesis of a more soluble molecular synthon. Suitable synthons were identified in $[MX_3(thf)_3]$ (M = Sc,[22] La, Lu; X = Cl, Br or $[YCl_2(thf)_5][YCl_4(thf)_2]$).[23,24,25,26,27] The higher solubility of these compounds comes with higher air and moisture sensitivity, but they are particularly important for reaction with less strongly coordinating ligands (e.g. non O-donor ligands). Alternatively, when the reactions do not require anhydrous conditions, the hydrated metal halide salts or the nitrates can be reacted directly with

the appropriate ligand.[28,29,30] Indeed, the reactions of $ScX_3 \cdot xH_2O$ and $YX_3 \cdot xH_2O$ (X = Cl, Br, I) with R_3PO and R_3AsO (R = Me, Ph) in ethanol produced the desired complexes, $[MX_2(R_3PO)]X$, showing coordination number of six in all cases (Figure 5.1) (in contrast to the reactions of $Sc(NO_3)_3$ and $Y(NO_3)_3$ with the same ligands, which gave complexes with coordination numbers from six to nine[28]). The analysis of the bond distances revealed a higher affinity of the metal ions towards chlorides compared to the other heavier halides for a fixed ligand.[30,29]

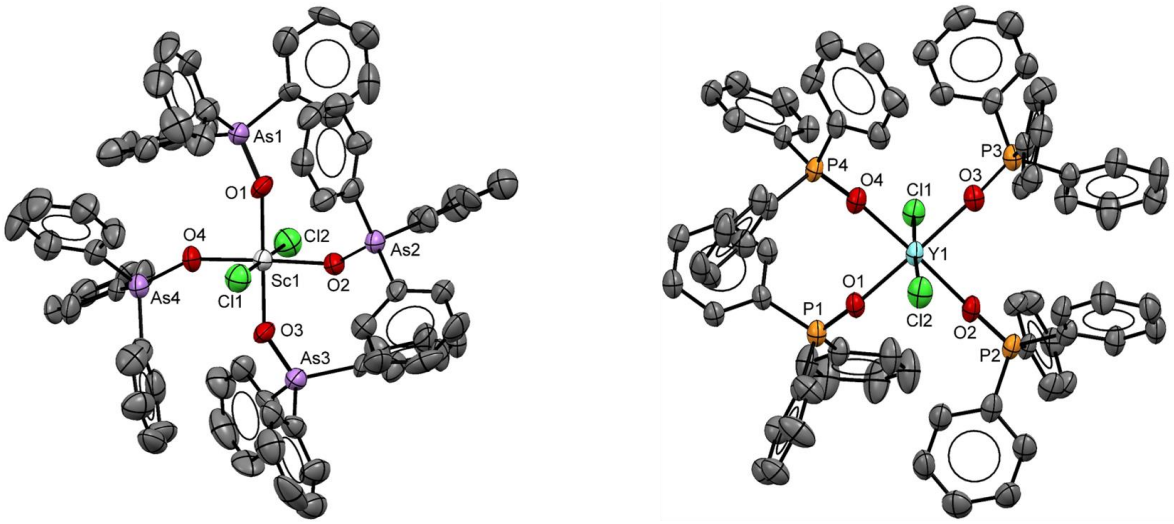

Figure 5.1. Crystal structure of the cations in $[ScCl_2(OAsPh_3)_4]Cl$ (left) and $[YCl_2(OPPh_3)_4]Cl \cdot 2EtOH \cdot H_2O$. Images redrawn from CCDC numbers 173060[29] and 173577.[30]

The use of LaI_3, LuI_3, ScI_3, YI_3, $[ScCl_3(thf)_3]$ or $[YCl_2(thf)_5][YCl_4(thf)_2]$ as molecular sources of the metal halides in reactions with the mixed oxa-thia and oxa-selena macrocycles, $[18]aneO_4S_2$, $[15]aneO_3S_2$ and $[18]aneO_4Se_2$ (Scheme 5.1), was successful in forming complexes in which the soft S- and Se-donor atoms coordinate to the metal.

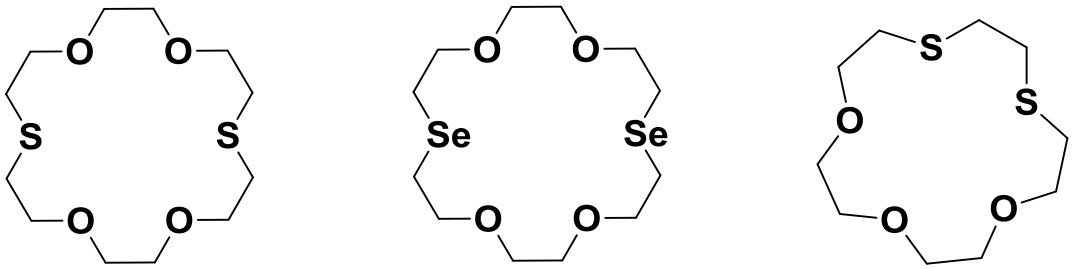

Scheme 5.1. Mixed oxa-thia and oxa-selena crowns employed for reactions with Group 3 ions.

These complexes represent rare examples of these hard metals coordinated to the neutral sulfur and selenium donor groups, proving that in the right conditions, when competition from other potential stronger ligands is eliminated, they can coordinate with soft-donor ligands.

Representative examples of the systems are shown in Figure 5.2.[24] These reactions must be performed in strictly anhydrous conditions to prevent water from coordinating to the metals.

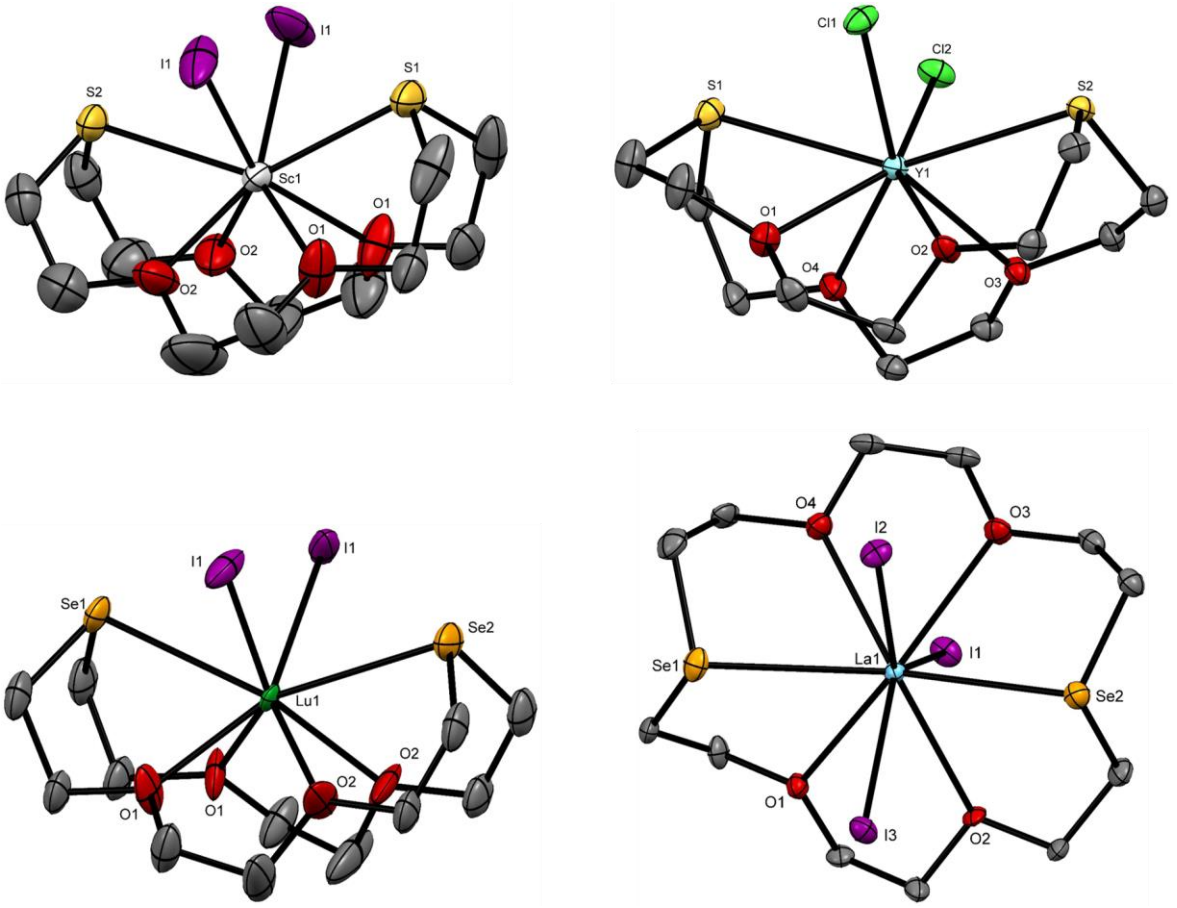

Figure 5.2. Top: crystal structure of $[ScI_2([18]aneO_4S_2)]I{\cdot}MeCN$ (left) and $[YCl_2([18]aneO_4S_2)][FeCl_4]$ (right); bottom: crystal structure of $[LuI_2([18]aneO_4Se_2)]I{\cdot}2MeCN$ (left) and $[LaI_3([18]aneO_4Se_2)]$ (right). Ellipsoids are drawn at 50 % probability level and H atoms are omitted for clarity. Iodide and the acetonitrile molecules in the crystal lattice of $[LuI_2([18]aneO_4Se_2)]I{\cdot}2MeCN$ and $[ScI_2([18]aneO_4S_2)]I{\cdot}MeCN$ and $FeCl_4^-$ in $[YCl_2([18]aneO_4S_2)][FeCl_4]$ are also omitted. Images redrawn from CCDC numbers 940220, 940225, 940227 and 940228.[24]

Figure 5.2 shows that the La(III) centre is nine-coordinate with the three iodide anions in the first coordination sphere, whereas only two iodide ions are coordinated to the smaller Sc(III), Y(III) and Lu(III) complexes, giving eight-coordinate complexes with a discrete iodide ion (or $FeCl_4^-$ for Y) balancing the charge. The difference in coordination numbers reflects the bigger radius of La(III) (Table 5.1).

Reactions of $[MCl_3(thf)_3]$ and $[YCl_2(thf)_5][YCl_4(thf)_2]$ with the N-donor ligands, Me_3-tacn, produced six-coordinate complexes $[MCl_3(Me_3\text{-tacn})]$, where the three nitrogen atoms and the three chloride atoms complete the octahedral configuration around the metal (Figure 5.3).[25]

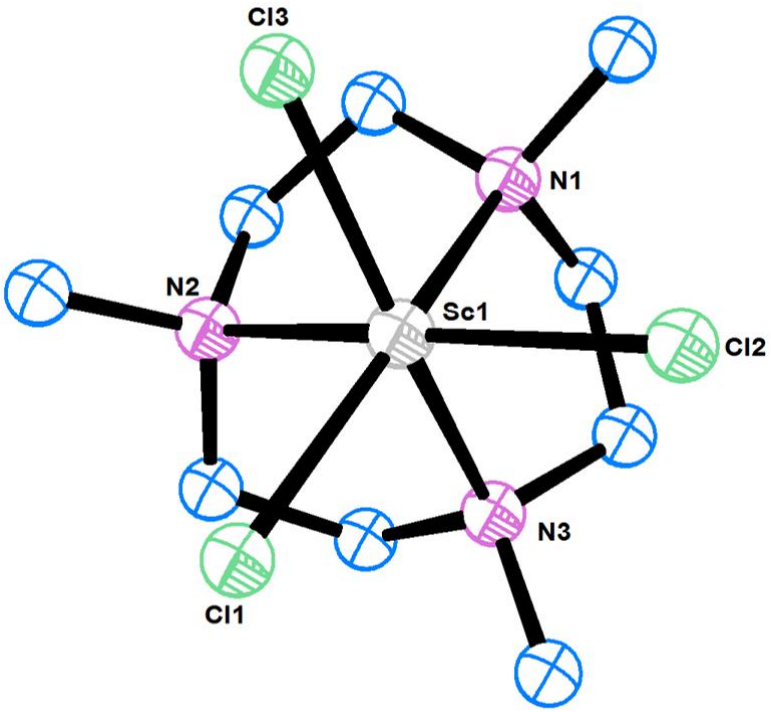

Figure 5.3. Crystal structure of [$ScCl_3(Me_3$-tacn)]. Ellipsoids are drawn at 50 % probability level and H atoms are omitted for clarity. Image redrawn from CCDC number 1219295.[25]

These complexes were first synthesised by the Bercaw Group who proceeded to substitute the chlorides with methyl groups for C-H bond activation applications.[25] The same strategy has been utilised for the activation of ethene polymerisation[26] and in the catalytic chemistry of cationic alkyl compounds.[27] This last study also reported the reaction with Me_3-triazacyclohexane, the complexes were compared with the analogues Me_3-tacn. Unsurprisingly, they found that both metals coordinate to the different ligands, but both prefer the Me_3-tacn based on macrocycle ring size/metal radius match.

A detailed and abstruse examination of the structural properties of the lanthanide series with terpy as ligand, $[LnCl(terpy)(OH_2)_x]Cl_2 \cdot y\text{-}xH_2O$ (x = 1, 2; y = 6 or 8), has been reported. The complexes showed coordination numbers of eight or nine and were obtained in aqueous EtOH solution by mixing the reagent in a 1:1 ratio.[31] Complexes of La(III) were also obtained with *ortho*-phenantroline and pyridine,[32,33] and the crystal structure of the seven-coordinate $[LaCl_3(py)_4] \cdot 0.5py$ was reported (Figure 5.4).

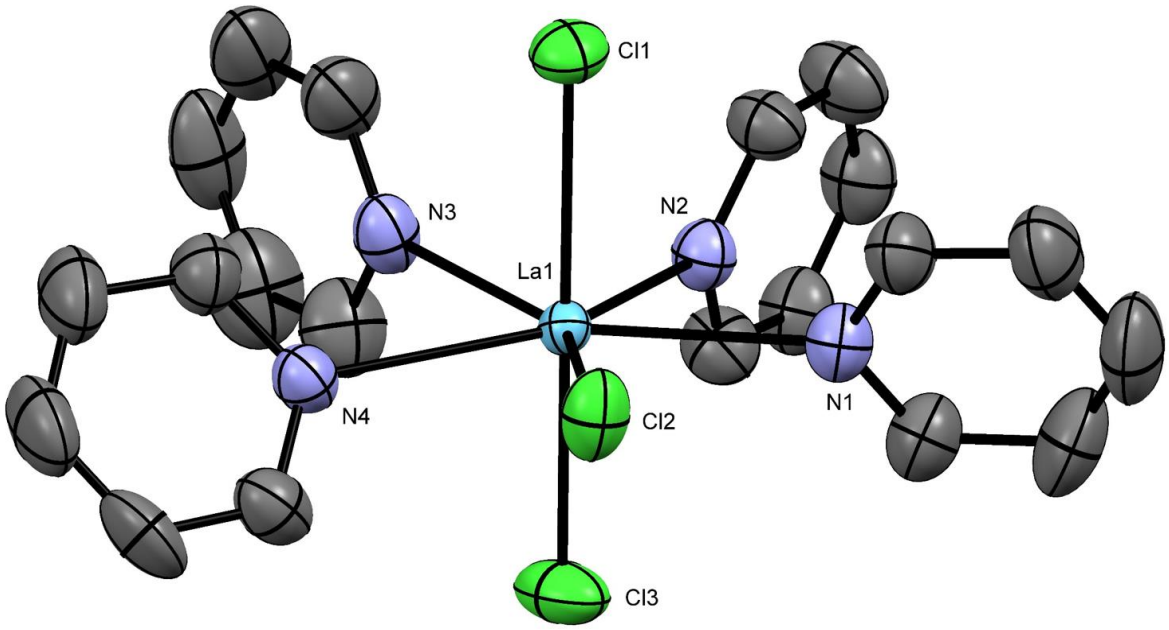

Figure 5.4. Crystal structure of the metal complex present in $[LaCl_3(py)_4]\cdot 0.5py$. Ellipsoids are drawn at 50 % probability level and H atoms and solvated pyridine are omitted for clarity. Image redrawn from CCDC number 171592.[33]

5.1.2 MF_3 (M = Sc, Y, La, Lu) coordination chemistry

The coordination chemistry of the Group 3 and f-block metal trifluorides has been even less developed compared to that of the heavier halides. This is most likely due to their poor solubility in most solvents, poor reactivity towards neutral ligands and, particularly for the Group 3 elements, their high cost and limited availability.[3,7] Complexes of these metal fluorides are limited to those containing charged N- or C-donor ligands,[3] such as $[\{Cp_2ScF\}_3]$,[34] $[\{Cp_2Y(\mu\text{-}F)(thf)_2\}_2]$,[15] $[Sc\{MeC(N(2,6\text{-}^iPrC_6H_3))CHC(Me)(NCH_2CH_2NMe)NH(2,6\text{-}^iPrC_6H_3)\}F]$[18] and $[Sc(\mu\text{-}F)_2\{Fe(C_5H_4NSi^tBuMe_2)_2\}]$.[16] Roesky and co-workers reported another example of a Sc-F complex, $[ScL(\mu\text{-}F)_2(SnMe_3Br)_2]$ (L^- = N,N′-(1,3-dimethyl-1,3-propanediylidine)bis(N′,N′-diethyl-1,2-ethanediamine), which was obtained by a halide exchange reaction using Me_3SnF as the fluoride source.[35] $[ScBr_2(L)]$ was reacted with 2 molar equivalents of Me_3SnF in toluene solution at room temperature, leading to a complex in which the bromides are replaced by fluorides at the Sc(III) centre and two Me_3SnBr molecules are linked through bridges via the fluorides (Figure 5.5).[35]

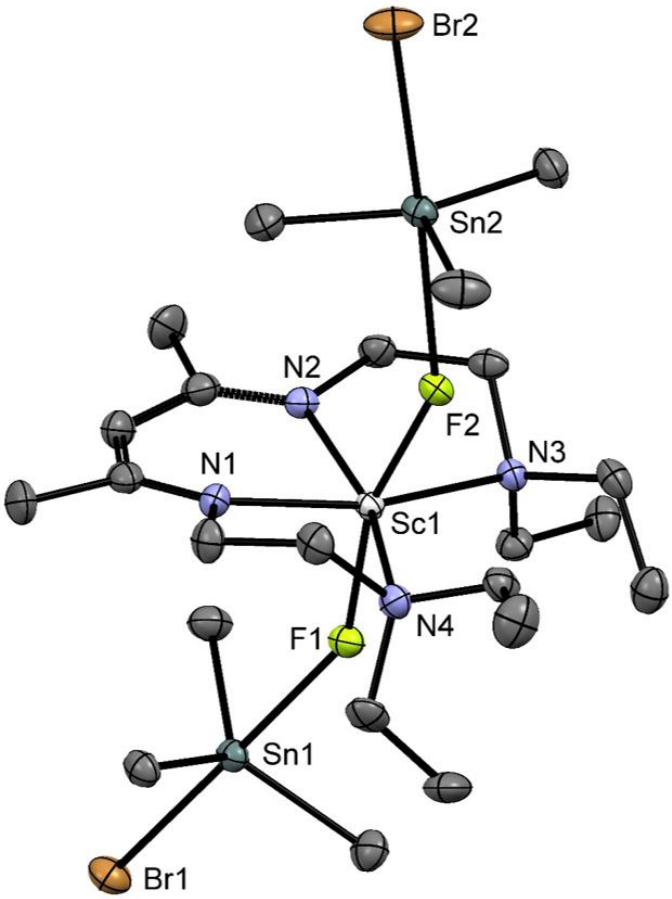

Figure 5.5. Crystal structure of $[ScL(\mu\text{-}F)_2(SnMe_3Br)_2]$ (L^- = N,N′-(1,3-dimethyl-1,3-propanediylidine)bis(N′,N′-diethyl-1,2-ethanediamine). Ellipsoids are drawn at 50 % probability level and H atoms and solvated pyridine are omitted for clarity. Selected bond lengths (Å) and angles (°): Sc1-F1 1.967(3), Sc1-F2 1.991(3), Sn1-F1 2.419(3), Sn2-F2 2.455(5), F1-Sc1-F2 162.20(2), Sc1-F1-Sn1 149.28(14), F1-Sn1-Br1 177.47(7).Image redrawn from CCDC number 199568.[35]

Examples of complexes having La-F or Lu-F bonds are extremely rare, with only three structures reported to-date, $[La(CF_3Form)_3]$ (CF_3Form = N,N'-bis(2-trifluoromethylphenyl)formamidine) and $[La(L)_3]$ (L = *p*-$HC_6F_4N(CH_2)_2NR_2$; R = Me, Et), in which the fluorides are part of the ligand itself (from studies looking into C-F bond activation).[36,37]

Considering the insolubility and inertness of these Group 3 and *f*-block MF_3, this Chapter explores possible routes in order to find an entry into their chemistry with the aim of obtaining complexes of the type $[MF_3(L)]$, where L is terpy or RMe_2-tacn (R = Bn, Me). The properties of the synthesised trifluoride complexes will then be evaluated with a view towards possible PET radiotracers.

5.2 Results and discussion

Three possible routes to Group 3 metal trifluoride complexes of RMe_2-tacn and terpy (L, R = Me, Bn) were identified:

- Direct reaction of the "hydrated" Group 3 metal trifluorides with neutral ligands;
- Chloride(iodide)/fluoride exchange by reaction of the pre-formed Group 3 metal trichloride or triiodide complexes, $[MX_3(L)]$ (X = Cl or I), with anhydrous $[Me_4N]F$;
- Chloride(iodide)/fluoride exchange by reaction of the pre-formed Group 3 metal trichloride or triiodide complexes, $[MX_3(L)]$ (X = Cl or I), with Me_3SnF.

5.2.1 Attempted synthesis of $MF_3 \cdot xH_2O$ (M = Sc, Y, La) for direct reaction with neutral ligands

This strategy had been successful with the Group 13 metal trifluorides (Chapter 4). The anhydrous MF_3 (M = Al, Ga, In) are insoluble and inert, but the hydrates, $MF_3 \cdot 3H_2O$, reacted with neutral ligands in hydrothermal conditions (180 °C, 15 hours) to form complexes of the type, $[MF_3(L)]$.[2] The same approach was undertaken with the MF_3 (M = Sc, Y, La), which are also insoluble and inert. However, the hydrated Group 3 metal trifluorides are not commercially available and only a few papers can be found in the literature in which the extent of hydration quoted is variable (typically less than one water molecule per metal). The synthesis of the $MF_3 \cdot xH_2O$ was, therefore, attempted. The reaction of metal salts with either KF or HF in water produced "$MF_3 \cdot xH_2O$" as white precipitates (Scheme 5.2).

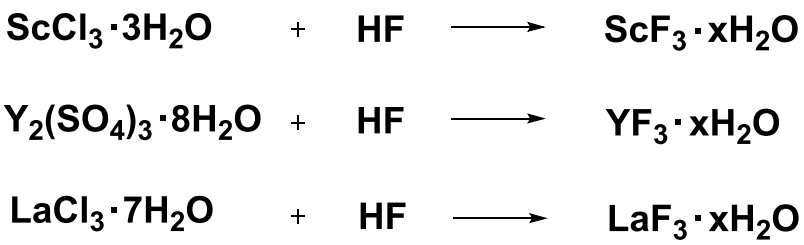

Scheme 5.2. Reaction scheme of the synthesis of $MF_3 \cdot H_2O$

$ScCl_3 \cdot 3H_2O$ was made from the oxide Sc_2O_3, from reaction with a 6 M HCl solution.[38] It turned out that the PXRD data from the products corresponds to the patterns reported for anhydrous MF_3 (Figures 5.6, 5.7 and 5.8).

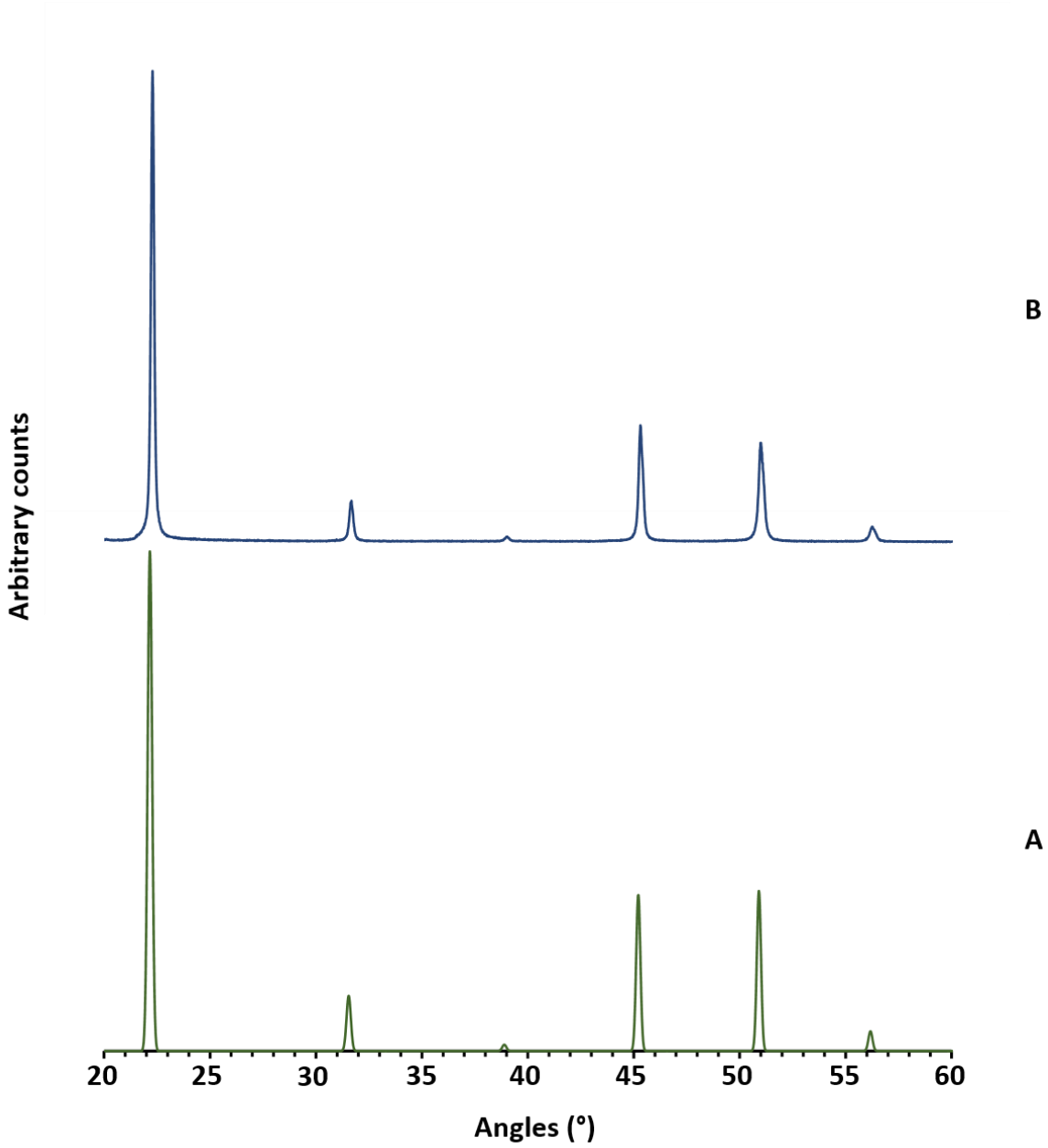

Figure 5.6. PXRD patterns obtained from the attempted synthesis of scandium fluoride hydrate. A: PXRD of anhydrous ScF_3 from the literature;[39] B: synthesised $ScF_3 \cdot xH_2O$.

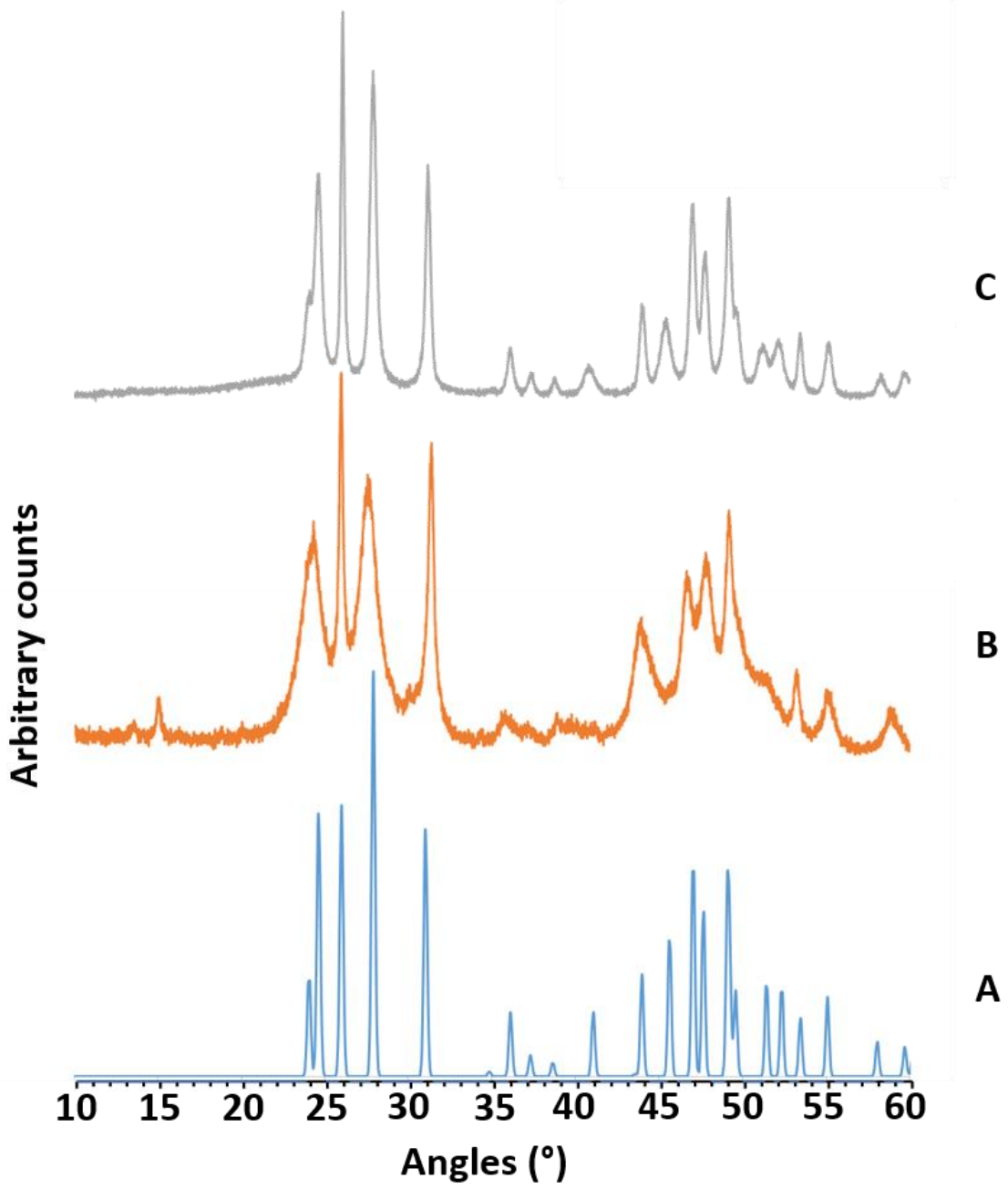

Figure 5.7. PXRD patterns obtained from the attempted synthesis of yttrium fluoride hydrate. A: PXRD of anhydrous YF_3 from the literature;[40] B: synthesised $YF_3 \cdot xH_2O$; C: synthesised $YF_3 \cdot xH_2O$ after heating under hydrothermal conditions (180 °C, 15 hours).

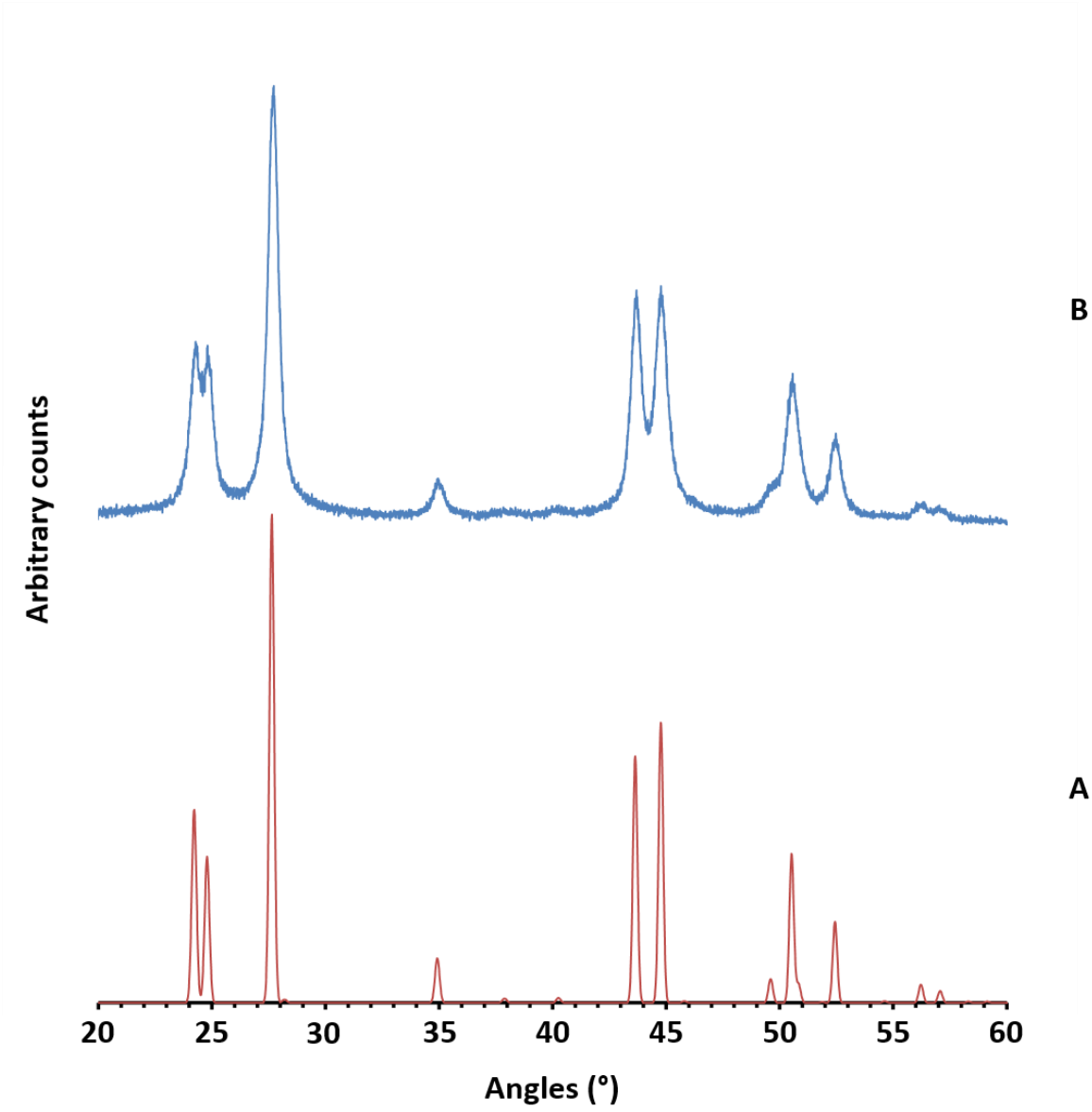

Figure 5.8. PXRD patterns obtained from the attempted synthesis of lanthanum fluoride hydrate. A: PXRD of anhydrous LaF_3 from the literature;[41] B: synthesised $LaF_3 \cdot xH_2O$.

$YF_3 \cdot xH_2O$ showed higher crystallinity after treatment in hydrothermal conditions (180 °C, 15 hours) (Figure 5.7). In the case of $ScCl_3 \cdot 3H_2O$, the use of KF as fluoride source gave mixtures of product and in one case pure KSc_2F_7 (Figure 5.9).

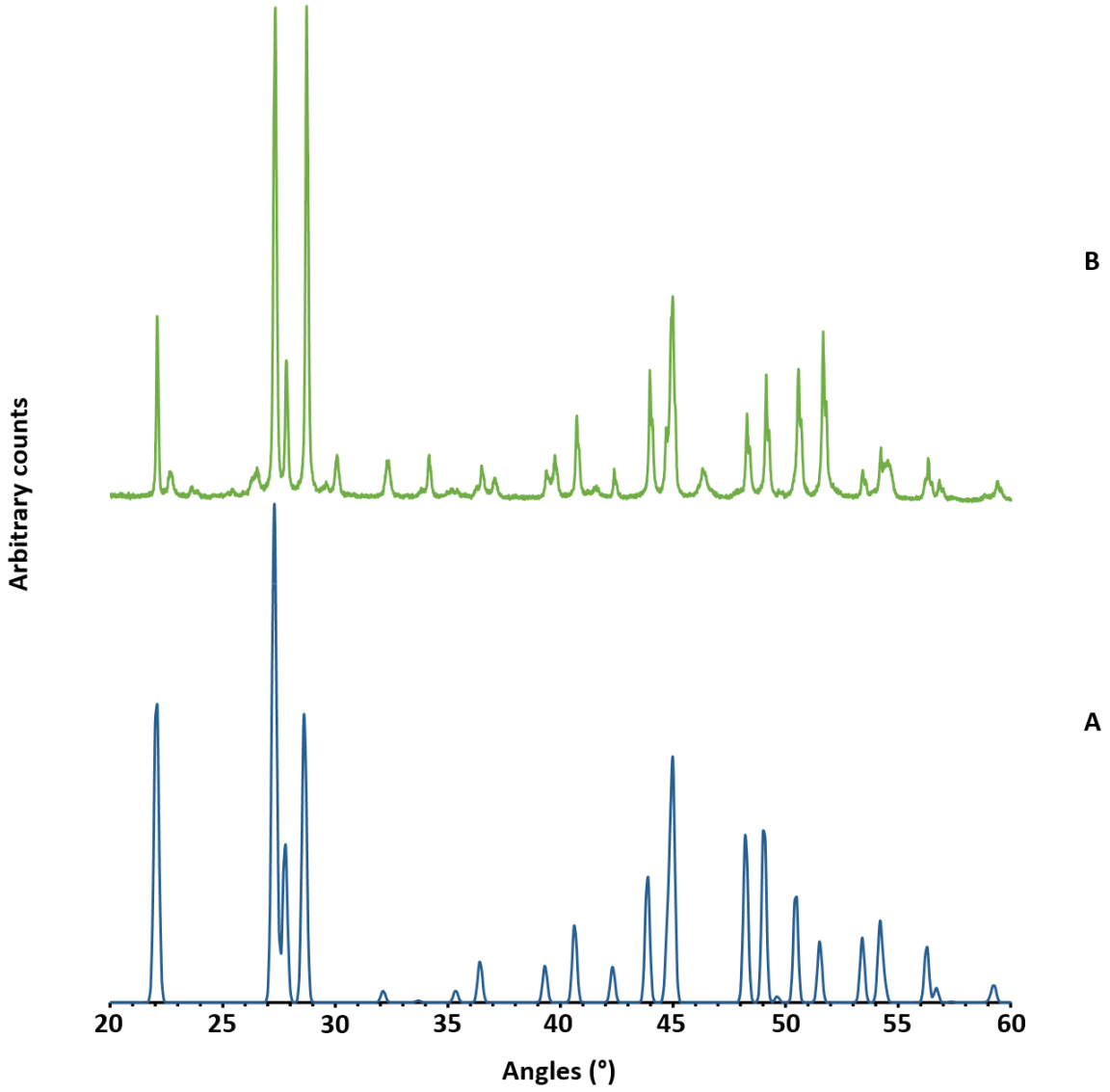

Figure 5.9. A: PXRD of KSc_2F_7 from the literature;[42] B: PXRD of the product obtained from KF and $ScCl_3{\cdot}3H_2O$ in water.

It was concluded, therefore, that the MF_3 "hydrates" were in fact extensively polymerised (fluoride bridged) and *anhydrous* and that the associated water molecules were not coordinated to the metal, but instead occupy voids in the crystal lattice or on the surface of the compound. As a result, they are unlikely to offer a viable entry into the chemistry of the MF_3 species with neutral ligands. Nonetheless, attempts to react the synthesised $MF_3{\cdot}xH_2O$ with terpy and Me_3-tacn in hydrothermal conditions (180 °C, 15 hours) were made. However, in all cases the unreacted MF_3 was recovered. Furthermore, the recovered $MF_3{\cdot}xH_2O$ showed increased crystallinity (sharper peaks in the PXRD patterns). These results are in contrast with the Group 13 $MF_3{\cdot}3H_2O$[43,44,2] and Group 4 $[MF_4(OH_2)_2]$ (M = Zr, Hf)[45] hydrates, in which the water molecules are coordinated to the metals and can be displaced by neutral ligands. Similar behaviour has been observed in $MF_4{\cdot}xH_2O$ (M = Ce, Th), which

have very limited coordination chemistry, suggesting that also in this case the water is not coordinated to the metal.[46]

5.2.2 Chloride/iodide precursor complexes

The second and third strategies identified for the formation of the trifluoride complexes of the Group 3 metals consider halide exchange reactions on the preformed chloride or iodide analogues, $[MX_3(L)]$, using $[Me_4N]F$ or Me_3SnF as fluoride sources. In this section the synthesis of the parent trichloride and triiodide complexes of M(III) (M = Sc, Y, La and Lu) with the ligands terpy and Me_3-tacn are discussed.

The chloride complexes were obtained starting with $[ScCl_3(thf)_3]$[22] and $[YCl_2(thf)_5][YCl_4(thf)_2]$[23] (made from $ScCl_3{\cdot}6H_2O$ and YCl_3 respectively), whereas YI_3 was reacted directly with the ligands, due to its higher solubility in weakly coordinating solvents. Since these compounds are moisture sensitive (YI_3 in particular), the reactions were performed in anhydrous conditions in MeCN.

$LaCl_3{\cdot}7H_2O$ and $LuCl_3{\cdot}6H_2O$ were used as the sources of the lanthanides and reacted in EtOH with the ligands. $[MCl_3(Me_3\text{-tacn})]$ (M = Sc, Y) were made as reported in the literature[25] and $[ScCl_3(BnMe_2\text{-tacn})]$ was prepared and characterised similarly.

The reaction of $[ScCl_3(thf)_3]$ with terpy in anhydrous MeCN gave $[ScCl_3(terpy)]$, in which the chlorides are coordinated to the metal in *a meridional* configuration (Figure 5.10).

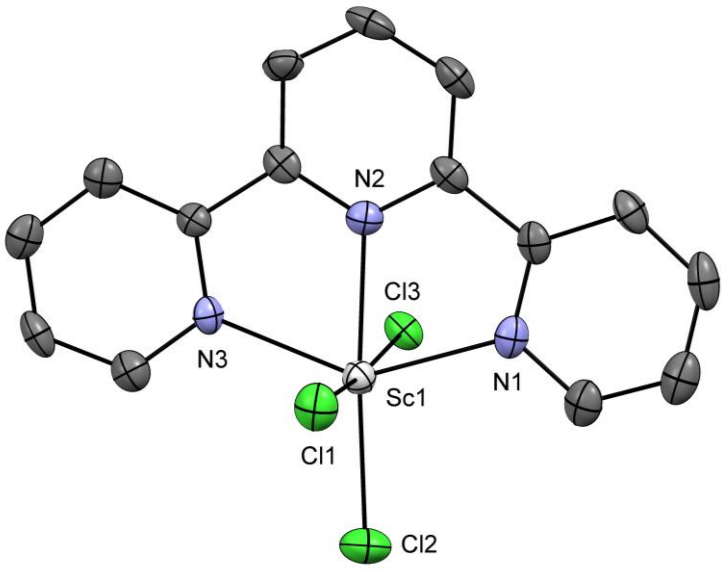

Figure 5.10. Structure of mer-$[ScCl_3(terpy)]$ with ellipsoids drawn at 50 % probability level. H atoms are omitted for clarity. Selected bond lengths (Å) and angles (°): Sc1–Cl1 = 2.414(2), Sc1–Cl2 = 2.396(2), Sc1–Cl3 = 2.451(2), Sc1–N1 = 2.229(4), Sc1–N2 = 2.231(5), Sc1–N3 = 2.248(4), Cl1–Sc1–Cl3 = 174.51(7), Cl2–Sc1–N2 = 174.2(1), N1–Sc1–N3 = 142.3(2), N1–Sc1–N2 = 71.3(2), N2–Sc1–N3 = 71.1(2), N2–Sc1–Cl3 83.7(1), Cl3–Sc1–Cl2 91.22(6), Cl2–Sc1–N1 = 105.9(1).

The complex has a distorted octahedral coordination environment around the metal centre due to the rigid terpy ligand. The angles involving the ligand are significantly less than the 180/90° expected for a regular octahedron, e.g. with N1-Sc1-N3 142.3°. The extended crystal structure shows π-stacking interactions (3.82 Å) between the aromatic rings of the ligand of adjacent molecules, connecting them into 1D zig-zag chains (Figure 5.11).

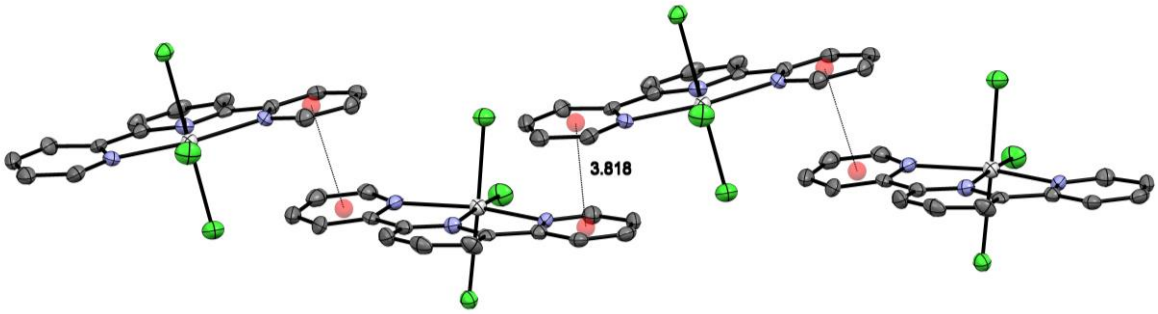

Figure 5.11. View of the π-stacking arrangement present in the X-ray crystal structure of [$ScCl_3$(terpy)].

The reaction of [$YCl_2(thf)_5$][$YCl_4(thf)_2$] with terpy in MeCN produced [YCl_3(terpy)(OH_2)], incorporating adventitious water (Figure 5.12).

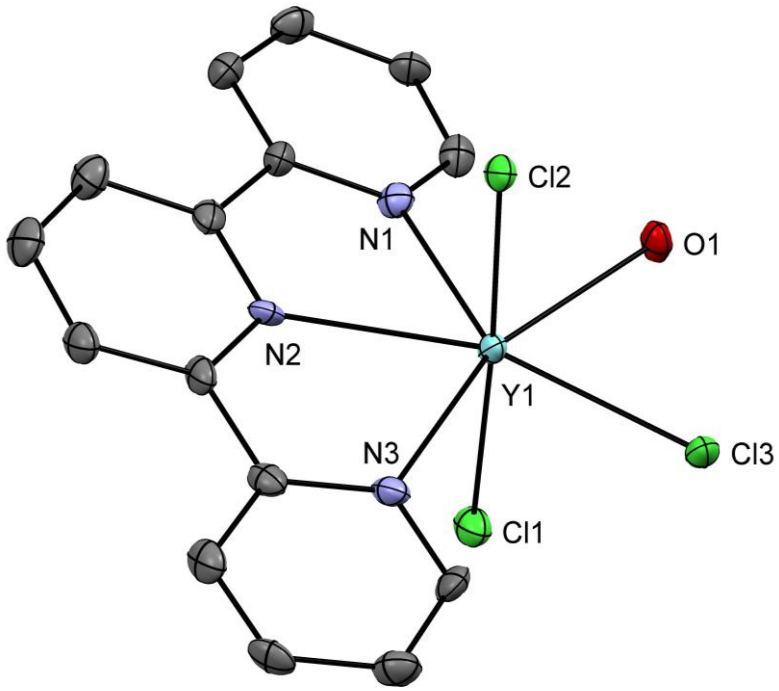

Figure 5.12. Crystal structure of [YCl_3(terpy)(OH_2)] with ellipsoid drawn at 50 % probability level. H atoms are omitted for clarity. Selected bond lengths (Å) and angles (°): Y1–Cl1 = 2.572(2), Y1–Cl2 = 2.611(2), Y1–Cl3 = 2.629(1), Y1–N1 = 2.507(5), Y1–N2 = 2.480(4), Y1–N3 = 2.514(5), Y1–O1 2.348(3), Cl2–Y1–Cl1 176.49(5), Cl3–Y1–Cl1 90.77(5), Cl1–Y1–O1 96.6(1), Cl1–Y1–N2 96.3(1), Cl2–Y1–N2 80.8(1), N2–Y1–N1 64.9(2).

The crystal structure (Figure 5.12) shows a pentagonal-bipyramidal coordination around the metal centre with the Y–Cl bond lengths in the axial positions shorter than that in the equatorial plane (~ 0.1 Å). The angles subtended at the yttrium centre and involving the nitrogen atoms are less than the 72° value expected for the perfect pentagonal-bipyramidal conformation, due to the rigid terpy ligand, and the equatorial plane is slightly puckered. Furthermore, the packing in the crystal structure shows both H-bonding (Cl···HOH distance 3.11 Å) between adjacent molecules to form associated dimers, and weak π-stacking (4.04 Å) linking the dimers into zig-zag chains (Figure 5.13). The bond lengths are generally shorter than in the eight-coordinate $[YCl(terpy)(OH_2)_4]Cl_2{\cdot}2H_2O$.[31]

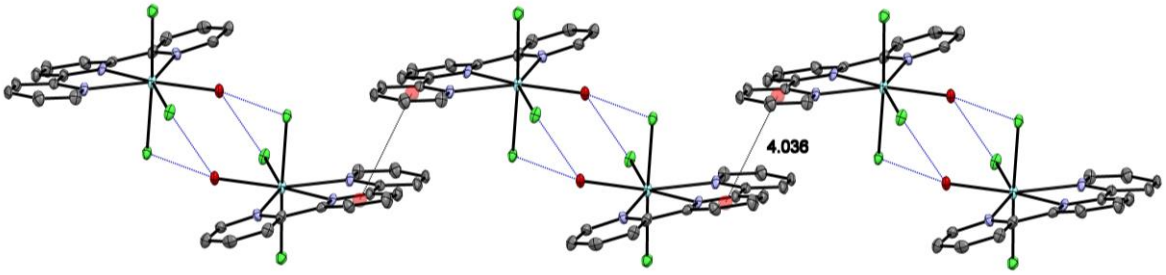

Figure 5.13. View of the zig-zag chain formed *via* H-bonding (blue dotted lines) and π-stacking (grey dotted lines) in the X-ray crystal structure of $[YCl_3(terpy)(OH_2)]$.

The reaction of $LuCl_3{\cdot}6H_2O$ with terpy in EtOH gave $[LuCl_3(terpy)(OH_2)]$ (Figure 5.14), which is isostructural with the Y(III) analogue and displays the same H-bonding and π-stacking interactions (Figure 5.15).

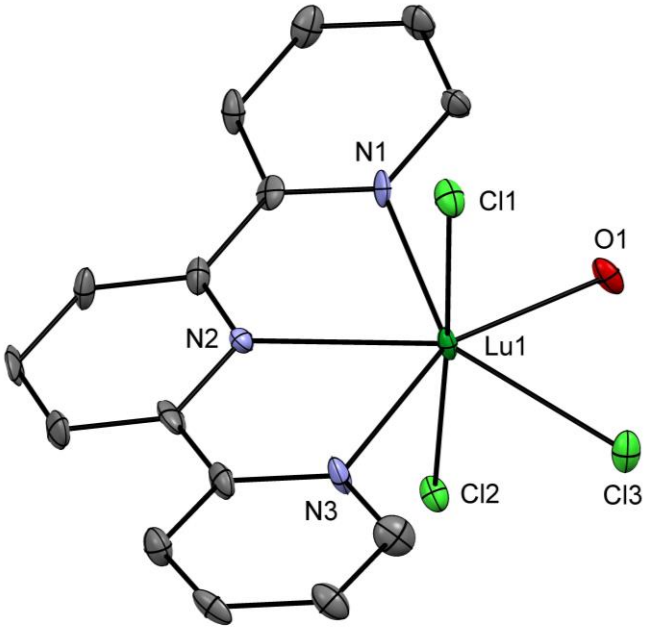

Figure 5.14. Crystal structure of $[LuCl_3(terpy)(OH_2)]$ with ellipsoid drawn at 50 % probability level. H atoms are omitted for clarity. Selected bond lengths (Å) and angles (°): Lu1-Cl1 = 2.5256(18), Lu1-Cl2 = 2.5681(18), Lu1-Cl3 = 2.6634(17), Lu1-O1 = 2.309(5), Lu1-N1 = 2.471(3), Lu1-N2 = 2.436(3), Lu1-N3 = 2.478(3), Cl1-Lu1-

Cl2 = 176.96(5), Cl1-Lu-Cl3 = 91.01(6), O1-Lu1-Cl1 = 96.16(13), O1-Lu1-Cl3 = 72.99(12), O1-Lu1-N1 = 73.61, O1-Lu1-N2 = 137.07(15), O1-Lu1-N3 = 154.89, N1-Lu1-Cl1 = 87.52(11), N1-Lu1-Cl2 92.61, N1-Lu1-N3 = 131.29(13).

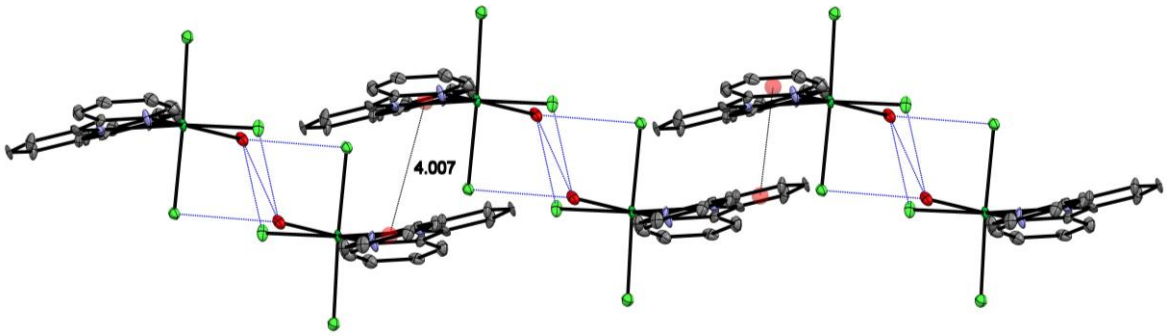

Figure 5.15. View of the zig-zag chain formed *via* H-bonding (blue dotted lines) and π-stacking (grey dotted lines) in the X-ray crystal structure of [$LuCl_3$(terpy)(OH_2)].

However, the reaction of $LaCl_3 \cdot 7H_2O$ with terpy in a 1:1 ratio in EtOH produced the eight-coordinate chloro-bridged dimer, [{La(terpy)(OH_2)Cl_2}$_2$(μ-Cl)$_2$] (Figure 5.16).

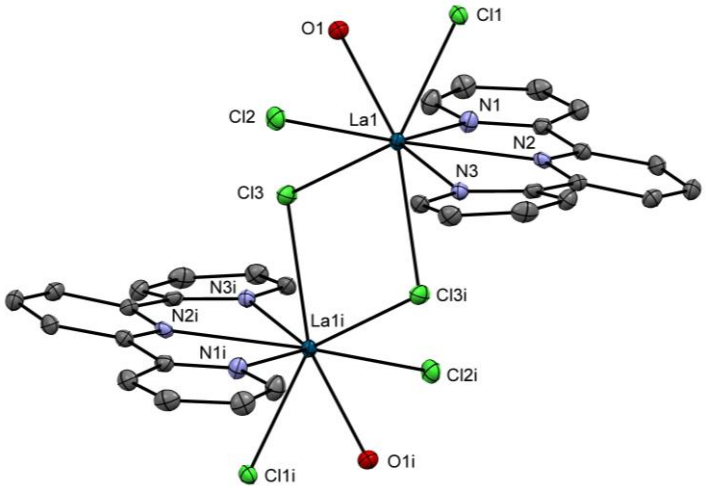

Figure 5.16. Crystal structure of [{La(terpy)(H_2O)Cl_2}$_2$(μ-Cl)$_2$] with ellipsoids drawn at 50 % probability level. H atoms are omitted for clarity. Selected bond lengths (Å) and angles (°): La1–Cl1 = 2.8385(9), La1–Cl2 = 2.8014(8), La1–Cl3 = 2.8895(9), La1–N1 = 2.638(3), La1–N2 = 2.678(3), La1–N3 = 2.658(3), La1–O1 = 2.576(3), La1–Cl3^{i} = 2.9209(9), Cl1–La1–Cl3 = 144.65(2), Cl1–La1–Cl2 = 86.82(2), Cl1–La1–O1 = 72.14(7), Cl2–La1–O1 = 78.77(7), Cl3–La1–O1 = 140.69(7), N3–La1–N1 123.52(9), N3–La1–O1 145.03(9), N3–La1–N2 = 62.21(9).

The packing of the structure also shows H-bonding involving the coordinated water molecule and the chlorides of adjacent molecules (Cl···HOH distance 3.13 Å) (Figure 5.17).

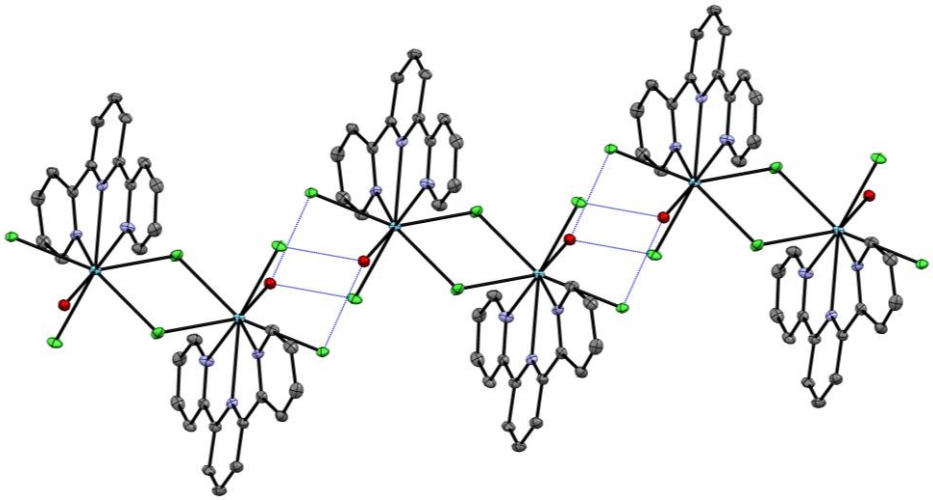

Figure 5.17. Hydrogen bonding network present in the X-ray crystal structure of [{La(terpy)(OH_2)Cl_2}$_2$(μ-Cl)$_2$].

Whilst the reaction of $LaCl_3 \cdot 7H_2O$ with Me_3-tacn produced [$LaCl_3$(Me_3-tacn)], characterised by ^{1}H NMR spectroscopy and microanalysis, the reaction of $LuCl_3 \cdot 6H_2O$ with the same ligand failed to produce the desired product (microanalysis results were always low in carbon and nitrogen). The reasons for this difference in reactivity are not clear.

Reacting YI_3 with Me_3-tacn in anhydrous MeCN gave the extremely moisture sensitive solid, [YI_3(Me_3-tacn)]·1.5CH_3CN (Figure 5.18).

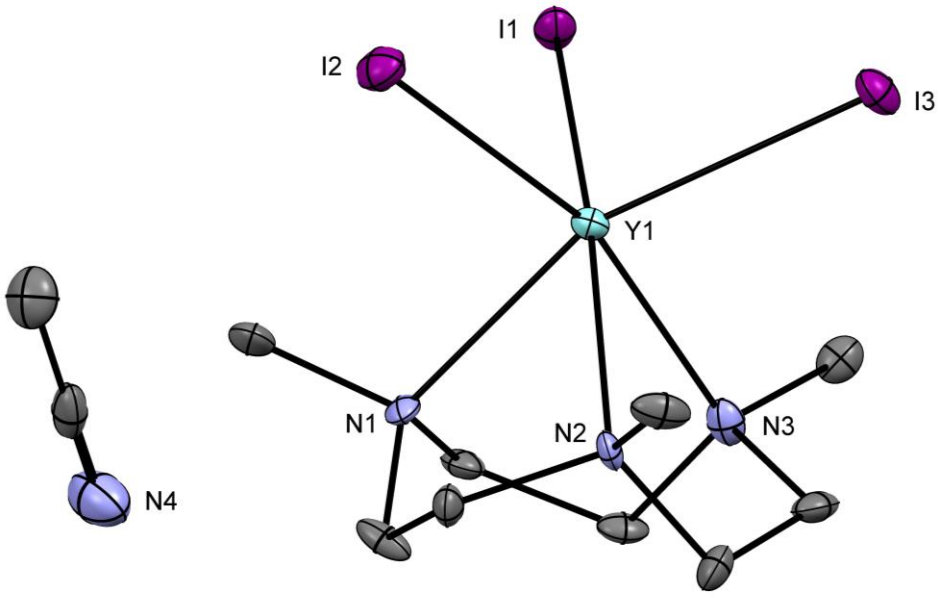

Figure 5.18. Structure of [YI_3(Me_3-tacn)]·CH_3CN with atom numbering scheme. Ellipsoids are drawn at the 50 % probability level and H atoms are omitted for clarity. Select bond lengths (Å) and angles (°): Y1–I1 = 2.9671(8), Y2–I2 = 2.9509(9), Y1–I3 = 2.9460(8), Y1–N1 = 2.468(6), Y1–N2 = 2.480(5), Y1–N3 = 2.467(7), I3–Y1–N1 = 160.9(1), I2–Y1–N3 = 162.3(2), I1–Y1–N2 = 161.6(1), I1–Y1–I2 = 99.59(2), I3–Y1–I2 = 98.87(2), I3–Y1–N2 = 94.5(1), N1–Y1–N2 = 72.0(2).

The structure shows an octahedral environment around the metal with the ligand coordinated in the expected *facial* configuration. Crystallisation from MeCN solution in the freezer produced a mixture of the desired complex (Figure 5.18) and another crystal morphology, which was also analysed by single crystal X-ray diffraction. This revealed the crystals to be [{YI_2(Me_3-tacn)}$_2$(μ-O)] (Figure 5.19), obtained from partial hydrolysis with adventitious trace water.

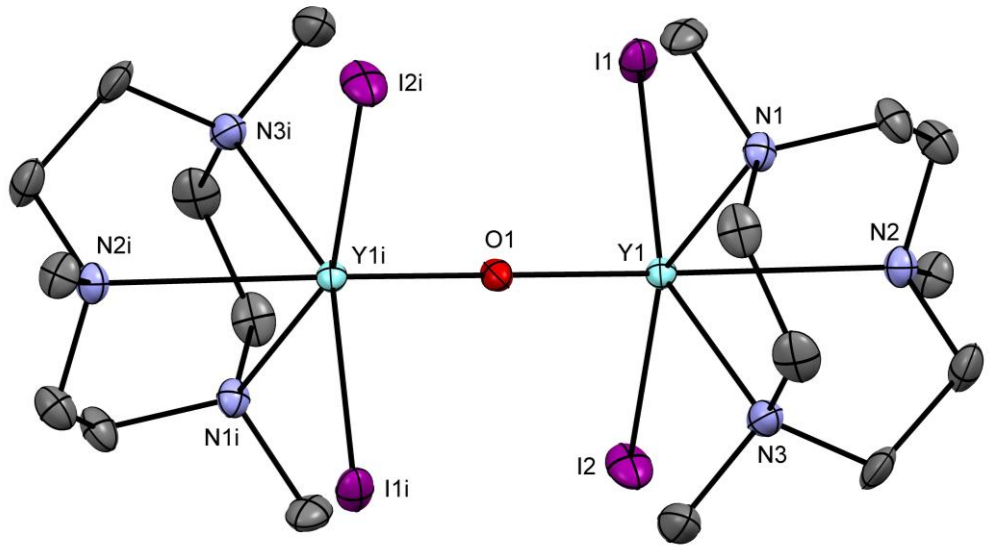

Figure 5.19. The structure of [{YI_2(Me_3tacn)}$_2$(μ-O)]·CH_3CN with atom numbering scheme. Ellipsoids are drawn at the 50 % probability level and H atoms and the MeCN solvent molecule are omitted for clarity. Selected bond lengths (Å) and angles (°): Y1–I1 = 3.0213(6), Y1–I2 = 2.9969(7), Y1–O1 = 2.0332(5), Y1–N2 = 2.580(5), Y1–N1 = 2.473(5), Y1–N3 = 2.495(5), Y1–O1–Y1 = 180.00(3), I2–Y1–I1 = 93.991(19), O1–Y1–I1 = 104.69(2), O1–Y1–I2 = 104.12(2), O1–Y1–N2 = 156.16(11), O1–Y1–N1 = 90.72(11), O1–Y1–N3 = 93.79(11).

The ^{1}H NMR spectra of the terpy complexes reported in this section showed the expected shifts of the resonances towards higher frequency upon coordination or, in the case of [YI_3(Me_3-tacn)], complex multiplets at 2.81 and 2.73 ppm, characteristic of the CH_2 groups of a tridentate tacn unit, as well as a singlet at 2.58 ppm, due to the ligand methyl groups, consistent with *facial* complexation of the Me_3-tacn.

Several attempts at the reaction of ScI_3 with Me_3-tacn produced only protonated ligand rather than the intended [ScI_3(Me_3-tacn)] (characterised by microanalysis, ^{1}H NMR spectroscopy and X-ray diffraction).

5.2.3 Chloride(iodide)/fluoride exchange using [Me_4N]F

The reaction of the trichloride precursors with [Me_4N]F as fluoride source were investigated. [Me_4N]F dissolves in most solvents providing a source of free F^- ions in solution. The reaction of [$ScCl_3$(Me_3-tacn)] with three mol. equivalents of [Me_4N]F in anhydrous CH_3CN solution successfully

produced the fluorinated complex, [ScF_3(Me_3-tacn)] (Scheme 5.3). The removal of [Me_4N]Cl from the solid product proved to be very difficult with the microanalysis showing a 1:1 ratio between the complex and [Me_4N]Cl (also confirmed in the ^1H NMR spectrum).

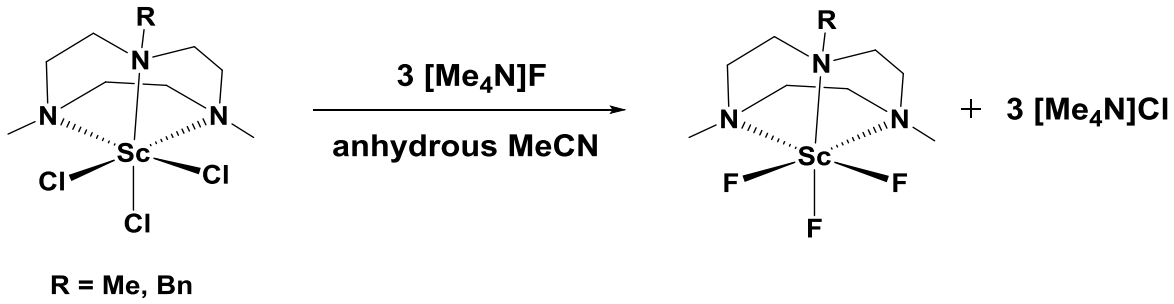

R = Me, Bn

Scheme 5.3. Cl/F exchange reactions of [$ScCl_3$(RMe_2-tacn)] using [Me_4N]F as source of fluoride ions.

However, $^{19}F\{^1H\}$ and ^{45}Sc NMR [I = 7/2; 100 % abundance; Q = −0.22 x 10^{-28} m^2] spectra for the product in CD_3CN show three broad resonances at 77.2, 40.1 and 7.7 ppm ($^{19}F\{^1H\}$) and 219, 155 and 104 ppm (^{45}Sc) (Figure 5.20), corresponding to [$ScFCl_2$(Me_3-tacn)], [ScF_2Cl(Me_3-tacn)] and [ScF_3(Me_3-tacn)], respectively (the partially fluorinated species were most likely obtained due to a deficit of [Me_4N]F present in solution as a result of the difficulty of weighting solids in the glovebox with a nitrogen stream or some ^{i}PrOH still present in [Me_4N]F from the drying step). The broadening of the ^{45}Sc peaks is due to the lower symmetry of the partially fluorinated complexes, which cause faster quadrupolar relaxation due to the higher electric field gradients.

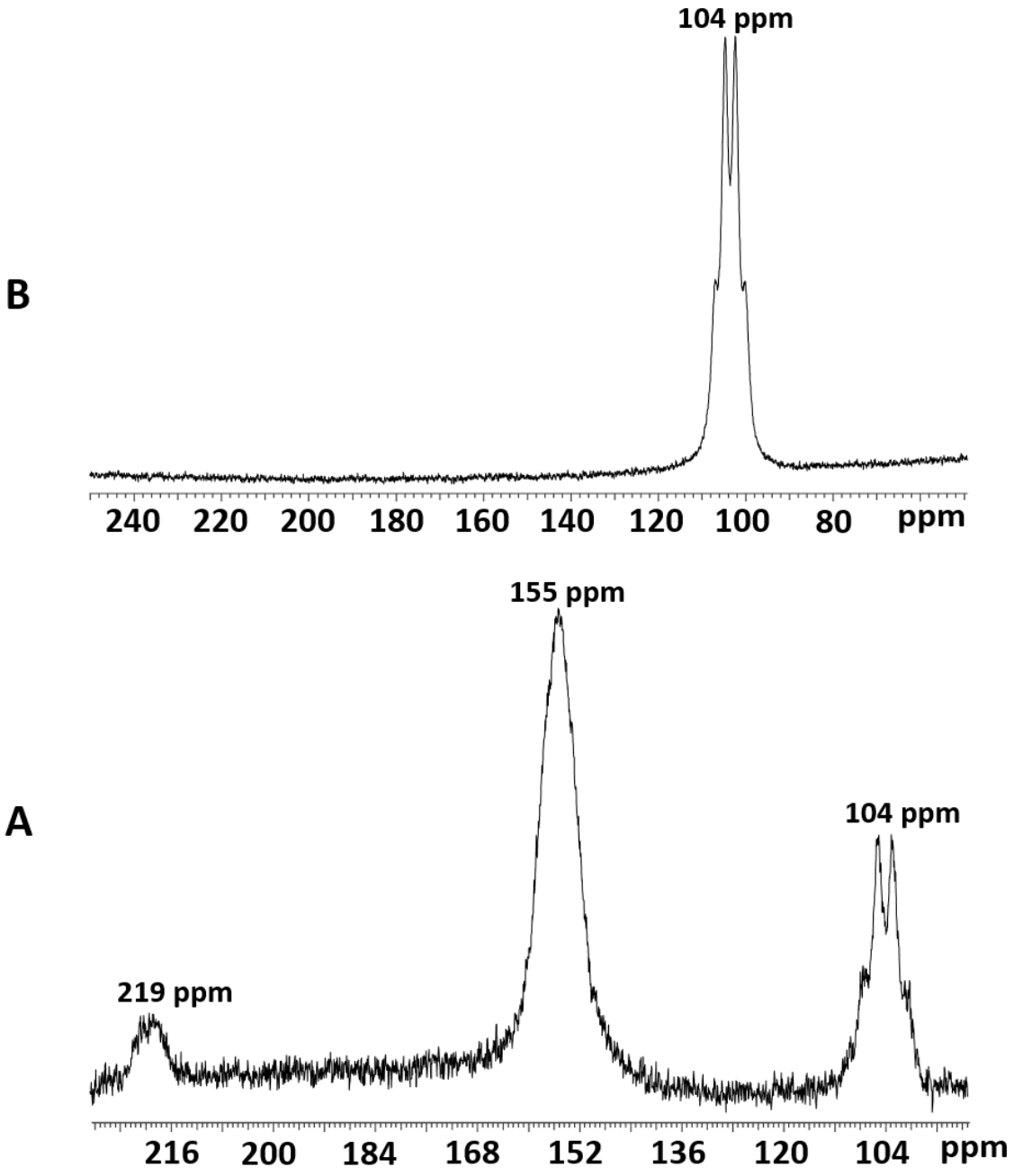

Figure 5.20. Fluorination of $[ScCl_3(Me_3tacn)]$: A: ^{45}Sc NMR spectrum showing the species $[ScFCl_2(Me_3tacn)]$ (219 ppm), $[ScF_2Cl(Me_3tacn)]$ (155 ppm) and $[ScF_3(Me_3tacn)]$ (104 ppm) when a deficit of $[NMe_4]F$ is used; B: ^{45}Sc NMR spectrum of $[ScF_3(Me_3tacn)]$ showing the quartet at 103.7 ppm ($^1J_{Sc\text{-}F}$ = 219 Hz).

Table 5.2 reports the $^{19}F\{^1H\}$ and ^{45}Sc chemical shifts for the scandium chloride and fluoride complexes. The observation of stepwise substitution on Sc(III) contrasts with the Group 13 chemistry where mono and di-fluoro species have never been observed. This is consistent with slower kinetics in the Sc(III) system.

Complex	$\delta(^{45}Sc)$ / ppm	$\delta(^{19}F\{^{1}H\})$ / ppm
$[ScCl_3(Me_3\text{-tacn})$	+300	-
$[ScCl_3(BnMe_2\text{-tacn})$	+302	-
$[ScFCl_2(Me_3\text{-tacn})]$	+219	+77.3
$[ScF_2Cl(Me_3\text{-tacn})]$	+155	+41.0
$[ScF_3(Me_3\text{-tacn})]$	+104 (q, $^{1}J_{Sc\text{-}F}$ = 219Hz)	+7.7
$[ScF_3(BnMe_2\text{-tacn})$	+104	+10.1
$[ScF_3(terpy)]$	+64	-37.7 [2F], -53.3 [F]
$[ScCl_3(terpy)]^a$	+254	-

Table 5.2. $^{19}F\{^{1}H\}$ and ^{45}Sc NMR data in CD_3CN. [a] spectra recorded in CD_2Cl_2.

$[ScF_3(Me_3\text{-tacn})]$ is the first example of a scandium fluoride complex with neutral ligands, therefore its chemical shifts cannot be compared directly with similar systems. However, the chemical shifts of the partially fluorinated complexes are reasonable compared to data on other scandium chloride complexes.[28,29] Adding a slight excess of $[Me_4N]F$ to the sample with the mixed chloro/fluoro complexes led to the formation of the completely fluorinated species, $[ScF_3(Me_3\text{-tacn})]$, whereas further addition of $[Me_4N]F$ cause the loss of the $^{19}F\{^{1}H\}$ and ^{45}Sc resonances, suggesting instability of the complex in the presence of an excess of fluoride anions in solution (possibly producing fluoroscandate species). Further confirmation of the sequential fluorination of the complex came from the single crystal X-ray analysis of $[ScF_2Cl(Me_3\text{-tacn})]$ (Figure 5.21).

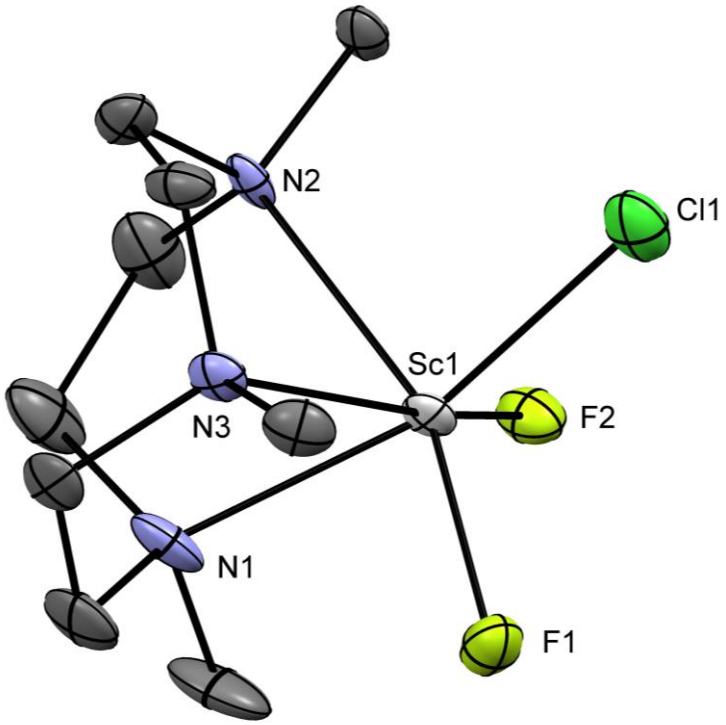

Figure 5.21. Crystal structure of [$ScF_2Cl(Me_3$-tacn)] with ellipsoids drawn at the 50 % probability level. H atoms are omitted for clarity. Select bond lengths (Å) and angles (°): Sc1–F1 = 1.947(3), Sc1–F2 = 1.940(3), Sc1–Cl1 = 2.444(2), Sc1–N1 = 2.339(5), Sc1–N2 = 2.364(4), Sc–N3 = 2.334(4), Cl1–Sc1–F1 = 101.7(1), Cl1–Sc1–N1 = 162.4(1), Cl1–Sc1–N2 = 89.9(1), F1–Sc1–F2 = 103.3(1), N2–Sc1–N3 = 74.6(1), F1–Sc1–N3 = 158.8(1).

The complex is six-coordinate with the three nitrogen atoms of the ligand coordinated to the metal in a *facial* configuration, while the three other positions are occupied by two fluorine atoms and one chlorine, with no evidence for disorder of the halides. As expected, the Sc–F bonds are significantly shorter than the Sc–Cl bond (1.940(3) and 1.947(3) against 2.444(2) Å).

The analogous [$ScCl_3(BnMe_2$-tacn)] shows similar behaviour with [NMe_4]F, with [$ScF_3(BnMe_2$-tacn)] showing a broad ^{45}Sc NMR resonance at 104 ppm (the increased broadenings due to the lower symmetry of the complex with the benzyl group compared to the Me_3-tacn analogue), with $\delta(^{19}F\{^1H\})$ = 10.1 ppm (Figure 5.22).

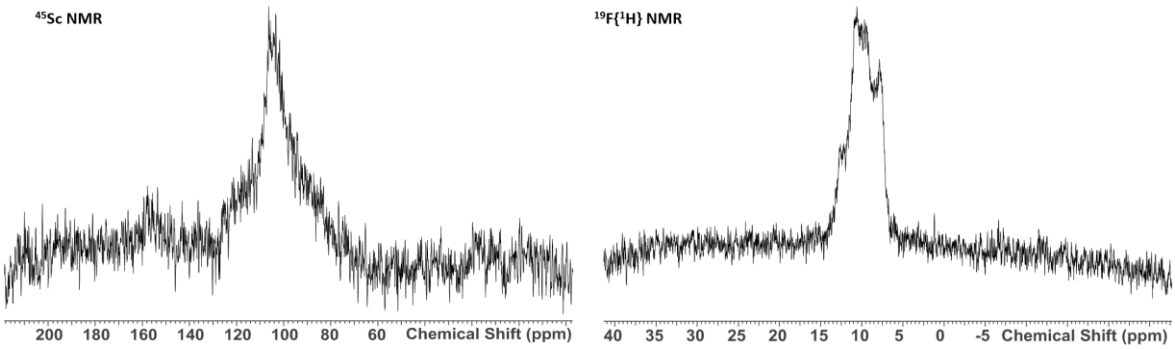

Figure 5.22. ^{45}Sc (left) and $^{19}F\{^{1}H\}$ (right) NMR spectra of $[ScF_3(BnMe_2\text{-tacn})]$ in CD_3CN.

Attempts to react $[ScCl_3(terpy)]$ with $[NMe_4]F$ in CH_3CN on an NMR scale caused complete loss of the resonances from the trichloro complex, without the appearance of any new resonances in either the ^{45}Sc or $^{19}F\{^{1}H\}$ spectra, most likely suggesting the formation of insoluble ScF_3 (white precipitate formed in solution).

The reaction of $[YCl_3(Me_3\text{-tacn})]$ with three mol. equivalents of $[NMe_4]F$ in CH_3CN resulted in a white precipitate that was insoluble in CH_3CN or CH_2Cl_2 and the ^{1}H NMR spectrum of the supernatant showed liberation of Me_3-tacn, whilst the $^{19}F\{^{1}H\}$ NMR spectrum showed only small amounts of free fluoride. Similar results were obtained using $[YI_3(Me_3\text{-tacn})]$, and it was concluded that Cl(I)/F exchange resulted in decomposition and loss of the Me_3-tacn from the yttrium. Similar decomposition occurred using $[LaCl_3(Me_3\text{-tacn})(OH_2)]$, $[LaCl_3(terpy)]$ and $[LuCl_3(terpy)]$.

5.2.4 Chloride/fluoride exchange reactions using Me_3SnF

The fluorination reactions of the chloride complexes was also investigated using Me_3SnF as fluoride source. Me_3SnF has a polymeric structure where the fluoride bridge to a tin atom in an adjacent molecule, forming a chain; it is poorly soluble in most solvents.[47,48,49] Its low solubility makes the addition of an excess into the reaction possible, without the risk of decomposition as observed in the reaction using an excess of $[Me_4N]F$ as fluoride source.

$[ScCl_3(Me_3\text{-tacn})]$ was reacted with Me_3SnF in MeCN solution. The addition of an excess of the fluoride source caused the formation of the completely fluorinated complex, $[ScF_3(Me_3\text{-tacn})]$. The $^{19}F\{^{1}H\}$ and ^{45}Sc NMR spectra of the complex are shown in Figure 5.23.

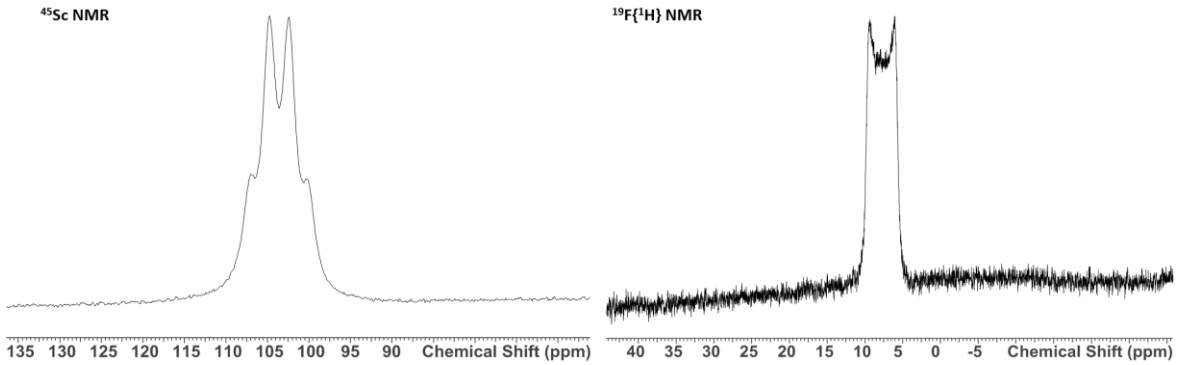

Figure 5.23. ^{45}Sc (left) and $^{19}F\{^{1}H\}$ (right) NMR spectra of $[ScF_3(Me_3\text{-tacn})]$ in CD3CN obtained using an excess of Me_3SnF.

The ^{45}Sc NMR spectrum shows a quartet at 104 ppm due to the coupling to the three equivalent fluorides $^{1}J_{Sc\text{-}F}$ 219 Hz (*facial* coordination to the metal); the ^{45}Sc magnetic properties mean that coupling is often seen in high symmetry systems (i.e. with the efg close to zero).[50,24,29,28] The $^{19}F\{^{1}H\}$ NMR spectrum shows a broad resonance at 7.7 ppm resulting from the partial collapse of the couplings to ^{45}Sc (I = 7/2, 100 %).

Further confirmation of the fluorination occurring in a stepwise manner came from a reaction in which a deficit of Me_3SnF was used, leading to the formation of the partially fluorinated complexes also in this case (chemical shifts consistent with those described above). The addition of more Me_3SnF results in the conversion of the mono- and di-fluoro species into the trifluorinated complex, $[ScF_3(Me_3\text{-tacn})]$ (Figure 5.24).

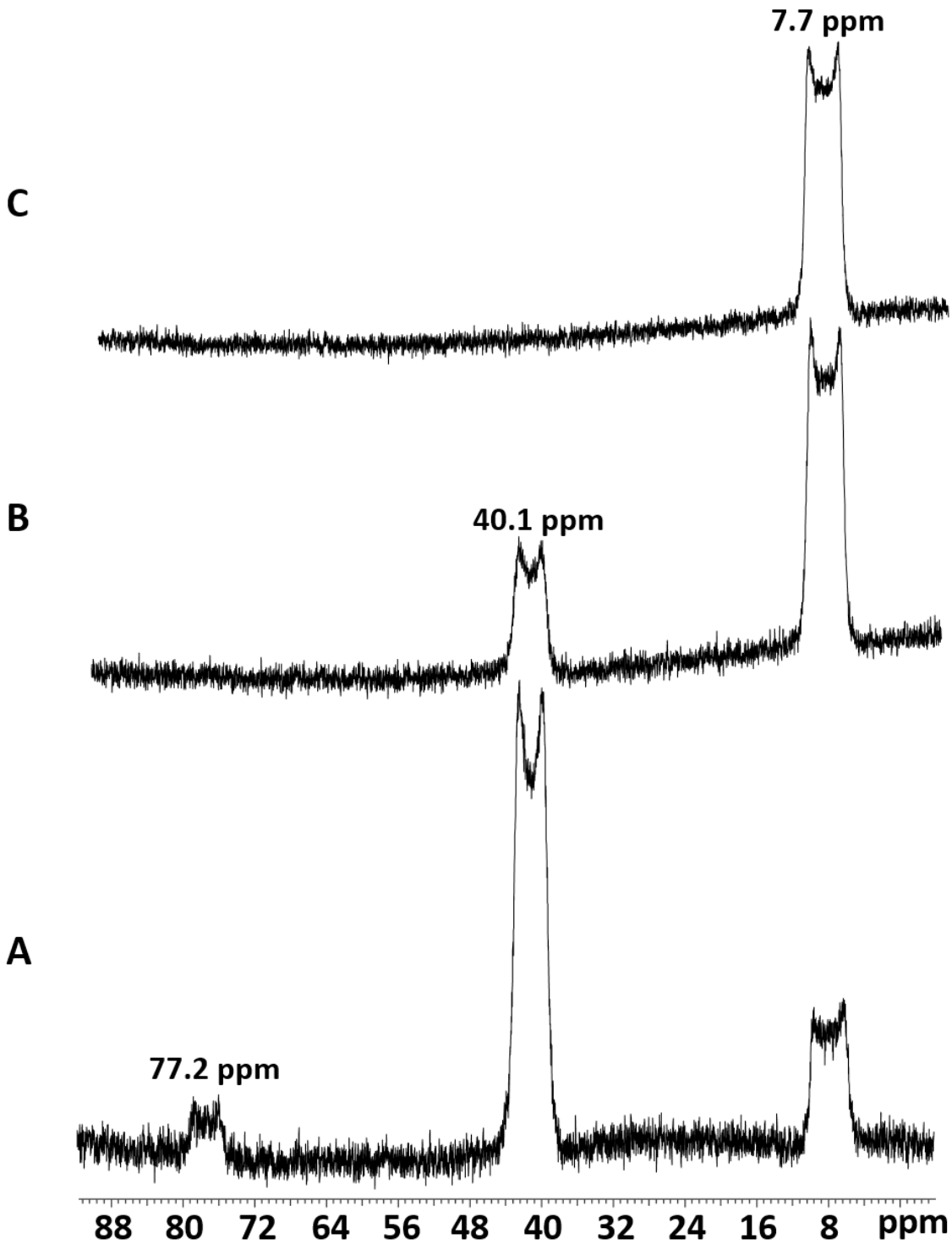

Figure 5.24. $^{19}F\{^{1}H\}$ NMR spectra of $[ScFCl_2(Me_3tacn)]$ (77.2 ppm), $[ScF_2Cl(Me_3tacn)]$ (40.1 ppm) and $[ScF_3(Me_3tacn)]$ (7.7 ppm). A: ~ 2.5 mol. equiv. of Me_3SnF were added to a CD_3CN solution of $[ScCl_3(Me_3tacn)]$; B: < 3 mol. equiv. of Me_3SnF were added to a CD_3CN solution of $[ScCl_3(Me_3tacn)]$; C: > 3 mol. equiv. of Me_3SnF were added to a CD_3CN solution of $[ScCl_3(Me_3tacn)]$.

However, the solid product isolated had a microanalysis corresponding to $[Sc(Me_3\text{-}tacn)F_2(\mu\text{-}F)SnMe_3Cl]$; note that whilst three molar equivalents of Me_3SnCl are produced in the reaction, the microanalytical data indicate that only one is retained in the scandium complex.

The microanalysis results were also confirmed by a single crystal X-ray analysis (Figure 5.25).

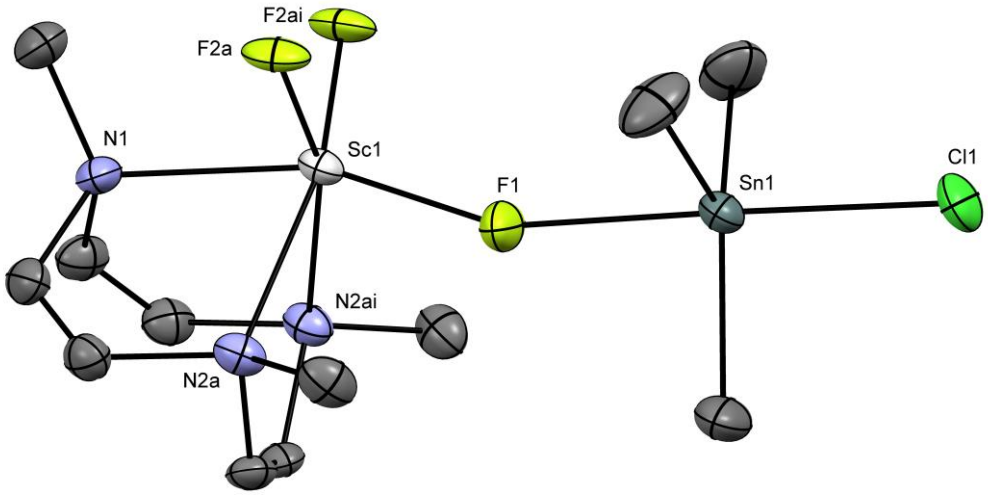

Figure 5.25. Crystal structure of [Sc(Me_3-tacn)F_2(μ-F)$SnMe_3Cl$)] with atom numbering scheme. Ellipsoids are shown at the 50% probability level and H atoms are omitted for clarity. Selected bond lengths (Å) and angles (°): Sc1–N1 = 2.334(6), Sc1–N2 = 2.351(4), Sc1–F1 =1.980(6), Sc1–$F2^a$ = 1.92(2), Sn1–F1 = 2.307(6), Sn1–Cl1 = 2.502(2), Sn1–C1 = 2.124(7), Sn1 - $C2^a$ = 2.153(3), N2–Sc1–N2 = 75.36(18), N1–Sc1–N2 = 74.92(14), $F2^a$–Sc1–N1 = 94.6(10), F1–Sc1–N1 159.7(3), F1–Sn–Cl1 = 178.7(2).

The three fluorides are coordinated to the scandium in a *facial* configuration and the three nitrogen atoms of the ligand complete the distorted octahedral geometry. However, one of the fluorides is bridging to Me_3SnCl. The Sc-F bond distance for the fluoride bridging Sc and Sn is 0.06 Å longer than that of the other two fluorides (identical by symmetry) (1.980(6) vs. 1.92(2) Å). The Sc-N bond distances are similar to those found in [$ScF_2Cl(Me_3$-tacn)]. The F-bound Me_3SnCl shows a trigonal bipyramidal geometry at Sn with F and Cl in axial positions with a near linear angle (F-Sn-Cl 178.7(2)°) and the methyl groups in the equatorial plane. The Sn-F and Sn-Cl bonds are longer than those in Me_3SnF (2.1620(7) Å)[49] and Me_3SnCl (2.430(2) Å)[51] polymers. Thus, [$ScF_3(Me_3$-tacn)] acts as a neutral Lewis base towards Me_3SnCl through the highly negative polarised ScF_3 unit, a behaviour already noted with the trivalent Group 13, Fe(III) and Cr(III) complexes, *fac*-[$MF_3(Me_3$-tacn)].[52,53] The only similar complex to have been reported is [$ScL(\mu\text{-}F)_2(SnMe_3Br)_2$] (Figure 5.5) ($L^-$ = N,N”-(1,3-dimethyl-1,3-propanediylidine)bis(N’,N’-diethyl-1,2-ethanediamine)), made from [$ScLBr_2$] and Me_3SnF.[35] In this case both fluorine groups bridge between scandium and a Me_3SnBr molecule, with Sc-F bond distances of 1.967(3) and 1.991(3) Å and Sn-F distances of 2.419(3) and 2.455(3) Å. While the Sc-F distances are comparable with the ones of the crystal reported here, the Sn-F bond distance is 0.1 Å longer, suggesting a stronger interaction of the [$ScF_3(Me_3$-tacn)] unit with the slightly more Lewis acidic Me_3SnCl.

The ^{45}Sc and $^{19}F\{^1H\}$ NMR spectra of [Sc(Me_3-tacn)F_2(μ-F)$SnMe_3Cl$] and [$ScF_3(Me_3$-tacn)] in CH_3CN are identical, as are the ^1H resonances of the Me_3-tacn moieties, whilst the ^1H NMR resonance of the Me_3SnCl in the former complex is consistent with the free organotin, indicating the adduct is

dissociated in solution. However, attempts to crystallise [ScF_3(Me_3-tacn)] from solutions of [Sc(Me_3-tacn)F_2(μ-F)$SnMe_3Cl$)] failed, with the bimetallic species reforming in the isolated solid. This contrasts with [ScL(μ-F)$_2$(Me_3SnBr)$_2$] (L^- = N,N''-(1,3-dimethyl-1,3-propanediylidine)bis(N',N'-diethyl-1,2-ethanediamine)) which decomposes when the mother liquor is removed.[35] Gently heating a finely ground sample of [Sc(Me_3-tacn)F_2(μ-F)Me_3SnCl] (40 °C) under vacuum leads to partial removal of the Me_3SnCl, but complete removal of the tin species could not be achieved without decomposition of the scandium moiety.

The reaction of [$ScCl_3$(terpy)] with three mol. equivalents of Me_3SnF gave similar results, but in this case two Me_3SnCl molecules interact with the ScF_3 unit, most likely due to the planar and less sterically demanding terpy ligand. [Sc(terpy)F(μ-F)$_2$($SnMe_3Cl$)$_2$] was characterised by microanalysis and $^{19}F\{^1H\}$ and ^{45}Sc NMR and IR spectroscopy (Figure 5.26)

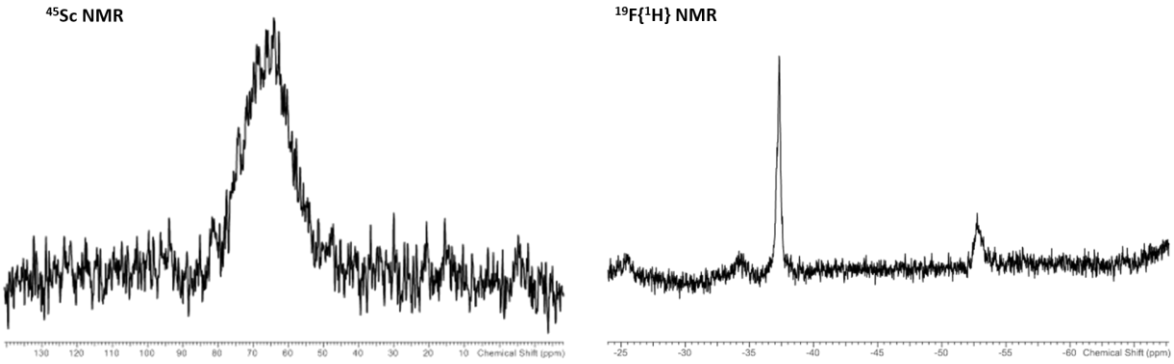

Figure 5.26. ^{45}Sc (left) and $^{19}F\{^1H\}$ (right) NMR spectra of [ScF_3(terpy)] in CD_3CN obtained using Me_3SnF.

The $^{19}F\{^1H\}$ NMR spectrum shows two resonances at −37.7 ([2F]) and −53.3 ([F]) ppm, due to the two fluorine environments present in the *meridional*-[ScF_3(terpy)] unit, while the ^{45}Sc NMR spectrum shows a broad resonance at 64 ppm. This compound, in contrast with [Sc(Me_3-tacn)F_2(μ-F)Me_3SnCl], appears to be unstable in solution and slowly decomposes.

The reaction of [YCl_3(Me_3-tacn)] with Me_3SnF in CH_3CN resulted in decomposition, and no YF_3 complex was identified.

5.2.5 Stability tests on [ScF_3(Me_3-tacn)]

The stability of [ScF_3(Me_3-tacn)] was challenged in the presence of competitive anions, water and heating and the experiments monitored by $^{19}F\{^1H\}$ and ^{45}Sc NMR spectroscopy. Since the halide exchange reactions on the chloride analogue were carried out in anhydrous conditions the stability of the formed scandium trifluoride complex in water was an important aspect in relation to the potential future application of this compound as a PET agent. The stability tests were performed on the Me_3-tacn complex since this ligand is more easily synthesised and it is reasonable to expect that the behaviour of [ScF_3(Me_3-tacn)] should replicate that of the $BnMe_2$-tacn analogue. However, the

$BnMe_2$-tacn complex would be used in radiolabelling experiments as the benzyl group provides a chromophore (detectable by UV-vis spectroscopy) and a site for functionalisation to attach a peptide. The $^{19}F\{^1H\}$ and ^{45}Sc NMR spectra of $[ScF_3(Me_3\text{-tacn})]$ in CD_3CN are shown in Figure 5.22. Water was added gradually into the NMR sample (1 drop, 2 drops and a 1:1 CD_3CN/H_2O solution).

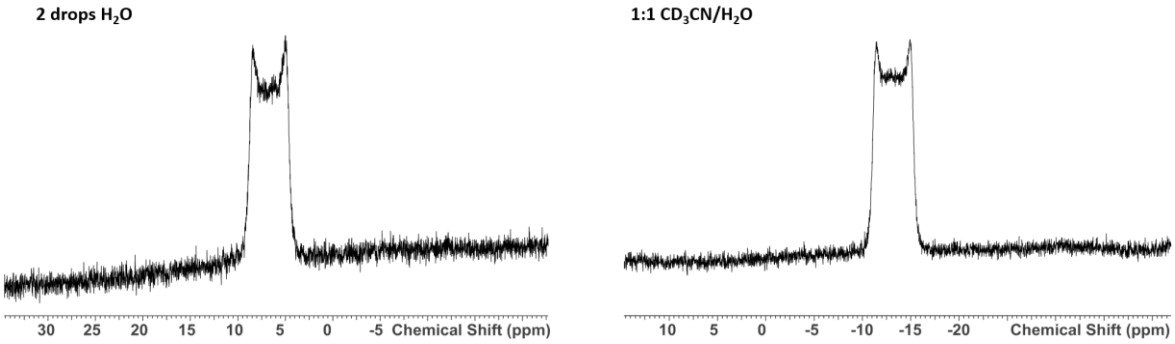

Figure 5.27. $^{19}F\{^1H\}$ NMR spectra of $[ScF_3(Me_3\text{-tacn})]$ in CD_3CN in the presence of two drops of water (left) δ = 6.7 ppm and in a 1:1 CD_3CN/H_2O solution (right) δ = −13.2 ppm.

Figure 5.27 shows that the complex is stable to the presence of water (1:1 CD_3CN/H_2O solution). It also shows that the complex resonance has shifted by ~ 20 ppm to lower frequencies upon the presence of water, suggesting a solvent dependant system (most likely involving H-bonding of the H_2O molecules via the fluoride ligands). The ^{45}Sc NMR spectrum was also acquired, showing the characteristic quartet due to the coupling to the three equivalent fluorides (also shifted at lower frequencies by ~7 ppm), undoubtedly providing evidence for the presence of the *fac*-$[ScF_3(Me_3\text{-tacn})]$ in solution (Figure 5.28).

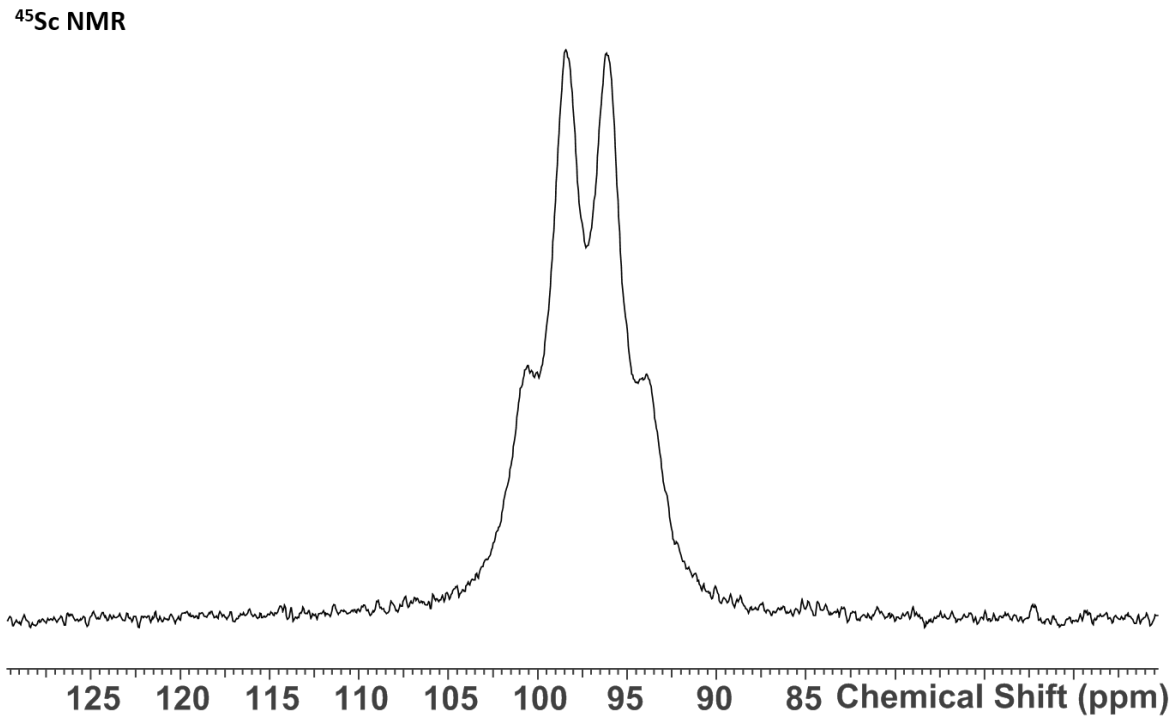

Figure 5.28. ^{45}Sc NMR of $[ScF_3(Me_3\text{-tacn})]$ in a 1:1 CD_3CN/H_2O solution δ = 97.2 ppm.

It was said that the halide exchange reaction on $[ScCl_3(Me_3\text{-tacn})]$ has to be carried out in anhydrous conditions, but the possibility of performing the reaction in the presence of water was also explored. As background, despite the moisture sensitivity of the $[MCl_3(Me_3\text{-tacn})]$ (M = Al, Ga), the radiolabelling experiments could be successfully carried out in aqueous MeCN solution.[2,54] In order to explore this possibility the halide exchange reaction on $[ScCl_3(Me_3\text{-tacn})]$ was performed *in situ* in an NMR tube using $[Bu_4N]F$ as fluoride source and CD_3CN as solvent. $[Bu_4N]F$ was obtained in a 1 M thf solution in which trace water was present. The addition of three mol. equivalents of $[Bu_4N]F$ into the NMR sample did not produce the desired product. The peak corresponding to the complex was not present in the $^{19}F\{^1H\}$ spectrum, while the ^{45}Sc NMR spectrum shows an eight-line pattern at 23.7 ppm, indicative of the formation of the fluoroscandate anion, ScF_7^{4-}, where the fluorides are fluxional (it should be noted that $[Sc(OH_2)_7]^{3+}$, used as reference in the ^{45}Sc experiments, is also seven-coordinate and H_2O and F^- have similar sizes)[55,56,57] (Figure 5.29).

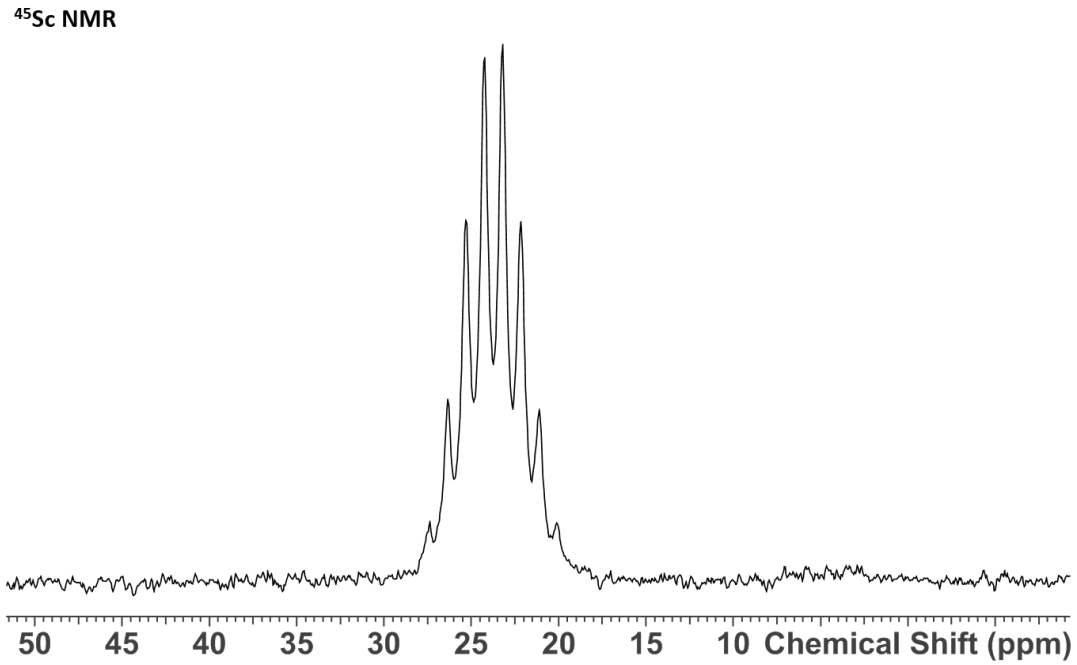

Figure 5.29. ^{45}Sc NMR spectrum obtained from the addition of three mol equiv. of $[Bu_4N]F$ in thf/H_2O to $[ScCl_3(Me_3\text{-tacn})]$.

The implication of these results is that the halide exchange reaction must be performed in strictly anhydrous conditions. However, once the scandium fluoride complex is formed, it is water stable.

Moreover, the $^{19}F\{^1H\}$ NMR spectrum of $[ScF_3(Me_3\text{-tacn})]$ was unchanged after 2 hours at 80 °C and after standing in a 1:1 CD_3CN/H_2O solution for 24 hours. The stability of the complex to a 10-fold excess of various competitive anions showed mixed results: $[ScF_3(Me_3\text{-tacn})]$ is stable to the presence of Cl^- and $CH_3CO_2^-$ ($^{19}F\{^1H\}$ and ^{45}Sc NMR spectra unchanged), but decomposes in the presence of PO_4^{3-}, CO_3^{2-}, and F^-, showing only F^- in the $^{19}F\{^1H\}$ NMR spectra in each case, and no ^{45}Sc resonance (all anions were added as sodium salts).

5.3 Conclusions

Among the three strategies identified for the synthesis of scandium fluoride complexes with neutral ligands, the halide exchange approach, in which the chlorides in [$ScCl_3$(Me_3-tacn)], [$ScCl_3$($BnMe_2$-tacn)] and [$ScCl_3$(terpy)] are replaced by fluorides, proved to be successful. [Me_4N]F or Me_3SnF were used as fluoride source producing different results: the reactions with Me_3SnF formed the unusual adducts, [Sc(Me_3-tacn)F_2(μ-F)$SnMe_3Cl$] and [Sc(terpy)F(μ-F)$_2$($SnMe_3Cl$)$_2$], whereas [ScF_3(Me_3-tacn)] and [ScF_3($BnMe_2$-tacn)] were obtained using [Me_4N]F. In both cases, the fluorination happens sequentially with the partially fluorinated species clearly visible in the $^{19}F\{^1H\}$ and ^{45}Sc NMR spectra. In the adducts [Sc(Me_3-tacn)F_2(μ-F)($SnMe_3Cl$)] and [Sc(terpy)F(μ-F)$_2$($SnMe_3Cl$)$_2$], the highly electron rich and polarised ScF_3 unit acts as a Lewis base towards Me_3SnCl. These compounds are the first examples of scandium fluoride complexes with neutral ligands. Since the scandium chloride complexes are moisture sensitive, the halide exchange reactions must be performed in strictly anhydrous conditions. *In situ* NMR reactions confirmed that if water is present during the halide exchange reaction, the fluorinated complex does not form. However, once [ScF_3(Me_3-tacn)] is formed, it is stable to the addition of water. Attempts to produce Y, La or Lu fluoride complexes either using [Me_4N]F or Me_3SnF failed. In this case, the use of larger ring tetra-azamacrocycles (cyclen or cyclam) may be better suited to accommodate the bigger radii of the metals.

In consideration of the potential application in PET imaging, [ScF_3(RMe_2-tacn)] is a promising system. [ScF_3($BnMe_2$-tacn)] must be synthesised in anhydrous conditions (from the chloride analogue), but its stability in water over a range of temperatures, as well as towards common ions, indicates that it may be worth further examination to establish whether it could be used as an ^{18}F carrier. Although the "ideal" precursor should be radiolabelled in aqueous solution, there are many examples of ^{18}F PET tracers whose synthesis require moisture exclusion in one or more steps (for example ^{18}F-FDG[58]). The use of tacn derivatives with anionic pendant arms, such as the H_2-R-nota type, may be better suited for the oxophilic Sc(III) ion (but also for Y and La or Lu).

In comparison with the Group 13 metal fluorides,[2] the systems discussed in this Chapter are less versatile in the sense that only the scandium fluoride complexes could be synthesised and only through halide exchange reactions, whose conditions need to be carefully controlled. The scandium fluoride complexes are also tolerant to a narrower selection of competitive anions. Furthermore, the chloride complexes show a range of coordination modes, with the Y and La terpy complexes being seven-coordinate. Apart from [$ScCl_3$(terpy)], whose coordination sphere does not contain water molecules, the other chloride complexes synthesised during this work all show extensive H-bonding and π-stacking interactions.

The attempts to synthesise $MF_3 \cdot xH_2O$ (M = Sc, Y, La) only produced the anhydrous form of these metal trifluorides (in contrast to the Group 13 hydrates synthesis[44]). The reactions with neutral ligands in hydrothermal conditions were unsuccessful suggesting that only the metal fluoride hydrates that contain water within the metal coordination sphere are likely to be viable synthons for neutral ligand complexes.

5.4 Experimental

All complex syntheses were carried out using standard Schlenk and vacuum line techniques. Samples were handled and stored in a glove box under a dry dinitrogen atmosphere to exclude moisture, which decomposes many of the samples. $[ScCl_3(thf)_3]$ and $[YCl_2(thf)_5][YCl_4(thf)_2]$ were prepared by the literature methods.[38,22,23] 2,2':6'2"-terpyridyl was obtained from Sigma-Aldrich and dried *in vacuo* prior to use. 1,4,7-trimethyl-1,4,7-triazacyclononane and 1,4-dimethyl-7-benzyl-1,4,7-triazacyclononane were prepared as described previously.[59,60] Anhydrous $[NMe_4]F$ was obtained by recrystallising the commercial sample (Aldrich) from ^{i}PrOH as described.[61] For further details regarding the instrumentation used see Appendix 1.

5.4.1 $ScF_3 \cdot xH_2O$

Sc_2O_3 (2.9 g, 0.021 mol), and a 6 M solution of HCl (43 mL) were heated to reflux for 3 h, during which period the mixture changed from a cloudy white suspension to a clear yellow solution. The solvent was removed in *vacuo* whilst heating at 65 °C. $ScCl_3 \cdot 6H_2O$ was obtained as a white solid. This was dissolved in water in a plastic beaker and 6 mL of 40 % $HF_{(aq)}$ (CARE) were added causing the precipitation of a white solid. The mixture was heated to boiling and the solvent evaporated, giving a white gel-like solid. A portion of the gel was suspended in water, causing the formation of the solid, which was isolated by evaporation of the solvent. The same procedure was repeated portion by portion and the solid combined (3.94 g, 93 %).

5.4.2 $YF_3 \cdot xH_2O$

Method 1: $Y_2(SO_4)_3 \cdot 8H_2O$ (3.0 g, 4.92 mmol) was dissolved in water. 5 mL of a solution of 40 % $HF_{(aq)}$ was added and a white precipitate formed. The precipitate was left to settle overnight. The solution was filtered and the solid washed with water and dried *in vacuo* (1.07 g, 75 %).

Method 2: $Y_2(SO_4)_3 \cdot 8H_2O$ (3.0 g, 4.92 mmol) was suspended in hot water (80 °C) until most of the solid dissolved. The liquid was decanted off from any residue and a solution of 40 % $HF_{(aq)}$ (3 mL) was added to the solution. A white solid precipitated immediately. The reaction was left stirring for 1.5 h and then the solid was left to settle overnight. The solution was decanted off and the solid dried overnight in a desiccator. (1.24 g, 86 %).

5.4.3 $LaF_3 \cdot xH_2O$

$LaCl_3 \cdot 7H_2O$ (5.0 g, 13.5 mmol) was dissolved in water (30 mL). 40 % $HF_{(aq)}$ (1.5 mL) was diluted in water (10 mL) and added dropwise to the solution, giving a white gelatinous material which was

stirred for 1 h. This solid was collected by evaporating the solvent off at 110 ˚C, leaving a fine white solid. Yield: 2.50 g, 95%.

5.4.4 [$ScCl_3$(terpy)]

A solution of terpy (0.055 g, 0.24 mmol) in 3 mL of CH_3CN was added to a solution of [$ScCl_3(thf)_3$] (0.076 g, 0.24 mmol) in 5 mL of CH_3CN, causing the immediate precipitation of a white solid. After a few minutes the solid was filtered off, washed with n-hexane and dried in *vacuo.* Yield: 0.054 g, 60%. Required for $C_{15}H_{11}Cl_3N_3Sc$: C, 46.8; H, 2.9; N, 10.9. Found: C, 46.7; H, 3.1; N, 11.1 %. IR (Nujol, ν/cm^{-1}): 292, 339, 337 (Sc–Cl). ^{1}H NMR (CD_2Cl_2, 298 K): δ = 9.25-9.20 (m, [2H], Ar), 8.30-8.24 (m, [7H], Ar), 7.80 (s, [2H], Ar). ^{45}Sc NMR (CD_2Cl_2, 298 K): δ = 254 (s, br). Colourless crystals were obtained from slow diffusion of Et_2O into a concentrated solution of the complex in CH_3CN.

5.4.5 [YCl_3(terpy)(OH_2)]

A solution of terpy (0.046 g, 0.20 mmol) was added to a solution of [$YCl_2(thf)_5$][$YCl_4(thf)_2$] (0.08 g, 0.09 mmol) in anhydrous CH_3CN, causing the immediate precipitation of a white solid. After 30 minutes, the white solid was filtered, washed with n-hexane and dried in *vacuo*. Yield: 0.051 g, 61%. Required for $C_{15}H_{13}Cl_3N_3OY$: C, 40.3; H, 2.9; N, 9.4. Found: C, 40.2; H, 3.0; N, 9.5 %. IR (Nujol, ν/cm^{-1}): 3338, 1641 (H_2O), 272, 262(sh) (Y–Cl). ^{1}H NMR (CD_3CN, 298 K): δ = 9.84-9.78 (m, [2H], Ar), 8.48-8.40 (m, [2H], Ar), 8.39-8.33 (m, [3H], Ar), 8.17-8.12 (m, [2H], Ar), 7.69-7.61 (m, [2H], Ar), 2.15 (s, H_2O). Colourless crystals were grown by placing the Schlenk tube containing the filtrate in the freezer (–18°C) for a few days.

5.4.6 [$LaCl_3$(terpy)(OH_2)]·4H_2O

$LaCl_3·7H_2O$ (0.108 g, 0.44 mmol) was dissolved in ethanol (10 mL). Terpy (0.098 g, 0.42 mmol) was suspended in ethanol (10 mL) and the reagents combined. A white precipitate formed, which was stirred for 45 min. The solvent was then removed via filtration and the solid washed with ethanol, then diethyl ether and dried *in vacuo.* Yield: 0.09 g, 40 %. Required for $C_{15}H_{21}Cl_3LaN_3O_5$: C, 31.7; H, 3.7; N, 7.4. Found: C, 31.8; H, 4.0; N, 6.9%. IR (Nujol, *ν*/cm^{-1}): 3369, 1633 (H_2O), 209, 205 (La-Cl). ^{1}H NMR (CD_3OD, 298 K): δ = 9.37-9.32 (m, br, [2H], Ar), 8.61-8.55 (m, br, [3H], Ar), 8.43-8.38 (m, br, [2H], Ar), 8.31-8.25 (m, br, [2H], Ar), 7.79-7.73 (m, br, [2H], Ar), 4.85 (H_2O). Colourless crystals of [{La(terpy)(OH_2)Cl_2}$_2$(μ-Cl)$_2$] were obtained by layering an ethanol solution of $LaCl_3·7H_2O$ with an equimolar solution of terpy in ethanol, and leaving undisturbed for 48 h.

5.4.7 [$LuCl_3(terpy)(OH_2)$]

$LuCl_3 \cdot 6H_2O$ (0.113 g, 0.29 mmol) was dissolved in ethanol (10 mL). Terpy (0.069 g, 0.30 mmol) was dissolved in ethanol (5 mL) and added dropwise. After stirring for 2 h, a white precipitate had formed. The precipitate was collected via filtration, washed with diethyl ether (2 mL) and then dried in a desiccator for one hour, leaving a white powder. Yield: 0.120 g, 77%. Required for $C_{15}H_{13}Cl_3LuN_3O$: C, 33.8; H, 2.5; N, 7.9. Found: C, 33.7; H, 2.5; N, 7.7%. IR (Nujol, ν/cm^{-1}) 3424, 1657 (H_2O) 205, 201 (Lu-Cl). ^{1}H NMR (CD_3OD, 298 K): δ = 9.41 (d, [2H], Ar), 8.72 (d, [2H], Ar), 8.67 (m, [3H], Ar), 8.51 (t, [2H], Ar), 8.35 (t, [2H], Ar). Colourless crystals of [$LuCl_3(terpy)(OH_2)$] were grown by layering an ethanol solution of $LuCl_3 \cdot 6H_2O$ with an equimolar solution of terpy in ethanol, and leaving undisturbed for one week.

5.4.8 [$ScCl_3(Me_3\text{-}tacn)$]

This was prepared by the literature method.[25] Required for $C_9H_{21}Cl_3N_3Sc$: C, 33.5; H, 6.6; N, 13.0. Found: C, 33.5; H, 6.7; N, 13.2 %. IR (Nujol, ν/cm^{-1}) 353, 330 (Sc–Cl). ^{1}H NMR (CD_3CN, 298 K): δ = 3.26-3.18 (m, [6H], CH_2), 2.96-2.90 (m, [6H], CH_2), 2.87 (s, [9H], CH_3). ^{45}Sc NMR (CD_3CN, 298 K): δ = 300 (s).

5.4.9 [$ScCl_3(BnMe_2\text{-}tacn)$]

[$ScCl_3(thf)_3$] (0.066 g, 0.2 mmol) was dissolved in 10 mL of acetonitrile. A solution of $BnMe_2$-tacn (0.051 g, 0.2 mmol) in 5 mL of acetonitrile was then added. The reaction was left stirring for 3 h and the solvent was removed *in vacuo* giving an off-white solid, which was washed with hexane (5 mL) and dried *in vacuo.* Yield: 0.079 g, 57%. Required for $C_{15}H_{31}Cl_3N_3Sc$: C, 45.2; H, 6.3; N, 10.5. Found: C, 45.3; H, 6.5; N, 10.7 %. IR (Nujol, ν/cm^{-1}): 333, 301 (br, Sc–Cl). ^{1}H NMR (CD_3CN, 298 K): δ = 7.38-7.32 (m, [5H], Ar), 3.85-3.79 (s, [2H], N-CH_2-Ar), 2.98 (s, [4H], CH_2), 2.81-2.75 (m, [8H], CH_2), 2.50 (s, [6H], CH_3). ^{45}Sc NMR (CD_3CN, 298 K) δ = 302 (s).

5.4.10 [$YCl_3(Me_3\text{-}tacn)$]

This was prepared by the literature method.[25] Required for $C_9H_{21}Cl_3N_3Y$: C, 29.5; H, 5.8; N, 11.5. Found: C, 29.8; H, 5.9; N, 11.3 %. IR (Nujol, ν/cm^{-1}): 323, 289 (Y–Cl). ^{1}H NMR (CD_3CN, 298 K): δ = 3.16-3.08 (m, [6H], CH_2), 2.94-2.87 (m, [6H], CH_2), 2.82 (s, [9H], CH_3).

5.4.11 [$YI_3(Me_3\text{-tacn})]\cdot 1.5CH_3CN$

YI_3 (0.122 g, 0.26 mmol) was suspended in 10 mL of acetonitrile. A solution of Me_3-tacn (0.044 g, 0.26 mmol) in 10 mL of acetonitrile was added. The reaction mixture was heated to 40 °C until a clear solution was obtained. After cooling, the volatiles were reduced *in vacuo* to 5 mL causing the precipitation of a white solid, which was filtered and dried *in vacuo* (0.078 g, 47%). Required for $C_9H_{21}I_3N_3Y\cdot 1.5CH_3CN$: C, 20.5; H, 3.7; N, 9.0. Found: C, 21.2; H, 3.9; N, 8.4 %. IR (Nujol, ν/cm^{-1}): 2253, 2187 (MeCN). ^{1}H NMR (CD_3CN, 298 K): δ = 3.46-3.40 (m, [6H], CH_2), 3.12 (s, [9H], CH_3), 2.94-2.89 (m, [6H], CH_2), 1.98 (s, CH_3CN). Crystals suitable for single crystal X-ray analysis were obtained from a separate reaction by placing the Schlenk flask in the freezer (−18 °C). After a few days, two different crystal morphologies were found, which were identified by single crystal X-ray diffraction to be $[YI_3(Me_3\text{-tacn})]\cdot CH_3CN$ and $[\{YI_2(Me_3\text{-tacn})\}_2(\mu\text{-O})]$, the latter formed via hydrolysis from trace water ingress into the flask during crystallisation in the freezer.

5.4.12 [$LaCl_3(Me_3\text{-tacn})(OH_2)$]

$LaCl_3\cdot 7H_2O$ (0.101 g, 0.41 mmol) was dissolved in ethanol (10 mL). Me_3-tacn (0.06 mL, 0.41 mmol) in ethanol (5 mL) was added to form a white precipitate. After stirring for 45 min., the solvent was removed *in vacuo* leaving a white sticky solid, which was dried in a desiccator for two hours. The solid was then washed with diethyl ether (3 mL) and dried again *in vacuo*, leaving a white powder. Yield: 0.09 g, 54%. Required for $C_9H_{23}Cl_3LaN_3O$: C, 24.9; H, 5.3; N, 9.7. Found: C, 25.6; H, 5.2; N, 10.0 %. IR (Nujol, ν/cm^{-1}): 3376, 1635 (H_2O), 207 (La–Cl). ^{1}H NMR (CD_3CN, 298 K): δ = 2.86-2.78 (m, [12H], CH_2), 2.57 (s, [9H], CH_3), 2.10 (H_2O). ^{1}H NMR (CD_3OD, 178 K): δ = 3.30 (H_2O), 2.92 (m, [6H], CH_2), 2.77 (m, [6H], CH_2), 2.62 (s, [9H], CH_3).

5.4.13 [$Sc(terpy)F(\mu\text{-}F)_2(SnMe_3Cl)_2$]

$[ScCl_3(terpy)]$ (0.05 g, 0.13 mmol) was suspended in CH_3CN (8 mL). A suspension of Me_3SnF (0.083 g, 0.45 mmol) in CH_3CN (15 mL) was added to the first one. After one hour most of the solid dissolved. The mixture was left stirring for 6 hours. The liquid was decanted *via* cannula and the solvent removed *in vacuo*, giving a slightly pink solid. The solid was washed with hexane and dried in *vacuo* (0.031 g, 33 %). Required for $C_{21}H_{29}Cl_2F_3N_3ScSn_2$: C, 34.4; H, 4.0; N, 5.7. Found: C, 34.8; H, 3.9; N, 6.9%. IR (Nujol, ν/cm^{-1}): 489, 509, 544 (Sc–F), 270 (Sn–Cl). ^{1}H NMR (CD_3CN, 298 K): δ = 8.68 (br, [2H], Ar-CH_2), 8.48 (br, [3H], Ar-CH_2), 8.05 (br, [2H], Ar-CH_2), 7.95 (br, [2H], Ar-CH_2), 7.45 (br, [2H], Ar-CH_2), 0.60 (s, $^2J_{SnH}$ = 64 Hz, Me_3SnCl)). ^{19}F{^{1}H} NMR (CD_3CN, 298 K): δ = −37.7 (br s, [2F]), −53.3 (br s, [F]). ^{45}Sc NMR (CD_3CN, 298 K): δ = 64 (s, br).

5.4.14 [$ScF_3(Me_3$-tacn)]

[$ScCl_3(Me_3$-tacn)] (0.05 g, 0.15 mmol) was dissolved in 10 mL of acetonitrile. [NMe_4]F (0.046 g, 0.46 mmol) was suspended in 10 mL of acetonitrile and added dropwise to the solution of the complex. The reaction was left stirring for 90 minutes. Some white solid was evident throughout the reaction. The volatiles were removed *in vacuo* and the resulting white solid was washed with CH_2Cl_2, filtered and dried *in vacuo* (0.041 g, 97%). Required for $C_9H_{21}F_3N_3Sc{\cdot}NMe_4Cl$: C, 40.8; H, 8.7; N, 14.6. Found: C, 41.7; H, 9.2; N, 14.6%. IR (Nujol, ν/cm^{-1}): 579, 546 (Sc–F). ^{1}H NMR (CD_3CN, 298 K): δ = 3.16 (s, [12H], CH_3), 2.75-2.87 (m, [12H], CH_2), 2.65 (s, [9H], CH_3). $^{19}F\{^1H\}$ NMR (CD_3CN, 298 K): δ = 41.6 (m, [$ScF_2Cl(Me_3$-tacn)]), 8.2 (m, [$ScF_3(Me_3$-tacn)]). ^{45}Sc NMR (CD_3CN, 298 K): δ = 157 (m, [$ScF_2Cl(Me_3$-tacn)]), 104 (quartet, [$ScF_3(Me_3$-tacn)], $^1J_{ScF}$ = 215 Hz).

5.4.15 [$Sc(Me_3$-tacn)F_2(μ-F)$SnMe_3Cl$]

Me_3SnF was ground and dried under *vacuo* for 30 mins. 10 mL of a MeCN solution containing [$ScCl_3(Me_3$-tacn)] (0.066 g, 0.20 mmol) was added to a solution of Me_3SnF (0.133 g, 0.72 mmol), giving a clear solution in 20 mins. The reaction mixture was stirred for 4 h. The solvent was then removed *in vacuo* and the white solid was dissolved in CH_2Cl_2 (5 mL). Hexane was added causing the precipitation of a white solid, which was filtered and dried in *vacuo* (0.078 g, 81 %). Required for $C_{12}H_{301}ClF_3N_3O_3ScSn$: C, 30.5; H, 6.4; N, 8.9. Found: C, 30.3; H, 6.5; N, 8.8 %. IR (Nujol, *ν*/cm^{-1}): 556, 547 (Sc–F), 269 (Sn–Cl). ^{1}H NMR (CD_3CN, 298 K): δ = 2.72-2.87 (m, [12H], CH_2), 2.61 (s, [9H], CH_3), 0.60 (s, [9H], Me_3SnCl). $^{19}F\{^1H\}$ NMR (CD_3CN, 298 K): δ = 7.7 (m). ^{45}Sc NMR (CD_3CN, 298 K): δ = 104 (q, $^1J_{ScF}$ = 227 Hz). Crystals of [$Sc(Me_3$-tacn)F_2(μ-F)$SnMe_3Cl$] were obtained from slow evaporation of a concentrated solution of the product in CH_3CN.

5.4.16 [$ScF_3(BnMe_2$-tacn)]

A suspension of [NMe_4]F (0.027 g, 0.38 mmol) in CH_3CN (5 mL) was added to a suspension of [$ScCl_3(BnMe_2$-tacn)] (0.038 g, 0.13 mmol) in CH_3CN (10 mL). The white precipitate present in solution was removed by filtration. The filtrate was taken to dryness in *vacuo* giving a light yellow solid (0.010 g, 57%). ^{1}H NMR (CD_3CN, 298 K): δ = 7.39-7.31 (m, [5H], Ar) 3.82 (s, [2H], N-CH_2-Ar), 2.98 (s, [4H], CH_2), 2.80-2.72 (m, [8H], CH_2), 2.50 (s, [6H], CH_3). $^{19}F\{^1H\}$ NMR (CD_3CN, 298 K): δ = 10.1 (br). ^{45}Sc NMR (CD_3CN, 298 K): δ = 104 (br).

5.4.17 X-ray experimental

Table 5.3. Crystal data and structural refinement details. [a]

Compound	$[ScCl_3(terpy)]$	$[YCl_3(terpy)(OH_2)]$	$[ScF_2Cl(Me_3\text{-}tacn)]$
Formula	$C_{15}H_{11}Cl_3N_3Sc$	$C_{15}H_{11}C_{l3}N_3OY$	$C_9H_{21}ClF_2N_3Sc$
M	284.58	444.53	289.70
Crystal system	monoclinic	triclinic	Monoclinic
Space group	P 2_1/c (14)	P -1 (2)	P 2_1/c (14)
a /Å	8.5434(12)	7.5645(7)	11.9938(9)
b /Å	13.9045(12)	9.9623(10)	6.8826(7)
c /Å	14.0175(16)	12.1261(11)	15.8721(19)
α/ °	90	70.174(9)	90
β /°	106.779(13)	83.413(7)	90.292(8)
γ/°	90	73.153(8)	90
U /Å^3	1594.3(3)	822.62(14)	1310.2(2)
Z	4	2	4
μ(Mo-K$_\alpha$)/mm^{-1}	0.961	4.037	0.768
F(000)	776	440	608
Total no. reflns	14466	10392	7726
R_{int}	0.149	0.088	0.175
Unique reflns	3144	3236	2566
No. of params, restraints	199, 0	208, 0	148, 0
R_1, wR_2 [$I > 2\sigma(I)$] [b]	0.070, 0.116	0.053, 0.117	0.071, 0.159
R_1, wR_2 (all data)	0.151, 0.145	0.083, 0.130	0.136, 0.196

Table 5.1 continued

Compound	$[YI_3(Me_3\text{-}tacn)]\cdot CH_3CN$	$[\{YI_2(Me_3\text{-}tacn)\}_2(\mu\text{-}O)]\cdot CH_3CN$	$[\{La(terpy)(OH_2)Cl\}_2(\mu\text{-}Cl)_2]$
Formula	$C_9H_{21}I_3N_3Y\cdot C_2H_3N$	$C_{18}H_{42}I_4N_6OY_2\cdot C_2H_3N$	$C_{30}H_{26}Cl_6La_2N_6O_2$
M	681.95	1085.05	993.09
Crystal system	monoclinic	triclinic	triclinic
Space group	P $2_1/c$ (14)	P -1 (2)	P-1 (2)
a /Å	10.5669(5)	8.6352(3)	9.7676(4)
b /Å	15.9059(7)	8.6395(3)	9.9809(4)
c /Å	11.7484(6)	23.7313(8)	10.3396(3)
α/ °	90	90.160(3)	94.048(3)
β /°	90.139(5)	90.941(3)	109.768(3)
γ/°	90	108.966(3)	113.865(4)
U /Å^3	1974.61(16)	1674.05(10)	841.92(6)
Z	4	2	1
μ(Mo-K_α)/mm^{-1}	7.639	7.161	3.018
F(000)	1264	1024	480
Total no. reflns	13372	11161	10844
R_{int}	0.065	0.027	0.057
Unique reflns	3887	6471	3299
No. of params, restraints	177, 0	317, 0	216, 0
R_1, wR_2 [$I > 2\sigma(I)$][b]	0.039, 0.065	0.035, 0.082	0.025, 0.057
R_1, wR_2 (all data)	0.052, 0.069	0.043, 0.085	0.029, 0.059

Table 5.1 continued

Compound	[Sc(Me$_3$-tacn)F$_2$(μ-F)SnMe$_3$Cl]	[LuCl$_3$(terpy)(OH$_2$)]
Formula	$C_{12}H_{30}ClF_3N_3ScSn$	$C_{15}H_{13}Cl_3LuN_3O$
M	472.49	532.60
Crystal system	monoclinic	triclinic
Space group	Cm (8)	P-1 (2)
a /Å	11.8495(10)	7.5588(5)
b /Å	9.2438(6)	10.0003(8)
c /Å	10.9099(7)	12.0814(9)
α/ °	90	69.953(7)
β /°	118.852(5)	82.993(6)
γ/°	90	72.341(7)
U /Å^3	1046.67(14)	817.31(11)
Z	2	2
μ(Mo-K$_\alpha$)/mm^{-1}	1.666	6.535
F(000)	476	508
Total no. reflns	5546	12609
R_{int}	0.037	0.114
Unique reflns	2729	3214
No. of params, restraints	132, 176	173, 4
R_1, wR_2 [$I > 2\sigma(I)$][b]	0.0271, 0.0636	0.043, 0.101
R_1, wR_2 (all data)	0.0275, 0.0638	0.051, 0.106

[a] Common items: T = 100 K; wavelength (Mo-Kα) = 0.71073 Å; ϑ(max) = 27.5°;

[b] $R_1 = \Sigma||F\sigma| - |Fc|| / \Sigma|Fo|$; $wR_2 = [\Sigma w(Fo^2 - Fc^2)^2 / \Sigma wFo^2]^{1/2}$.

5.5 References

1. Bhalla, R.; Levason, W.; Luthra, S. K.; McRobbie, G.; Sanderson, G.; Reid, G., *Chem. Eur. J.* **2015**, *21*, 4688.

2. Bhalla, R.; Darby, C.; Levason, W.; Luthra, S. K.; McRobbie, G.; Reid, G.; Sanderson, G.; Zhang, W., *Chem. Sci.* **2014**, *5*, 381.

3. Sears, J. M.; Boyle, T. J., *Coord. Chem. Rev.* **2017**, *340*, 154.

4. Aldridge, S.; Downs, A. J., *The Group 13 Metals Aluminium, Gallium, Indium, Thallium - Chemical Patterns and Peculiarities,* Wiley, **2011**.

5. Fisher, K. J., *Comprehensive Coordination Chemistry II,* ed. J.A. McCleverty and T.J. Meyer, Elsevier Pergamon, **2004**, Vol. *3*, 1.

6. Bunzli, J. C., *Acc. Chem. Res.* **2006**, *39*, 53.

7. Wilkinson, G.; Gillard, R. D.; McCleverty, J. A., *Comprehensive Coordination Chemistry I,* Pergamon, Oxford, **1987**, Vol. *3*, 1060.

8. Evans, W. J., *Coord. Chem. Rev.* **2000**, *206*, 263.

9. Anwander, R.; Dolg, M.; Edelmann, F. T., *Chem. Soc. Rev.* **2017**, *46*, 6697.

10. Mao, J.; Jin, Z., *Polyhedron* **1994**, *13*, 319.

11. Klein, J. M.; Clegg, J. K.; Saggiomo, V.; Reck, L.; Luning, U.; Sanders, J. K., *Dalton Trans.* **2012**, *41*, 3780.

12. Rogers, R. D.; Etzenhouser, R. D.; Murdoch, J. S., *Inorg. Chim. Acta* **1992**, *196*, 73.

13. Rakhmatullin, A.; Polovov, I. B.; Maltsev, D.; Allix, M.; Volkovich, V.; Chukin, A. V.; Boca, M.; Bessada, C., *Inorg. Chem.* **2018**, *57*, 1184.

14. Mountford, P.; Ward, B. D., *Chem Commun.* **2003**, 1797.

15. Xie, Z.; Chui, K.; Yang, Q.; Mak, T. C. W.; Sun, J., *Organometallics* **1998**, *17*, 3937.

16. Huang, W.; Diaconescu, P. L., *Organometallics* **2016**, *36*, 89.

17. Zeimentz, P. M.; Arndt, S.; Elvidge, B. R.; Okuda, J., *Chem. Rev.* **2006**, *106*, 2404.

18. Chu, J.; Han, X.; Kefalidis, C. E.; Zhou, J.; Maron, L.; Leng, X.; Chen, Y., *J. Am. Chem. Soc.* **2014**, *136*, 10894.

19. Greve, B. K.; Martin, K. L.; Lee, P. L.; Chupas, P. J.; Chapman, K. W.; Wilkinson, A. P., *J. Am. Chem. Soc.* **2010**, *132*, 15496.

20. Hu, L.; Chen, J.; Sanson, A.; Wu, H.; Guglieri Rodriguez, C.; Olivi, L.; Ren, Y.; Fan, L.; Deng, J.; Xing, X., *J. Am. Chem. Soc.* **2016**, *138*, 8320.

21. Chen, J.; Gao, Q.; Sanson, A.; Jiang, X.; Huang, Q.; Carnera, A.; Rodriguez, C. G.; Olivi, L.; Wang, L.; Hu, L.; Lin, K.; Ren, Y.; Lin, Z.; Wang, C.; Gu, L.; Deng, J.; Attfield, J. P.; Xing, X., *Nat. Commun.* **2017**, *8*, 14441.

22. Manzer, L. E., *Inorg. Synth.* **1982**, *21*, 1579.

23. Sobota, P.; Utko, J.; Szafert, S., *Inorg. Chem.* **1994**, *33*, 5203.

24. Champion, M. J.; Farina, P.; Levason, W.; Reid, G., *Dalton Trans.* **2013**, *42*, 13179.

25. Hajela, S.; Schaefer, P. W.; Bercaw, E. J., *J. Organomet. Chem.* **1997**, *532*, 45.

26. Bartlett, S. A.; Cibin, G.; Dent, A. J.; Evans, J.; Hanton, M. J.; Reid, G.; Tooze, R. P.; Tromp, M., *Dalton Trans.* **2013**, *42*, 2213.

27. Tredget, C. S.; Lawrence, S. C.; Ward, B. D.; Howe, R. G.; Cowley, A. R.; Mountford, P., *Organometallics* **2005**, *24*, 3136.

28. Deakin, L.; Levason, W.; Popham, M. C.; Reid, G.; Webster, M., *J. Chem. Soc., Dalton Trans.* **2000**, 2439.

29. Hill, N. J.; Levason, W.; Popham, M. C.; Reid, G.; Webster, M., *Polyhedron* **2002**, *21*, 1579.

30. Hill, N. J.; Levason, W.; Popham, M. C.; Reid, G.; Webster, M., *Polyhedron* **2002**, *21*, 445.

31. Kepert, C. J.; Lu, W. M.; Skelton, B. W.; White, A. H., *Aust. J. Chem.* **1994**, *47*, 365.

32. Khorasani-Motlagh, M.; Noroozifar, M.; Niroomand, S.; Patrick, B. O., *Inorg. Chim. Acta* **2012**, *383*, 72.

33. Li, J.-S.; Neumüller, B.; Dehnicke, K., *Z. Anorg. Allg. Chem.* **2002**, *628*, 45.

34. Bottomley, F.; Paez, D. E.; White, P. S., *J. Organomet. Chem.* **1985**, *291*, 35.

35. Neculai, Ana M.; Neculai, D.; Nikiforov, Grigori B.; Roesky, Herbert W.; Schlicker, C.; Herbst-I rmer, R.; Magull, J.; Noltemeyer, M., *Eur. J. Inorg. Chem.* **2003**, *2003*, 3120.

36. Deacon, G. B.; Forsyth, C. M.; Junk, P. C.; Kelly, R. P.; Urbatsch, A.; Wang, J., *Dalton Trans.* **2012**, *41*, 8624.

37. Deacon, G. B.; Junk, P. C.; Werner, D., *Eur. J. Inorg. Chem.* **2015**, 1484.

38. Hayes, P. G.; Piers, W. E., *Inorg. Synth.* **2010**, *35*, 20.

39. Fedorov, P. P.; Trnovtsova, V.; Kocherba, G. I.; Sobolev, B. P., *Kristallografiya* **1995**, *40*, 716.

40. Cheetham, A. K.; Norman, N.; Hope, H.; Kjekshus, A.; Klewe, B.; Powell, D. L., *Acta Chem. Scand.* **1974**, *28a*, 55.

41. Zalkin, A.; Templeton, D. H.; Hopkins, T. E., *Inorg. Chem.* **1966**, *5*, 1466.

42. Gude, K.; Hebecker, C., *Z. Naturforsch.* **1985**, *40b*, 726.

43. Bhalla, R.; Levason, W.; Luthra, S. K.; McRobbie, G.; Monzittu, F. M.; Palmer, J.; Reid, G.; Sanderson, G.; Zhang, W., *Dalton Trans.* **2015**, *44*, 9569.

44. Bhalla, R.; Burt, J.; Hector, A. L.; Levason, W.; Luthra, S. K.; McRobbie, G.; Monzittu, F. M.; Reid, G., *Polyhedron* **2016**, *106*, 65.

45. Benjamin, S. L.; Levason, W.; Pugh, D.; Reid, G.; Zhang, W. J., *Dalton Trans.* **2012**, *41*, 12548.

46. Champion, M. J. D.; Levason, W.; Reid, G., *J. Fluorine Chem.* **2014**, *157*, 19.

47. Murphy, E. F.; Murugavel, R.; Roesky, H. W., *Chem. Rev.* **1997**, *97*, 3425.

48. Beckmann, J.; Horn, D.; Jurkschat, K.; Rosche, F.; Schürmann, M.; Zachwieja, U.; Dakternieks, D.; Duthie, A.; Lim, Allan E. K., *Eur. J. Inorg. Chem.* **2003**, *2003*, 164.

49. Chaudhary, P.; Bieringer, M.; Hazendonk, P.; Gerken, M., *Dalton Trans.* **2015**, *44*, 19651.

50. Mason, J., *Multinuclear NMR,* ed. Plenum, New York, **1987**.

51. Lefferts, J. L.; Molloy, K. C.; Hossain, M. B.; van der Helm, D.; Zuckerman, J. J., *J. Organomet. Chem.* **1982**, *240*, 349.

52. Bhalla, R.; Levason, W.; Luthra, S. K.; McRobbie, G.; Reid, G.; Sanderson, G.; Zhang, W., *Chem Commun.* **2014**, *50*, 12673.

53. Pedersen, K. S.; Lorusso, G.; Morales, J. J.; Weyhermuller, T.; Piligkos, S.; Singh, S. K.; Larsen, D.; Schau-Magnussen, M.; Rajaraman, G.; Evangelisti, M.; Bendix, J., *Angew. Chem. Int. Ed.* **2014**, *53*, 2394.

54. Levason, W.; Luthra, S. K.; McRobbie, G.; Monzittu, F. M.; Reid, G., *Dalton Trans.* **2017**, *46*, 14519.

55. Yamaguchi, T.; Niihara, M.; Takamuku, T.; Wakita, H.; Kanno, H., *Chem. Phys. Lett.* **1997**, *274*, 485.

56. Cotton, S. A., *Comments Inorg. Chem.* **1999**, *21*, 165.

57. Migliorati, V.; D'Angelo, P., *Inorg. Chem.* **2016**, *55*, 6703.

58. Hamacher, K.; Coenen, H. H.; Stocklin, G., *J. Nucl. Med.* **1986**, *27*, 235.

59. Belousoff, M. J.; Duriska, M. B.; Graham, B.; Batten, S. R.; Moubaraki, B.; Murray, K. S.; Spiccia, L., *Inorg. Chem.* **2006**, *45*, 3746.

60. Wieghardt, K.; Chaudhuri, P.; Nuber, B.; Weiss, J., *Inorg. Chem.* **1982**, *21*, 3086.

61. Christe, K. O.; Wilson, W. W.; Wilson, R. D.; Bau, R.; Feng, J. A., *J. Am. Chem. Soc.* **1990**, *112*, 7619.

Chapter 6: **Exploring the stability of transition metal (Cr^{3+}, Mn^{3+}, Fe^{3+}, Co^{3+}) fluoride complexes in aqueous media**

6.1 Introduction

The journey across the periodic table to investigate some of the metals in the oxidation state +3 for application in PET imaging, terminates with the first row of transition metals, Cr^{3+}, Mn^{3+}, Fe^{3+} and Co^{3+}. It started from the highly stable Group 13 metal fluorides of aluminium and gallium, which are highly promising systems for peptide conjugation and *in vivo* studies, and it moved to the larger and more oxophilic Group 3 elements (and La and Lu). The synthesis to form the Group 3 fluoride complexes required more stringent reaction conditions, but also show positive aspects, in particular, the stability of the ScF_3-tacn system in water. The transition metal ions, Cr^{3+}, Mn^{3+}, Fe^{3+} and Co^{3+}, are the subject of this Chapter. Ti^{3+} and V^{3+} were not considered as the former is very readily oxidised, while the latter is also likely to form V(IV) *in vivo* (the green $[VF_3(tacn)]$ is oxidised to $[VOF_2(tacn)]$ (blue) within 24 hours by simply adding a few drops of water to a methanol solution of $[VF_3(tacn)]$).[1] In contrast to the systems discussed in the previous Chapters, these metal ions do not have closed shell electronic configurations, but rather have partially filled *d* orbitals and, for some of them, multiple oxidation states are accessible. For each metal, the different d^n configurations (Table 6.1) correspond to different properties, such as ligand substitution kinetics or the ease with which they change oxidation state.

Metal(III)	Electronic Configuration	*d*-orbital Configuration (O_h)		Free Ion Term	Ground State Molecular Term (O_h)	
Cr	$[Ar]3d^3$	$t_{2g}^3e_g^0$		^4F	$^4A_{2g}$	
Mn	$[Ar]3d^4$	$t_{2g}^4e_g^0$ (LS)	$t_{2g}^3e_g^1$ (HS)	^5D	$^3T_{1g}$ (LS)	^5E_g (HS)
Fe	$[Ar]3d^5$	$t_{2g}^5e_g^0$ (LS)	$t_{2g}^3e_g^2$ (HS)	^6S	$^2T_{2g}$ (LS)	$^6A_{1g}$ (HS)
Co	$[Ar]3d^6$	$t_{2g}^6e_g^0$ (LS)	$t_{2g}^4e_g^2$ (HS)	^5D	$^1A_{1g}$ (LS)	$^5T_{2g}$ (HS)

Table 6.1. Electronic configuration of the M(III) used in this work. O_h: octahedral symmetry; CN: coordination number; LS: low spin; HS: high spin.

Another implication of their electronic configurations is that in the majority of cases NMR spectroscopy cannot be used to investigate solution speciation, since these metals have unpaired electrons and, hence, are paramagnetic (apart from the low spin d^6 Co(III)). Instead, UV-vis spectroscopy will give some insight into these systems. In this Chapter the synthesis and

characterisation of the distorted octahedral complexes of the type $[MF_3(L)]$ (M = Cr^{3+}, Mn^{3+}, Fe^{3+}, Co^{3+}; L = terpy, Me_3-tacn) are described, along with an assessment of their stability in water to the presence of competitive anions, increased temperature and changes in pH by means of UV-vis spectroscopy. The stability tests were performed on the Me_3-tacn complexes, as they are usually more stable than terpy complexes, thanks to the macrocyclic effect and the ^{18}F-radiolabelling experiments will be performed in the future on the related $BnMe_2$-tacn complexes; nonetheless, stability tests were also performed on $[CrF_3(terpy)]$ for comparison. Moreover, while the syntheses of the complexes are performed by direct reaction of the hydrates, $FeF_3{\cdot}4H_2O$ and $CoF_2{\cdot}4H_2O$, or anhydrous MnF_3 and $[CrF_3(py)_3]$ with the appropriate ligand, Cl/F halide exchange reactions on $[MCl_3(Me_3\text{-tacn})]$ (M = Cr, Fe) are explored using (non-radioactive) $[Me_4N]F$ to evaluate the possibility of ^{18}F-radiolabelling through Cl/^{18}F substitution. The synthesis of the known $[CrF_3(L)]$, $[MnF_3(terpy)]$ and $[FeF_3(Me_3\text{-tacn})]$, as well as the novel $[MnF_3(Me_3\text{-tacn})]$, $[FeF_3(terpy)]$ and $[CoF_3(L)]$ (L = terpy, Me_3-tacn) are reported.

These metals have been extensively studied for decades, so the coordination chemistry of the metal fluorides towards neutral N-donor ligands will be discussed only briefly in this introduction. A comprehensive review on the coordination chemistry of fluoride complexes (including these transition metal fluorides) has been published recently.[2]

6.1.1 Chromium(III)

The thermodynamic stability of the d^3 electronic configuration in a octahedral geometry, makes Cr(III) complexes almost exclusively six-coordinate. Thanks to the favourable energetic properties and the kinetic inertness associated, these complexes, in particular with ammonia and diamines as ligands, were the basis upon which the coordination chemistry and inorganic electronic spectroscopy were developed in the early days.[3,2] Apart from several hydrated species of Cr(III) fluoride,[4] complexes of CrF_3 with neutral O-donor ligands are scarce. The majority of the complexes reported are based on mono-, bi-, tri- and tetra-dentate N-donor ligands. The synthesis and detailed studies of the absorption and emission spectra of the chromium halide complexes with ligands such as 1,2-diaminoethane, 1,3-diaminopropane and 1,2-diaminocyclohexane, have been reported.[5,6,7,8,9,10,11] In these studies, the complexes were obtained as cationic or anionic species by direct reaction of $CrF_3{\cdot}3.5H_2O$ with the ligand, by halide exchange reactions from the bromide or chloride complexes, or by reaction of the trichloride hydrate in HF solution with the ligand.[12] The crystal structures of the chromium fluoride complexes with py,[13,14,15] 2,2'-bipy,[16,17] 1,10-phen[18] have also been reported, as well as *fac*-$[CrF_3(Me_3\text{-tacn})]$,[13] *fac*-$[CrF_3(tacn)]$[19] and *mer*-$[CrF_3(terpy)]$[13] (Figure 6.1).

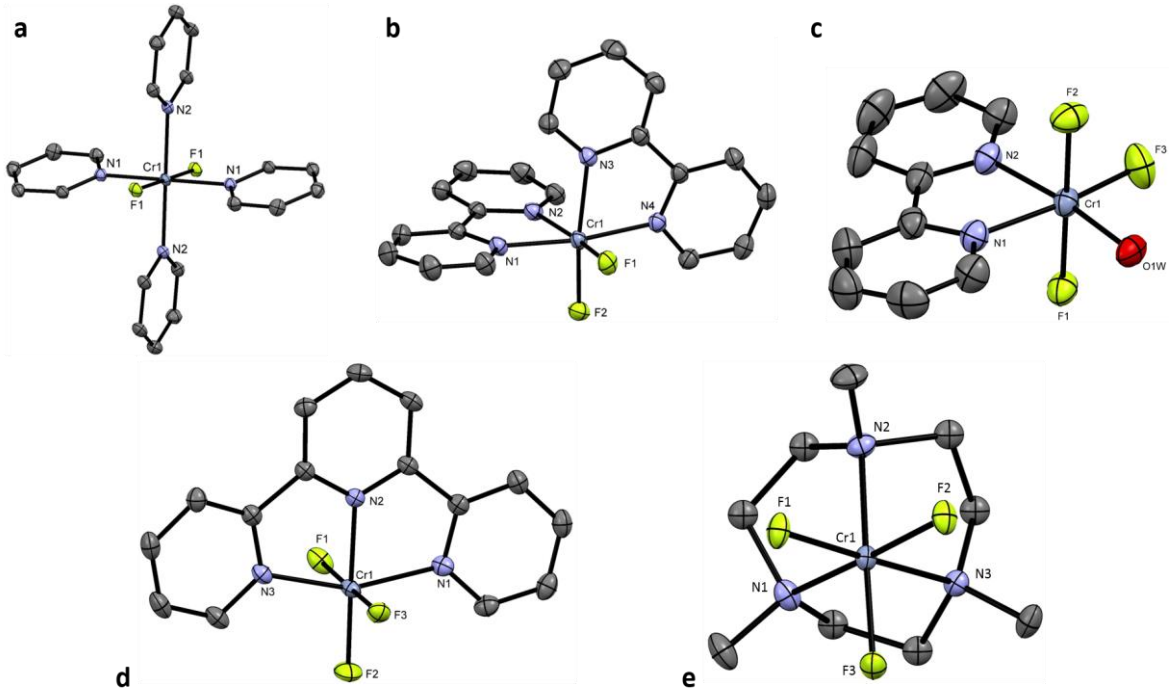

Figure 6.1. Crystal structure of the $[CrF_2(py)_4]^+$ (a) and $[CrF_2(bipy)_2]^+$ (b) cations, and the neutral $[CrF_3(bipy)(OH_2)]$ (c), $[CrF_3(terpy)]$ (d) and $[CrF_3(Me_3\text{-}tacn)]$ (e) (all of which crystallise as hydrates). Ellipsoids are drawn at 50 % probability level and H atoms, ClO_4^- and water molecules in the lattice are omitted. Images redrawn from CCDC numbers 963439,[15] 636269,[16] 669357,[17] 767059[13] and 961243.[20]

Interestingly, the species $[CrF_3(Me_3\text{-}tacn)]$, $[CrF_3(terpy)]$ and $[CrF_2(py)_4]^+$ act as metallo-ligands towards alkali metal salts producing hypsochromic shifts in the visible spectra. This effect depends not only on the presence of the cation, but also on the solvent in which the experiment is carried out (solvatochromism is often seen in chromium(III) fluoride complexes).[13] The ability to act as metallo-ligands toward alkali metals was also observed with the Group 13 metal fluoride species, $[GaF_3(BnMe_2\text{-}tacn)]$.[21] Chromium and gadolinium heterobimetallic species, in which fluoride anions bridge the two metals, have been reported in studies focusing on the magnetic properties of these compounds (e.g. single molecule magnets).[20,22,23]

Complexes of Cr(III) fluoride with tetradentate acyclic and macrocyclic N_4-donor ligands have also been reported.[24,25] They usually have one or two fluorides coordinated to the metal and, therefore, they are bi- or mono-cationic, respectively (Figure 6.2). These complexes were prepared by reacting $[CrF_2(py)_4][ClO_4]$ with the appropriate tetradentate ligand in 2-methoxyethanol. Their spectroscopic properties were analysed in detailed.[26,27]

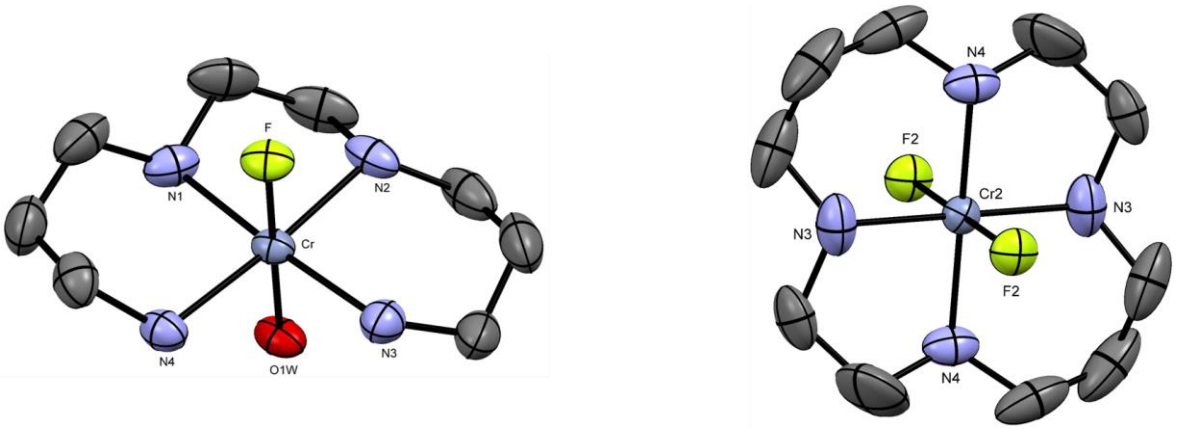

Figure 6.2. Crystal structure of [CrF(1,10-diamino-4,7-diazadecane)(OH_2)][ClO_4]$_2$·H_2O (left) and [CrF_2([14]aneN_4)][ClO_4]·H_2O (right). Ellipsoids are drawn at 50 % probability level. H atoms, ClO_4^- anions and lattice water molecules in the lattice are omitted for clarity. Images redrawn from CCDC numbers 702417[24] and 252076.[26]

As already mentioned, the stability of the Cr(III)-d^3 complexes has allowed for the electronic spectroscopic properties of these systems to be studied. In principle, all three spin-allowed *d-d* transitions can be observed but in practise this is only true when in the presence of a near ultra-violet transparent ligand.[3] The first allowed *d-d* transition ($^4T_{2g}\leftarrow{}^4A_{2g}$) in octahedral Cr(III) species gives a direct measure of the energy gap between the *d* orbitals (Δ_o)[13] and the lowest energy spin-forbidden transition ($^2E_{2g}\leftarrow{}^4A_{2g}$) is also often observed in the spectra.

6.1.2 Manganese(III)

Several octahedral manganese(III) fluoride complexes with neutral N-donor ligands are known. Reaction of MnF_3 in neat pyridine leads to [$MnF_3(py)_3$],[28] whereas reaction of [MnO(OH)] in aqueous HF in the presence of 2,2'-bipy or 1,10-phen forms the six-coordinate complexes, [MnF_3(2,2-bipy)(OH_2)] and [MnF_3(1,10-phen)(OH_2)], in which a water molecule completes the octahedral configuration (Figure 6.3).[29,30,31] In these complexes, the fluorides are arranged in a *meridional* configuration. The chloride analogues are also known.[31] The use of 4,4'-bipy produced a polymeric structure in which the ligand links the MnF_3 unit in a 2D chain and orthogonal Mn-F-Mn links the chains producing a 3D structure.[32]

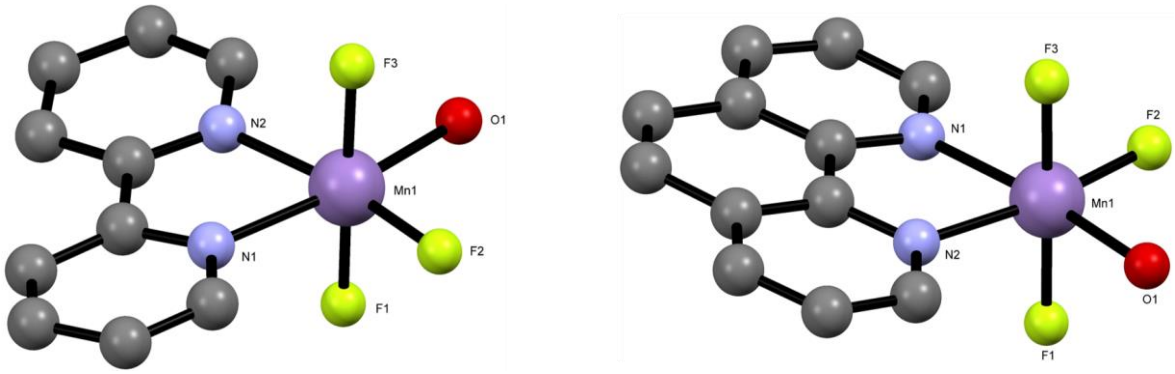

Figure 6.3. Crystal structure of $[MnF_3(2,2\text{-bipy})(OH_2)]\cdot H_2O$ (left) and $[MnF_3(phen)(OH_2)]\cdot H_2O$ (right). H atoms and lattice water molecules are omitted for clarity. Images redrawn from CCDC numbers 1224526[29] and 632138.[30]

The reaction of MnF_3 with terpy in methanol gives *mer*-$[MnF_3(terpy)]\cdot H_2O\cdot MeOH$. A single crystal X-ray analysis of the compound shows an elongation along the N2-Mn-N3 axis of the structure due to a Jahn-Teller distortion, characteristic of high spin Mn(III) (Figure 6.4).[33]

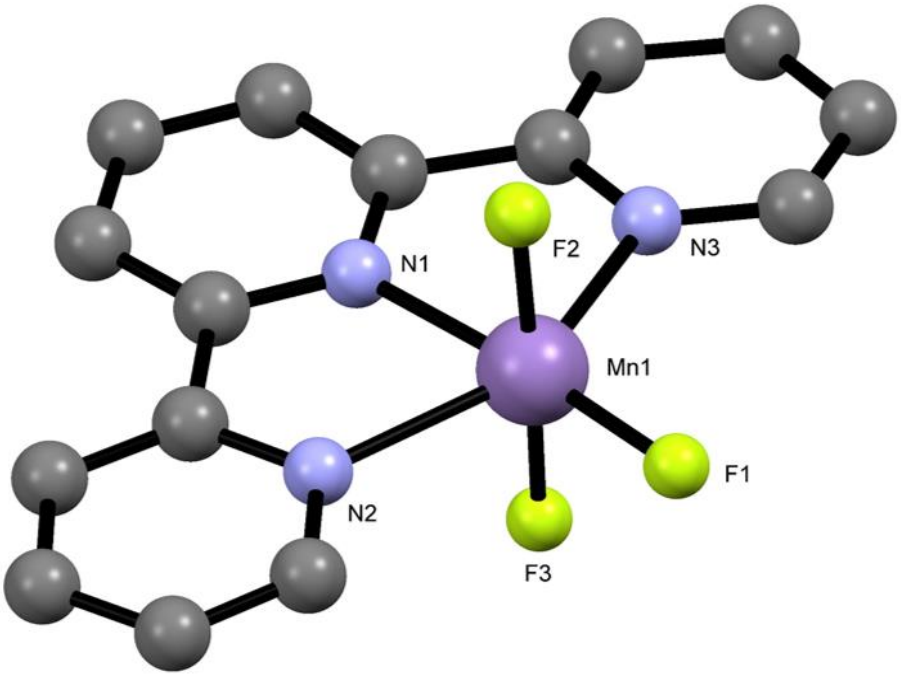

Figure 6.4. Crystal structure of $[MnF_3(terpy)\cdot H_2O\cdot MeOH$. Selected bond lengths (Å) and angles (°): Mn1-F1 = 1.8342(6), Mn1-F2 = 1.8137(7), Mn1-F3 = 1.8511(6), Mn1–N1 = 2.0952(8), Mn1–N2 = 2.2561(9), Mn1-N3 = 2.2370(9), F2-Mn1-F1 = 93.20(3), F2-Mn1-F3 = 175.34(3), F1-Mn1-N1 = 175.53(3), F2-Mn1-N3 = 90.27(3), N2-Mn1-N3 = 149.51(3), N1-Mn1-N3 = 74.87(3), N1-Mn1-N2 = 74.69(3). H atoms and solvent molecules in the lattice are omitted for clarity. Image redrawn from CCDC numbers 223613.[33]

The structures of the complexes $[MnF_3(bpea)]$[34] (bpea = N,N-bis(2-pyridylmethyl)ethylamine)) and the dinuclear $[\{MnF_2(Me_3\text{-tacn})\}_2(\mu\text{-F})][PF_6]$[35] (Figure 6.5) have been reported and their magnetic properties studied. The complexes were made by reaction of MnF_3 with the appropriate ligand in MeOH solution, with the addition of NH_4PF_6 in the Me_3-tacn system to form the dinuclear species.

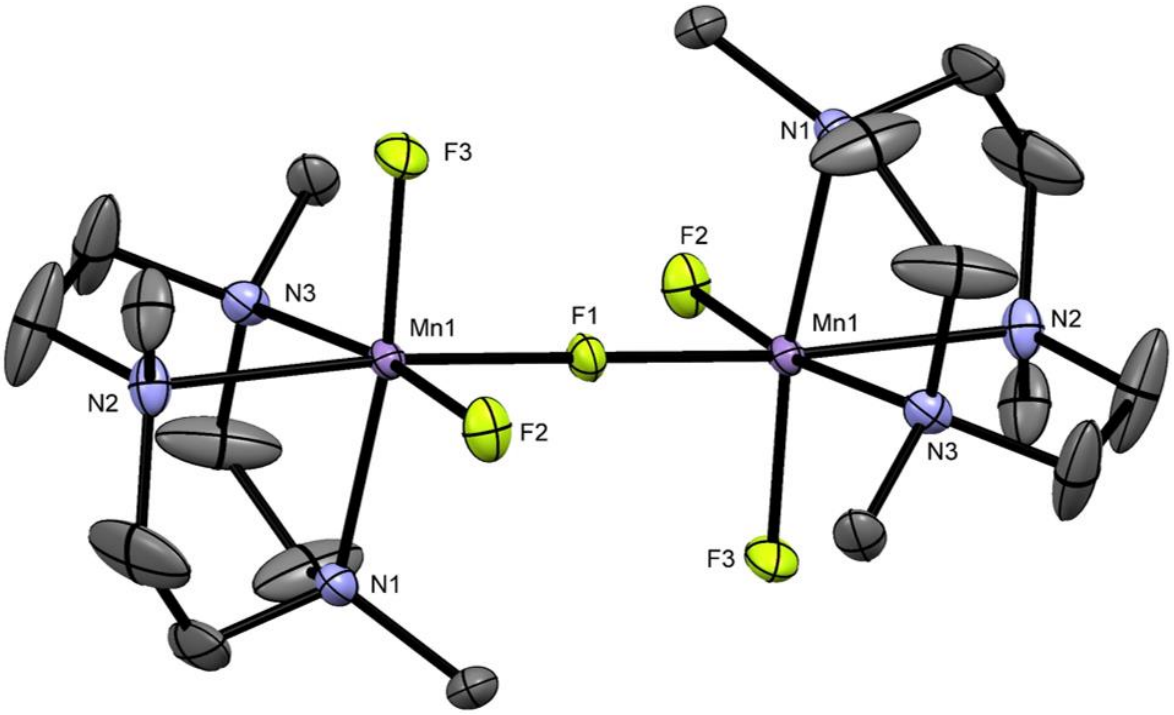

Figure 6.5. Crystal structure of [{$MnF_2(Me_3\text{-}tacn)\}_2(\mu\text{-}F)$][$PF_6$]. Ellipsoids are drawn at 50 % probability level. H atoms and PF_6^- anions are omitted for clarity. Images redrawn from CCDC number 986307.[35]

The crystal structures of several aquo-fluoromanganates(III) are described in the literature, including $[MnF_5(OH_2)]^{2-}$, $[MnF_4(OH_2)_2]^-$ and the dinuclear $[Mn_2(\mu\text{-}F)_2F_6(OH_2)]^{2-}$.[36,37,38]

An octahedral complex in a d^4 electron configuration can be either low or high spin. However, the majority of the Mn(III) complexes show a high spin configuration. The ground state for a high spin d^4 configuration is ^5E_g, whereas $^3T_{1g}$ is the ground state in the low spin case. Another interesting feature in a d^4 system is the possibility of Jahn-Teller distortions, with the removal of the degeneracy of the ground states to give a distorted octahedron.[3] Although these electronic transitions are often not resolved in UV-vis spectra, the Jahn-Teller effect is expected to be greater for a high spin system. The energy level diagram for a distorted octahedron with axial elongation is shown in Scheme 6.1.

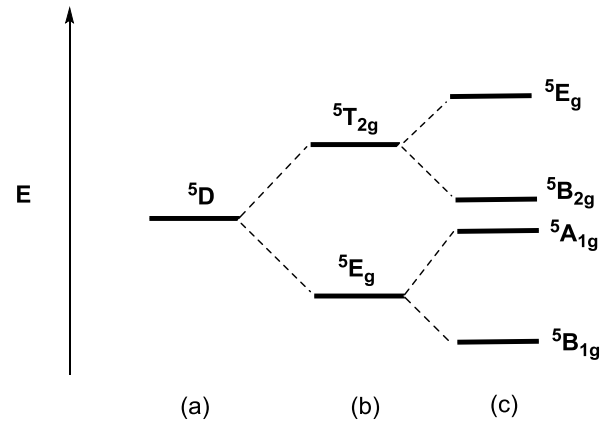

Scheme 6.1. Energy level diagram for a d^4 ion. (a) free ion; (b) octahedral splitting; (c) tetragonal elongation (along z axis) energy level splitting.

6.1.3 Iron(III)

Iron(III) fluoride complexes with neutral ligands are scarce. *Mer*-$[FeF_3(NH_3)_3]$[39] was obtained by reaction of $FeF_3{\cdot}3H_2O$ in liquid ammonia whilst the complexes of the type $[FeF(L_1)][PF_6]$ and $[FeF(L_2)][PF_6]$ were obtained from the chloride analogues using $AgPF_6$ or KPF_6 (Scheme 6.2).[40]

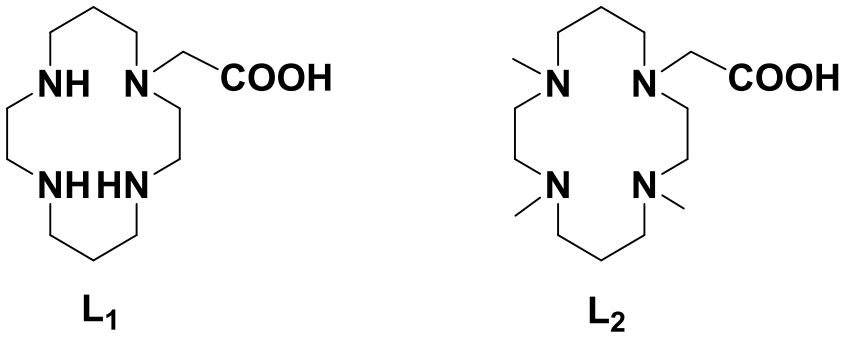

Scheme 6.2. N_4-macrocycles.

The complex with L_2 is high spin whereas the other one is low spin. The reaction of $FeF_3{\cdot}3H_2O$ with Me_3-tacn in boiling dmf produces the *facially* coordinated complex, $[FeF_3(Me_3\text{-tacn})]{\cdot}H_2O$ (Figure 6.6).[20]

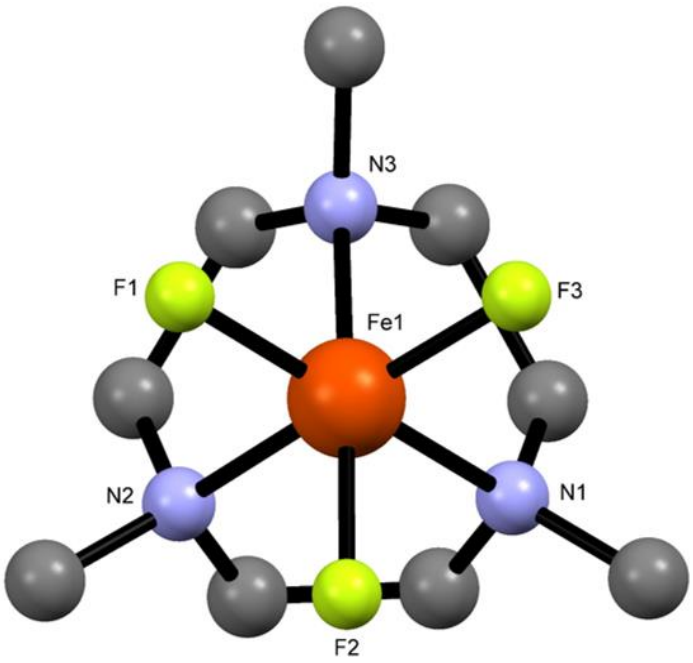

Figure 6.6. Crystal structure of $[FeF_3(Me_3\text{-tacn})]\cdot H_2O$. H atoms and the water molecule in the lattice are omitted for clarity. Images redrawn from CCDC number 961244.[20]

Complexes of iron(III) chloride with N-donor ligands are much more common than the trifluorides. The crystal structure of $[FeCl_3(L)]$ (L = terpy, Me_3-tacn, $(CN)_3$-tacn, tacn, Me_3-triazacyclohexane), $[FeCl_3(L)(OH_2)]$ (L = 2,2'-bipy, 1,10-phen) and $[FeCl_3(py)_3]$ have been reported.[41,42,43,44,45,46,47]

Examples of anionic fluoroferrate(III) complexes with aquo ligands are: $[FeF_5(OH_2)]^{2-}$ and $[Fe_2F_8(OH_2)_2]^{2-}$.[48,49]

Complexes of transition metals in a d^5 high spin configuration have a $^6A_{1g}$ ground state and the absence of any other spin sextet term makes all the *d-d* transitions spin-forbidden. As a result, the electronic spectra of Fe(III) in high spin complexes are generally very weak. Moreover, the oxidising Fe(III) can lead to ligand to metal charge transfer transitions that obscure the already low intensity d-d transitions.[3] The spin-forbidden transitions which can be observed are: $^4T_{2g} \leftarrow {}^6A_{1g}$ and $^4T_{1g} \leftarrow {}^6A_{1g}$. Low spin Fe(III) complexes are uncommon and would not be expected with fluoride co-ligands.

6.1.4 Cobalt(III)

The low spin d^6 configuration of Co(III) in an octahedral ligand field results in stable and diamagnetic complexes and its coordination chemistry, in particular with a range of amine ligands, has long been known.[50] However, these are usually less stable compared to the Cr(III) analogues. Some recently reported examples of Co(III) fluoride complexes with N-donor ligands include, *mer*-$[CoF_3(NH_3)_3]$,[51] *trans*-$[CoF_2(py)_4][ClO_4]$[52] and *cis*-$[CoF_2\{N(CH_2CH_2CH_2NH_2)_3\}]^+$.[53] No crystal structures of Co(III) trifluoride complexes with neutral N- or O-donor ligands have been reported.

In a similar way to the Cr(III) d^3 systems reported above, the kinetically inert low spin d^6 configuration in an octahedral ligand field has allowed for extensive study of the electronic properties of these systems. Although d^6 high spin species are known, they are almost exclusively found in Fe(II) systems.[3] Co(III) complexes adopt the low spin d^6 configuration in almost all cases. For these, the low spin octahedral ground state molecular term is $^1A_{1g}$ and there are two spin-allowed electronic transitions to $^1T_{1g}$ and $^1T_{2g}$.

6.2 Results and discussion

The complexes [MF_3(L)] (M = Cr, Mn, Fe, Co; R = terpy, Me_3-tacn) were prepared in alcoholic (butanol or methanol) or dmf solutions at room temperature or under reflux using modified literature methods (except for the Co(III) complexes, which are new, see experimental section) (Scheme 6.3). The complexes were characterised by IR spectroscopy, microanalysis and UV-vis spectroscopy and were generally the same colour as those reported in the literature (with a few exceptions, for example, the reported colour of [FeF_3(Me_3-tacn)] is green,[20] however in this work the complex was obtained as a pale yellow powder). Although some of the syntheses were carried out in anhydrous conditions (as some of the starting materials are oxygen/moisture sensitive), all of the products are air stable and can be stored outside a glovebox for several months. [CrF_3(Me_3-tacn)] and [FeF_3(Me_3-tacn)] were also obtained by halide exchange reactions in anhydrous MeCN solution from the chloride analogues.

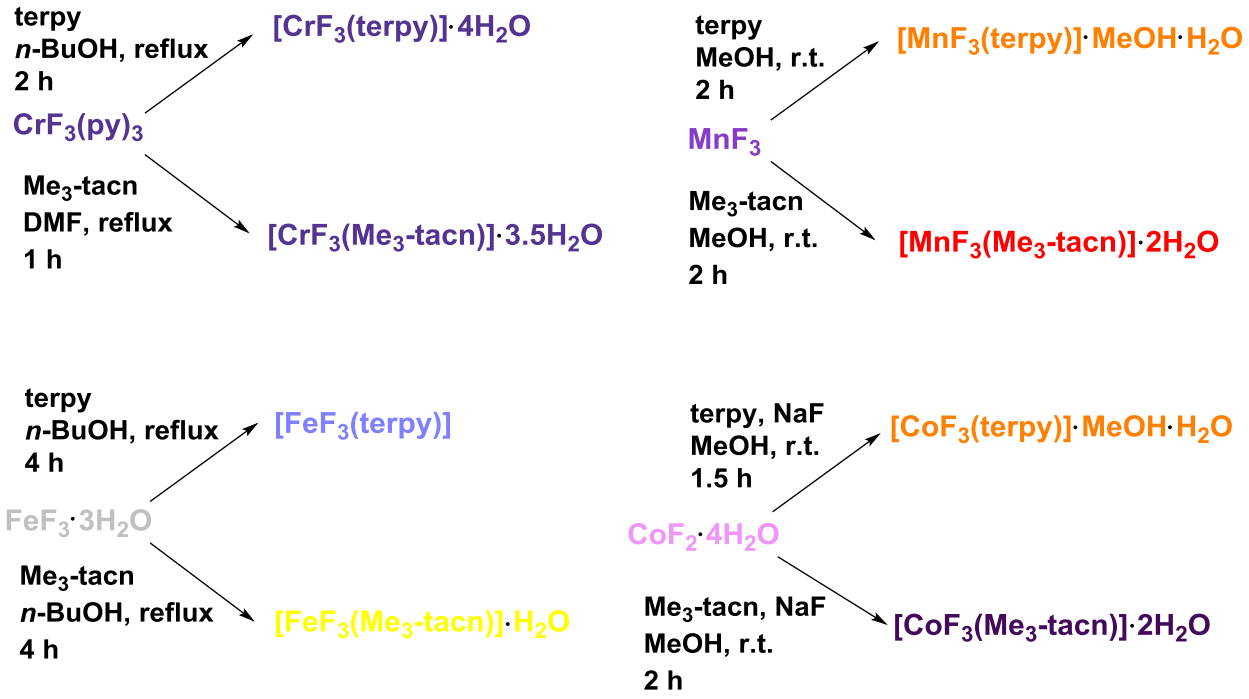

Scheme 6.3. Synthesis of the complexes [MF_3(L)] (M = Cr, Mn, Fe, Co; L = terpy, Me_3-tacn).

6.2.1 [CrF_3(L)] (L = terpy, Me_3-tacn)

Mer-[CrF_3(terpy)]·$4H_2O$ and *fac*-[CrF_3(Me_3-tacn)]·$3.5H_2O$ were obtained as purple solids in good yields by reaction of [$CrF_3(py)_3$] with the ligands in *n*-BuOH or dmf respectively, following the methods reported in the literature.[13] The complexes were characterised by IR, microanalysis and UV-vis spectroscopy in the solid state and in solution. The difference in the degree of hydration with lattice water, between [CrF_3(terpy)]·$4H_2O$ and the [CrF_3(terpy)]·$2.5H_2O$ reported in the literature, is not uncommon for MF_3-complexes, whose three fluorides are often involved in H-

bonding and the degree of interaction with water can vary for a given complex, depending upon the work-up and the drying conditions used. The IR spectra show peaks for water, and for the Cr-F groups one very broad band is seen for $[CrF_3(terpy)]\cdot 4H_2O$ (three bands are expected, but not resolved) and two bands for $[CrF_3(Me_3\text{-tacn})]\cdot 3.5H_2O$, as expected for a *facial* octahedral configuration in C_{3v} symmetry. The diffuse reflectance and solution UV-vis spectra of *fac*-$[CrF_3(Me_3\text{-tacn})]\cdot 3.5H_2O$ and *mer*-$[CrF_3(terpy)]\cdot 4H_2O$ are shown in Figures 6.7 and 6.8.

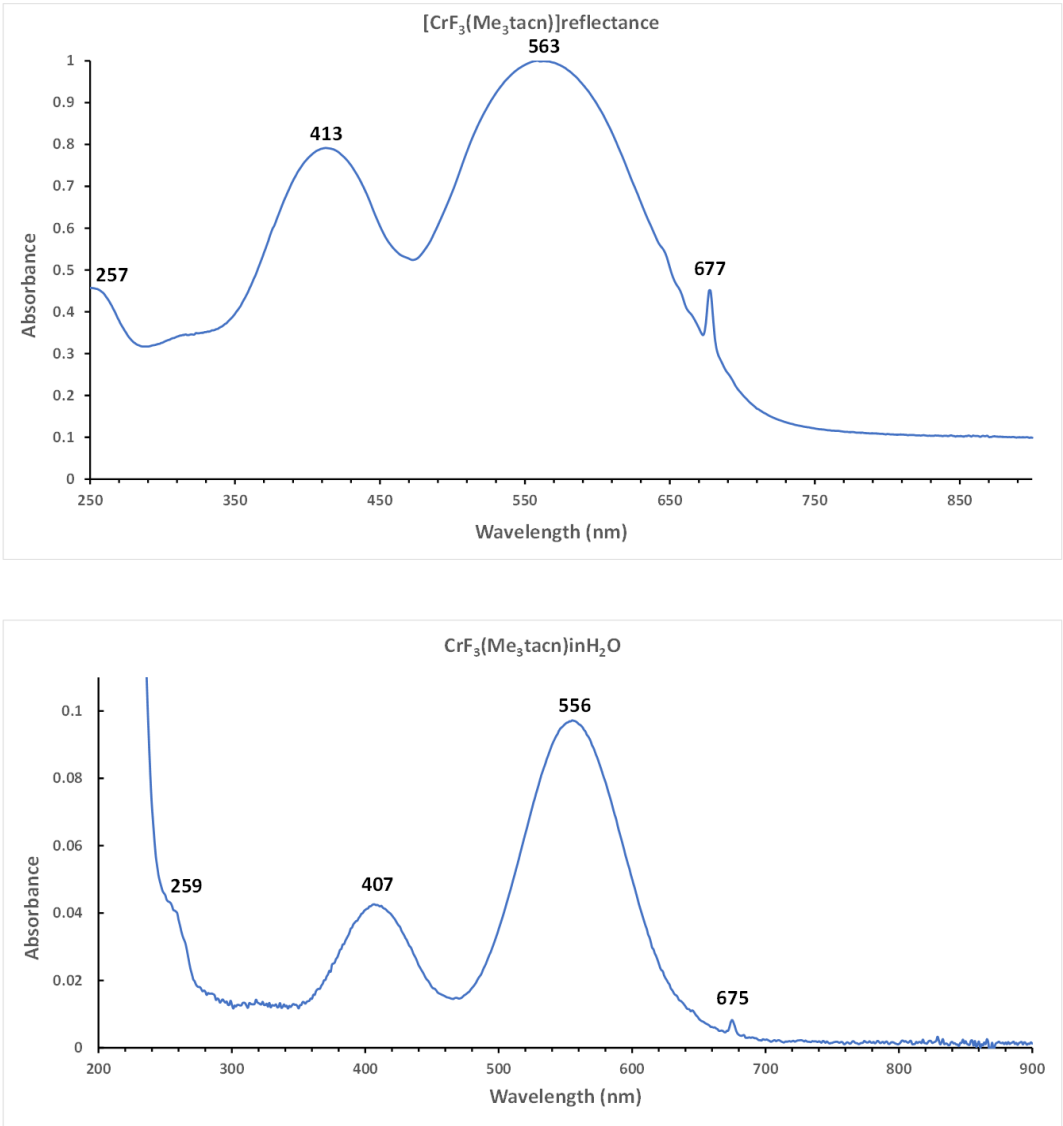

Figure 6.7. UV-vis spectra of $[CrF_3(Me_3\text{-tacn})]\cdot 3.5H_2O$. A: diffuse reflectance; B: 10^{-3} M in H_2O.

A

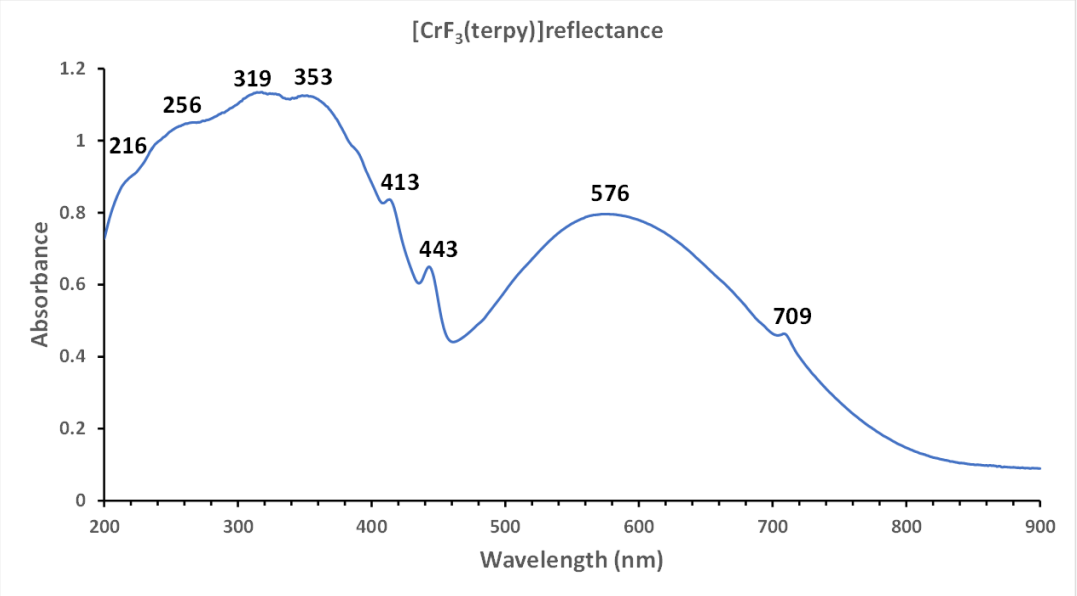

B

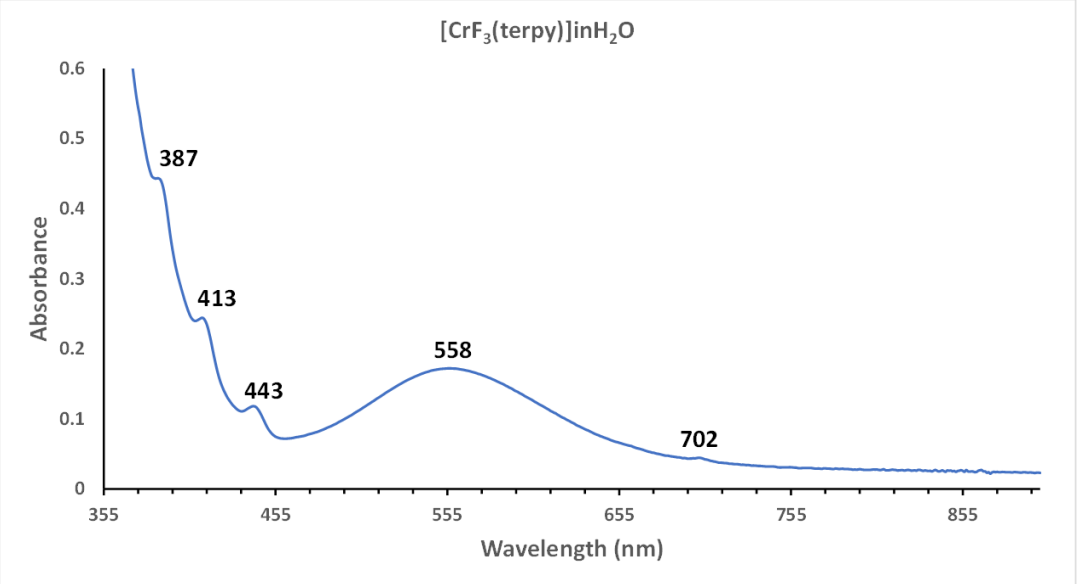

Figure 6.8. UV-vis spectra of $[CrF_3(terpy)]\cdot 4H_2O$. A: diffuse reflectance; B: 10^{-3} M in H_2O.

The UV-vis spectra of a 10^{-3} M solution of $[CrF_3(Me_3\text{-tacn})]\cdot 3.5H_2O$ in water and the diffuse reflectance spectra (Figure 6.7) are very similar, showing two main bands at ~ 17800 and ~ 24400 cm^{-1} (~ 560 and 410 nm), which correspond to the spin-allowed electronic transitions $^4T_{2g} \leftarrow {}^4A_{2g}$ and $^4T_{1g} \leftarrow {}^4A_{2g}$ respectively (note that although the symmetry in the metal complexes is lower than O_h, resolved splittings were not resolved, hence local O_h symmetry is assumed for the analysis). The first transition is also a measure of $10D_q$ for the complex. In addition, the spectra show a weaker band at ~ 39800 cm^{-1} (~ 250 nm) which corresponds to the third spin-allowed transition in a d^3 system ($^4T_{1g} \leftarrow {}^4A_{2g}$) and a sharp and very weak band at ~ 14800 cm^{-1} (~ 675 nm) due to the spin-forbidden transitions $^2E_g, {}^2T_{1g} \leftarrow {}^4T_{2g}$.

Likewise, the solution and diffuse reflectance spectra for $[CrF_3(terpy)]\cdot 4H_2O$ are also very similar (Figure 6.8). The strong bands at high energies present in both spectra are due to ligand to metal

charge transfer transitions, σN→Cr and π-π* transitions due to the aromatic rings in terpy (these transitions are beyond the solvent cut-off in the solution spectra). The band at ~ 17500 cm^{-1} (~ 570 nm) can be identified as the $^4T_{2g}\leftarrow{}^4A_{2g}$ transitions and corresponds to $10D_q$. The spin-forbidden transitions $^2E_g,{}^2T_{1g}\leftarrow{}^4T_{2g}$ are also visible in the spectra at ~ 14200 cm^{-1} (~ 705 nm). The data are in good agreement with the literature and with similar systems.[13,3]

6.2.1.1 Stability tests

The stability of both complexes was challenged in the presence of competitive anions (Cl^-, F^-, CO_3^{2-}, PO_4^{3-}, $MeCO_2^-$ in a 1:1 complex:anion ratio), pH range, elevated temperature (10^{-3} M solution of the complex were heated to 80 °C for 2 hours) and time (a 10^{-3} M aqueous solution over one week). The stability was followed by UV-vis spectroscopy. The spectra of the experiments in the presence of competitive anions and pH (from pH 4 to pH 11) were acquired at t = 0 and again after 4 hours. In particular, changes in the position of the bands or appearance/disappearance of bands were taken as an indication of the instability of the complexes during the experiments. The results of the stability test on $[CrF_3(Me_3\text{-tacn})]\cdot 3.5H_2O$ are shown in Figure 6.9.

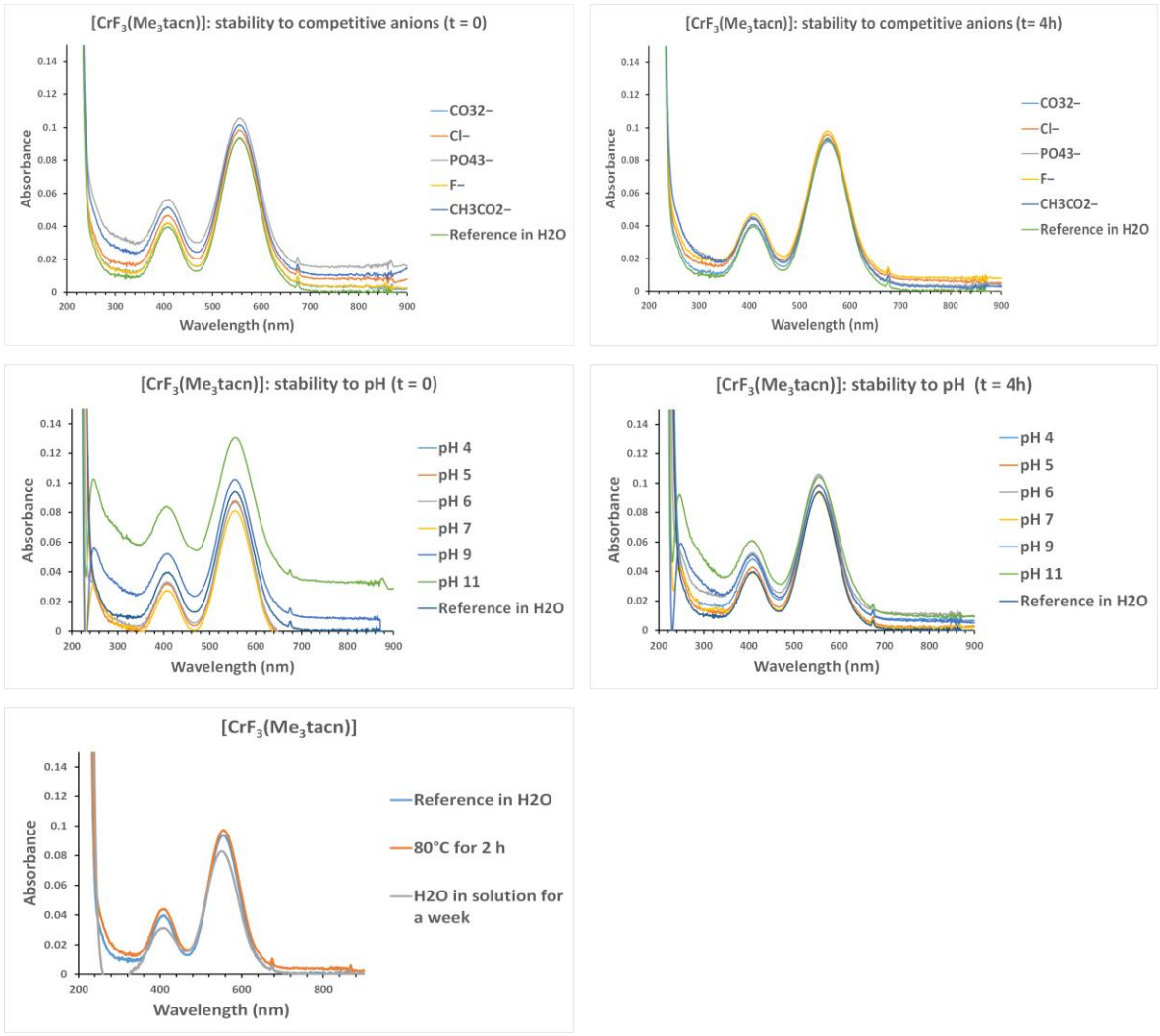

Figure 6.9. Stability tests on $[CrF_3(Me_3\text{-tacn})]\cdot 3.5H_2O$.

The spectra show that the complex is stable in all conditions with the position of the bands unchanged. The spectra of $[CrF_3(terpy)]\cdot 4H_2O$ (Figure 6.10) show slightly different behaviour.

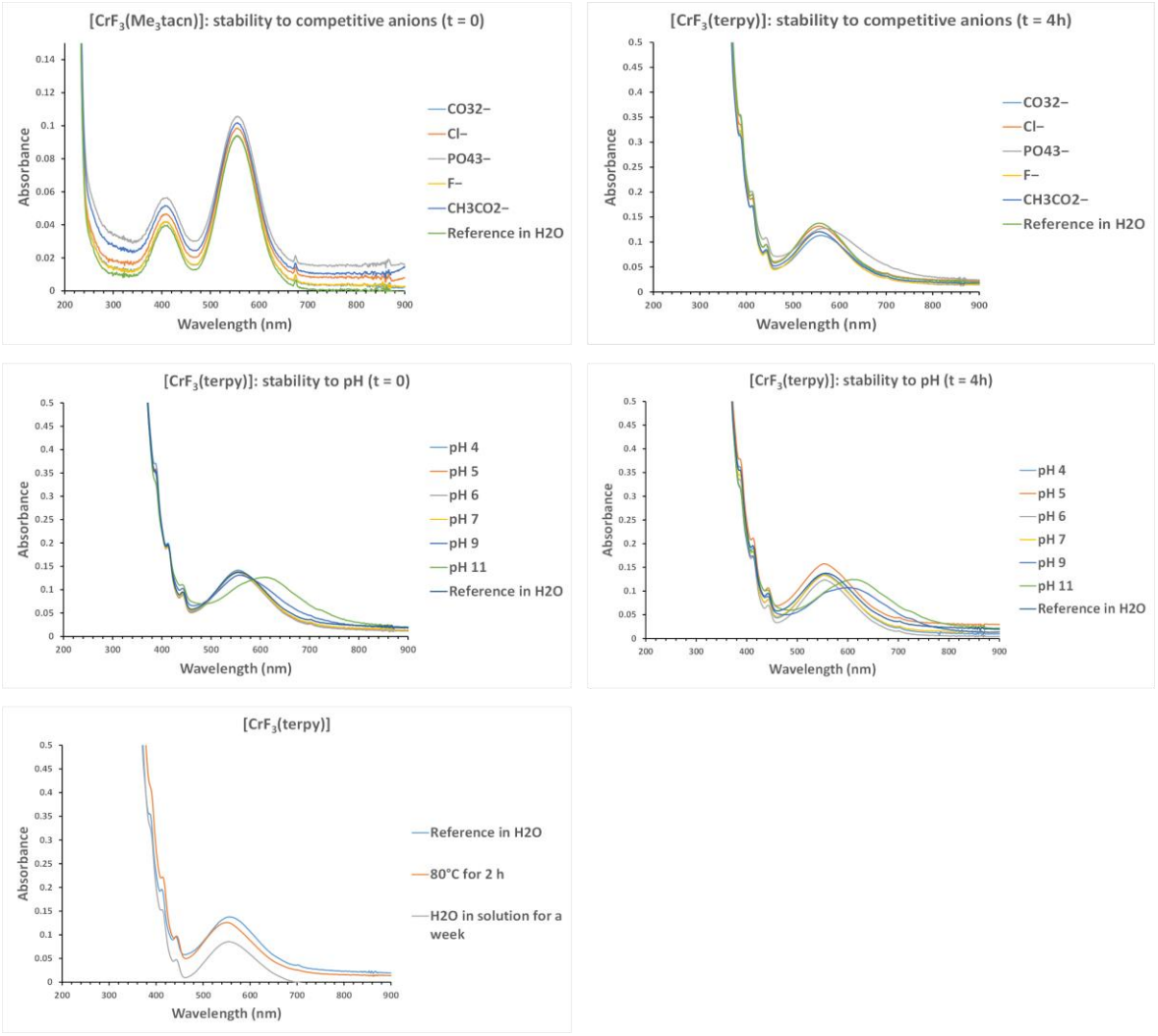

Figure 6.10. Stability tests on $[CrF_3(terpy)]\cdot 4H_2O$.

The spectra of the complex in the presence of competitive anions in the ratio 1:1 show that it is stable at t = 0. However, in the presence of PO_4^{3-} the spectra acquired after 4 hours show a small shift of the band at 558 nm (~ 10 nm) towards lower energy, indicating that the complex might be less stable in this condition. This solution had pH ~ 8/9 and considering that there is also a shift of the same band at pH 9 and 11 (spectra at t = 4 hours), the instability might be due to a pH affect rather than the presence of the PO_4^{3-} anions. The complex is stable up to pH 7, after heating at 80 °C for 2 hours and is unchanged after one week in aqueous solution.

6.2.1.2 Halide exchange reaction on $[CrCl_3(Me_3\text{-tacn})]$

Since the radioactive $[^{18}F]F^-$ can be incorporated into the Al(III) and Ga(III) complexes described in Chapters 2 and Chapter 3 through halide exchange reactions, this possibility was also explored for the Cr(III) analogue using the non-active $[^{19}F]F^-$. $[CrCl_3(Me_3\text{-tacn})]$ was treated with 4 mol. equiv. of $[Me_4N]F$ in refluxing MeCN solution and the mixture was reacted for 24 hours. The crude solid obtained was analysed by IR spectroscopy and compared with the IR spectra of $[CrCl_3(Me_3\text{-tacn})]$

and [CrF_3(Me_3-tacn)]. Figure 6.11 shows that the CrF_3-complex (ν(Cr-F) = 511 and 541 cm^{-1}) is formed during the reaction, but it appears that some $CrCl_3$-complex (ν(Cr-Cl) = 327 and 340 cm^{-1}) and/or mixed chloride/fluoride species are still present even after 24 hours under reflux. This is not surprising given the expected slow substitution kinetics in the d^3 systems.

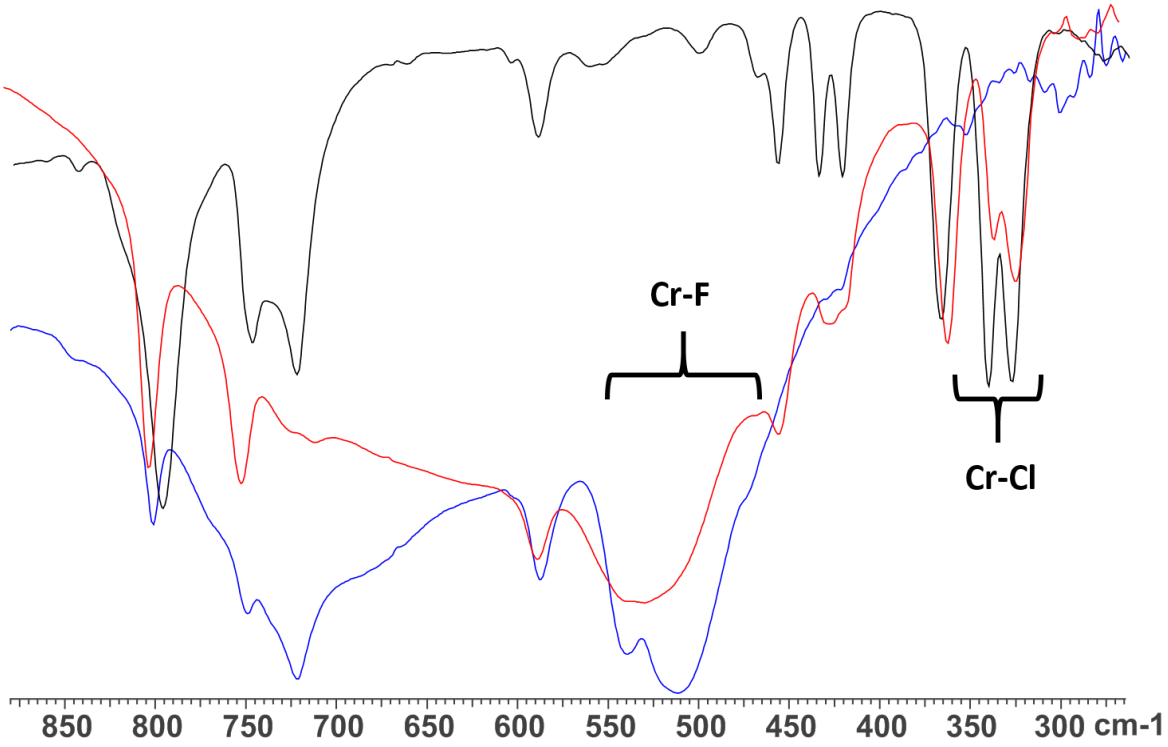

Figure 6.11. Comparison of the IR spectra of [$CrCl_3$(Me_3-tacn)] (black), [CrF_3(Me_3-tacn)] (blue) and crude of the halide exchange reaction [$CrCl_3$(Me_3-tacn)] + 4 [Me_4N]F (red).

6.2.2 [MnF_3(L)] (L = terpy, Me_3-tacn)

The reactions of MnF_3 with terpy or Me_3-tacn in MeOH solution at room temperature produce the species [MnF_3(terpy)]·MeOH·$3H_2O$ (orange solid) and [MnF_3(Me_3-tacn)]·$3H_2O$ (deep red solid). While the terpy complex has been reported previously,[33] [MnF_3(Me_3-tacn)]·$3H_2O$ has not, although the related dinuclear species, [{MnF_2(Me_3-tacn)}$_2$(μ-F)][PF_6], can be found in the literature.[35] The complexes were characterised by IR spectroscopy, microanalysis and UV-vis spectroscopy and the molecular composition of [MnF_3(Me_3-tacn)] was confirmed by a single crystal X-ray structure analysis (Figure 6.12). The presence of MeOH in [MnF_3(terpy)]·MeOH·$3H_2O$ was confirmed by ^{1}H NMR spectroscopy (δ = 3.28 (OH), 2.15 (CH_3OH)).

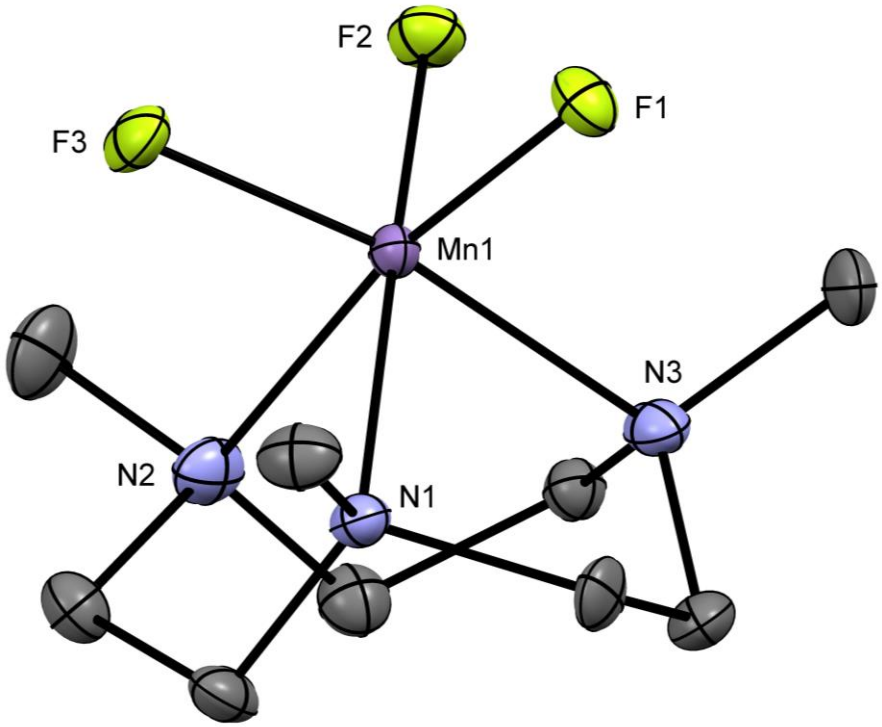

Figure 6.12. Crystal structure of $[MnF_3(Me_3\text{-tacn})]\cdot 4H_2O$ with ellipsoids drawn at the 50 % probability level. H atoms and water molecules are omitted for clarity. Select bond lengths (Å) and angles (°): Mn1–F1 = 2.017(2), Mn1–F2 = 1.852(2), Mn1–F3 = 1.848(2), Mn1–N1 = 2.080(3), Mn1–N2 = 2.267(3), Mn1–N3 = 2.096(3), F1–Mn1–N1 = 91.29(10), F3–Mn1–N3 = 170.31(11), F2–Mn1–N1 = 172.65(10), F1–Mn1–F3 = 94.88(9), F1–Mn1–F2 = 94.43(9), N1–Mn1–N2 = 80.92(11), N1-Mn1-N3 = 83.43(11).

The structure shows a distorted octahedral environment with the fluorides coordinated to the metal in *facial* configuration. The Mn-F3 and Mn-N3 bond lengths are elongated by ~ 0.17 Å and ~ 0.18 Å compared to the other Mn-F and Mn-N distances, respectively. This significant difference in the bond lengths is consistent with a Jahn-Teller distortion in the high spin d^4 configuration.[3] As confirmation of this, the complex has a magnetic moment of 4.94 BM consistent with the high spin configuration.[54] The tetragonal elongation in $[\{MnF_2(Me_3\text{-tacn})\}_2(\mu\text{-F})][PF_6]$ is observed along the axis on which Mn-$F_{bridging}$ and Mn-N trans to it lie. The distances of these bond lengths are ~ 0.18 and 0.23 Å longer than the other Mn-N and Mn-F bonds, respectively.[35] The Mn-$F_{terminal}$ distance in $[\{MnF_2(Me_3\text{-tacn})\}_2(\mu\text{-F})][PF_6]$ is ~ 0.03 Å shorter than Mn1-F1 and Mn1-F2 in $[MnF_3(Me_3\text{-tacn})]\cdot 2H_2O$. The carbon atoms in the ring were disordered and were modelled with the split occupancy factors, accordingly. Extensive H-bonding involving the water molecules and the fluorides is also present (Figure 6.13). The same H-bonding pattern was observed in $[GaF_3(Me_3\text{-tacn})]\cdot H_2O$.[55]

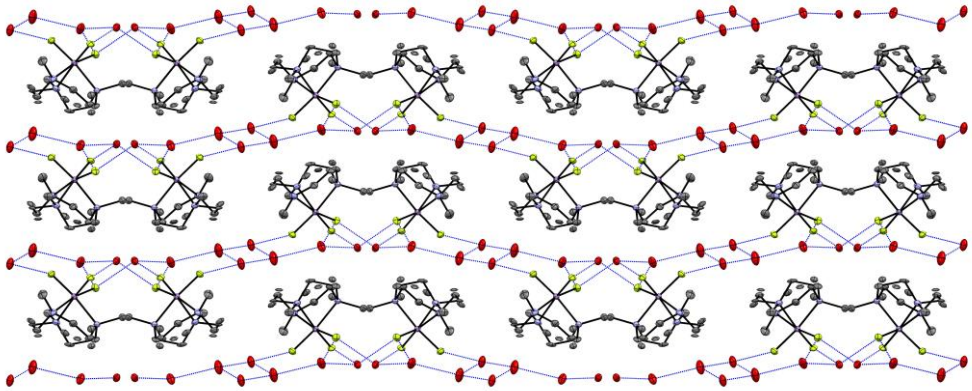

Figure 6.13. H-bonding interaction present in $[MnF_3(Me_3\text{-tacn})]\cdot 4H_2O$ (blue dots).

The UV-vis diffuse reflectance and solution (10^{-3} M concentration of the complex in MeCN) spectra are shown in Figure 6.14 and Figure 6.15.

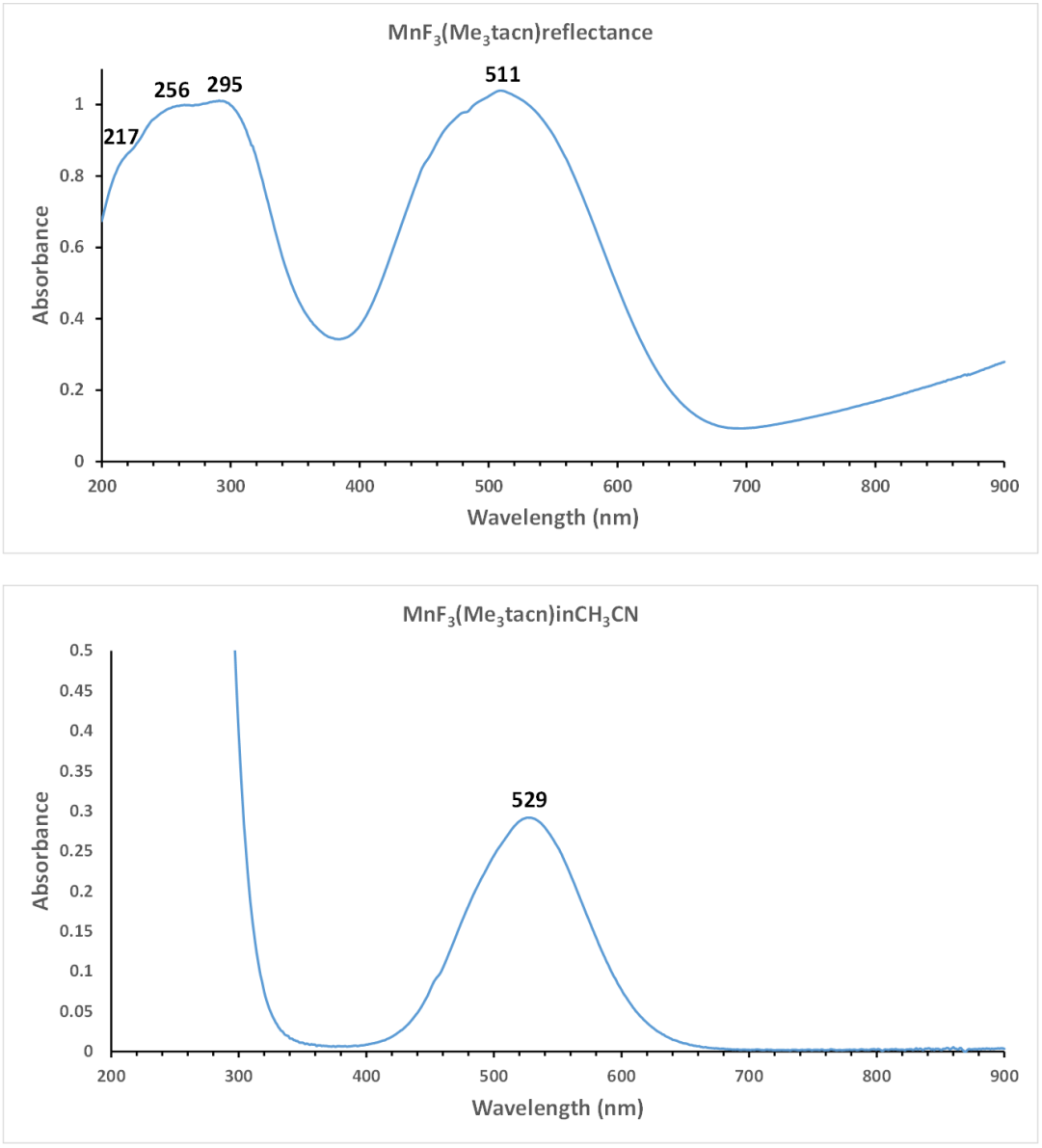

Figure 6.14. UV-vis spectra of $[MnF_3(Me_3\text{-tacn})]\cdot 2H_2O$. A: diffuse reflectance; B: 10^{-3} M in MeCN.

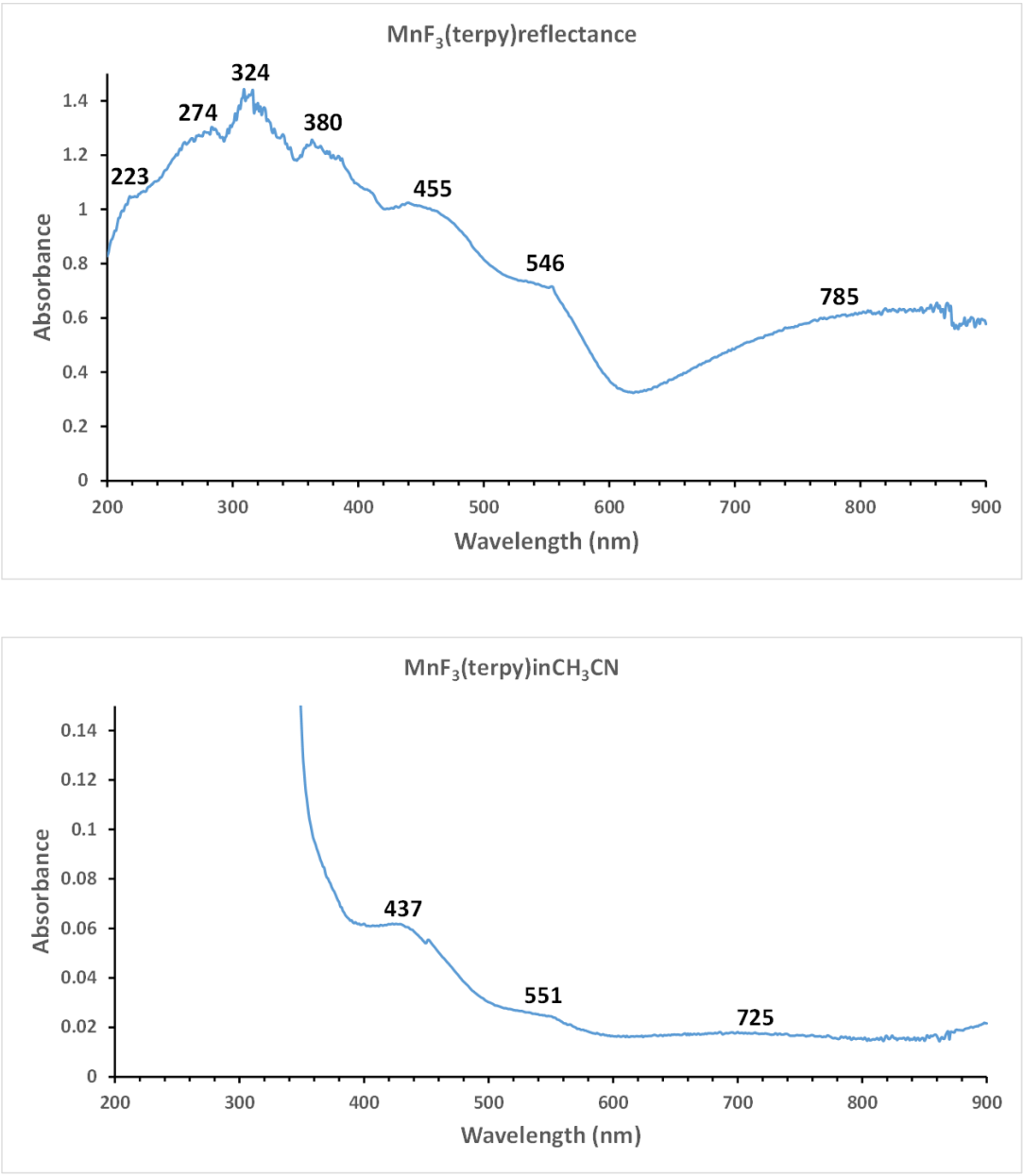

Figure 6.15. UV-vis spectra of $[MnF_3(terpy)]\cdot MeOH\cdot 3H_2O$. A: diffuse reflectance; B: 10^{-3} M in MeCN.

The ground state in an octahedral d^4 high spin configuration is ^5E_g and only one spin-allowed transition is predicted: $^5T_{2g}\leftarrow{}^5E_g$. However, since a high spin d^4 configuration is affected by Jahn-Teller distortion through elongation along the axial direction, the single transition is often split into multiple transitions: ^5E_g transforms into $^5B_{1g}$ and $^5A_{1g}$, and $^5T_{2g}$ transforms into $^5B_{2g}$ and ^5E_g (Scheme 6.1).[3] Strictly, the coordination geometry gives C_{3v} symmetry, which could also result in splitting of the bands. The $[MnF_3(Me_3\text{-tacn})]\cdot 2H_2O$ spectra of the solid and solution (Figure 6.14) show intense bands in the ultraviolet region due to ligand to metal charge transfer transitions, and one single d-d transition at ~ 19230 cm^{-1} (~ 520 nm) generically assigned to $^5T_{2g}\leftarrow{}^5E_g$ since splitting is not resolved. The data resemble those of the related dimer $[\{MnF_2(Me_3\text{-tacn})\}_2(\mu\text{-}F)][PF_6]$.[35]

The UV-vis spectra of the lower symmetry complex, $[MnF_3(terpy)]\cdot MeOH\cdot 3H_2O$ (Figure 6.15), again show strong absorptions at high energy due to the ligand to metal charge transfer transitions, σN→Mn, and π-π* transitions. In addition, three separate bands at ~ 13000, 18200 and 22400 cm^{-1} (~ 770, 550 and 445 nm respectively) are present. These are tentatively assigned to the resolved transitions $^5A_{1g}\leftarrow{}^5B_{1g}$, $^5B_{2g}\leftarrow{}^5B_{1g}$, $^5E_g\leftarrow{}^5B_{1g}$ respectively. The $^5B_{2g}\leftarrow{}^5B_{1g}$ transition is also a measure of $10D_q$. The metal centre symmetry is C_{2v} and it is possible that both this and the Jahn-Teller effect result in greater splitting of the bands. The spectrum is similar to that of some other Mn(III) complexes.[3,35]

Since the $MnCl_3$-complexes are unstable and have a short shelf-life,[56] the halide exchange reaction to synthesise $[MnF_3(Me_3\text{-tacn})]$ was not pursued.

6.2.2.1 Stability tests

The stability of $[MnF_3(Me_3\text{-tacn})]\cdot 2H_2O$ was investigated under the same conditions as those described above for $[CrF_3(Me_3\text{-tacn})]\cdot 3.5H_2O$. The results are shown in Figure 6.16.

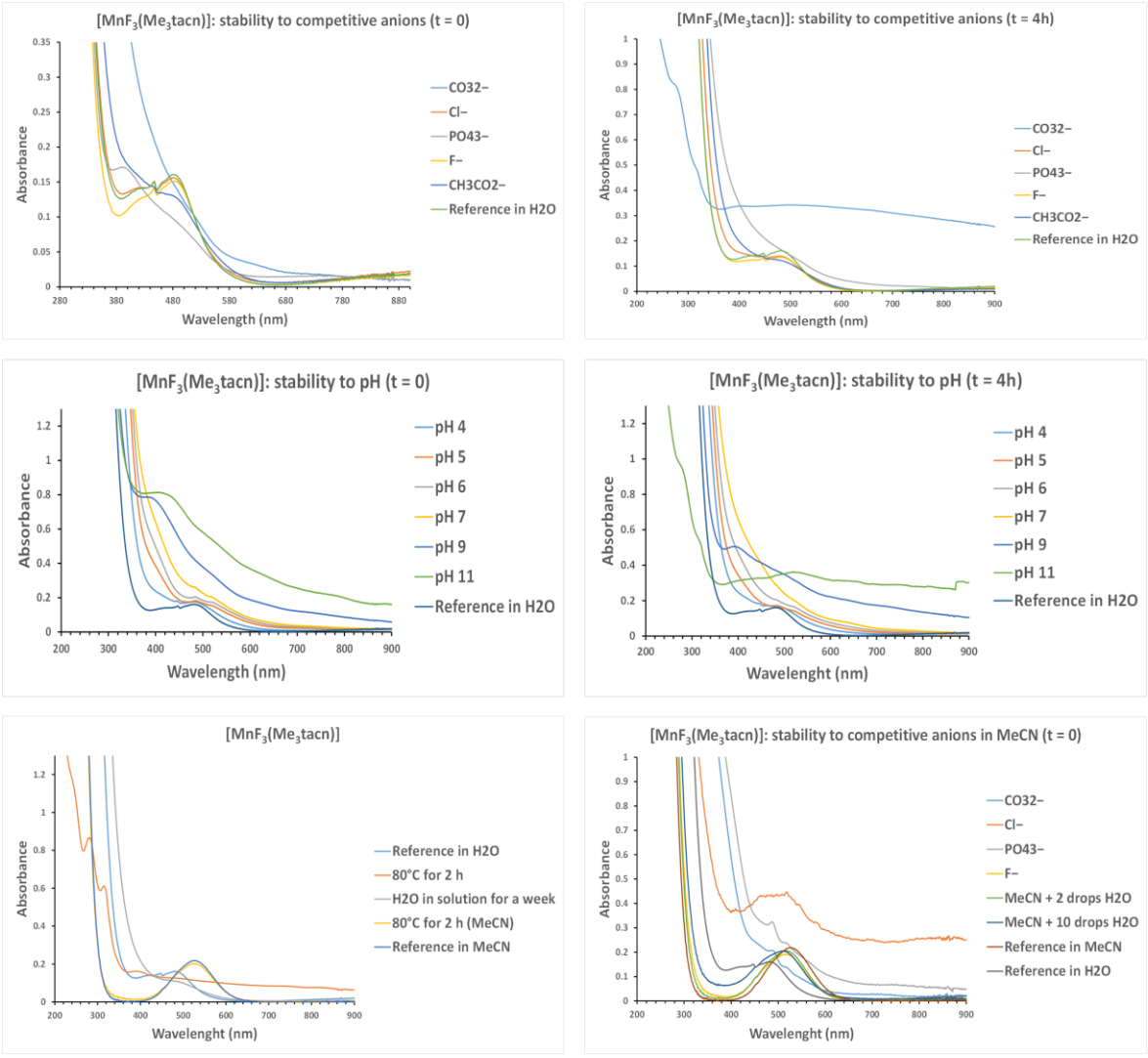

Figure 6.16. Stability tests on $[MnF_3(Me_3\text{-tacn})]\cdot 2H_2O$.

The UV-vis spectrum of a 10^{-3} M aqueous solution of $[MnF_3(Me_3\text{-tacn})]\cdot 2H_2O$ shows the main band shifted by 40 nm to higher energy compared to that in MeCN, possibly due to a solvatochromic effect (instability of the complex in water should not be excluded, see below). The stability of the Mn(III) complex is inferior to that of the Cr(III) analogue, as expected for a d^4 system. $[MnF_3(Me_3\text{-tacn})]\cdot 2H_2O$ is stable to the presence of chloride and fluoride but it is unstable to phosphate, carbonate and acetate at t = 0, with no significant further change observed after 4 hours (salts added in a 1:1 ratio with the complex). Moreover, pH > 4 causes decomposition of the complex, as is also observed upon heating (80 °C for 2 hours) and prolonged exposure in aqueous solution (1 week). Decomposition of the sample was clearly observable as a black solid precipitated (most likely MnO_2 or Mn_2O_3). The possibility that the complex is not stable in water (although the crystals for the single crystal X-ray analysis were grown in water) was considered and its stability to competitive anions (1:1 complex:anions ratio) was checked in MeCN solution (bottom right in Figure 6.16). The data show that the complex is stable to Cl^-, F^- and at pH 8 and that it is not stable to CO_3^{2-} and PO_4^{3-}, confirming the results in water. Since the salts employed are not soluble in MeCN they were

dissolved in 2-10 drops of water and added to the MeCN solution of the complex. Even the addition of two drops of water cause a small shift to higher energy of the main band.

Considering the extra stability conferred by the macrocyclic affect to the Me_3-tacn complexes compared to the terpy ones and the already problematic stability of $[MnF_3(Me_3\text{-tacn})]\cdot 2H_2O$, the stability tests on $[MnF_3(terpy)]\cdot MeOH\cdot 3H_2O$ were not carried out.

6.2.3 $[FeF_3(L)]$ (L = terpy, Me_3-tacn)

$[FeF_3(Me_3\text{-tacn})]\cdot H_2O$ was obtained as a pale yellow solid after reaction of $FeF_3\cdot 3H_2O$ with Me_3-tacn in refluxing butanol. This method differs from that reported in the literature.[20] The IR spectrum of the complex shows two ν(Fe-F) bands at 512 and 529 cm^{-1}, consistent with *facial* coordination of the three fluorides in C_{3v} symmetry. The product was shown to be analytically pure by microanalysis. $[FeF_3(terpy)]$, made using the same method, was obtained as a light purple powder and characterised similarly. The UV-vis spectra of the complexes are shown in Figure 6.17 and Figure 6.18.

A

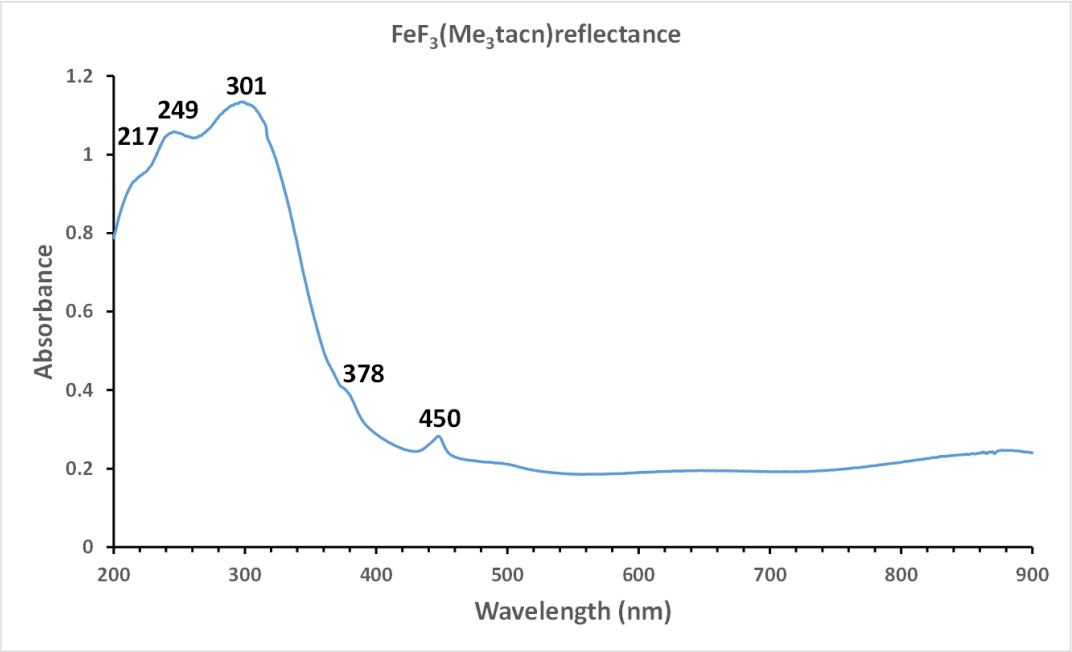

B

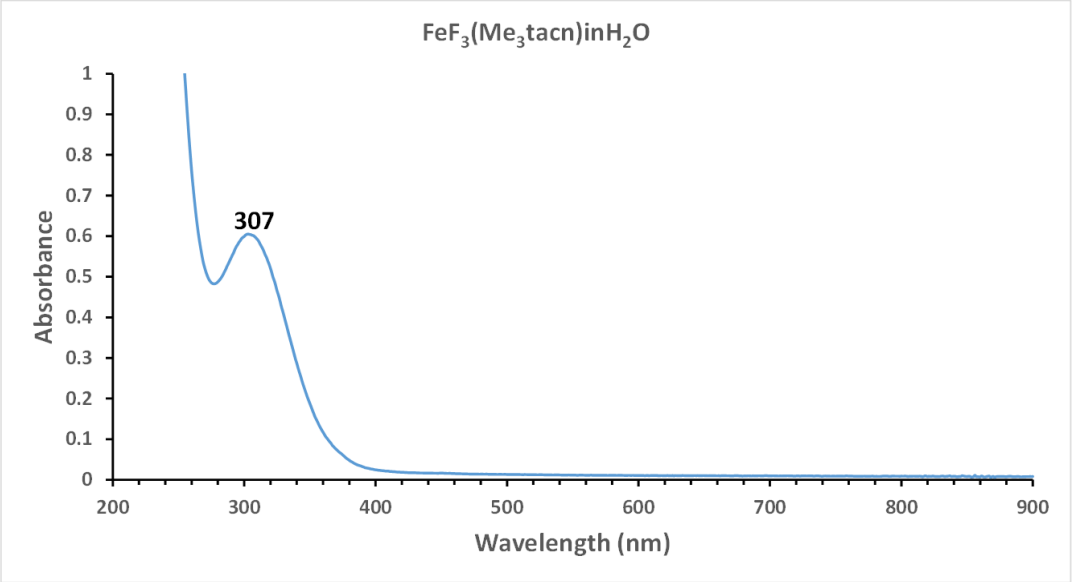

Figure 6.17. UV-vis spectra of [FeF_3(Me_3-tacn)]·H_2O. A: diffuse reflectance; B: 10^{-2} M in H_2O.

A

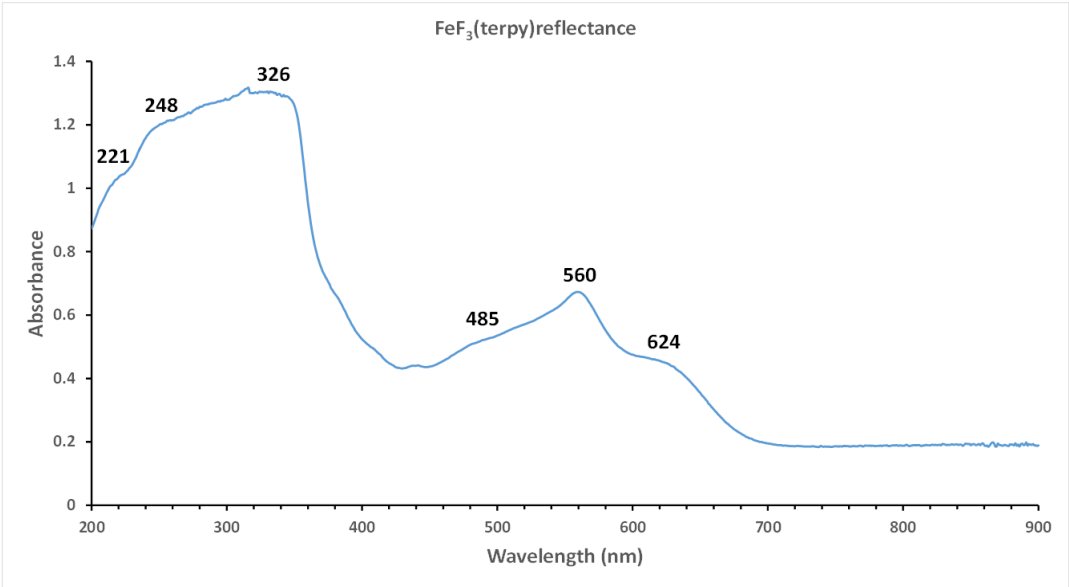

B

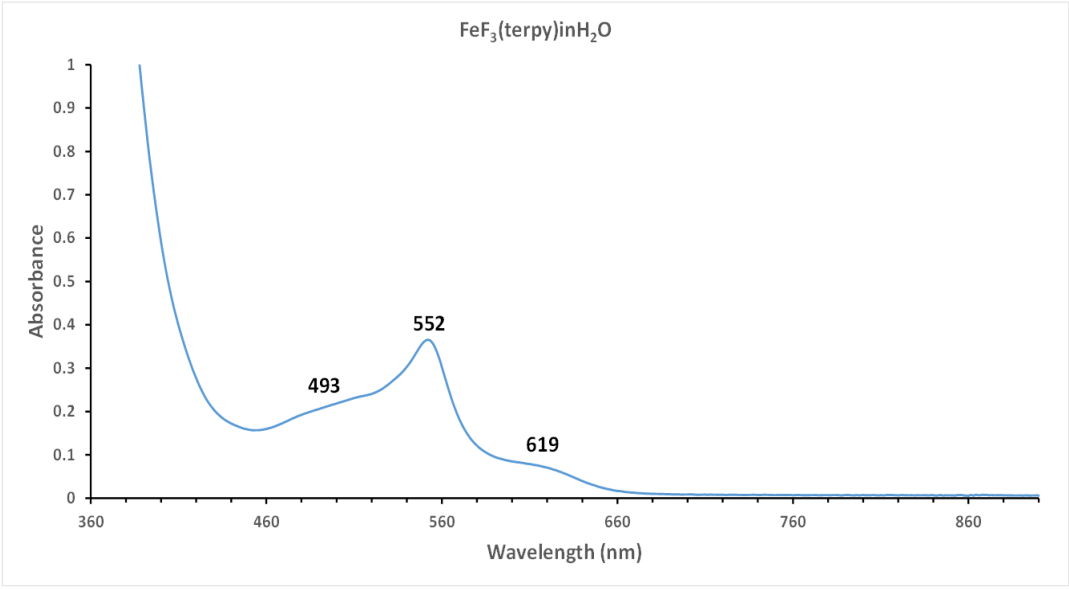

Figure 6.18. UV-vis spectra of [FeF_3(terpy)]. A: diffuse reflectance; B: 10^{-2} M in H_2O.

The electronic transitions in a d^5 high spin systems with a ground state $^6A_{1g}$ are all spin-forbidden and weak bands in the visible region are therefore expected. The UV-vis spectrum of [FeF_3(Me_3-tacn)]·H_2O shows the ligand to metal charge transfer transitions at energies above 33200 cm^{-1} (> 300 nm) and very weak bands at 22222 and 26455 cm^{-1} (450 and 378 nm) in the diffuse reflectance spectra, which can be assigned to the spin-forbidden transitions from $^6A_{1g}$ to spin quartet levels ($^4T_{1g}$, $^4T_{2g}$, $^4A_{1g}$, ^4E_g). These transitions are more resolved in the [FeF_3(terpy)] spectra and can be assigned by comparison with similar systems[3] as follow: $^4T_{1g}\leftarrow{}^6A_{1g}$ at ~ 16000 cm^{-1} (~ 625 nm), $^4T_{2g}\leftarrow{}^6A_{1g}$ at ~ 18000 cm^{-1} (~ 555 nm) and $^4A_{1g}$,$^4E_g\leftarrow{}^6A_{1g}$ at ~ 20500 cm^{-1} (~ 490 nm).

6.2.3.1 Stability tests

The stability of $[FeF_3(Me_3\text{-tacn})]\cdot H_2O$ was challenged in the same conditions as reported above with the difference that the anions were added in a 10-fold excess to the solution of the complex. The results are shown in Figure 6.19.

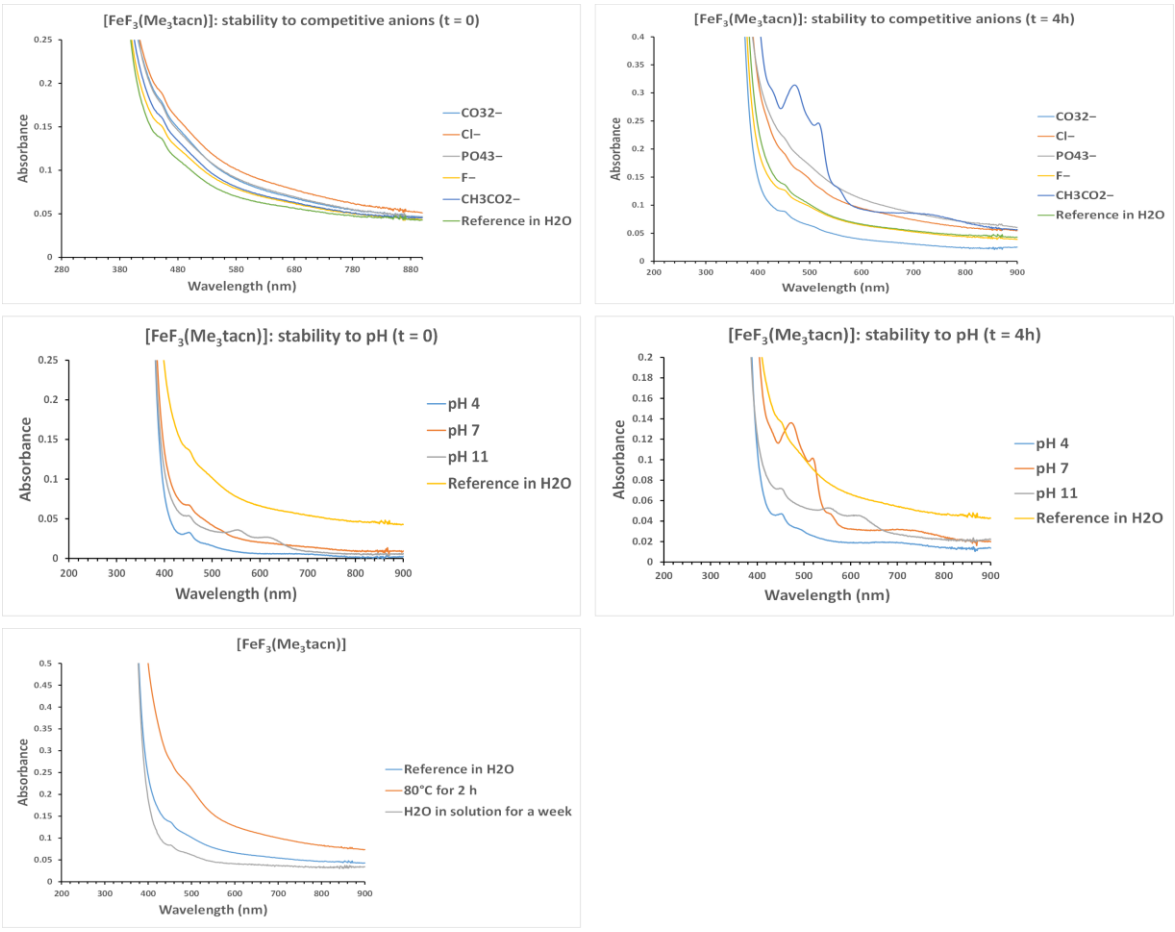

Figure 6.19. Stability tests on $[FeF_3(Me_3\text{-tacn})]\cdot H_2O$.

It can be seen that the complex is stable to the presence of a 10-fold excess of all the anions studied at t = 0. However, the spectra acquired after 4 hours show that the presence of excess carbonate anions causes decomposition of the complex. Similar behaviour was observed in the pH 7 experiments (stable at t = 0 and unstable at t = 4 hours), whereas the complex is unstable at pH 11 from t = 0. The complex is stable after 2 hours at 80 °C in water and is unchanged after one week in aqueous solution.

6.2.3.2 Halide exchange reaction on $[FeCl_3(Me_3\text{-tacn})]$

The halide exchange reaction of $[FeCl_3(Me_3\text{-tacn})]$ in the presence of an excess of $[Me_4N]F$ (4 mol. equiv.) in refluxing MeCN was investigated. The target product was successfully isolated after work up of the reaction and characterised by IR spectroscopy and microanalysis. A comparison between the IR spectra of the parent $FeCl_3$- and FeF_3-complexes and the product obtained from the halide

exchange reaction is shown in Figure 6.20. The shift in the Fe-F bands in the IR spectra of the trifluoride complex made by halide exchange reaction may reflect a different degree of hydration in the compound. This reaction appears to be successful in a much shorter time than for the kinetically inert Cr(III) system and future studies will be carried out in order to test radiofluorination of this system.

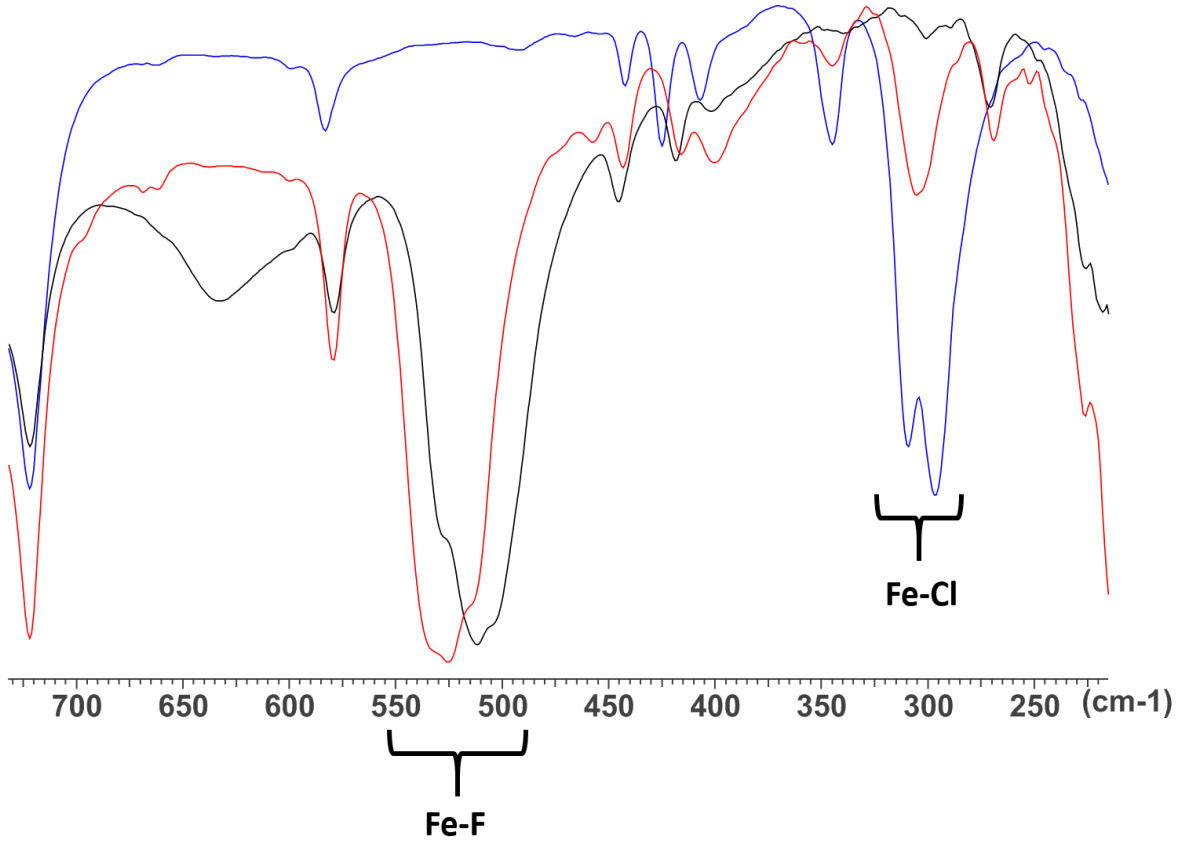

Figure 6.20. Comparison of the IR spectra of [$FeCl_3$(Me_3-tacn)] (blue), [FeF_3(Me_3-tacn)] (black) and [FeF_3(Me_3-tacn)] from the halide exchange reaction (red).

6.2.4 [CoF_3(L)] (L = terpy, Me_3-tacn)

[CoF_3(Me_3-tacn)]·2H_2O and [CoF_3(terpy)]·MeOH·H_2O were made by oxidising $Co^{II}F_2$·4H_2O to Co(III) in air in the presence of NaF and the appropriate ligand, to form the desired complex. The reactions were carried out in MeOH solution at room temperature. The complexes were characterised by ^{1}H, $^{19}F\{^{1}H\}$, ^{59}Co, IR, UV-vis spectroscopy and microanalysis. The presence of MeOH in [CoF_3(terpy)]·MeOH·H_2O was confirmed by ^{1}H NMR spectroscopy. The $^{19}F\{^{1}H\}$ NMR spectra of the complexes show broad resonances, with no resolved $^{1}J_{F\text{-}Co}$ coupling, at −151 ppm ([CoF_3(Me_3-tacn)]·2H_2O) and −116 ppm ([CoF_3(terpy)]·MeOH·H_2O). These low spin d^6 systems are diamagnetic and allow for NMR spectroscopic data to be obtained. The $^{19}F\{^{1}H\}$ and ^{59}Co NMR of [CoF_3(terpy)]·MeOH·H_2O are shown in Figure 6.21.

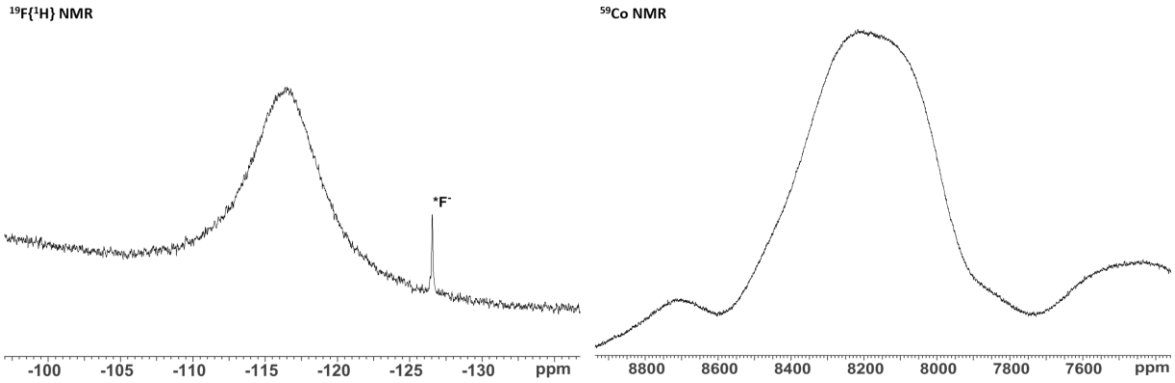

Figure 6.21. $^{19}F\{^{1}H\}$ (left) and ^{59}Co NMR (right) spectra of $[CoF_3(terpy)]\cdot MeOH\cdot H_2O$.

The UV-vis spectra are shown in Figures 6.22 and 6.23.

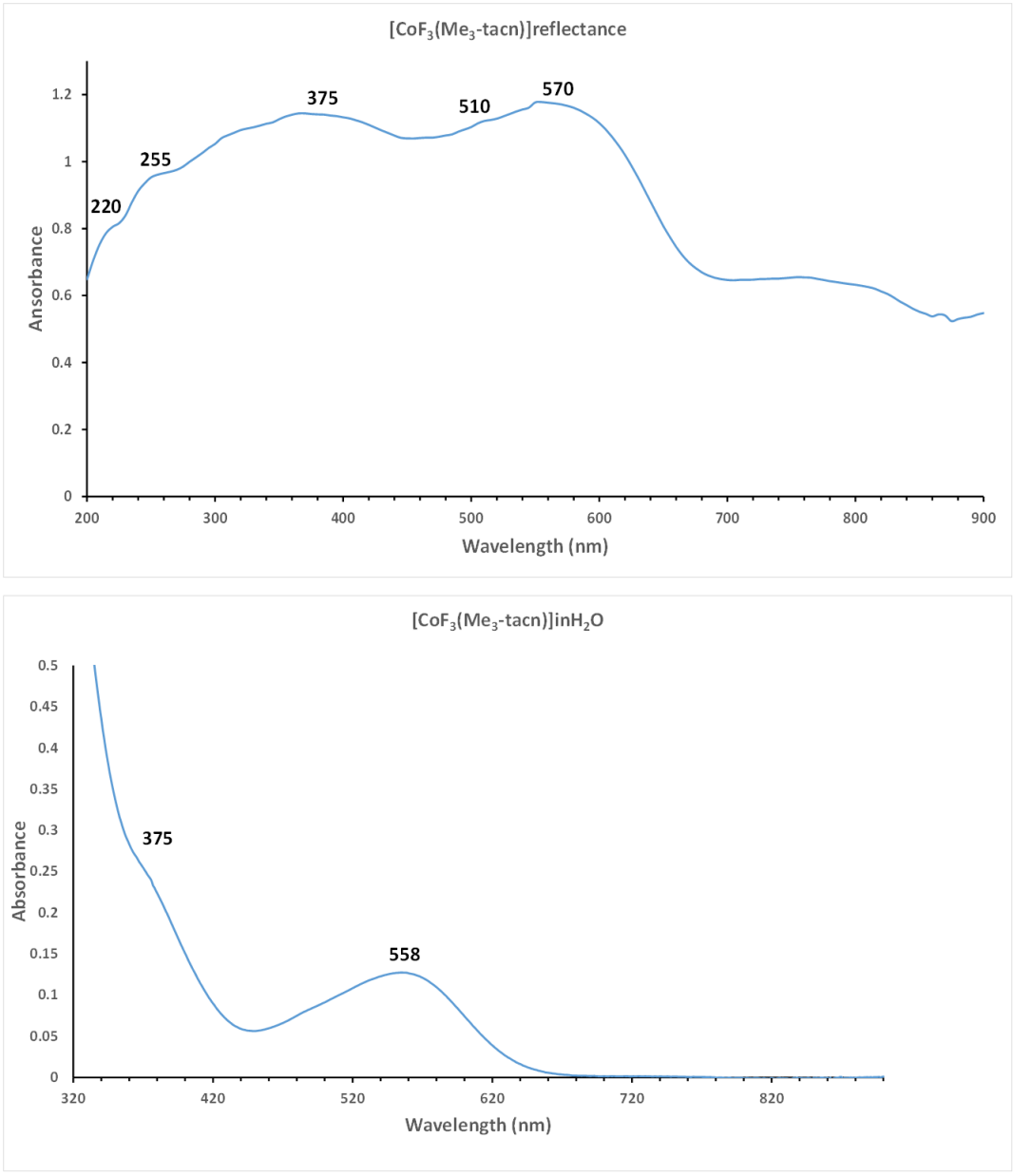

Figure 6.22. UV-vis spectra of $[CoF_3(Me_3\text{-}tacn)]\cdot 2H_2O$. A: diffuse reflectance; B: 10^{-3} M in H_2O.

A

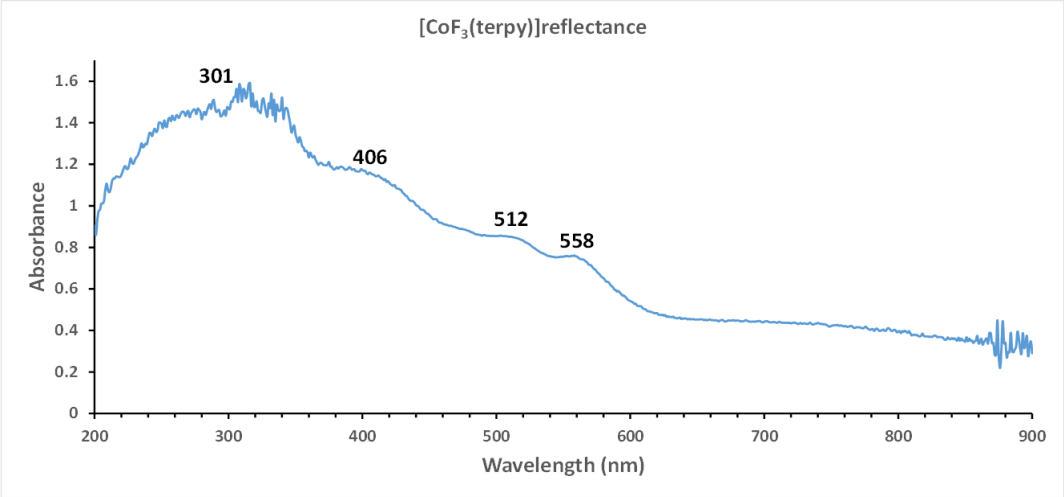

B

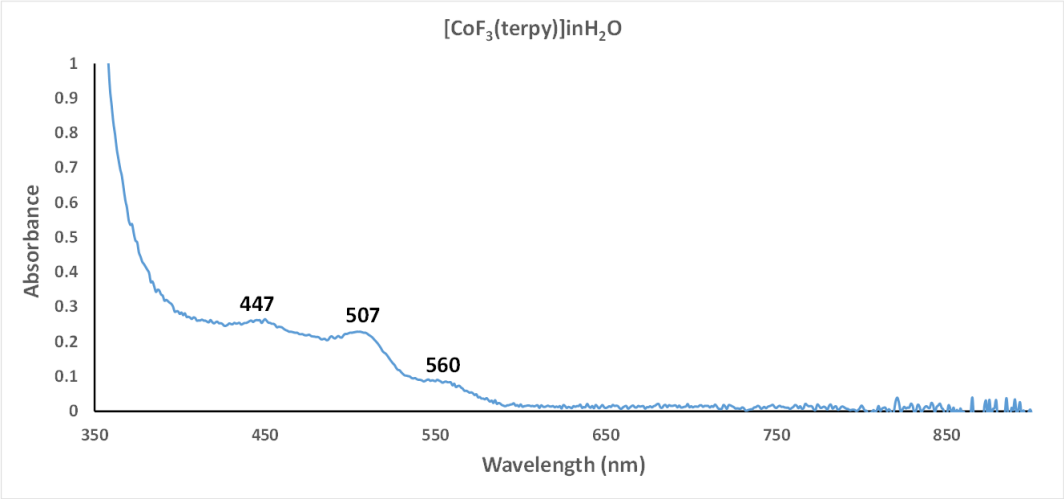

Figure 6.23. UV-vis spectra of $[CoF_3(terpy)]\cdot MeOH\cdot H_2O$. A: diffuse reflectance; B: 10^{-3} M in H_2O.

Two spin-allowed transitions are predicted for a low spin d^6 system.[3] These two transitions are present in the spectra of $[CoF_3(Me_3\text{-tacn})]\cdot 2H_2O$ (solid and solution) at ~ 17500 and 26650 cm^{-1} (~ 570 and 375 nm), and are assigned to $^1T_{1g}\leftarrow{}^1A_{1g}$ and $^1T_{2g}\leftarrow{}^1A_{1g}$ respectively. However, the $[CoF_3(terpy)]\cdot MeOH\cdot H_2O$ show three bands close to each other at 17900, 19600 and 24000 cm^{-1} (~ 560, 510 and 420 nm). The *mer*-$[CoF_3(terpy)]\cdot MeOH\cdot H_2O$ has C_{2v} symmetry and, as discussed for the MnF_3-terpy complex above, the splitting is greater than in the Me_3-tacn complex. The $^1T_{1g}$ level split into three components and the transitions observed are therefore assigned to $^1B_{1g}\leftarrow{}^1A_{1g}$, $^1B_{2g}\leftarrow{}^1A_{1g}$, $^1B_{3g}\leftarrow{}^1A_{1g}$ (from low to high energy).[3,57,58] In this case, the second spin-allowed transition $^1T_{2g}\leftarrow{}^1A_{1g}$ is masked by the ligand to metal charge transfer and/or π-π^* bands involving the terpy ligand.

Crystals of $[CoF_3(Me_3\text{-tacn})]\cdot 4H_2O$ suitable for single crystal X-ray analysis were obtained by slow evaporation of a concentrated solution of the complex in water. The structure shows, as for $[MnF_3(Me_3\text{-tacn})]\cdot 4H_2O$, disorder in the carbon atom positions in the ring of the macrocycle and only one part is shown in Figure 6.24A. The complex is isostructural to $[MnF_3(Me_3\text{-tacn})]\cdot 4H_2O$ and shows the same H-bonding pattern in the lattice (Figure 6.24B).

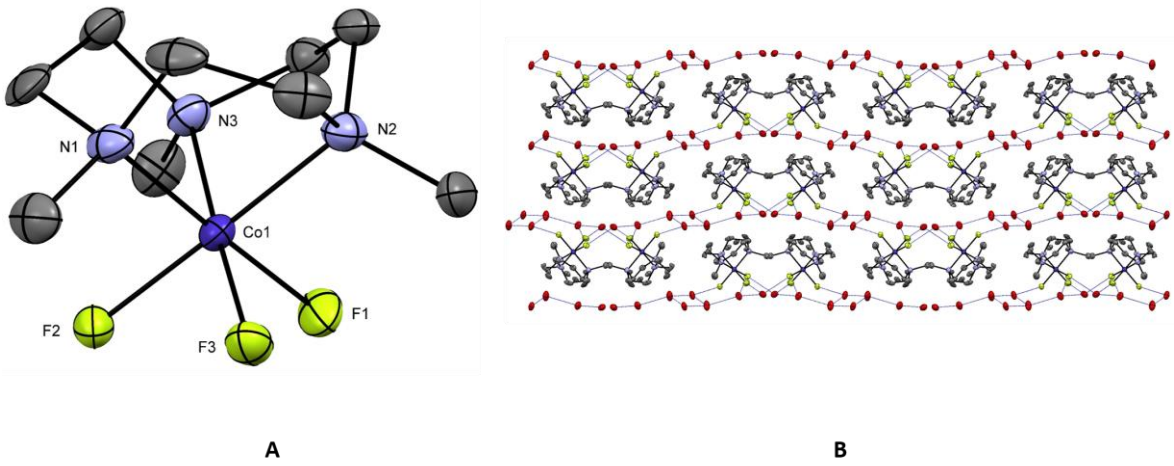

Figure 6.24 A: Crystal structure of $[CoF_3(Me_3\text{-tacn})]\cdot 4H_2O$ with ellipsoids drawn at the 50 % probability level. H atoms and water molecules are omitted for clarity. Select bond lengths (Å) and angles (°): Co1–F1 = 1.857(3), Co1–F2 = 1.871(2), Co1–F3 = 1.871(3), Co1–N1 = 1.960(4), Co1–N2 = 1.960(4), Co1–N3 = 1.958(4), F1–Co1–N1 = 178.30(14), F3–Co1–N3 = 178.13(14), F2–Co1–N1 = 91.39(14), F1–Co1–F3 = 88.29(13), F1–Co1–F2 = 89.92(12), N1–Co1–N2 = 87.62(16), N1-Co1-N3 = 87.95(15). B: H-bonding interaction present in $[CoF_3(Me_3\text{-tacn})]\cdot 4H_2O$ (blue dots).

6.2.4.1 Stability tests

The stability of $[CoF_3(Me_3\text{-tacn})]\cdot 2H_2O$ to the presence of a 15-fold excess of competitive anions (Cl^-, F^-, CO_3^{2-} added as sodium salts and ascorbic acid), a range of pH (4, 7, and 11), heat and time was followed by UV-vis spectroscopy on a 10^{-3} M solution of the complex in water. As for the other systems, the spectra were acquired at two time points (t = 0 and t = 4 hours). Figure 6.25 shows the results of these experiments.

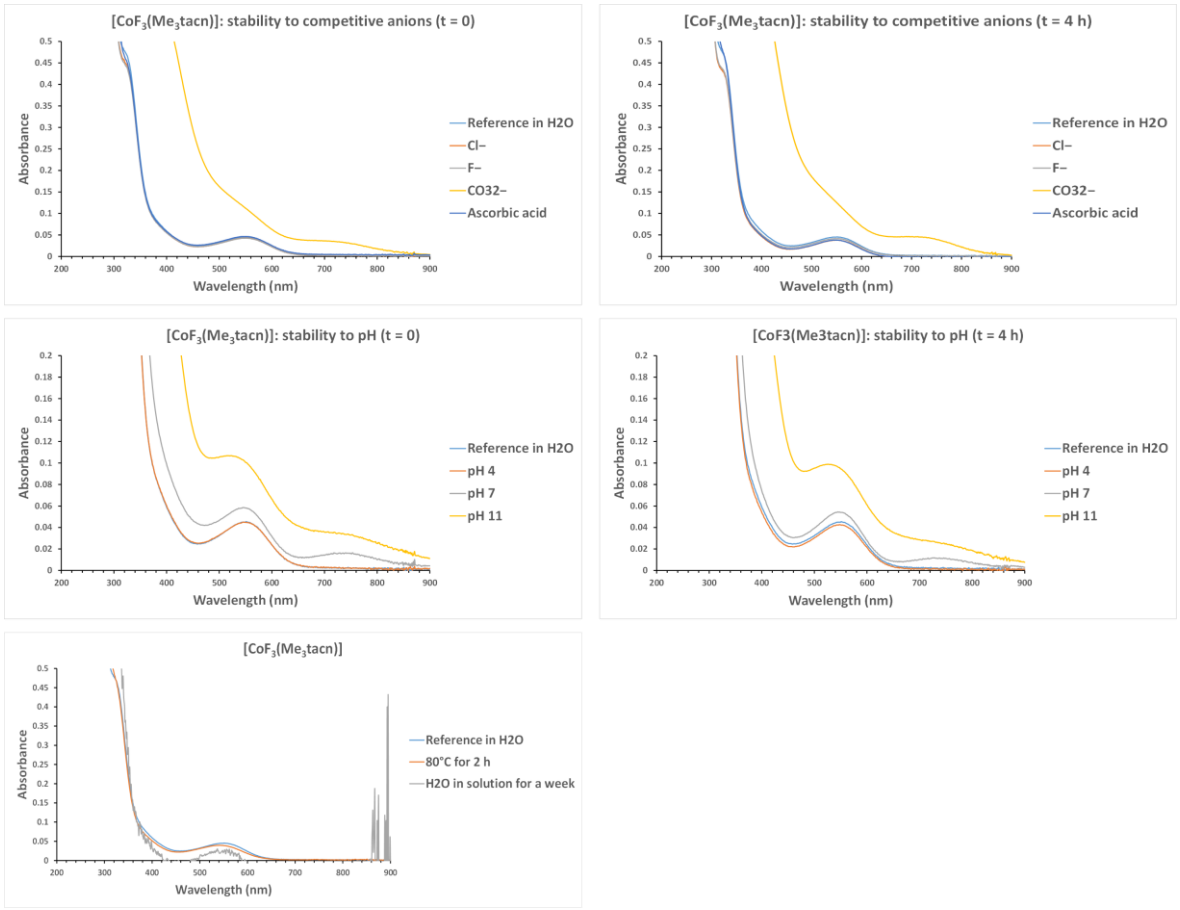

Figure 6.25. Stability tests on $[CoF_3(Me_3\text{-tacn})]\cdot 2H_2O$.

The complex proved to be highly stable in all of the test conditions. The spectra were unchanged after 4 hours in the presence of the chloride and fluoride anions, from pH 4 to 11, after two hours at 80 °C and after a week in water. Moreover, the stability of the complex was challenged by the presence of a 15-fold excess of the mildly reducing agent ascorbic acid, showing very good stability in this case as well. The only experiment in which the complex was not stable was the one in the presence of a 15-fold excess of carbonate (pH of the solution ~ 9-10).

6.3 Conclusions

The distorted octahedral complexes, $[MF_3(L)]$ (M = Cr, Mn, Fe, Co; L = terpy, Me_3-tacn), were synthesised and fully characterised. The Mn(III) (d^4) and Fe(III) (d^5) complexes are high spin systems whereas the Co(III) (d^6) analogues are low spin. The UV-vis spectroscopic data are consistent with these electronic configurations and the bands are assigned accordingly. Crystal structures of the isostructural $[MnF_3(Me_3\text{-tacn})]\cdot 4H_2O$ and $[CoF_3(Me_3\text{-tacn})]\cdot 4H_2O$ were also acquired, showing once again the tendency of the MF_3 moiety to interact with water through H-bonding.[55]

The complexes were synthesised and studied in order to explore their potential for further applications as PET imaging agents and, in particular, the preliminary stability studies over a range of physiological relevant conditions were carried out. The stability tests were performed on $[CrF_3(L)]$, $[MnF_3(Me_3\text{-tacn})]$, $[FeF_3(Me_3\text{-tacn})]$ and $[CoF_3(Me_3\text{-tacn})]$ in the presence of competitive anions, changes in pH, in solution at elevated temperature and prolonged exposure in solution. The results show that, as expected, the kinetically inert d^3 and low spin d^6 systems are more stable than the other metals (Mn(III) d^4 and Fe(III) d^5) and that $[CrF_3(Me_3\text{-tacn})]$ is more stable than $[CrF_3(terpy)]$. Given the kinetically lability and tendency to reduction and disproportionation of the d^4 Mn(III) systems, $[MnF_3(Me_3\text{-tacn})]$ proved to be (unsurprisingly) the least stable of the systems studied, whilst $[FeF_3(Me_3\text{-tacn})]$ showed good stability to the presence of competitive anions, heating and time. However, the observed instability at pH > 7 may be detrimental for the future possible application in PET.

The ideal precursor in a Cl/F halide exchange reaction is a system whose properties are a trade-off between thermodynamic stability, kinetic inertness and sufficient lability. Thermodynamic stability is important because a certain degree of stability should be maintained during the radiolabelling reaction, while at the same time remaining sufficiently labile so that the Cl/F exchange occurs in a relatively short time (when the ^{18}F half-life of 110 minutes is considered). Stability of the final product should of course be maintained during the post-labelling manipulation and the PET scan. The Cl/F exchange reactions on $[CrCl_3(Me_3\text{-tacn})]$ and $[FeCl_3(Me_3\text{-tacn})]$ in anhydrous MeCN (reflux) using $[Me_4N]F$ as fluoride source were explored. The reaction of $[CrCl_3(Me_3\text{-tacn})]$ was incomplete after 24 hours with both the chloride and fluoride species evident in the IR spectra, whereas the reaction of $[FeCl_3(Me_3\text{-tacn})]$ with $[NMe_4]F$ showed promising results with complete conversion of the chloride precursor to the fluoride analogue.

Alternatively, $[^{18}F]F^-$ can be introduced into the complex through $^{18}F/^{19}F$ isotopic exchange reactions (Chapter 3). In this regard, the high stability of the complexes $[CrF_3(Me_3\text{-tacn})]$ and $[CoF_3(Me_3\text{-tacn})]$ make them promising systems to explore this route.

6.4 Experimental

Complex synthesis were generally carried out in atmospheric conditions. Anhydrous conditions were used as stated in the methods. $[CrCl_3(thf)_3]$ was prepared by the literature method.[59] 2,2':6'2"-terpyridyl was obtained from Sigma-Aldrich. 1,4,7-trimethyl-1,4,7-triazacyclononane was prepared as described previously.[60] Anhydrous $[NMe_4]F$ was obtained by recrystallising the commercial sample (Aldrich) from ^{i}PrOH as described.[61] For further details regarding the instrumentation used see Appendix 1.

6.4.1 $[CrF_3(py)_3]\cdot 3.5H_2O$

This was prepared by the literature method.[62] $[Cr(NO_3)_3]\cdot 9H_2O$ (4 g, 0.01 mol) was dissolved in water (20 mL) to give a deep blue solution, which was filtered and cooled in an ice bath. KF (1.8 g, 0.03 mol) was dissolved in water (15 mL) and also cooled before being slowly added to the $[Cr(NO_3)_3]\cdot 9H_2O$ solution, resulting in a purple precipitate. The solid was filtered, washed with ice-cold ethanol and water and dried for 1 hour *in vacuo*. Yield 1.50 g. The purple solid was then added to pyridine (50 mL) and heated to let the pyridine-water azeotrope evaporate. The colour of the solution changed from violet to blue and back to violet. When nearly fully evaporated, more pyridine (15 mL) was added and then heated until most of the solvent evaporated. The purple solid was filtered, washed with acetone and diethyl ether and dried overnight *in vacuo* (1.52g, 43 %). Required for $C_{15}H_{15}N_3F_3Cr\cdot 3.5H_2O$: C, 44.0; H, 5.4; N, 10.3. Found: C, 44.1; H, 4.3; N, 11.0 %. IR (Nujol, ν/cm^{-1}): 3391, 1659 (H_2O), 571, 559 (Cr–F). UV-Vis (diffuse reflectance)/cm^{-1}: 14144, 17361, 21277, 26596, 31646, 38168, 45872. UV-Vis $[CrF_3(py)_3]\cdot 3.5H_2O]$ = 10^{-3} M in water/cm^{-1} (ε/M^{-1} cm^{-1}): 18051 (95), 26385 (110), 28902 (136), 31546 (203).

6.4.2 $[CrF_3(terpy)]\cdot 4H_2O$

This was prepared by the literature method.[13] $[CrF_3(py)_3]$ (150 mg, 0.43 mmol) and terpy (107 mg, 0.46 mmol) were dissolved in butan-1-ol (12 mL) and heated under reflux for 2 hours. The colour of the solution changed from violet to blue to green to blue. Half of the solvent was evaporated, and the reaction mixture was cooled resulting in a blue precipitate. Water (10 drops) and acetone (5 mL) was added while stirring and a purple precipitate formed. The solid was filtered and washed in acetone before being dried under vacuum (139 mg, 92 %). Required for $C_{15}H_{11}N_3F_3Cr\cdot 4H_2O$: C, 43.5; H, 4.6; N, 10.1. Found: C, 43.5; H, 4.2; N, 10.0 %. IR (Nujol, ν/cm^{-1}): 3370, 1664 (H_2O), 552 (br, Cr–F). UV-Vis (diffuse reflectance)/cm^{-1}: 14104, 17361, 22573, 24213, 28329, 31348, 39063, 46296. UV-Vis $[CrF_3(terpy)\cdot 4H_2O]$ = 10^{-3} M in water/cm^{-1} (ε/M^{-1} cm^{-1}): 14245 (45), 17921 (172), 22573 (118), 24213 (244), 25840 (443).

6.4.3 $[CrF_3(Me_3\text{-tacn})]\cdot 3.5H_2O$

Method 1: This was prepared by the literature method.[13] $[CrF_3(py)_3]$ (185 mg, 0.53 mmol) was dissolved in dmf (10 mL) and Me_3-tacn (97 mg, 0.57 mmol) was added. The reaction mixture was heated under reflux for 50 mins and a colour change from violet to green was observed. The reaction mixture was filtered, yielding a green solid and blue filtrate. The solvent was evaporated from the filtrate, resulting in a deep blue solid which was dissolved in water (7 mL), to which acetone (150 mL) was added resulting in a purple precipitate. The acetone was removed and the solid dried under vacuum (79 mg, 53 %). Required for $C_9H_{21}N_3F_3Cr\cdot 3.5H_2O$: C, 31.5; H, 8.2; N, 12.2. Found: C, 30.8; H, 8.8; N, 13.2 %. IR (Nujol, ν/cm^{-1}): 3376, 1662 (H_2O), 541, 511 (Cr–F). UV-Vis (diffuse reflectance)/cm^{-1}: 14771, 17762, 24213. UV-Vis $[CrF_3(Me_3\text{-tacn})\cdot 3.5H_2O]$ = 10^{-3} M in water/cm^{-1} (ε/M^{-1} cm^{-1}): 14815 (8), 17986 (97), 24570 (43).

Method 2: $[CrCl_3(Me_3\text{-tacn})]$ (50 mg, 0.15 mmol) was dissolved in 10 mL of MeCN giving a green solution and a suspension of $[Me_4N]F$ (56 mg, 0.60 mmol) in MeCN (5 mL) was added. The mixture was heated to reflux for 24 hours after which time the solution became of a darker green colour. The solvent was removed *in vacuo* and an IR on the crude product was acquired showing the presence of both Cr-F and Cr-Cl bands. IR (Nujol, ν/cm^{-1}): 539, 507 (Cr-F), 343, 333(Cr-Cl).

6.4.4 $[CrCl_3(Me_3\text{-tacn})]$

Reactions carried out in anhydrous conditions using Schleck and glove box techniques.

This was prepared from a different method reported in the literature.[60] $[CrCl_3(thf)_3]$ (170 mg, 0.46 mmol) was dissolved in CH_2Cl_2 to give a purple solution, to which Me_3-tacn (94 mg, 0.55 mmol) was added resulting in a green solution. The reaction mixture was stirred at room temperature for 1 hour. A green solid was filtered from the reaction mixture, washed with diethyl ether (10 mL) and dried under vacuum (78 mg, 52 %). Required for $C_9H_{21}N_3Cl_3Cr$: C, 32.8; H, 6.4; N, 12.8. Found: C, 32.6; H, 6.5; N, 12.6 %. IR (Nujol, ν/cm^{-1}): 340, 327 (Cr–Cl). UV-Vis (diffuse reflectance)/cm^{-1}: 14144, 15898, 21505, 38610, 45662.

6.4.5 $[MnF_3(terpy)]\cdot MeOH\cdot 3H_2O$

This was prepared by a modified method in the literature[33] in anhydrous conditions using Schleck and glove box techniques but product treated as air stable. Terpy (115 mg, 0.49 mmol) was dissolved in 6 mL of methanol and MnF_3 (50 mg, 0.45 mmol) was added resulting in a brown solution with a small amount of black precipitate. The reaction mixture was stirred at room temperature for 2 hours before filtering to remove the black solid. Diethyl ether (20 mL) was added yielding an orange precipitate. The solvents were removed and the solid dried under vacuum (81 mg, 52 %).

Required for $C_{15}H_{11}N_3F_3Mn{\cdot}MeOH{\cdot}3H_2O$: C, 44.6; H, 4.9; N, 9.7. Found: C, 45.1; H, 4.8; N, 9.0 %. IR (Nujol, *v*/cm^{-1}): 3410, 1640 (H_2O), 597, 573 (Mn–F). ^1H NMR (CD_3CN, 298 K): δ = 3.28 (s, OH), 2.15 (s, CH_3OH). UV-Vis (diffuse reflectance)/cm^{-1}: 12739, 18315, 21978, 26316, 30864, 26738, 44843. UV-Vis [MnF_3(terpy)·MeOH·$3H_2O$] = 10^{-3} M in water/cm^{-1} (ε/M^{-1} cm^{-1}): 15552 (160), 18182 (172). UV-Vis [MnF_3(terpy)·MeOH·$3H_2O$] = 10^{-3} M in MeCN/cm^{-1} (ε/M^{-1} cm^{-1}): 13793 (17), 18149 (24), 22883 (60).

6.4.6 [MnF_3(Me_3-tacn)]·$2H_2O$

Reaction carried out in anhydrous conditions using Schleck and glove box techniques but product treated as air stable. This was prepared by a different method from the one reported literature.[35] MnF_3 (91 mg, 0.55 mmol) in MeOH was added to a MeOH solution of Me_3tacn (94 mg, 0.55 mmol), forming a green solution. The reaction was left stirring at room temperature for 22 hours after which time the solution was deep red. The solvent was removed *in vacuo* and the resulting red solid was washed in diethyl ether (10 mL) before being dried *in vacuo* (121 mg, 78 %). Required for $C_9H_{21}N_3F_3Mn{\cdot}MeOH{\cdot}3H_2O$: C, 33.9; H, 7.9; N, 13.2. Found: C, 33.8; H, 7.7; N, 13.0 %. IR (Nujol, *v*/cm^{-1}): 3438, 1664 (H_2O), 585, 553 (Mn–F). UV-Vis (diffuse reflectance)/cm^{-1}: 19569, 33898, 39063, 46083. UV-Vis [MnF_3(Me_3-tacn)·$2H_2O$] = 10^{-3} M in water/cm^{-1} (ε/M^{-1} cm^{-1}): 20534 (169), 22222 (143), 23810 (130). UV-Vis [MnF_3(Me_3-tacn)·$2H_2O$] = 10^{-3} M in MeCN/cm^{-1} (ε/M^{-1} cm^{-1}): 18904 (292). μ_{eff} = 4.94 BM (298 K). Crystals suitable for single crystal X-ray diffraction analysis were obtained by slow evaporation of a concentrated solution in water of the complex.

6.4.7 [FeF_3(terpy)]

$FeF_3{\cdot}3H_2O$ (72 mg, 0.43 mmol) was suspended in 15 mL of butan-1-ol and a solution of terpy (101 mg, 0.43 mmol) in butan-1-ol was added. The mixture was heated to reflux for 4 hours, resulting in a clear red/purple solution. The mixture was left cooling to room temperature and the solvent was removed *in vacuo* giving a fine pink/purple powder, which was washed with Et_2O and dried *in vacuo* (79 mg, 52 %). Required for $C_{15}H_{11}F_3N_3Fe$: C, 47.1; H 4.0; N 11.00. Found: C, 46.4; H, 4.2; N, 10.6 %. IR (Nujol, *v*/cm^{-1}): 550, 518 (Fe–F). UV-Vis (diffuse reflectance)/cm^{-1}: 16026, 17857, 20619, 30675, 40323, 45249. UV-Vis [FeF_3(terpy)] = 10^{-2} M in water/cm^{-1} (ε/M^{-1} cm^{-1}):16155 (7), 18116 (37), 20284 (21).

6.4.8 [FeF_3(Me_3-tacn)]·H_2O

This was synthesised using different methods from the one reported in the literature.[20]

Method 1: $FeF_3 \cdot 3H_2O$ (88 mg, 0.53 mmol) was suspended in 15 mL of butan-1-ol and a solution of Me_3-tacn (90 mg, 0.53 mmol) in butan-1-ol was added. The mixture was heated to reflux for 4 hours, resulting in a clear yellow solution. The mixture was left cooling to room temperature and the solvent was removed *in vacuo* giving a pale yellow solid, which was washed with Et_2O and dried *in vacuo* (60 mg, 40 %). Required for $C_9H_{21}F_3N_3Fe \cdot H_2O$: C, 35.8; H 7.7; N 13.9. Found: C, 35.6; H, 8.1; N, 13.1 %. IR (Nujol, ν/cm^{-1}): 3439, 1664 (H_2O), 529, 512 (Fe–F). UV-Vis (diffuse reflectance)/cm^{-1}: 22222, 26455, 33223, 40161, 46083. UV-Vis [$FeF_3(Me_3\text{-tacn}) \cdot H_2O$] = 10^{-2} M in water/cm^{-1} (ε/M^{-1} cm^{-1}): 32573 (60).

Method 2: [$FeCl_3(Me_3$-tacn)] (45 mg, 0.15 mmol) was dissolved in 10 mL of MeCN giving a yellow solution, and a suspension of [Me_4N]F (56 mg, 0.60 mmol) in MeCN (5 mL) was added. The mixture was heated to reflux for 4 hours. The solvent was removed *in vacuo* giving a yellow/orange pale solid. CH_2Cl_2 was added and filtered, obtaining a clear yellow solution. The solvent was removed *in vacuo* giving a yellow solid (16 mg, 42 %). Required for $C_9H_{21}F_3N_3Fe \cdot 2.5H_2O$: C, 32.8; H 8.0; N 12.8. Found: C, 33.7; H, 6.3; N, 11.3 %. IR (Nujol, ν/cm^{-1}): 536, 525 (Fe-F).

6.4.9 [$FeCl_3(Me_3$-tacn)]

This compound was made from a modified method reported in the literature.[63] $FeCl_3$ (0.06 g, 0.36 mmol) was dissolved in diethyl ether (5 mL) forming a brown solution and a diethyl ether (3 mL) solution of Me_3-tacn (0.07 mL, 0.36 mmol) was added. The mixture was stirred for 15 minutes and the solvent removed under *vacuum* giving a yellow solid. The solid was washed with diethyl ether and dried under *vacuum* (0.11 g, 92%). Required for $C_9H_{21}Cl_3N_3Fe$: C, 32.4; H 6.4; N 12.6. Found: C, 32.3; H, 6.4; N, 12.6 %. IR (Nujol, ν/cm^{-1}): 308, 298 (Fe-Cl). UV-Vis (diffuse reflectance)/cm^{-1} (nm): 17857(560), 25316(395), 32787(305), 44053(227).

6.4.10 [CoF_3(terpy)]·MeOH·H_2O

$CoF_2 \cdot 4H_2O$ (150 mg, 0.89 mmol) was suspended in MeOH (5 mL). A solution of terpy (222 mg, 0.98 mmol) in MeOH (5mL) was added dropwise into the first solution. The mixture turned deep orange/brown within 20 minutes. NaF (15 mg, 0.36 mmol) was added to the mixture. The reaction mixture was left stirring for 90 minutes, filtered and the solvent removed *in vacuo* giving an orange solid. This solid was washed with Et_2O and dried *in vacuo* (243 mg, 76 %). Required for $C_{15}H_{11}F_3N_3Co \cdot MeOH \cdot H_2O$: C, 48.1; H 4.3; N 10.5. Found: C, 48.1; H, 4.5; N, 10.7 %. IR (Nujol, ν/cm^{-1}): 3377, 1654 (H_2O), 665, 651, 637 (Co–F). ^{1}H NMR (D_2O, 298 K): δ = 9.07 (s, [2H], Ar-CH_2), 8.63 (d, [3H], Ar-CH_2), 8.20 (t, [2H], Ar-CH_2), 7.39 (t, [2H], Ar-CH_2), 7.31 (d, [2H], Ar-CH_2), 3.23 (s, CH_3OH). ^{19}F{^{1}H} NMR (D_2O, 298 K): δ = −116 (br s). ^{59}Co NMR (D_2O, 298 K): δ = 8179 (br s, HWHM = 396 ppm).

UV-Vis (diffuse reflectance)/cm^{-1}: 17291, 19531, 24631, 32223. UV-Vis [$CoF_3(Me_3$-tacn)·MeOH·H_2O] = 10^{-3} M in water/cm^{-1} (ε/M^{-1} cm^{-1}): 17857 (75), 19724 (228), 22371 (262).

6.4.11 [$CoF_3(Me_3$-tacn)]·$2H_2O$

$CoF_2·4H_2O$ (72 mg, 0.42 mmol) was suspended in MeOH (5 mL). A solution of Me_3-tacn (72 mg, 0.42 mmol) in MeOH (5mL) was added dropwise into the first solution. The mixture turned brown and black within 20 minutes. NaF (13 mg, 0.31 mmol) was added to the mixture. The reaction mixture was left stirring for 2 hours, filtered and the solvent removed *in vacuo* giving a brown solid. This solid was washed with Et_2O and dried *in vacuo* (243 mg, 76 %). The solid turned purple overnight. Required for $C_9H_{21}F_3N_3Co·2H_2O$: C, 33.4; H 7.8; N 13.0. Found: C, 33.2; H, 7.9; N, 12.9 %. IR (Nujol, *v*/cm^{-1}): 3353, 1656 (H_2O), 591, 574 (Co–F). ^{1}H NMR (D_2O, 298 K): δ = 3.12 (m, [6H], CH_2), 3.02 (m, [6H], CH_2), 2.84 (s, [9H], CH_3). ^{19}F{^{1}H} NMR (D_2O, 298 K): δ = −151 (br s). ^{59}Co NMR (D_2O, 298 K): δ = 8280 (br s, HWHM = 428 ppm). UV-Vis (diffuse reflectance)/cm^{-1}: 12739, 17544, 19608, 26667, 39216, 45455. UV-Vis [$CoF_3(Me_3$-tacn)·$2H_2O$] = 10^{-3} M in water/cm^{-1} (ε/M^{-1} cm^{-1}): 17921 (127), 26667 (242).

6.4.12 X-ray experimental

Table 6.2. Crystal data and structural refinement details. [a]

Compound	$[MnF_3(Me_3\text{-tacn})]\cdot 4H_2O$	$[CoF_3(Me_3\text{-tacn})]\cdot 4H_2O$
Formula	$C_9H_{21}F_3MnN_3\cdot 4(H_2O)$	$C_9H_{21}CoF_3N_3\cdot 4(H_2O)$
M	355.55	359.03
Crystal system	orthorhombic	orthorhombic
Space group	Pbca (61)	Pbca (61)
a /Å	8.9041(2)	8.74923(7)
b /Å	13.2669(3)	13.14407(11)
c /Å	26.9700(6)	26.2569(3)
α/ °	90	90
β /°	90	90
γ/°	90	90
U /Å^3	3185.96(12)	3019.55(5)
Z	8	8
μ(Mo-K$_\alpha$)/mm^{-1}	0.875	1.186
F(000)	1505	1518
Total no. reflns	32812	30727
R_{int}	0.0584	0.0248
Unique reflns	3124	2973
No. of params, restraints[b]	254, 276	253, 243
R_1, wR_2 [$I > 2\sigma(I)$][c]	0.0691, 0.1160	0.0586, 0.1427
R_1, wR_2 (all data)	0.0663, 0.1170	0.0586, 0.1427

[a] Common items: T = 100 K; wavelength (Mo-Kα) = 0.71073 Å; ϑ(max) = 27.5°;

[b] The high number of restrains is due to the disorder associated to the carbon atoms in the macrocycle ring.

[c] $R_1 = \Sigma||F\sigma| - |Fc|| / \Sigma|Fo|$; $wR_2 = [\Sigma w(Fo^2 - Fc^2)^2 / \Sigma wFo^2]^{1/2}$;

6.5 References

1. Knopp, P.; Wieghardt, K., *Z. Naturforsch.* **1991**, *46b*, 1077.
2. Benjamin, S. L.; Levason, W.; Reid, G., *Chem. Soc. Rev.* **2013**, *42*, 1460.
3. Lever, A. B. P., *Inorganic Electronic Spectroscopy,* Elsevier, **1984**, Vol. *33*.
4. Herbstein, F. H.; Kapon, M.; Reisner, G. M., *Zeitschrift Fur Kristallographie* **1985**, *171*, 209.
5. Brencic, J. V.; Leban, I., *Z. Anorg. Allg. Chem.* **1981**, *480*, 213.
6. Wendlandt, W. W.; Sveum, L. K., *J. Inorg. Nucl. Chem.* **1967**, *29*, 975.
7. Vaughn, J. W.; Marzowski, J., *Inorg. Chem.* **1973**, *12*, 2346.
8. Schlaefer, H. L.; Gausmann, H.; Zander, H. U., *Inorg. Chem.* **1967**, *6*, 1528.
9. Vaughn, J. W., *Inorg. Chem.* **1981**, *20*, 2397.
10. Schaffer, C. E.; Lang, J. M.; Drickamer, H. G., *Inorg. Chem.* **1996**, *35*, 5072.
11. Flint, C. D.; Matthews, A. P.; O'Grady, P. J., *Journal of the Chemical Society, Faraday Trans. 2* **1977**, *73*, 655.
12. Casabo, J.; Solans, A.; Diaz, C.; Ribas, J.; Segui, A.; Corbella, M., *Transition Met. Chem.* **1985**, *10*, 128.
13. Birk, T.; Magnussen, M. J.; Piligkos, S.; Weihe, H.; Holten, A.; Bendix, J., *J. Fluorine Chem.* **2010**, *131*, 898.
14. Fochi, G.; Straehle, J.; Gingl, F., *Inorg. Chem.* **1991**, *30*, 4669.
15. Moon, D.; Choi, J. H., *Acta Crystallogr., Sect. E: Struct. Rep. Online* **2013**, *69*, m514.
16. Yamaguchi-Terasaki, Y.; Fujihara, T.; Nagasawa, A.; Kaizaki, S., *Acta Crystallogr., Sect. E: Struct. Rep. Online* **2007**, *63*, m593.
17. Liu, H. X., *Acta Crystallogr., Sect. E: Struct. Rep. Online* **2009**, *65*, m1093.
18. Birk, T.; Bendix, J.; Weihe, H., *Acta Crystallogr., Sect. E: Struct. Rep. Online* **2008**, *64*, m369.
19. Kirk, A. D.; Namasivayam, C., *Inorg. Chem.* **1988**, *27*, 1095.
20. Pedersen, K. S.; Lorusso, G.; Morales, J. J.; Weyhermuller, T.; Piligkos, S.; Singh, S. K.; Larsen, D.; Schau-Magnussen, M.; Rajaraman, G.; Evangelisti, M.; Bendix, J., *Angew. Chem. Int. Ed.* **2014**, *53*, 2394.
21. Bhalla, R.; Levason, W.; Luthra, S. K.; McRobbie, G.; Reid, G.; Sanderson, G.; Zhang, W., *Chem Commun.* **2014**, *50*, 12673.
22. Birk, T.; Pedersen, K. S.; Thuesen, C. A.; Weyhermuller, T.; Schau-Magnussen, M.; Piligkos, S.; Weihe, H.; Mossin, S.; Evangelisti, M.; Bendix, J., *Inorg. Chem.* **2012**, *51*, 5435.

23. Dreiser, J.; Pedersen, K. S.; Piamonteze, C.; Rusponi, S.; Salman, Z.; Ali, M. E.; Schau-Magnussen, M.; Thuesen, C. A.; Piligkos, S.; Weihe, H.; Mutka, H.; Waldmann, O.; Oppeneer, P.; Bendix, J.; Nolting, F.; Brune, H., *Chem. Sci.* **2012**, *3*, 1024.

24. Choi, J. H.; Lee, U., *Acta Crystallogr. Sect. E: Struct. Rep. Online* **2008**, *64*, m1186.

25. Bang, E.; Pedersen, E.; Svanholt, H.; Almenningen, A.; Bastiansen, O.; Fernholt, L.; Gundersen, G.; Nielsen, C. J.; Cyvin, B. N.; Cyvin, S. J., *Acta Chem. Scand.* **1978**, *32a*, 833.

26. Choi, J. H.; Oh, I. G.; Ryoo, K. S.; Lim, W. T.; Park, Y. C.; Habibi, M. H., *Spectrochim. Acta A* **2006**, *65*, 1138.

27. Vagnini, M. T.; Rutledge, W. C.; Hu, C.; VanDerveer, D. G.; Wagenknecht, P. S., *Inorg. Chim. Acta* **2007**, *360*, 1482.

28. Sawodny, W.; Rau, K. M.; Bolkart, W., *J. Fluorine Chem.* **1989**, *43*, 119.

29. Nunez, P.; Elias, C.; Fuentes, J.; Solans, X.; Tressaud, A.; deLucas, M. C. M.; Rodriguez, F., *J. Chem. Soc., Dalton Trans.* **1997**, 4335.

30. Biju, A. R.; Rajasekharan, M. V., *J. Mol. Struct.* **2008**, *875*, 456.

31. Goodwin, H. A.; Sylva, R. N., *Aust. J. Chem.* **1967**, *20*, 629.

32. Darriet, J.; Massa, W.; Pebler, J.; Stief, R., *Solid State Sci.* **2002**, *4*, 1499.

33. Mantel, C.; Hassan, A. K.; Pecaut, J.; Deronzier, A.; Collomb, M. N.; Duboc-Toia, C., *J. Am. Chem. Soc.* **2003**, *125*, 12337.

34. Albela, B.; Carina, R.; Policar, C.; Poussereau, S.; Cano, J.; Guilhem, J.; Tchertanov, L.; Blondin, G.; Delroisse, M.; Girerd, J. J., *Inorg. Chem.* **2005**, *44*, 6959.

35. Pedersen, K. S.; Sigrist, M.; Weihe, H.; Bond, A. D.; Thuesen, C. A.; Simonsen, K. P.; Birk, T.; Mutka, H.; Barra, A. L.; Bendix, J., *Inorg. Chem.* **2014**, *53*, 5013.

36. Rother, G.; Worzala, H.; Bentrup, U., *Z. Anorg. Allg. Chem.* **1998**, *624*, 1706.

37. Jacobs, U.; Schröder, L.; Massa, W.; Elías, C.; Fuentes, J.; Núñez, P.; Bentrup, U., *Z. Anorg. Allg. Chem.* **1998**, *624*, 1471.

38. Rother, G.; Stief, R.; Bentrup, U.; Massa, W., *J. Fluorine Chem.* **2011**, *132*, 740.

39. Kraus, F.; Baer, S. A., *Z. Naturforsch.* **2011**, *66b*, 865.

40. Berry, J. F.; Bill, E.; Garcia-Serres, R.; Neese, F.; Weyhermuller, T.; Wieghardt, K., *Inorg. Chem.* **2006**, *45*, 2027.

41. Cotton, S. A.; Franckevicius, V.; Fawcett, J., *Polyhedron* **2002**, *21*, 2055.

42. Zhang, Z.; Geng, Z.-R.; Kan, X.-W.; Zhao, Q.; Li, Y.-Z.; Wang, Z.-L., *Inorg. Chim. Acta* **2010**, *363*, 1805.

43. Hoser, A.; Kałuski, Z.; Januszczyk, M.; Pietrzak, J.; Głowiak, T., *Acta Crystallogr., Sect. C: Cryst. Struct. Commun.* **1983**, *39*, 1039.

44. Healy, P. C.; Patrick, J. M.; Skelton, B. W.; White, A. H., *Aust. J. Chem.* **1983**, *36*, 2031.

45. Eckenhoff, W. T.; Biernesser, A. B.; Pintauer, T., *Inorg. Chim. Acta* **2012**, *382*, 84.

46. Köhn, R. D.; Kociok-Köhn, G., *Angew. Chem. Int. Ed.* **1994**, *33*, 1877.

47. Banerjee, A.; Panda, M.; Tolla, A. S.; Li, J.; Brennessel, W. W.; Loloee, R.; Chavez, F. A., *Z. Anorg. Allg. Chem.* **2012**, *638*, 1473.

48. Ali, A. B.; Grenèche, J.-M.; Leblanc, M.; Maisonneuve, V., *Solid State Sci.* **2009**, *11*, 1631.

49. Bentrup, U.; Massa, W., *Z. Naturforsch., B: J. Chem. Sci.* **1991**, *66*, 395.

50. McCleverty, J. A.; Meyer, T. J., *Comprehensive Coordination Chemistry II,* Pergamon, Oxford, **2004**, Vol. *6*.

51. Mitsutsuka, Y.; Tursun, E.; Nakahara, M., *Bull. Chem. Soc. Jpn.* **1990**, *63*, 260.

52. Glerup, J.; Schaffer, C. E.; Springborg, J., *Acta Chem. Scand.* **1978**, *32*, 673.

53. Massoud, S. S.; Milburn, R. M., *Polyhedron* **1989**, *8*, 2389.

54. Figgis, B. N.; Lewis, J., The Magnetic Properties of Transition Metal Complexes. In *Prog. Inorg. Chem.*, John Wiley & Sons, Inc.: 2007; pp 37-239.

55. Bhalla, R.; Darby, C.; Levason, W.; Luthra, S. K.; McRobbie, G.; Reid, G.; Sanderson, G.; Zhang, W., *Chem. Sci.* **2014**, *5*, 381.

56. Nachtigall, O.; Pataki, A.; Molski, M.; Lentz, D.; Spandl, J., *Z. Anorg. Allg. Chem.* **2015**, *641*, 1164.

57. Bagger, S.; Jensen, H. P., *Acta Chem. Scand.* **1978**, *32*, 659.

58. Laier, T.; Schaffer, C. E.; Springborg, J., *Acta Chem. Scand.* **1980**, *34*, 343.

59. Herwig, W.; Zeiss, H., *J. Org. Chem.* **1958**, *23*, 1404.

60. Wieghardt, K.; Chaudhuri, P.; Nuber, B.; Weiss, J., *Inorg. Chem.* **1982**, *21*, 3086.

61. Christe, K. O.; Wilson, W. W.; Wilson, R. D.; Bau, R.; Feng, J. A., *J. Am. Chem. Soc.* **1990**, *112*, 7619.

62. Andersen, P.; Døssing, A.; Glerup, J.; Rude, M.; Brekke, T.; Aksnes, D. W.; Tokii, T., *Acta Chem. Scand.* **1990**, *44*, 346.

63. Chaudhuri, P.; Winter, M.; Wieghardt, K.; Gehring, S.; Haase, W.; Nuber, B.; Weiss, J., *Inorg. Chem.* **1988**, *27*, 1564.

Chapter 7: **Summary and outlook**

The work described in this Thesis has considerably advanced the Group 13 metal-chelate systems, and has explored new platforms, for possible PET applications. The complex, [$Ga^{18}F^{19}F_2$($BnMe_2$-tacn)], was successfully ^{18}F-radiolfuorinated through $^{18}F/^{19}F$ isotopic exchange reactions starting with a sub-30 nM concentration of precursor (0.01 mg). The radiolabelling reaction proceeds in an aqueous MeCN solution at moderate temperature (80 °C) without the need of a Lewis acid promoter. Since the [^{18}F]F^- target water is used directly as received from the cyclotron and the purification of the radiolabelled compound is achieved through a simple SPE protocol, the total manipulation time (not optimised) of the process is about 20 minutes; a very short time in consideration of the half-life of fluorine-18 (110 minutes). The considerably reduced quantity of precursor required, in comparison to the Cl/^{18}F halide exchange reaction on [$GaCl_3$($BnMe_2$-tacn)] (1 mg, 2.63 μM), as well as the mild reaction conditions employed, make this result a key advance towards the synthesis of a new generation of ^{18}F-radiotracers based on GaF_3-complexes. The next step towards this goal would be the conjugation of biomolecules, such as PSMA and folate, through the functionalisation of the benzyl group of the ligand $BnMe_2$-tacn, in order to selectively target specific receptors overexpressed at the surface of diseased cells. PSMA is overexpressed in prostate cancer, whereas folate receptors are overexpressed on the surface of many tumour types, such as ovarian cancers. PSMA has been extensively studied and it can be used as benchmark for comparison and evaluation of the systems, whereas folate would be more exploratory with the aim of obtaining selective images of the tumour at an early stage. If successful, this could provide earlier and more informative disease diagnosis than the existing C-^{18}F based radiotracers (whose synthesis often requires reaction conditions that are often not compatible with biomolecules).

The ^{18}F-radioflurination of [$AlCl_3$($BnMe_2$-tacn)] by Cl/^{18}F halide exchange reactions has also demonstrated that the metal can greatly influence the radiolabelling conditions. Indeed, [$AlCl_3$($BnMe_2$-tacn)] and the gallium analogue, [$GaCl_3$($BnMe_2$-tacn)], can be radiolabelled using very different reaction conditions: [$AlCl_3$($BnMe_2$-tacn)] was successfully radiolabelled at pH 4 (sodium acetate buffer solution) with heating (80 °C), whereas [$GaCl_3$($BnMe_2$-tacn)] was radiolabelled in an aqueous MeCN solution at room temperature.

During this work, other metals in the 3+ oxidation state have been explored in order to assess their possible application as PET radiotracers. The group 3 metals, Sc(III) and Y(III), the lanthanides La(III) and Lu(III), and some of the metals in the first row of the transition metals (Cr(III), Mn(III), Fe(III) and Co(III)) have been investigated. Among these systems, [ScF_3($BnMe_2$-tacn)] has shown the most promise. Although its synthesis through Cl/^{19}F halide exchange reactions using the non-active [^{19}F]F^- in a preparative scale, requires the exclusion of moisture, the system is certainly worth further study

for the incorporation of ^{18}F. Given the oxophilic nature of Sc(III), the functionalisation of the tacn ligand with carboxylate pendant arms should also be considered. This strategy, or the use of N_4-macrocyles, may also be better suited for the larger metals, Y(III), La(III) and Lu(III).

From the analysis of the first row of transition metals, the complexes, [CrF_3(Me_3-tacn)], [FeF_3(Me_3-tacn)] and [CoF_3(Me_3-tacn)], have been identified as the systems which most merit further study. The thermodynamic stability and kinetic inertness of d^3 systems has prevented complete conversion to [CrF_3(Me_3-tacn)] through Cl/^{19}F halide exchange reactions using the chloride analogue, [$CrCl_3$(Me_3-tacn)], to be achieved within a time compatible with the half-life of fluorine-18. However, the stability tests performed on [CrF_3(Me_3-tacn)] have shown that the complex is stable in all the conditions tested. For this reason, $^{18}F/^{19}F$ isotopic exchange reactions on the parent complex [CrF_3($BnMe_2$-tacn)] may be successful in obtaining the desired radioactive product. Similarly, the high stability of [CoF_3(Me_3-tacn)] suggests that, also in this case, $^{18}F/^{19}F$ isotopic exchange reactions should be considered as a method to introduce [^{18}F]F^- into [CoF_3($BnMe_2$-tacn)].

[FeF_3(Me_3-tacn)] was successfully obtained through Cl/^{19}F halide exchange reactions from the chloride analogue (MeCN solution under reflux for 4 hours). Future work will involve further investigation of this reaction in a preparative scale in order to establish whether shorter reaction time and milder reaction conditions can be employed for the complete fluorination of [$FeCl_3$(Me_3-tacn)]. If successful, the knowledge acquired during the preparative scale reactions will be applied to the radiolabelling reactions.

Appendix 1 – General Experimental Techniques

Where required all reactions were conducted using Schlenk, vacuum line and glove-box techniques under a dry dinitrogen atmosphere. Solvents were dried and degassed prior to use. Et_2O and thf were distilled over Na/benzophenone ketyl; hexane and toluene over Na wire; CH_2Cl_2, $CHCl_3$ and MeCN were distilled over CaH_2 and MeOH was dried over Mg/I_2. Reactions performed under aqueous conditions utilised freshly distilled H_2O. All commercial reagents (obtained from Sigma-Aldrich, Strem, Alfa Aesar) were used as received. All ligands were prepared *via* literature methods.

Infra-red spectra were recorded over a range of 4000-200 cm^{-1} using a Perkin Elmer Spectrum 100 spectrometer. Samples were prepared as Nujol mulls between CsI plates. NMR spectra were recorded on a Bruker AV400 or DPX400 spectrometers. ^{1}H and $^{13}C\{^{1}H\}$ NMR spectra were referenced to the solvent resonances. $^{19}F\{^{1}H\}$ spectra were referenced to $CFCl_3$, ^{27}Al to aqueous $[Al(H_2O)_6]^{3+}$, ^{71}Ga to aqueous $[Ga(H_2O)_6]^{3+}$ pH 1, ^{45}Sc to $[Sc(H_2O)_7]^{3+}$ in water at pH 1 and ^{59}Co to $[Co(CN)_6]^{3-}$. ESI mass spectrometry was recorded using a Waters (Manchester, UK) mass spectrometer equipped with a single quadrupole analyser. Sample were introduced to the mass spectrometer *via* flow injection using a Waters 600 pump (flow rate 0.1 mL/min MeCN) and Waters 2700 autosampler. Microanalyses were performed by London Metropolitan University.

UV/visible spectra were recorded in solution (water or MeCN) and as powdered solids, using the diffuse reflectance attachment, in a Perkin Elmer 750S spectrometer. Magnetic measurements were made on a Johnson Matthey magnetic balance.

Single crystal X-ray data were collected using a Rigaku AFC12 goniometer equipped with an enhanced sensitivity (HG) Saturn724+ detector mounted at the window of an FR-E+ SuperBright molybdenum rotating anode generator with HF or VHF Varimax optics using Mo-Kα radiation (λ = 0.71073 Å). Crystals were held at 100 K under a nitrogen gas strem (Oxford Cryostream). Solution and refinement of structures was carried out using SHELX-97,[1] with hydrogen atoms added to the model in calculated positions using default C-H distances. Where additional restraints were required, details are provided in the cif file for each structure, or are discussed in the text.

Powder X-ray diffraction data were collected on a Bruker D2 diffractometer using Cu-K_α X-rays and refined using the GSAS package.[2,3]

Radiolabelling experiments were performed using $[^{18}F]F^-$ obtained by proton irradiation of $[^{18}O]H_2O$ (97 atom %, Rotem Industries Ltd., Israel) with a CTI RDS 112 cyclotron (11 MeV, 30 µA beam current) and analysed on an Agilent 1290 HPLC system with an Agilent 1260 DAD UV detector (G4212B). Dionex Chromeleon 6.8 Chromatography data recording software was used to integrate the UV and radiochemical peak areas. Column: Phenomenex Luna 5 µm C18(2) 250 x 4.6 mm.

Mobile phase A: 10 mM ammonium acetate. B: MeCN. Flow rate: 1 mL min^{-1} Gradient: 0-15 min (10- 90 % B), 15- 20 min (90 % B), 20- 21 min (90- 10 % B), 21- 26.5 min (10 % B).

References

1. Sheldrick, G. M., *Acta Crystallogr A* **2008**, *64*.

2. Toby, B. H., *J. Appl. Crystallogr.* **2001**, *34*.

3. Larson, A. C.; Von Dreele, R. B. *General Structure Analysis System (GSAS)*; 2004; pp 86-748.

Appendix 2 – Crystallographic Information Files

Cif files are located on a CD attached to the back of the thesis.

The filenames correspond to the complexes as follow:

$[Me_2NH_2][\textit{trans}\text{-}GaF_4(OH_2)_2]$	141311fmm10
$[GaF_3(OH_2)_2(DMSO)]$	2014fmm10
$[GaF_3(OH_2)_2(pyNO)]\cdot pyNO\cdot H_2O$	2015FMM32r
$[GaF_4(pmdtaH)]\cdot 2H_2O$	2015FMM29r-190315
$[Me_2N(CH_2)_2NMe(CH_2)_2]_2[Ga_2F_8(OH_2)_2]\cdot 2H_2O$	2015fmm31-b
$[GaF_3(OH_2)(py)_2]\cdot H_2O$	2015FMM7662-03r
$[ScCl_3(terpy)]$	2016FMM7662-36r0
$[YCl_3(terpy)(OH_2)]$	2016FMM7662-39Ar
$[ScF_2Cl(Me_3\text{-}tacn)]$	2016FMM7662-33Dr
$[YI_3(Me_3\text{-}tacn)]\cdot CH_3CN$	2016FMM7662-37A2ndr
$[\{YI_2(Me_3\text{-}tacn)\}_2(\mu\text{-}O)]\cdot CH_3CN$	2016FMM7662-37Ar
$[\{La(terpy)(OH_2)Cl\}_2\ (\mu\text{-}Cl)_2]$	2016rnw7945-05r
$[Sc(Me_3\text{-}tacn)F_2(\mu\text{-}F)SnMe_3Cl]$	2016FMM7662-54-2r_ml
$[LuCl_3(terpy)(OH_2)]$	2016rnw7945-09ar
$[MnF_3(Me_3\text{-}tacn)]\cdot 4H_2O$	FMM_TM52017k
$[CoF_3(Me_3\text{-}tacn)]\cdot 4H_2O$	2017FMM-8148-31k